

Immunophilin Ligand Design

by

George A. Kontopidis

Doctor of Philosophy

(Ph.D)

The University of Edinburgh

1999



The work presented in this thesis is the original work of the author, except where specific reference is made to other sources. It has not submitted in part, or in whole, for any other degree. Some of the results have already been published.

ΜΗΔΕΝ ΑΓΑΝ

ΠΛΑΤΩΝ

Nothing to excess

PLATO

ΑΦΙΕΡΩΝΕΤΑΙ
ΣΤΗ ΣΥΖΥΓΟ ΜΟΥ
Στελλα

**DEDICATED
TO MY WIFE
Stella**

Acknowledgements

I want to thank my supervisor, Prof. Malcolm D. Walkinshaw for his advice and encouragement during this project, and the great patience showed throughout the course of my work for this thesis. I am indebted to my supervisor Dr. Paul Taylor for instructing me in the tools and techniques of crystallography and for the computing help.

I am also indebted to Ms Jacqueline Dornan for her advice on procedures and techniques in the laboratory, and encouragement and help at all stages of this work.

I am further indebted to Dr Dimitri Alexeev for sharing his considerable experience and knowledge in the field of protein crystallography and for his friendship.

I would like to thank all the members of the Institute of Cell and Molecular Biology and the Department of Biochemistry, with special thanks to Dr David Apps for their help and support during this work.

Finally, I would like to thank my wife for her support, understanding and patience during this study.

I am pleased to acknowledge the financial support of the Novartis Pharma Basel.

Summary

The general aim of the project is to predict and select small molecule ligands which may bind to 3D protein templates. Proteins from the immunophilin family were used. Immunophilins are a class of proteins, which bind immunosuppressive drugs and also catalyse the *cis*↔*trans* isomerisation of peptidyl-prolyl bonds. Two families of immunophilins have been established: cyclophilin (Cyp) which binds the immunosuppressive drug cyclosporin A (CsA) and FKBP which binds the immunosuppressive drug of FK506 and rapamycin. The proteins used are cyclophilin A (165 residues, MW 17.8 kDa) cyclophilin B (184 residues, MW 22kda), FKBP-12 (107 residues, MW 12 kDa) and cyclophilin *Brugia* (177 residues, MW 20 kDa).

Where required proteins were produced and purified in house. Cyp-A and Cyp-B were expressed in *E.coli* and purified using chromatographic techniques. CypBr was provided as a fusion protein which then cleaved and purified in house. The purity of the initial protein samples were tested with SDS gels and then the samples were concentrated to an appropriate concentration for crystallization. Crystals of Cyp-A and of FKBP-12 were obtained of orthorhombic space group $P2_12_12_1$ and monoclinic space group C2 respectively. Two new crystals of CypBr were obtained a trigonal and tetragonal form. Molecular replacement methods were used to solve the crystal structure of the tetragonal form of CypBr using Cyp-A as starting model. The final R factor was 19,9 % and $R_{\text{free}}=23,4$ %. Atomic co-ordinates are deposited in the Brookhaven Database with the code 1A58.

The putative ligands were selected by two different methods, by structure similarity and using the docking program LIDAEUS, which was developed in house by Dr P. Taylor. Twenty nine small molecules were selected from a small molecule database and were tested with a fluorescence assay, a PPIase assay and x-ray crystallography for binding activity. Six new ligands have been discovered which bind to Cyp-A. In

this work the IC_{50} (concentration in which half inhibition occurred) of the putative ligands were determined by rotamase inhibition assay. In addition the binding of the ligands was also confirmed by crystallographic experiments. The X-ray structures of 3-acetyl-1 methyl piperidine, ethyl-piperidine glyoxylate, dimethyl sulfoxide, tetramethylene sulfoxide, cyclopentanone and 5,5-dimethyl-1,3-cyclohexanedione bound to Cyp-A have been solved and refined with Rfactors for each structure of less than 20%.

The structural analysis of the native and ligand structures revealed a hydrophobic pocket surrounded by residues Asn 102, Met 61, Arg 55 and His 122, a hydrogen bond donor site of the main chain nitrogen Asn 102, and another hydrogen bond donor site of the guanidinium of Arg 55.

The six novel ligands have been classified into 3 different families of compounds. 3-Acetyl-1 methyl piperidine and ethyl-piperidine glyoxylate belong to the piperidine family and shares structural similarities with a natural substrate of Cyp-A the dipeptide Ala-Pro. Dimethyl sulfoxide (DMSO), tetramethylene sulfoxide and cyclopentanone form the DMSO family and they do not share any similarities with known Cyp-A ligand. Only one compound has been discovered in the third family. This compound 5,5-dimethyl-1,3-cyclohexanedione also known as dimedone shows some structural similarities with the Val 11 residue of the Cyp-A ligand cyclosporin.

Abbreviations

$A_{1\text{mg/ml}}^{1\text{cm}}$	Absorbance coefficient
ACMPIP	1-Acetyl-3-methyl piperidine
AS _{sat}	Ammonium sulphate saturate
BCA	Bicinchonic acid protein assay method
BSA	Bovine serum albumin
B factor	Temperature factor
Cyp-A	Human cyclophilin A protein
CypA-AlaPro	Human cyclophilin A protein complex with Ala-Pro dipeptide
CypA-AAPF	Human cyclophilin A protein complex with N-succinyl-Ala-Ala-Pro-Phe-p-nitroanilide
Cyp-B	Human cyclophilin B protein
BrCyp	20 kD Cyclophilin from <i>Brugia malay</i>
CSD	Cambridge Structure Database
DCH	5,5-Dimethyl-1-3-Cyclohexanedione
DMSO	Dimethylsulfoxide
ETPIP	Ethyl-piperidine glyoxylate
FKBP-12	Human FK506 binding protein
FK506	Immunosuppressive drug, FK506
CsA	Immunosuppressive drug, cyclosporin A
IAA	3-β-Indoleacrylic acid
ISIS	Integrated Scientific Information System
LB	Luria-Bertani medium
LB _{amp}	Luria-Bertani medium contain 50μg/ml ampicillin
M9CA	M9 Minimal Medium contain 1% Casamino acid
M9CA _{amp}	M9 Minimal Medium contain 1% Casamino acid and 50μg/ml ampicillin
MBP	Maltose binding protein
OD ₆₀₀	Optical density at 600nm
PEG	Polyethylene glycol
PNT	Cyclopentanone
SDS	Sodium dodecyl sulphate
SDS-PAGE	Sodium dodecyl sulfate-polyacrylamide gel electrophoresis
TMSO	Tetramethylene sulfoxide
TRP	Tryptophan
PPIase	Peptidyl Prolyl Cis-Trans Isomerisation
Hepes	N-[2-Hydroxyethyl]piperazine-N'-[2-ethanesulfonic acid])
Tris	(Tris[hydroxyethyl]aminomethane)
Bis-Tris	(bis[2- Hydroxyethyl]iminotris[hydroxyethyl]methane
TFE	2, 2, 2-Trifluoroethanol

Table of Contents

1. Introduction.....	1.1
1.1 Ligand Design.....	1.1
A) Structural similarities.....	1.3
B) Docking Programme.....	1.4
1.2 Databases.....	1.5
A) ISIS.....	1.6
B) CSD.....	1.7
1.3 Immunophilins.....	1.7
A) Biological activities of Immunophilins.....	1.9
B) Mechanism of PPIase.....	1.12
C) Cyclophilins.....	1.15
1. Cyclophilin structures.....	1.15
D) FKPBs.....	1.17
1. FKBP structures.....	1.17
2. Protein Production.....	2.1
2.1 Introduction.....	2.1
2.2 Material & Methods.....	2.1
A) Storage of bacterial lines.....	2.1
B) Cyp-A & Cyp-B material and methods.....	2.2
1. Cells lines.....	2.2
2. Expression in <i>E.coli</i>	2.2
3. Small scale expression in <i>E.coli</i>	2.2
4. Large scale expression in <i>E.coli</i>	2.3
C) FKBP-12 material and methods.....	2.3

1.	Plasmid.....	2.3
2.	Bacterial strain.....	2.4
3.	Bacterial transformation.....	2.4
4.	FKBP-12 expression in <i>E.coli</i>	2.5
2.3	Results.....	2.6
A)	Expression of Cyp-A & Cyp-B.....	2.6
B)	FKBP-12.....	2.8
1.	Bacteria transformation	2.8
2.	FKBP-12 expression in <i>E.coli</i>	2.8
2.4	Discussion.....	2.9
3.	Protein Purification.....	3.1
3.1	Introduction.....	3.1
3.2	Purification strategy.....	3.1
A)	Cyp-A.....	3.3
B)	Cyp-B.....	3.4
C)	BrCyp.....	3.3
3.3	Material & Methods.....	3.5
A)	Columns and Equipments.....	3.5
B)	Purification procedures in Cyp-A.....	3.5
1.	Cell lysis.....	3.5
2.	Purification of Cyp-A.....	3.6
C)	Purification procedures in Cyp-B.....	3.7
1.	Cell lysis.....	3.7
2.	Purification of Cyp-B.....	3.7
D)	Purification of BrCyp.....	3.7
3.4	Results.....	3.8
1.	Cyp-A.....	3.8

2.	Cyp-B.....	3.13
3.	BrCyp.....	3.15
3.5	Discussion.....	3.16
1.	Cyp-A.....	3.17
2.	Cyp-B.....	3.18
3.	BrCyp.....	3.18
4.	Protein Characterisation.....	4.1
4.1	Introduction.....	4.1
4.2	Material &Methods.....	4.2
A)	Protein Determination.....	4.2
1.	BCA method.....	4.2
2.	Bradford method.....	4.3
3.	Extinction Coefficient	4.4
B)	Fluorescence Spectroscopy.....	4.5
C)	PPIase assay.....	4.11
1.	Rotamase activity assay.....	4.12
2.	IC ₅₀	4.13
4.3	Results.....	4.15
A)	Fluorescence Spectroscopy.....	4.15
1.	FKBP-12.....	4.15
2.	Cyp-A.....	4.17
B)	PPIase assay.....	4.19
1.	PPIase activity.....	4.19
2.	Determination of IC ₅₀ for Cyp-A ligands.....	4.22
2.	Determination of K _d	4.32
4.4	Discussion.....	4.33
A)	Protein determination.....	4.33

B)	Fluorescence spectroscopy.....	4.33
C)	PPIase assay.....	4.34

5. Crystallization5.1

5.1 Introduction.....5.1

5.2 Methods & Material.....5.2

A) Proteins.....5.2

1) Cyp-A.....5.2

2) Cyp-B.....5.2

3) BrCyp.....5.2

4) FKPB-12.....5.3

B) Crystallization and crystal handling.....5.3

1. Crystallization by vapour diffusion.....5.3

2. Screening.....5.3

3. Seeding.....5.4

4. Soaking.....5.5

A) Soaking ligands into Cyp-A crystals.....5.5

B) Soaking ligands into FKBP-12 crystals.....5.7

C) Soaking ligands into BrCyp crystals.....5.7

5. Co-crystallization.....5.7

5.3 Results.....5.8

1. Crystallization of native cyclophilin A, cyclophilin B, FKBP-12 in forms suitable for soaking experiments with novel ligands.....5.9

A) Cyclophilin A.....5.9

1. Crystallization.....5.9

2. Co-crystallization.....5.10

B) Cyclophilin B.....5.11

1.	Crystallization.....	5.11
C)	FKBP-12.....	5.11
1.	Crystallization.....	5.11
2.	Soaking.....	5.13
D)	BrCyp.....	5.13
1.	Crystallization.....	5.13
2.	Soaking.....	5.15
A)	Soaking Cyclophilin A crystals.....	5.15
B)	Soaking FKBP-12 crystals.....	5.19
C)	Soaking BrCyp crystal.....	5.19
5.4	Discussion.....	5.20

6.	X-ray Diffraction Data.....	6.1
6.1.	Introduction.....	6.1
6.2.	Material and Methods.....	6.1
1.	Data Collection Strategy.....	6.1
2.	X-ray source.....	6.2
3.	X-rays Detector.....	6.3
4.	Cryoprotection Mounting.....	6.4
5.	Data reduction.....	6.5
A)	Visualisation of diffraction image.....	6.6
B)	Indexing of the diffraction pattern.....	6.6
C)	Refinement of the crystal and detector parameters.....	6.6
D)	Scale and merge of the integrated reflections.....	6.7
6.	Ice removal.....	6.8
7.	Data collection set-up.....	6.9
6.3.	Results.....	6.10

1.	Cryoprotectors.....	6.10
2.	Data collection.....	6.11
	A) Cyp-A.....	6.11
	B) FKBP-12.....	6.16
	C) BrCyp.....	6.16
6.4.	Discussion.....	6.17
7.	Structure determination.....	7.1
7.1	Introduction.....	7.1
7.2	Material and Methods.....	7.3
1.	Molecular replacement.....	7.3
2.	Refinement.....	7.6
	A) Adding water molecules.....	7.6
	B) Addition of Ligands.....	7.7
3.	Evaluating errors of the model.....	7.7
	A) Ramachandran Plot.....	7.7
	B) Ω , Z and X angles.....	7.8
	C) Bad contacts and hydrogen bond energies.....	7.8
7.3.	Results	7.9
A)	Cyp-A.....	7.9
1.	Introduction	7.9
2.	Overview (ligand, Rfactors, native).....	7.11
3.	Stereochemical quality of CypA-ligand complexes and comparison.....	7.15
4.	Temperature factor evaluation and comparison.....	7.22
5.	Native structure (unliganded).....	7.24
6.	DMSO family.....	7.31
1.	DMSO.....	7.31

2.	TMSO	7.38
A)	Structural similarities and selection of TMSO ligand.....	7.38
B)	Refinement of TMSO data.....	7.40
3.	PNT.....	7.48
7.	Piperidine family.....	7.52
1.	ETPIPG.....	7.53
2.	ACMPIP.....	7.61
8.	Dimedone.....	7.66
A)	Selection and modification of the putative ligands.....	7.66
B)	Refinement of DCH data.....	7.68
B)	FKBP-12.....	7.72
1.	Introduction.....	7.72
2.	Overview.....	7.74
3.	Cyclooctanone.....	7.74
4.	Cyclohexanone.....	7.77
5.	Pregnane.....	7.79
C).	BrCyp.....	7.81
1.	Introduction.....	7.81
2.	Refinement of BrCyp data.....	7.81
A)	Trigonal form.....	7.81
B)	Tetragonal form.....	7.82
7.4.	Discussion.....	7.86
A)	Cyp-A.....	7.86
1.	Native.....	7.87
2.	DMSO.....	7.88
3.	TMSO.....	7.90
4.	PENT.....	7.96
5.	ETPIPG.....	7.99

6.	ACMPIP.....	7.102
7.	DCH.....	7.106
B)	FKBP-12.....	7.110
C)	BrCyp.....	7.116
8.	Conclusion.....	8.1
	1 Cyp-A.....	8.1
	2. FKBP-12.....	8.4
	3. BrCyp.....	8.4
9.	Appendix.....	9.1
	Appendix 1.....	9.1
	Appendix 2.....	9.2
	References.....	10.1

List of Figures

Figure 1.1: Selection of compounds based on structural similarities.....	1.3
Figure 1.2: Representation of docking program LIDAEUS.....	1.4
Figure 1.3: <i>Cis</i> ↔ <i>trans</i> isomerisation of peptidyl-prolyl bonds.....	1.7
Figure 1.4: Chemical formula of cyclosporin A and FK506.....	1.8
Figure 1.5: Topology of CypA.....	1.16
Figure 1.6: Topology of FKBP-12.....	1.18
Figure 2.1: SDS-PAGE of <i>E.coli</i> /7264 121 pellets induced with IPTG.....	2.6
Figure 2.2: SDS_PAGE of <i>E.coli</i> /101-521 1C pellets induced with IPTG.....	2.7
Figure 2.3: SDS-PAGE of <i>E.coli</i> /BL21(DE3)/pFKBP333.....	2.8
Figure 3.1: SDS-PAGE of cell extract and supernatant of <i>E.coli</i> /101-521 1C.....	3.9
Figure 3.2: SDS-PAGE of Cyp-A. Eluted fractions from Sepharose column.....	3.9
Figure 3.3: SDS-PAGE Cyp-A. Eluted fractions from mono-S column.....	3.10
Figure 3.4: SDS-PAGE Cyp-A. Eluted fractions from size exclusion column.....	3.11
Figure 3.5: SDS-PAGE. Eluted fractions from size exclusion column (cont).....	3.12
Figure 3.6: SDS-PAGE Cyp-B. Eluted fractions from mono-S column.....	3.13
Figure 3.7: SDS-PAGE Cyp-B. Eluted fractions from size exclusion column.....	3.14
Figure 3.8: SDS-PAGE BrCyp. Eluted fractions from mono-Q column.....	3.15
Figure 3.9: SDS-PAGE BrCyp. Past through of mono-Q column.....	3.16
Figure 4.1: Fluorescence titration of FKBP-12 with 5-Beta-Pregnane-3,20-dione..	4.7
Figure 4.2: Fluorescence emission titration of Cyp-A with CsA.....	4.8
Figure 4.3: Representation of <i>cis</i> ↔ <i>trans</i> isomerisation of peptidyl-prolyl bonds..	4.11
Figure 4.4: PPIase assay.....	4.12
Figure 4.5: Chymotrypsin-coupled assay of rotamase activity of Cyp-A.....	4.20
Figure 4.6: Chymotrypsin-coupled assay of rotamase activity of Cyp-B.....	4.21
Figure 4.7: Chymotrypsin-coupled assay of rotamase activity of BrCyp.....	4.22
Figure 4.8: PPIase assay with various amounts of Cyp-A.....	4.25
Figure 4.9: Expression of readings at absorbance units around 0.76 from Fig.4.8..	4.26
Figure 4.10: Protein concentration plotted against velocity.....	4.27
Figure 4.11: PPIase assay with various amounts of CsA.....	4.28
Figure 4.12: Readings at absorbance units around 0.76 from Fig.4.11.....	4.29
Figure 4.13: Plot of velocity against CsA concentration.....	4.30
Figure 5.1: Improvement of quality and size in Cyp-A crystal.....	5.10
Figure 5.2 .Results of streak seeding technique in FKBP-12.....	5.12
Figure 5.3. Crystal of FKBP-12 grew after macroseeding.....	5.13
Figure 5.3. Crystal of FKBP-12 grew after macroseeding.....	5.14
Figure 5.5. Improvement of quality in BrCyp crystals Tetragonal form.....	5.15

Figure 7.1: X-ray structure of Cyp-A.....	7.10
Figure 7.2: Ramachandan plot for Cyp-A complexed with PNT.....	7.17
Figure 7.3: Main chain parameters for Cyp-A complexed with PNT.....	7.20
Figure 7.5: Difference electron density map (1Fo-1Fc) of unliganded Cyp-A.....	7.25
Figure 7.6: Difference electron density map (2Fo-1Fc) of unliganded Cyp-A.....	7.26
Figure 7.7: Contacts of solvent molecules in the cyclophilin binding site.....	7.27
Figure 7.7A: Overlay of native CypA (this work) with the 2cpl native structure....	7.30
Figure 7.8: Difference electron density map (1Fo-1Fc) for the ligand DMSO.....	7.33
Figure 7.9: Difference electron density map (2Fo-1Fc) for the ligand DMSO.....	7.34
Figure 7.10: Contacts of DMSO ligand with surrounding atoms of the protein.....	7.36
Figure 7.11: Selection of compounds based in structural similarities.....	7.38
Figure 7.11: Difference electron density map (1Fo-1Fc) for the ligand TMSO.....	7.40
Figure 7.12: Difference electron density map (2Fo-1Fc) for the ligand TMSO.....	7.41
Figure 7.13: Difference electron density map for the ligand TMSO and W_310....	7.43
Figure 7.14: Two alternative positions of the ligand TMSO.....	7.45
Figure 7.15: Contacts of the TMSO ligand with surrounding atoms.....	7.47
Figure 7.16: Difference electron density map (1Fo-1Fc) for the ligand PNT.....	7.49
Figure 7.17: Difference electron density map (2Fo-1Fc) for the ligand PNT.....	7.50
Figure 7.18: Contacts of PNT ligand with surrounding atoms of the protein.....	7.51
Figure 7.19A: (1Fo-1Fc) map for the ligand ETPIPG.....	7.54
Figure 7.20: Difference electron density map (2Fo-1Fc) for the ligand ETPIPG....	7.55
Figure 7.21: Alternate conformations ALT1 and ALT2 for the ligand ETPIPG.....	7.56
Figure 7.22: Difference electron density map (2Fo-1Fc) for the ligand ETPIPG....	7.57
Figure 7.23: ALT1 and ALT2 of ETPIPG in the binding site of CypA.....	7.58
Figure 7.23A: Contacts of conformer 1 of ETPIPG with surrounding atoms.....	7.60
Figure 7.23B: Contacts of conformer 2 of ETPIPG with surrounding atoms.....	7.61
Figure 7.24: Difference electron density map (1Fo-1Fc) for the ligand ACMPIP..	7.62
Figure 7.25: Difference electron density map (2Fo-1Fc) for the ligand ACMPIP..	7.63
Figure 7.26: (2Fo-1Fc) electron density map for the side chain of Arg 55.....	7.64
Figure 7.27: Contacts of the ACMPIP ligand with surrounding atoms.....	7.65
Figure 7.29: Modifications applied in the ligand (TDD).....	7.67
Figure 7.30: Difference electron density map (1Fo-1Fc) for the ligand DCH.....	7.68
Figure 7.31: Difference electron density map (1Fo-1Fc) for the ligand DCH.....	7.69
Figure 7.32: Difference electron density map (2Fo-1Fc) for the ligand DCH.....	7.70
Figure 7.33: Contacts of the DCH ligand with surrounding atoms.....	7.71
Figure 7.33A: Structure of FK506.....	7.73
Figure 7.34: Difference electron density map (1Fo-1Fc) for the oct_1 data set.....	7.75
Figure 7.35: Difference electron density map (1Fo-1Fc) for the ligand oct_2.....	7.76
Figure 7.36: Difference electron density map (2Fo-1Fc) for the ligand oct_2.....	7.77
Figure 7.37: Difference electron density map (1Fo-1Fc) for the hex data set.....	7.78
Figure 7.38: Difference electron density map (1Fo-1Fc) for the hex data set.....	7.79
Figure 7.39: Difference electron density map (1Fo-1Fc) for the prg1 data set.....	7.80
Figure 7.41: Mass spectrum of BrCyp.....	7.84

Figure 7.42: The side chains of the two cysteines (Cys 43 and 173) of BrCyp.....	7.85
Figure 7.43: Overlay of native CypA with the CypA-DMSO complex.....	7.89
Figure 7.44: Overlay of CypA with TMSO and DMSO bound in binding site.....	7.91
Figure 7.45: Overlay of CypA-TMSO (Model 3) and native structure.....	7.92
Figure 7.46: Contacts of site 1 of TMSO ligand with surrounding atoms.....	7.94
Figure 7.47: Contacts of site 2 of TMSO ligand with surrounding atoms.....	7.95
Figure 7.48: Overlay of PNT, ACPIP and ETPIPG structures.....	7.97
Figure 7.49: Overlays of native CypA with the CypA-PNT complex.....	7.98
Figure 7.50: Overlay of ETPIPG and CypA-AlaPro (1cyh) complex structures.....	7.99
Figure 7.51: Overlays of native CypA with the CypA-ETPIPG complex.....	7.101
Figure 7.52: Contacts of ETPIPG (ALT1) with side chain of His 126.....	7.102
Figure 7.53: Overlay of CypA-ACMPIP and CypA-ETPIPG (ALT1) structures.....	7.104
Figure 7.54: Overlays of native CypA with the CypA-ACMPIP complex.....	7.105
Figure 7.55: Overlay of native CypA with the CypA-DCH complex.....	7.107
Figure 7.56: Chemical formula of the immunosuppressant drug cyclosporin.....	7.108
Figure 7.57: Overlay of complex CypA-DCH with the CypA-CsA complex.....	7.109
Figure 7.58: Overlay of native FKBP12 structure with the FKBP12-oct.....	7.111
Figure 7.59: Native FKBP-12 structure with waters in the binding site.....	7.112
Figure 7.60: An overlay of different structures of cyclooctanone found in CSD.....	7.113
Figure 7.61: Overlay of FKBP12-FK506 with the FKBP12-oct1 complex.....	7.114
Figure 7.62: Overlay of CypA with BrCyp.....	7.117
Figure 7.63: The octapeptide loop of BrCyp.....	7.118
Figure 7.64: Overlay of the active site of BrCyp with the CypA.....	7.120
Figure 7.65: CypA-CsA structure complex shows how CsA binds to CypA.....	7.121
Figure 7.66: The active site of BrCyp occupied by a neighbouring molecule.....	7.123

1 Introduction

In the early days of drug discovery, drugs were found from natural products by chance observations. The conceptual breakthrough facilitating rational drug discovery was that any drug has a specific target at the cellular level.

If nothing is known about the structure of the target protein there is no other way to find a drug except by screening large numbers of natural and synthetic substances to find one which shows binding activity. There are cases in which the natural ligand of the protein is known while the protein shape is unknown. In both cases a useful strategy in the design of a new drug or ligand is the trial and error modification of a lead. The increased potency or decreased toxicity monitored in conjunction with biological and physiological evaluation (Greer et al. 1994) must also be considered in the drug development process.

In recent years drug design has utilised knowledge of the structure of the target molecule. The structure based methodology can yield putative drugs more quickly and less expensively. The final products are custom tailored to their targets, they tend to be more potent, less toxic and more specific than drugs discovered in other ways (Bugg et al. 1993). This approach requires selecting a protein target molecule which plays a critical role in a physiologically relevant biological pathway. If the natural ligand is also known, it is helpful to have a three-dimensional structure of the complex as a starting point for development.

1.1 Ligand Design

The three-dimensional structure of the target protein is the first step in structure based design of a new ligand (Verlinde and Hol 1994). The next step is to find a lead or candidate ligand which fits geometrically and chemically into the binding pocket of the protein.

A 'lead' ligand as determined by X-ray crystallography or NMR methods can be used to direct the atom-by-atom modification in order to design a new ligand or improve the lead (Salemme et al. 1997). This method is called the **extending ligand or structural similarity** method and based on the principle that compounds with similar structure are going to have similar conformation and thus bind the same 3D template.

When a 'lead' ligand is not available the target protein must serve as a template. A number of methods have recently been proposed that attempt to automatically design new ligands for a given protein structure (Verlinde and Hol 1994). In the first step the binding pocket of the protein is defined and characterised. Most programs developed for *de novo* construction try to assemble novel molecules from "pieces". These "pieces" can be either atoms (**docking method**) or larger, chemically reasonable fragments (**linking recognition fragments method**).

In the docking method the protein template is used to select potential ligands using a computational docking procedure which involves matching and fitting ligand atoms onto the protein surface (Böhm 1996). Orientation of the ligand in the active site is generated such that a chemical and shape complementarity between the ligand and the binding site cavity has to be fulfilled.

The linking recognition fragments method incorporates different functional groups or small molecules bound to the target protein into a single, larger molecule (Verlinde and Hol 1994; Böhm 1995). The fragments are taken from a large small-molecule database. In the current work only the structural similarity method and the docking method were used for ligand design. The three dimensional structure of the ligand is required in all of the above techniques

A) Structural similarities

Structural similarity provides a method to select new ligands. The principle is that compounds with similar structure are going to have similar conformation and thus bind the same 3D template. The method is schematically described in Figure 1.1.

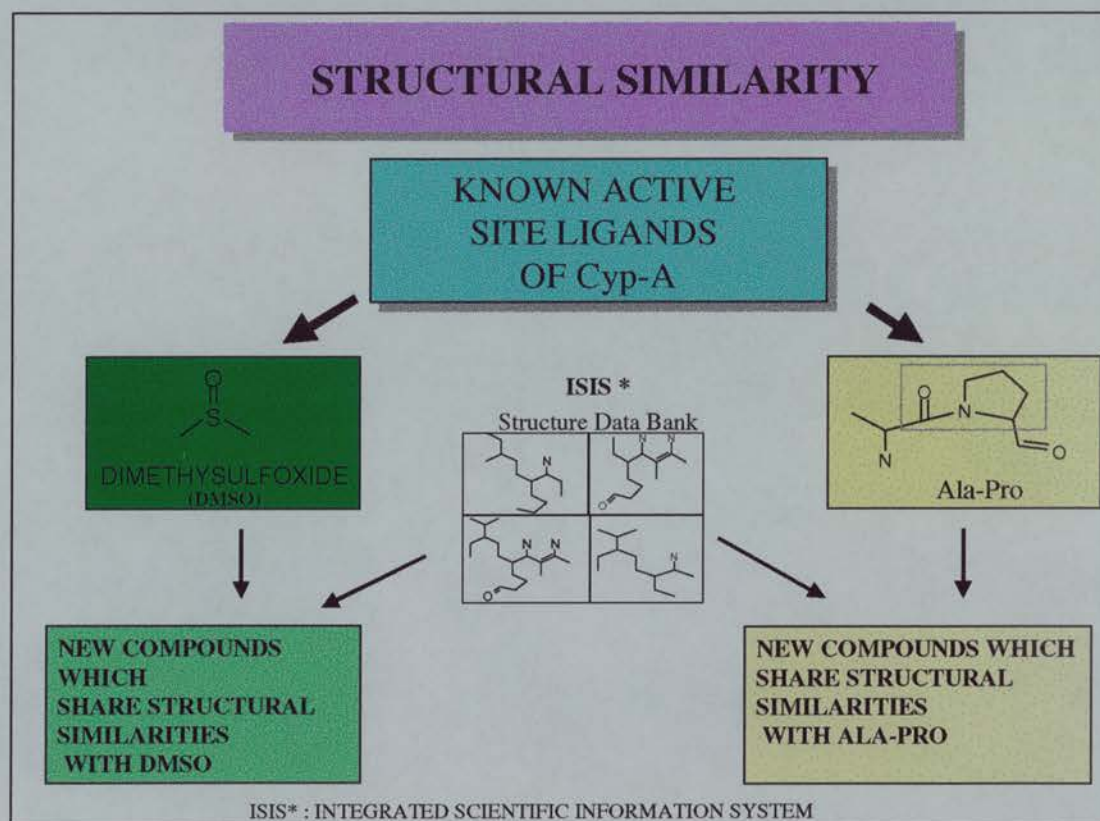


Fig. 1.1: Selection of compounds based on structural similarities

The first step is a careful inspection of the residues around the candidate atom. At this point the possibility of hydrogen bonding, electrostatic, hydrophobic and van der Waals interactions should be examined. The next important step is the comparison of the native (unbound) structure with the bound one. This will give a clear view of the rigid and flexible domains of the binding site. Furthermore the water molecules which have been replaced by the ligand (if any) can be marked.

The water molecules in the native structure are very important since they give us an idea which part of the ligand could be modified by extension, and try replacing one or more of these water molecules. The water molecules also indicate favoured sites for hydrophilic interaction or hydrogen bonding.

B) Docking Programme

The docking program LIDAEUS was developed in house by Dr P. Taylor. The process of how the program works is given below and schematically in Figure 1.2.

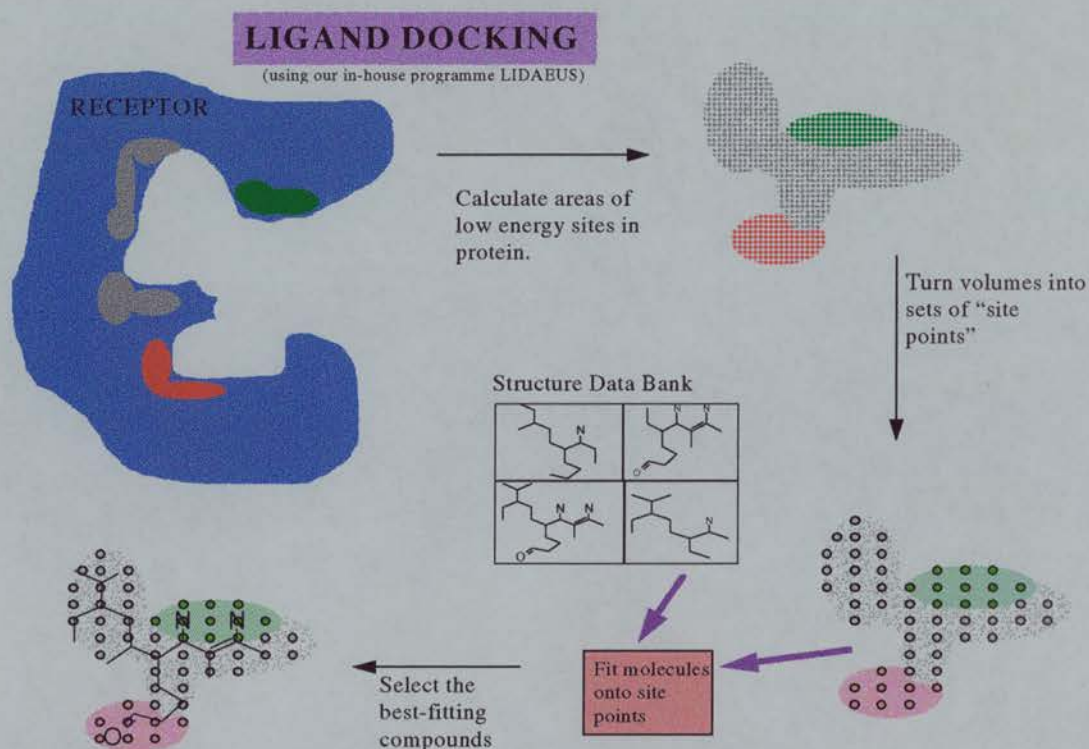


Fig. 1.2: Representation of how docking program **LIDAEUS** is working.

The program calculates the interaction energy between a "probe atom" and the protein on a 3D grid of site points around the protein sites. Carbon and oxygen atoms are used as probe atoms for the calculation. Carbon atom probes map out favoured

areas for hydrophobic interaction and oxygen atom for hydrogen bonding and hydrophilic interactions. The next step is to turn these volumes into site points and generate a negative template of the active site of the target protein. This negative template has the geometrical and chemical properties of putative ligands. The final step is the search for ligands in a database (Maybridge Fine Chemicals was used) which can fit in the above site points and select the best-fitting ligand. The list of the ligands found in the above database were commercially available.

Selection then was based on molecular weight and hydrophobicity. The most hydrophilic ligands were selected from the list generated by LIDAEUS. Hydrophobicity was a criterion for discarding molecules since occupancy of the binding sites in the crystal is proportional to concentration of the ligand in the solution. Furthermore small molecules can easily go through crystal channels and reach the binding site so molecules with a molecular weight larger than 300 were not used for soaking.

1.2 Databases

There are several large databases of small molecules (ISIS, CSD, and Maybridge Fine Chemicals). These databanks contain either three dimensional data as obtained from X-ray/NMR structure analysis or 2D atomic connectivities. When a 3D structure is not available, structure-generation programs that convert two dimensional connection tables into three dimensional structures are used, for example WITNOTP (Widmer 1997) or SYBYL (SYBYL a molecular modeling program, Tripos Inc., University of Georgia, St. Louis Missouri).

In the current work the following databases have been used:

- When a lead compound was available ISIS (Integrated Scientific Information System) was used to search for ligands with structural similarities.

- CSD (Cambridge Structural Database) was mainly used in order to find the experimentally obtained 3D structure of a ligand when only 2D atomic connectivities were known.
- Maybridge Fine Chemicals was the database used by the docking program LIDAEUS.

A) ISIS

The ISIS database contains about 238,000 compounds and the number is increasing daily.

Molecules in this data bank are in 2D atomic connectivities. (some entries are in 3D in the latest version of the software)

The main advantage of this databank is that all molecules are commercially available. Every compound listed has useful supplementary information such as suppliers, degree of purity and price. The availability makes the time between finding a lead and testing it shorter combined with the available information on price makes this a very efficient way forward both financially and experimentally.

The search for structure similar compounds is performed as follows:

- The lead compound was drawn in ISIS draw in 2D atomic connectivities.
- The 2D atomic connectivities were put in query window of the ISIS program.
- The actual search was performed by search tool. This tool allows you to specify the degree of similarity between the search structure and the target structure. Values range from 0 (no similarity) to 100 (an exact match).
- Hits generated from the above procedure were inspected manually. Large molecular weight (>300) molecules are put in second priority since the soaking technique was used and it would be difficult for them to penetrate the crystal lattice and reach the binding site.

The 3D structure of the ligands was generated afterwards using the WITNOTP program.

B) CSD

The Cambridge Structural Database contains some 197000 3D entries (September 1999) of small molecules. The main disadvantage of the database is that the compounds can not be ordered and tested quickly. The database was used for the comparison of structures generated by WITNOTP. If the candidate molecule is not in the database the closest derivative was used for comparison with the experimental 3D structure.

1.3 Immunophilins

Immunophilins are a class of proteins which bind immunosuppressive drugs and also catalyse the *cis*↔*trans* (Fig. 1.3) isomerisation of peptidyl-prolyl bonds. Immunophilins are ubiquitous proteins, found in organisms as diverse as plants, bacteria and mammals (Galat and Metcalfe 1995; Trandinh et al. 1992).

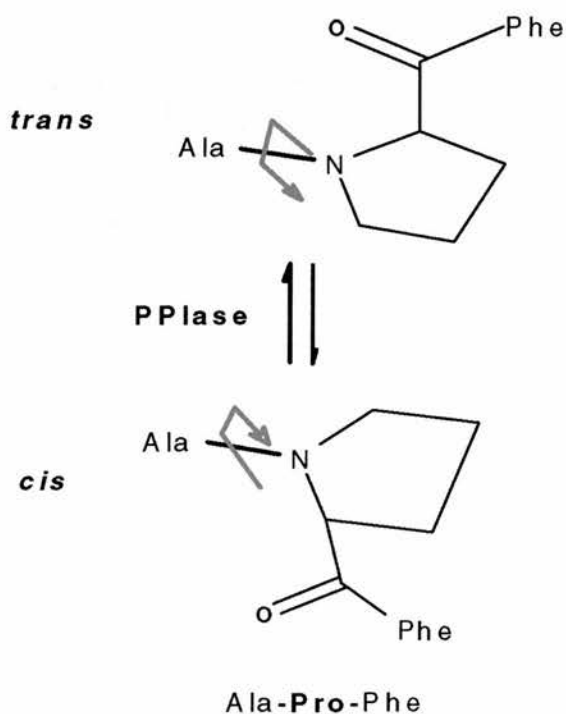


Fig. 1.3: Schematic presentation of *cis*↔*trans* isomerisation of peptidyl-prolyl bonds

Two families of immunophilins have been established: cyclophilin (Cyp) and FKBP. Cyclophilin (Cyp) was discovered in 1984 as a cytosolic receptor of the immunosuppressive drug CsA (Fig.4) (Handschumacher et al., 1984) while FKBP was identified as the binding protein of FK506 (Fig. 1.4) in 1989 (Siekierka et al., 1989; Harding et al., 1989). There is no sequence homology or obvious structural similarity between cyclophilin and FKBP (Walkinshaw et al. 1992).

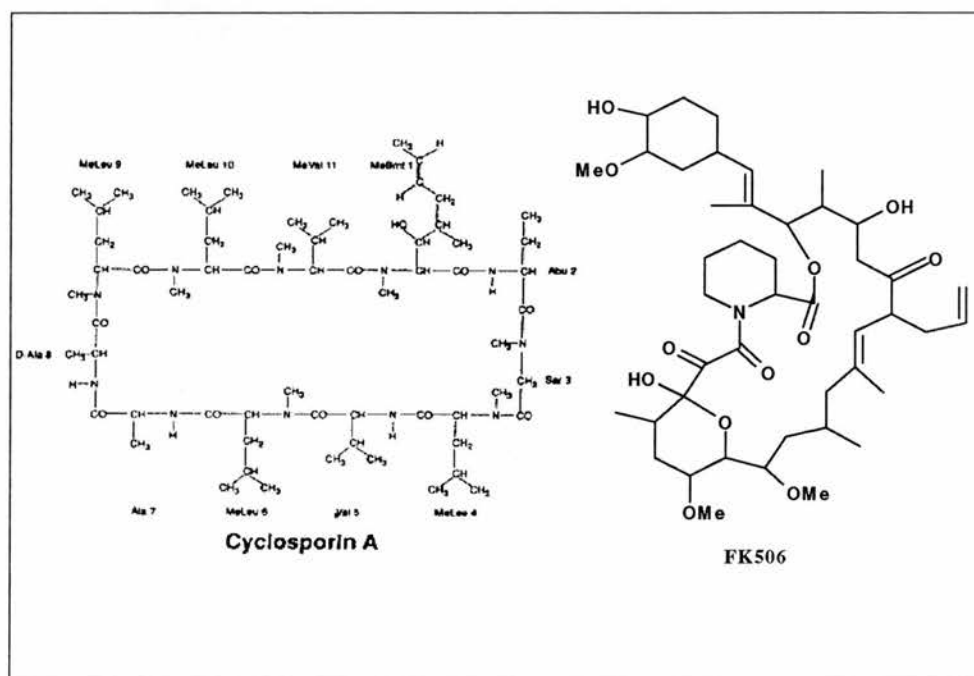


Fig. 1.4: Chemical formula of the immunosuppressive drugs cyclosporin A and FK506.

PPIase activity and T cell activation are two independent properties of immunophilins but both relate with the same binding site of the proteins. Bierer et al. (1990) and Kimball et al. (1991) demonstrate the failure of PPIase activity to mediate T cell activation, implying that the immunophilin-drug complex causes immunosuppression but not the immunophilin alone. PPIase activity of peptidylproline isomerases may be completely abolished by the immunosuppressive drugs CsA and FK506 suggesting that the binding site of these drugs and PPIase activity site are the same (Harding et

al. 1989; Takahashi et al. 1989). Indeed, x-ray structures of CypA with the substrate ac-Ala-Ala-Pro-Ala-amc in the Kallen and Walkinshaw structure (1991) and with CsA (Mikol et al. 1993) showed that both bound in the same binding pocket.

A) Biological activities of Immunophilins

Despite the chemical dissimilarity of the ligands and the structural difference between the two immunophilin families, there is an intriguing overlap of biochemical and biological activity. Immunophilins have been found to be involved in a number of cellular processes (Galat and Metcalfe 1995). Both cyclophilin and FKBP are involved in signal transduction in human T cell activation (Showstack et al. 1989; Metcalfe and Richards 1990) and also in protein folding by PPIase activity (Fischer et al. 1984; Harding et al. 1989; Fischer and Schmid, 1990). Other interesting biological functions are the binding into HIV-1 virions of hCypA (Thali et al. 1994; Braaten et al. 1996), phototransduction in *Drosophila* (Baker et al. 1994), transporting of procollagen (Smith et al. 1995) and the formation of avia progesterone receptor (Johnson and Toft 1994).

Signal transduction in human T cell

Since its first clinical trial in 1976, CsA (Fig 1) has been widely used as an immunosuppressive drug to prevent rejection following bone marrow and organ transplantation, and has also been the subject of a clinical trial in the treatment of autoimmune diseases (Starzl et al. 1989); Showstack et al. 1989). FK506 (Fig 1.4) possesses very similar immunosuppressive properties both *in vivo* and *in vitro*, but is 10 to 100 times more efficient than CsA (Thomson, 1989; Metcalfe and Richards, 1990).

Both CsA and FK506 inhibit early events in T lymphocyte activation and block lymphokine driven differentiation and proliferation of effector T cells (Emmel et al. 1989). Calcineurin, a serine/threonine phosphatase and a calmodulin binding protein

(Klee et al., 1988) has been identified as a receptor for both Cyp-CsA and FKBP-FK506 complexes *in vitro* (Liu et al., 1991). Inhibition of calcineurin will inactivate the dephosphorylation of a lymphocyte-specific transcription factor, NF-ATp, and therefore prevent the movement of NF-ATp from the cytoplasm to the nucleus where it binds to the promoter of the interleukin-2 gene and stimulates expression of the gene in the T-cell activation pathway (Loh et al. 1996; Luo et al. 1996).

PPIase activity

Another unexplained coincidence between the two immunophilin families is their shared peptidyl-prolyl isomerase activity (Galat and Metcalfe 1995). There is no apparent sequence similarity between the PPIase domains of the cyclophilins and FKBP (Harding et al. 1989). PPIase was the activity which originally led to the isolation of cyclophilin, (Fischer et al. 1984). The sequence of this cyclophilin (Fischer et al. 1989a) appeared to be identical with a protein which was shown to be the major target of CsA in bovine thymocytes (Handschumacher et al. 1984).

For proteins to adopt the correctly folded conformation, the Xaa-Pro amide bonds must be in the correct *cis* or *trans* configuration. *In vitro* studies show that the *cis/trans* isomerisation of some X-Pro bonds is the rate-limiting step in the refolding process (Lang et al. 1987). Depending on the nature of the substrate, CyP and FKBP can accelerate the rate of folding of proteins or oligopeptides by over 10 times the rate observed without isomerase (Fischer and Schmid, 1990) even at PPIase concentration as low as 0.1 μM . At concentration about 30 μM , which is close to the *in vivo* concentration of some cyclophilins (Harding et al. 1986), the refolding of RNase T1 was essentially instantaneous. PPIase has also been shown to accelerate the refolding process on bovine carbonic anhydrase II (Fransson et al. 1992). Other proteins reported to involve cyclophilins in their folding are collagen (Bachinger

1987), ribonuclease (Lang et al. 1987) and chymotrypsin inhibitor 2 (Jackson and Fersht 1991).

Incorporation into HIV-1 virions

Cyclophilin A has been reported to interact with the HIV-1 Gag protein (Thali et al. 1994 ; Franke et al. 1994). Furthermore, cyclosporine A inhibits the production of replication-competent HIV-1 virions by disrupting the Gag-CypA interaction (Thali et al. 1994; Braaten et al. 1996). The high CsA affinity to CypA (nanomolar range), significantly inhibits the incorporation of CypA into HIV-1 virions (K_d of Gag-CypA interaction is in micromolar range) and thus reduces HIV-1 infectivity. The anti-HIV-1 activity of CsA seems to be independent of its immunosuppressive activity since non-immunosuppressive CsA derivative can act as HIV virion inhibitors (Papageorgiou et al. 1996a, b).

***In vivo* protein activities by Immunophilins**

DmCyp-26 is a tissue specific cyclophilin and an integral ER protein. This 26 kDa PPIase is expressed in the photoreceptor cells of *Drosophila melanogaster* by the *ninaA* gene. DmCyp-26 has been shown to be required for the transport of the folded isoforms of rhodopsin (Rh1 and Rh2) from the rough endoplasmic reticulum through the cytoplasm to the cell surface (Baker et al. 1994).

Another related example of chaperone function is the folding of procollagen I. Cyclophilin has been implicated in the formation of collagen triple helices in the endoplasmic reticulum of fibroblast cells where the folding of procollagen I is slowed by 40% in the presence of 5 mM CsA (Steinman et al. 1991). Cyclophilin has also been shown to catalyse the folding of thermally denatured type III collagen

(Compton et al. 1992). Also the hCypB and Hsp-47 has been shown to act together to transport collagen from the endoplasmic reticulum (Smith et al. 1995).

CsA has been shown to retard the folding and secretion of transferrin from the HepG2 cells. Additionally folding and glycosylation which takes place in the endoplasmic reticulum (ER) was not affected by FK506 or rapamycin. It thus suggested that an ER-cyclophilin aids the formation of the prefolded segments of transferrin which facilitate the formation of correct disulphide bridges and secretion of the protein to the extracellular milieu (Lodish and Kong 1991).

B) Mechanism of PPIase

The torsion angle of a peptide (OC-N) bond could be in *cis* or in *trans* conformation (see Fig. 3). Because of the steric interference the *trans* form is energetically favorable and the *cis* form is rare in the native structure of proteins. The only exception is proline which has higher probability (0.1-0.3) to form a *cis* conformation compared to the other 19 common amino acids which have a probability of 10^{-3} (Galat and Metcalfe 1995).

The higher probability of proline *cis* peptide bonds could be due to a lower activation energy barrier (13 kcal/mol, Schulz and Schirmer 1979) for an X-Pro bond which for other peptide bonds is estimated to be between 18-21 (Jorgensen and Gao 1988). The corresponding difference between the *cis* and *trans* states of Xaa-Pro amide bonds is estimate to be only 0.5 kcal/mol (Kallen and Walkinshaw 1992). PPIases enzymatic activity can reduce the rotational energy barrier and speed up the *cis-trans* isomerisation. Several different mechanisms have been proposed to explain the reaction, and are listed below.

Tetrahedral intermediate

Measurements of the secondary deuterium effect on the hCypA-CsA complex had led to a suggestion that the complex was due to formation of a tetrahedral intermediate (Fischer et al. 1989a). In this mechanism a tetrahedral intermediate, hemithioorthoamide, was proposed by the nucleophilic addition of a cysteine or nucleophilic residue to the carbonyl carbon of the Xaa-Pro peptide bond (Fischer et al. 1989b). However, NMR studies on the FKBP12-FK506 complex and CypA-CsA complex had shown that only the *trans* form of the ligands were bound to the immunophilins without formation of tetrahedral intermediate (Harrison and Stein 1990b). Also the crystal structure of Ala-Pro with CypA revealed no cysteine or nucleophilic residue close to the carbonyl carbon (Ke et al. 1993).

Catalysis by distortion

This mechanism proposes that the C-N bond is rotated and this distorted intermediate is stabilised in the cyclophilin binding site. This mechanism is supported by kinetic isotropic studies and the solvent deuterium isotropic effect (Harrison and Stein 1990a). However all published structures of cyclophilin A with linear peptides except the HIV-1 capsid protein bind to hCypA in the *cis* conformation (Taylor et al. 1997).

Catalysis by protonation

The mechanism proposes a protonation of the C-N peptide bond by side chain residues like threonine, tyrosine or serine or maybe a hydrogen bond to the lone pair of the nitrogen atom (Fischer et al. 1989b; Kofron et al. 1991). Molecular orbital calculations show that the protonation reaction of amide atom can reduce the energy barrier of *cis-trans* isomerisation as it can deconjugate the OC-N peptide bond and

the double bond character of the C-N bond is weaker (Armbuster and Pulman 1974). However this mechanism is not proven by structural results since in the complexes of CypA with linear peptides there are no proton-donor groups such as serine, threonine or tyrosine close to the amide nitrogen (Zhao and Ke 1996 a; Zhao and Ke 1996 b; Ke et al. 1993).

Catalysis by desolvation

It has been shown that the rate of *cis-trans* isomerisation is accelerated in nonpolar solvents (Radzicka et al. 1992; Eberhardt et al. 1992). The mechanism suggests that the first step of the reaction is the desolvation of the substrate. The above is also supported by the structures of peptides contained a proline residue. The proline ring makes strong hydrophobic interactions with the hydrophobic pocket of cyclophilin.

Solvent assisted mechanism

The mechanism is based in the structures of hCypA with Ala-Pro (Ke et al. 1993) and most recently with a series of dipeptide Ser-Pro, His-Pro and Gly-Pro complexes (Zhao and Ke 1996 a). The solvent-assisted mechanism is similar to the proposal of “catalysis by distortion” (Harrison and Stein 1990a) but pinpoints water instead of protein residues as the chemical group to cause distortion of the amide bond. A conserved water molecule in the unligated and in the complexed structure in the binding site appears to be the candidate. A rotation between -50° to -90° of the C-N peptide bond (due to thermal movement) would bring the amide bond to the transition state which can be stabilised through a hydrogen bond between the carbonyl oxygen and the candidate water molecule. However this water molecule is not observed in the CypA-AAPF complex so the solvent-assisted mechanism is not verified on the basis of the tetrapeptide structure. This raises the question whether the dipeptide and

tetrapeptide have different *cis-trans* isomerisation mechanisms or that the dipeptides are competitive inhibitors of the CypA.

C) Cyclophilins

Cyclophilins are abundant and ubiquitous proteins in both prokaryotic and eukaryotic organisms (Koletsky et al., 1986). About 50 members of the family have been reviewed (Galat and Metcalfe 1995) and the number is growing. The majority of prokaryotic and yeast Cyps have an acidic pI whereas those from mammals are basic. The molecular mass of known cyclophilins vary from 15kDa for a *Bacillus subtilis* cyclophilin (Herrler et al. 1994) to 159 kDa (Anderson et al. 1993). Cyclophilins with low molecular weight are relatively hydrophobic molecules whereas big cyclophilins like Cyp-160 have both highly hydrophobic domains intertwined with those rich in charged residues (Galat and Metcalfe 1995). The dissociation constants to CsA can vary significantly for different members of the family. An 18kDa cyclophilin from *E.coli* has a K_i of 8.8 μ M while the same size human cyclophilin has a K_i of 17nM (Taylor et al. 1997).

1. Cyclophilin structures

Cyclophilin structures from human, yeast, parasite and bacteria have been solved by X-ray crystallography or NMR and they share similar structural features (Taylor et al. 1997). The most common features of cyclophilins are the 8 antiparallel β -stranded barrel capped by two α -helices (Fig. 1.5). The main sequence differences between different members of the family are located on the external loops.

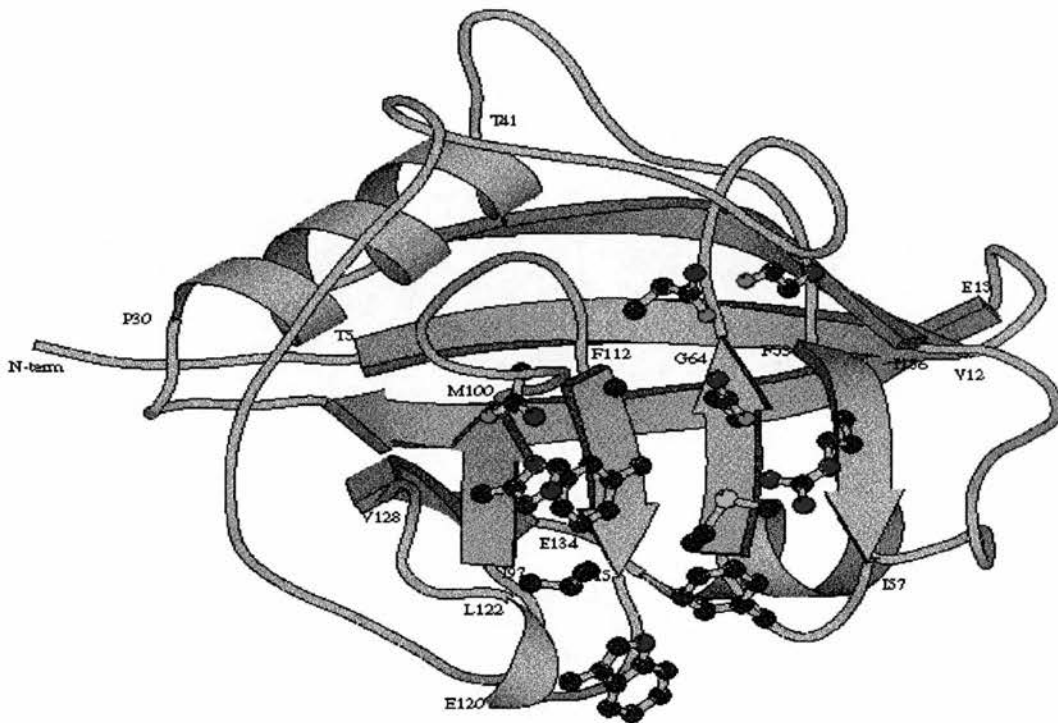


Fig. 1.5: Topology of CypA. Helices, β -stands and loops are shown (Kraulis 1991). Residues which interact with CsA are highlighted.

The topology of cyclophilins is unique and unlikely to be related to retinol-binding protein, superoxide dismutase, steptavidin or trosephosphate isomerases structures which also contain eight-standed β -barrels. The main difference with cyclophilins is that the centre of the barrel is completely filled with hydrophobic residues and the ends of the barrel are blocked off at each end by two stretches of α -helices.

The X-ray structures of hCypA with 11 cyclosporin derivatives show that there are small alterations in the structure of CypA upon binding with cyclosporins (Kallen et al. 1998). A similar result was derived from NMR studies on the hCypA-CsA complex (Theriault et al. 1993). This also applied with different crystal forms where the decameric (Pflugl et al. 1993) and the monomeric forms (Mikol et al. 1993) of CypA-CsA complex, have an rms deviation between the two structures of less than

0.5 Å for the backbone atoms. A number of complexes of cyclophilins with linear peptides have been solved (Taylor et al. 1997). The overall structure of CypA complexed with peptides is similar to those of the unligated CypA.

D) FKPBs

A number of FKPBs have been discovered from different sources (prokaryotes and eukaryotes) with a molecular weight from 12kDa up to 52kDa (Galat and Metcalfe 1995). The pI of the family is acidic for prokaryotic and basic for mammalian cell. Most FKPBs bind both FK506 or rapamycin (Galat et al. 1992). The FK506 binding domain of the family is conserved from FKBP-12 through FKBP-52 and the latter has all the hydrophobic residues which make interaction with FK506 in the FKBP12-FK506 structure (Galat and Metcalfe 1995).

1. FKBP structures

X-ray and NMR structures of hFKBP-12 (van Duyne et al. 1991) and bFKBP-12 (Moore et al. 1991) revealed that the protein fold is a five stranded anti-parallel β -sheet which wraps around an α -helix (Fig. 1.6). Insignificant structural changes occurred in hFKBP-12 upon complex formation with FK506 (Galat and Metcalfe 1995). All prolines of hFKBP-12 are in *trans* conformation. X-ray structures of FKBP complexes with FK506 and the antagonist L-685,818 show essentially identical protein-ligand interactions (Becker et al. 1993).

Fig. 1.6: Topology of FKBP-12. Helices, β -stands and loops are shown (Kraulis 1991).

2. Protein Production

2.1 Introduction

A large amount of protein is required for crystallization trials. The only way to keep up with the high demand of a protein is to overexpress the gene in bacteria. The ability to overexpress genes in bacteria has improved enormously over the past few years. The most commonly used microorganism to overexpress protein is *Escherichia coli*. Two cell lines of *E.coli* were provided by Sandoz for the production of Cyp-A and Cyp-B. Also a gene for FKBP-12 production was kindly provided by Fujisawa Pharmaceutical Co., Ltd, Japan.

2.2 Material & Methods

A) Storage of bacterial lines

A single colony obtained from a LB_{amp} (Luria-Bertani agar plate containing 50µg/ml ampicillin) plate was inoculated into fresh LB_{amp} medium. The culture was incubated at 37°C with constant shaking until the OD₆₀₀ reached 0.4. The cell pellet from this culture was resuspended in sterile 15% (v/v) glycerol. The suspension was flash frozen in liquid nitrogen and kept at -70°C in aliquots of 100 µl.

B) Cyp-A & Cyp-B material and methods

1. Cell lines

The cell lines were *E.coli* strain 101-521 1C for expression of Cyp-A and strain 7264 121 for expression of Cyp-B. Both strains contain an IPTG (isopropyl- β -D-thiogalactopyranoside) promoter and are ampicillin resistant.

2. Expression in *E.coli*

The same growth protocol was followed for *E.coli/101-521 1C* and *E.coli/7264 121* strain.

The protocol was as follows:

Small scale expression in *E.coli*

1. A single colony was isolated from a *E.coli* culture by streaking on an LB_{amp} plate at room temperature. In the streaking technique, a sterilised wire is dipped into a suspension of microorganisms and it is then used to make a series of parallel, nonoverlapping streaks on the surface of solidified agar plate (Stanier et al 1986 page 17)
2. From a single colony, 30 ml LB_{amp} broth (A1 culture) was inoculated at 37°C.
3. When the OD₆₀₀ of A1 culture reached OD₆₀₀~0.3, 1 ml was transferred and used to inoculate 30 ml of LB_{amp} broth (named as B1 culture) and was kept at 37°C for future use. The rest of the A1 culture was induced by adding 0.4 mM of IPTG.
4. After 4 hours, 0.5 ml of the A1 culture was centrifuged and the supernatant was discarded. The cells were suspended in 20 μ l sample buffer (0.06 M Tris-Cl, pH6.8, 2% SDS [Sodium dodecyl sulphate], 10% glycerol, 0.025% Bromophenol Blue). Finally the sample was heated at 95 °C for 4 min. The sample was run in 15

% SDS-PAGE to confirm the expression of the protein.

5. If the results of SDS-PAGE were positive the protocol was carried out using large scale cultures.

Large scale expression in *E.coli*

1. Six litres of LB_{amp} medium was divided equally into six 2 L flasks and inoculated with the 30 ml B1 culture, of small scale expression and grown at 37°C in a shaker incubator.
2. When OD₆₀₀ reached ~0.3 the cultures were induced by adding 0.4 mM of IPTG and were grown for further 4 hours (OD₆₀₀~2.2).
3. The culture was centrifuged and the supernatant was discarded. The cells were kept at -20°C at this stage.

C) FKBP-12 material and methods

1. Plasmid

The plasmid *pFKBP333* is ampicillin resistant and has an *E.coli* TRP (tryptophan) promoter upstream of the gene for FKBP-12. Therefore, FKBP-12 shall be expressed when *E.coli/pFKBP333* is cultivated in M9CA (M9 Minimal Medium contain 1% Casamino acid) broth. 3-β-indoleacrylic acid (IAA) is used to induced expression of recombinant proteins under the control of the tryptophan promoter in plasmid expression systems.

2. Bacterial strain

The bacterial strain *BL21(DE3)* (Sambrook et al 1989 Book3) was used for the transformation. This particular *E.coli* strain has a very fast growth rates and is employed for high-level expression.

3. Bacterial transformation

A modified calcium transformation method was used adapted from Sambrook et al 1989 (Book 1).

At an OD_{600} of 0.28 the number of viable cells is 10^8 cells/ml for this strain. For efficient transformation that number should not exceed 10^8 cells/ml (Sambrook et al 1989 Book 1). All materials used were sterile.

The protocol was as follows:

1. Pick single colony, inoculate 10 ml of M9CA, incubate overnight at 37°C in a shaking incubator.
2. Inoculate 100 ml M9CA with 0.5 ml of the overnight culture in a 250 ml flask and grow for ~2 hours at 37°C in the shaker until OD_{600} is approximately 0.25.
3. Divide into 2x50 ml Falcon tubes and cool on ice for 10 min.
4. Centrifuge at 2500 g for 5 min at 4°C. Discard the supernatant
5. Resuspend in 50 ml 100 mM $CaCl_2$ and leave on ice for 30 min to 4 hours.
6. Spin as above and resuspend in 5 ml $CaCl_2$.
7. A chilled pipette is used to transfer 90 μ l of suspension of competent cells to a microfuge tube. Add 10 μ l of DNA (no more than 50 ng in a volume of 10 μ l).

Mix the contents by swirling gently and leave on ice from 30 min to 1 hour.

8. Heat shock at 42°C water bath for 2 min.
9. Add 1 ml M9CA and culture for 30 min at 37°C without shaking.
10. Prepare plate of media containing ampicillin 50 µg/ml and transfer the appropriate volume (up to 200 µl per 90-mm plate) of transformed competent cells. Gently spread the transformed cells over the surface of the agar plate.

4. FKBP-12 expression in *E.coli*

The transformed bacteria grew in M9CA_{amp} (M9 Minimal Medium contain 1% Casamino acid and 50 µg/ml ampicillin).

Protocol

- A single colony of *E.coli/BL21(DE3)/pFKBP333* was cultivated in 10 ml M9CA_{amp} broth at 37°C until OD₆₀₀ is approximately 0.6.
- 1 ml of the culture with OD₆₀₀~0.6 inoculates 100 ml M9CA_{amp} broth at 37°C.
- When the OD₆₀₀ of 100 ml culture reached 0.3, induce by adding 1 ml of IAA 2.5 mg/ml in 95% ethanol.
- After 4 hours 0.5 ml of the 100 ml culture was centrifuged and the supernatant was discarded. The cells were suspended in 100 µl sample buffer (0.06 M Tris-Cl, pH6.8, 2% SDS [Sodium dodecyl sulphate], 10% glycerol, 0,025% Bromophenol Blue). Finally the sample was heated at 95 °C for 4 min.
- The sample was run in SDS-PAGE (Sodium dodecyl sulfate-polyacrylamide gel electrophoresis).

2.3 Results

A) Expression of Cyp-A & Cyp-B

SDS-PAGE gels of cell extracts from both bacterial strains indicated that expression of Cyp-A and Cyp-B was successful for both proteins (Fig.2.1 and 2.2).

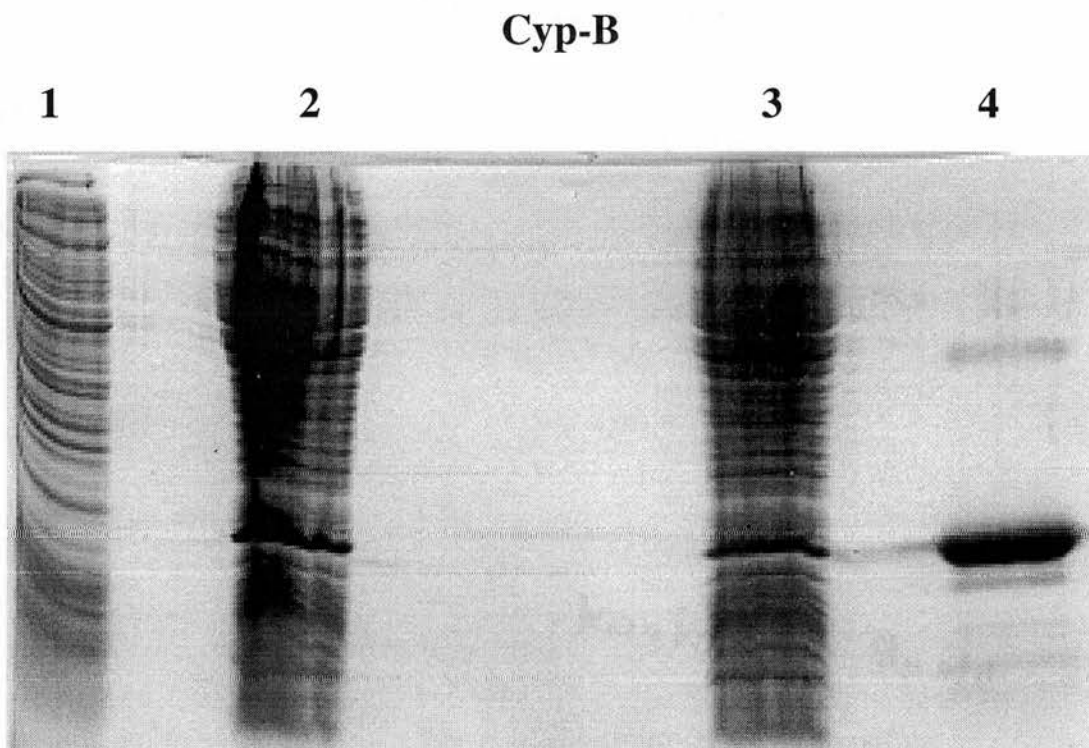


Fig.2.1: SDS-PAGE (15 %) of *E.coli*/7264 121(Cyp-B) induced with IPTG (400 μ M). Lane 1: uninduced pellets. Lanes 2 & 3: induced pellets. Lane 4: Cyp-B standard. A strong band of molecular weight identical to the Cyp-B (Lane 4) in lanes 2 and 3 indicated that expression of Cyp-B was successful.

The effect of IPTG concentration and induction time on the expression of Cyp-A was investigated.

Cultures of *E.coli*/101-521 1C in LB_{amp} induced at different growth times and IPTG

concentration. Results of that experiment can be seen in SDS-PAGE (Fig.2.2). The variation of the time and IPTG concentration can be seen in Table 2.1.

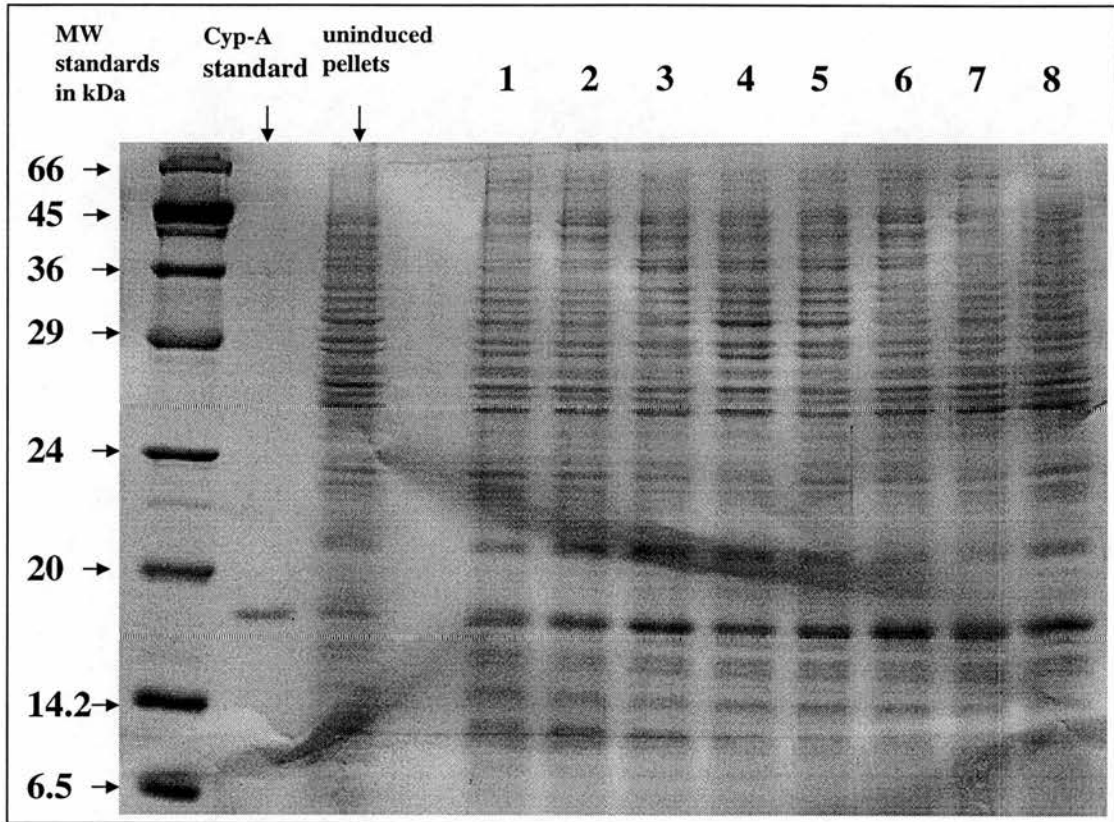


Fig. 2.2: SDS_PAGE (15 %) of *E.coli/101-521 IC* pellets induced with different IPTG concentration at different growth phase (determine by OD₆₀₀). The concentration of IPTG was used in each experiment given in Table 2.1.

Table 2.1: IPTG concentration tested for determination of optimum expression in *E.coli/101-521 IC*. The numbers in mM present IPTG concentration. The numbers in the first row corresponds to the numbers of wells in Figure 2.1.

Growth phase (OD ₆₀₀)	1	2	3	4	5	6	7
0.2						0.6 mM	0.2 mM
0.45	1.2 mM	0.6 mM	0.2 mM				
0.8				0.6 mM	0.2 mM		

The large scale production gave around 6.7 g (wet weight) pellets per litre of culture.

B) FKBP-12

1. Bacterial transformation

E.coli/ BL21(DE3)/pFKBP333 cells after transformation were plated on an ampicillin 50 µg/ml plate. Many colonies grew which is an indication that the transformation actually took place since the bacteria were not ampicillin resistant previously.

2. FKBP-12 expression in *E.coli*

E.coli/BL21(DE3)/pFKBP333 grew under expression conditions for FKBP-12. Cell extract and culture medium were tested for FKBP-12 in SDS-PAGE (12%).

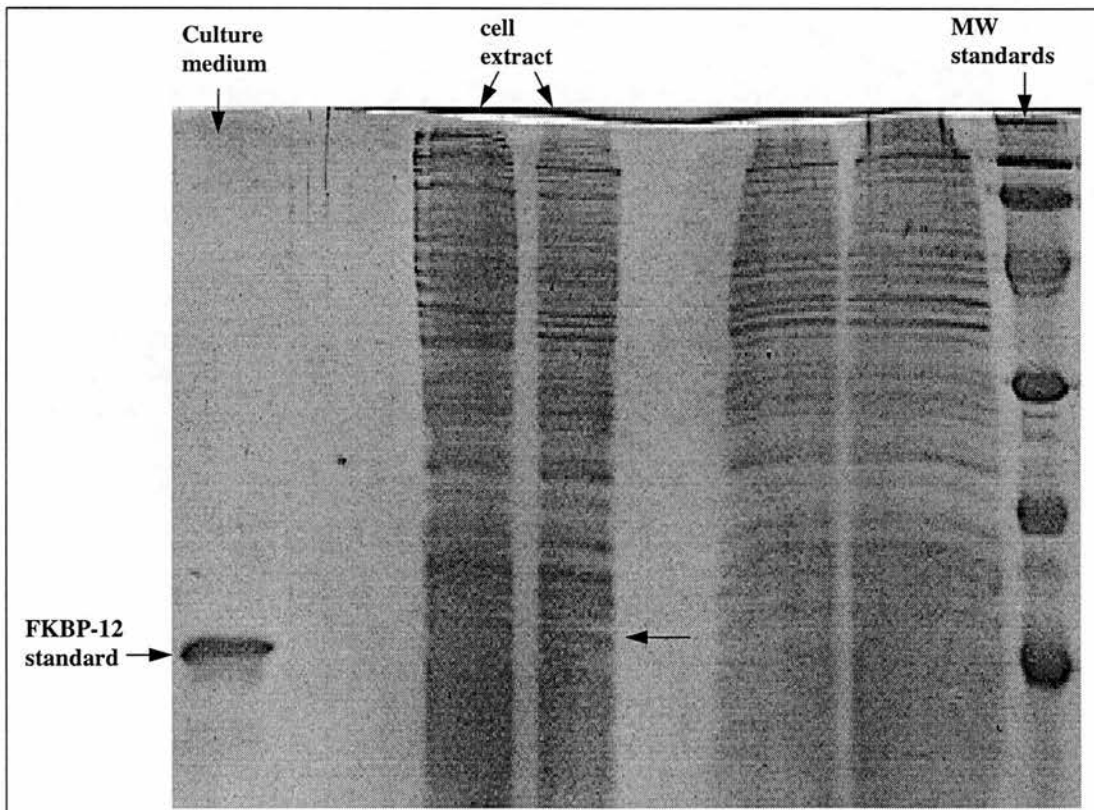


Fig.2.3: SDS-PAGE (12%) of *E.coli/BL21(DE3)/pFKBP333* cell extract sample and culture medium. Lane 1: FKBP-12 standard. Lane 2: Culture medium. Lane 3 and 4: Cell extract. Lane 5: Molecular weight standards.

2.4 Discussion

The transformation of *E.coli/BL21(DE3)/pFKBP333* was achieved since the bacteria became ampicillin resistant. Nevertheless the expression system for FKBP-12 was not so efficient and the band corresponding to FKBP-12 was not clearly seen in the gel. Due to low yield the system was not used for production of the protein. No more work was carried out with this expression system and no other promoters were used in order to increase the production of the protein.

Both expression systems for Cyp-A and Cyp-B seemed to work well. Results of expression of both *E.coli* strains are presented in the Fig.2.1 (Cyp-B) and Fig 2.2 (Cyp-A). Sample pellets of *E.coli/101-521 1C* run in SDS-PAGE (Fig. 2.2) indicates that better expression occurred when the induction takes place at OD₆₀₀ between 0.2 to 0.45 and with an IPTG concentration of 0.2 to 0.6 mM. The uninduced pellets of *E.coli/101-521 1C* in Fig. 2.2 contain a protein of similar MW to Cyp-A. That protein could be indeed Cyp-A. This could be caused by basal transcription level or traces of lactose in the media, lactose has the same effect as the IPTG.

3. Protein Purification

3.1 Introduction

The degree of purity of the protein plays an important role in enzymatic and fluorescence studies and especially in crystallogenes. Only when an enzyme has been purified can the assay be regarded as reliable. The same principle applies to fluorescence studies. The concept of purity can be applied to protein conformation and only one conformer of that protein is acceptable. Denatured protein has the same molecular weight but is inactive and the difference in the shape may prevent crystallization of the native form (Lorber and Giegé 1990). The main goal of purification is to purify the protein in a single form and to maintain the initial features and shape.

Three proteins have been purified in the current work Cyp-A, Cyp-B and BrCyp. The amino acid sequence of each protein is shown in appendix 1. Cyp-A and Cyp-B are both produced intracellularly so cell lysis was required. The BrCyp was supplied as an MBP fusion protein. The reason of using fusion protein with MBP is that can be purified on amylose resin as a single product.

3.2 Purification strategy

The proteins in cells are compartmentalised and therefore separated from other proteins with proteolytic activity. Cells lysis results in disruption of these barriers with the exposure of proteins to proteases and to a different environment in the cells. The potential for degradation then is inevitable during the course of the purification. For the above reasons the purification of all proteins in this work was carried out at 4°C and as quickly as possible. Additionally benzamidine and EDTA were added as protease inhibitors (Deutscher 1990) and β-mercaptoethanol was added to prevent

oxidation of the protein (see materials and methods section).

Many techniques have been developed to purify proteins including ion-exchange chromatography, gel filtration and hydrophobic interaction chromatography (Rossomando 1990 and Stellwagen 1990). Previous work on Cyp-A (Handschumacher et al 1984 and Holzman et al 1990), Cyp-B (Spik et al 1991) and BrCyp (Page *et al* 1995) showed that a combination of ion-exchange chromatography and (or) gel filtration was sufficient for purification for all of them. Therefore the same purification techniques were employed during the course of this work. Nevertheless modifications of the existing methods were required since the sources which the proteins come from and cell lysis were different. Handschumacher et al purified human cyclophilin A from human spleen. Holzman et al (1990) and Liu et al (1990) expressed and purified human cyclophilin A from different *Escherichia coli* strains (and with a different cell lysis procedure). Spik et al (1991) expressed and purified human cyclophilin B from a different *Escherichia coli* strain and with a different cell lysis procedure.

Ion-exchange chromatography separates molecules based on differences in their surface charges. Attraction takes place between molecules of opposite electric charge. The stationary phase of an ion exchange packing consists of functional groups which they have either a positive charge (anion exchanger), used to separate negatively charged molecules (anions), or a negative charge (cation exchanger), used to separate positively charged molecules (cations) (Rossomando, E. 1990).

Gel filtration (also known as size exclusion chromatography) separates molecules based on differences in their size. The stationary phase consists of particles with a distribution of pore sizes. If molecules are small enough, the pores are so large that the molecules can penetrate all of the internal volume of the particles. The large molecules on the other hand are excluded from the internal volume and therefore emerge first from the column while the small molecules emerge later. The

dimensions important to gel filtration are the diameter of the pores that access the internal volume and the hydrodynamic diameter of the molecules (Stellwagen 1990).

A) Cyp-A

All purification steps, including cell lysis took place at 4°C since previous purification work on Cyp-A was done at this temperature (Liu et al 1990) and for reasons described above.

The pH was adjusted to 7.5 during cell lysis for optimum activity of lysozyme. The pH of cell extract was then adjusted from 7.5 to 6.8. Since cation exchange chromatography was employed for purification, the protein should be positively charged in order to bind to the stationary phase. Two isoelectric forms of cloned human cyclophilin A have been reported, alkaline (pI > 9.0) (Liu et al 1990) and neutral (pI > 7.4) (Holzman et al 1990). Both of these isoelectric forms of Cyp-A are reported to have the same cDNA sequence. A possible explanation given from Holzman et al (1990) is that the proteins were cloned from different cell types and therefore may represent different gene products with different sequence. Obviously one of the above reported values for pI should be wrong. The pI value of the protein is very important for the design of purification procedure, and since it was not clear which pI value is the right one a pH of 6.8 was used for loading the protein into the columns. When pH is 6.8 a protein which has pI values above 6.8 (both reported values in literature are above 6.8) should be positively charged and should bind to a cation exchanger column. A pH of 6.8 was therefore used for loading the protein into the columns in order to be sure that the protein will be positively charged.

B) Cyp-B

All purification steps including the lysis of the cell took place at 4°C. Cyp-B has been cloned in *E.coli* and was purified from the same source (Spik et al 1991, Price et al 1991) by cation exchange chromatography. Spik et al (1990) used a pH 6.0 to load the protein to the column. The experimental pI had not been determined for cyclophilin B cloned in *E.coli*/7264 121. The theoretical pI can be calculated based on amino acid sequence. The theoretical value was calculated using programs available on Web pages (<http://www.embl-heidelberg.de>) of EMBL (European Molecular Biology Laboratory). The program determined the pI using literature values (Lehninger et al 1993). The calculated value of the isoelectric point for Cyp-B was 9.76. A pH of 6.8 was therefore used for loading the protein into the columns in order to be sure that the protein will be positively charged.

C) BrCyp

BrCyp original was isolated and cloned from the nematode parasite *Brugia malayi* by Page et al (1995). The protein was supplied as BrCyp fusion protein with maltose-binding protein by Dr Page (Wellcome Unit of Molecular Parasitology, Glasgow University, Glasgow). The cleavage and the purification of the cleavage products was carried out in house. The rest of the purification was carried out as described in Page *et al* (1995).

3.3 Material & Methods

The following material and equipment used in the current work was obtained from Pharmacia Biotech.

A) Columns and Equipment

- FPLC and GradiFrac system

The following columns were used for purification.

- SP Sepharose; a cation exchanger (40 ml) column
- SOURCE 15S; a strong cation exchanger (8 ml) column
- 30 Q; a strong anion exchanger (10 ml) column
- Sephacryl S-200 HR; a gel filtration (120ml) column

B) Purification procedures in Cyp-A

1. Cell lysis

Pellets were produced and frozen as previously described (see Protein production chapter). Pellets were resuspended at 10 % (w/v) in 50 mM Hepes pH 7.5 , 5 mM benzamidine, 5 mM β -mercaptoethanol, and 5 mM EDTA (ethylenediaminetetracetic acid). Digestion of the cell walls followed addition of lysozyme to 0.1 % (w/v) in the above solution and incubation for 1 hour. The suspension was mixed from time to time.

The cell extract was centrifuged in a BECKMAN Avanti J-25 centrifuge at 16000 x g for 30 min. The supernatant pH was adjusted to 6.8 with 1 M Hepes pH 6.6. The pH was monitored by narrow-range pH sticks. Supernatant was filtered first through

glass filter (glass prefilters cellulose acetate BDH) and then through 0.45 μm (PVDF syringe filters 25 mm BDH) to remove large particulates which may block the SP Sepharose column in next step.

2. Purification of Cyp-A

SP Sepharose, a cation exchanger from Pharmacia Biotech, was used for the first purification step. 40 ml SP Sepharose was equilibrated in 50 mM Hepes pH 6.8, 5 mM β -mercaptoethanol, and 5 mM EDTA (buffer **A**) for one hour.

The supernatant at this stage contained large amounts of protein which could block a column. Protein extract was therefore bound in batch mode to resin pre-equilibrated in buffer **A**. The resin/extract slurry was incubated for one hour with mixing from time to time. The slurry was packed into an XK26/20 column.(Pharmacia). The column was washed to base-line with buffer **A** and eluted with the same buffer containing 0.5 M NaCl (buffer **B**). The eluted material was then concentrated by ultrafiltration to 3 ml (Amicon YM 10 membranes) and dialysed (cellulose ester membrane MWCO 3.5 PIERCE) against 4 litres of buffer **A** by stirring overnight.

The next purification step was a strong cation exchanger column. The 3 ml sample from above was loaded on an 8 ml mono-S column (SOURCE 15S Pharmacia Biotech) with buffer **A**, washed to base-line with the same buffer and eluted with buffer **B**. Elution of Cyp-A was carried out with about 250 mM of NaCl. The eluted material was then concentrated by ultrafiltration to 3 ml (Amicon YM 10 membranes).

The final purification step made use of size exclusion chromatography with a Sephacryl S-200 HR column (120ml). The column was washed to base-line with buffer **A**. The sample applied to the column was not more than 3 ml. The applied volume to the column should be as small as possible (in order to reduce

bandspreading) for better separation. Buffer A was used for elution with flow rate of 0.5 ml/min. Size exclusion chromatography also ensured that the eluted protein contained no salt.

C) Purification procedures in Cyp-B

1. Cell lysis

The method was the same as for Cyp-A plus one additional filtration with 0.2 µm (PVDF syringe filters 25 mm BDH) before the sample was introduced into the Mono-S column.

2. Purification of Cyp-B

Filtered material was loaded onto a Mono-S cation exchanger column (SOURCE 15S Pharmacia Biotech) equilibrated with buffer A (*as above*) and eluted with a linear gradient of 1 M NaCl in buffer A. The next purification step was size exclusion chromatography with Sephacryl S-200 HR column (120ml).

D) Purification of BrCyp

The starting material was recombinant cyclophilin MBP fusion protein and provided by Dr Page (Wellcome Unit of Molecular Parasitology, Glasgow University, Glasgow) in Tris 20 mM pH 7.4 and glycerol 40 %. The supplied material was dialyzed against 200 volumes of Tris 20 mM pH 8.0.

The cleavage and purification procedure was adapted from Page *et al* 1995. After a couple of trials it was found that the best cleavage was obtained in 20 mM Tris pH 8.0, 100 mM CaCl₂ and 150 mM NaCl. Cleavage took place for 12 hours at room

temperature in a solution of 0.7 mg/ml fusion protein, 10 µg/ml factor-Xa, 20 mM Tris pH 8.0 100 mM CaCl₂ and 150 mM NaCl. The first step was the cleavage of fusion protein by factor-Xa purified in our laboratory by Dr Husi.

The cleaved material was dialyzed (Amicon YM 10 membranes cellulose ester membrane MWCO 3.5 PIERCE) against 200 volumes of Tris 20 mM pH 6.9. The dialyzed material was loaded onto a Mono-Q anion exchanger column (10 ml 30 Q Pharmacia Biotech) equilibrated with buffer Tris 20 mM pH 6.9 and eluted with a linear gradient of 1 M NaCl in the previous buffer. Finally the flow-through (BrCyp was not bound) was concentrated using a 10 kDa cut off membrane (Amicon YM 10 membranes).

3.4 Results

1. Cyp-A

After cell lysis most of the Cyp-A was released into the supernatant Fig. 3.1. This material was then loaded on to the Sepharose column. Eluted fractions of Sepharose column can be seen in Fig. 3.2. Fraction 6 contains a large amount of Cyp-A but it was contaminated with lysozyme (strong band at 14 kDa). Fraction 7 was considered as more “pure” and after dialysis was loaded on the mono-S column.

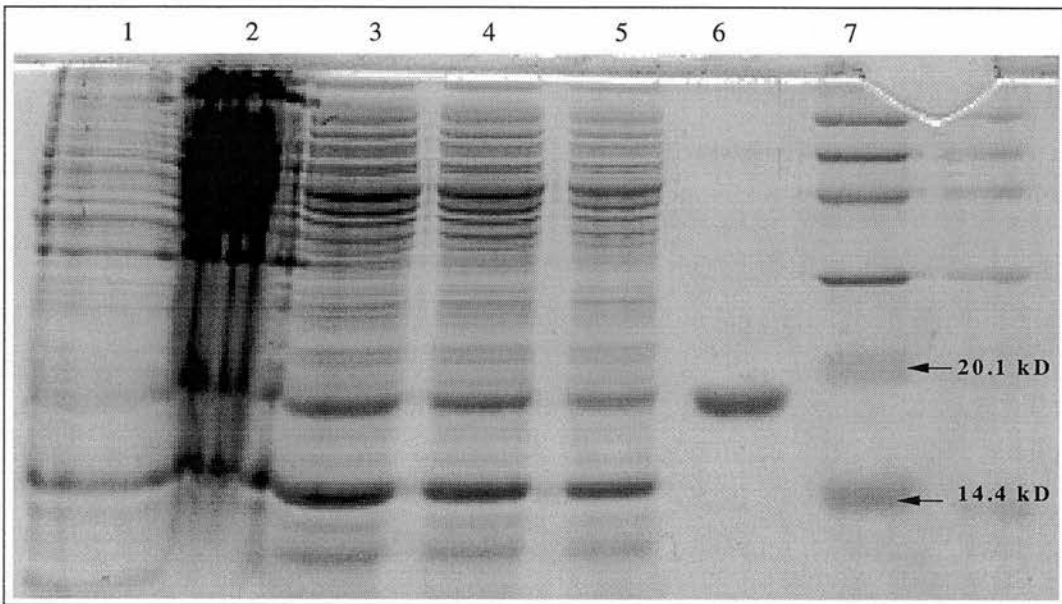


Fig. 3.1: SDS-PAGE (15 %). Cell extract and supernatant of *E.coli/101-521 IC*. Lane 1: *E.coli* pellets. Lane 3 to 5: Supernatant. Lane 6: Cyp-A standard. Lane 7 MW standards

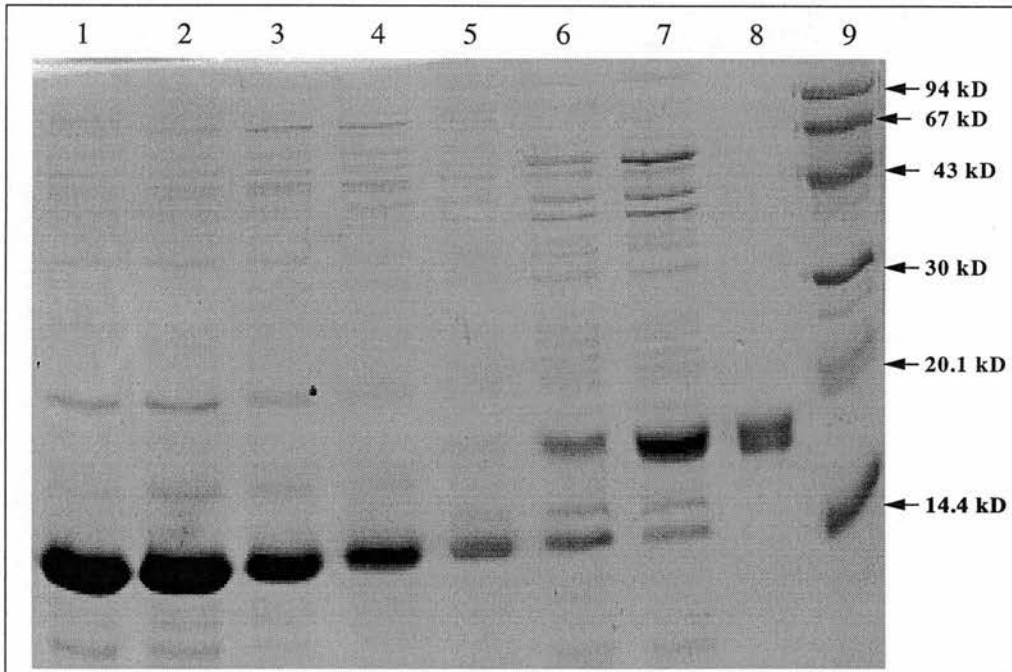


Fig. 3.2: SDS-PAGE (15 %). Eluted fractions from Sepharose column. Lane 7: Fraction containing Cyp-A which was used for further purification. Lane 8: Cyp-A standard. Lane 9: MW standards.

The degree of purity of eluted samples from the mono-S column was high Fig. 3.3. Fractions 4 and 5 in Figure 3.3 were contaminated with high MW proteins (65 to 94 kDa) which can be easily separated using gel filtration so these two fractions were loaded together in the size exclusion column. Fractions 6, 7 and 8 (Figure 3.3) were contaminated with high MW proteins (65 to 94 kDa) and low MW proteins (25 to 30 kDa) which would be difficult to separate since there almost the same size as Cyp-A. These fractions were collected, concentrated and loaded onto a size exclusion column as another batch.

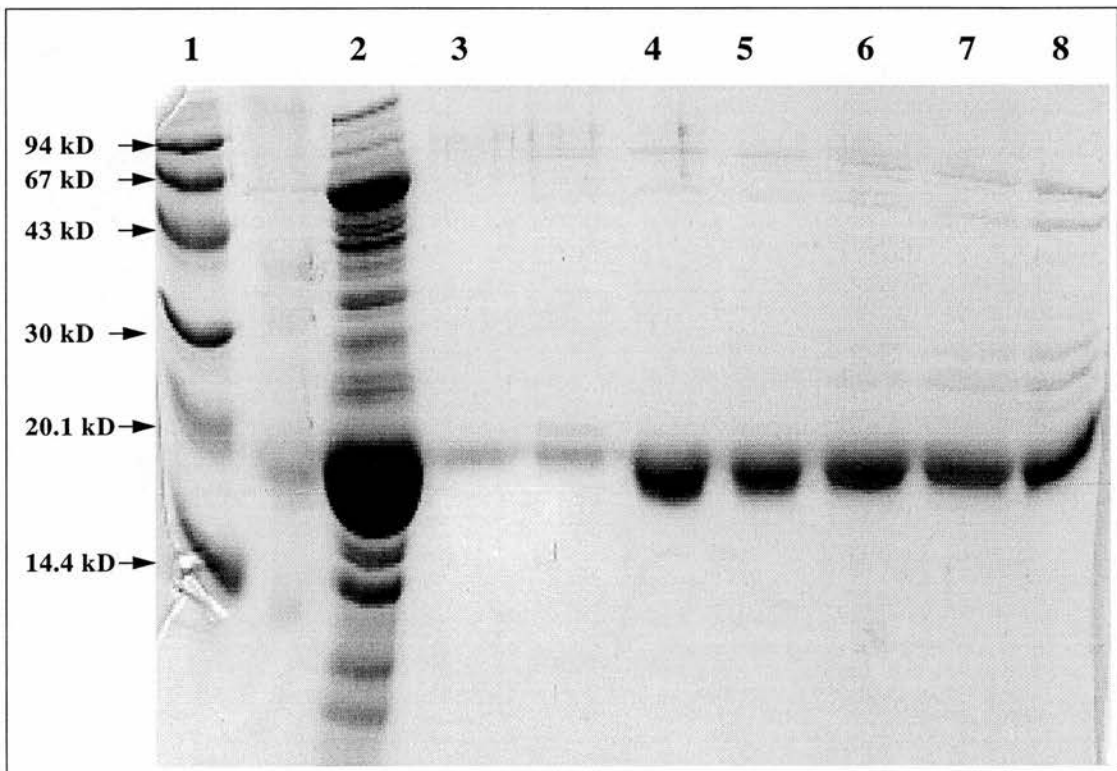


Fig. 3.3: SDS-PAGE (15 %). Eluted fractions from mono-S column. Lane 1: MW standards. Lane 2: Loaded material in mono-S column. Lane 3: Cyp-A standard.

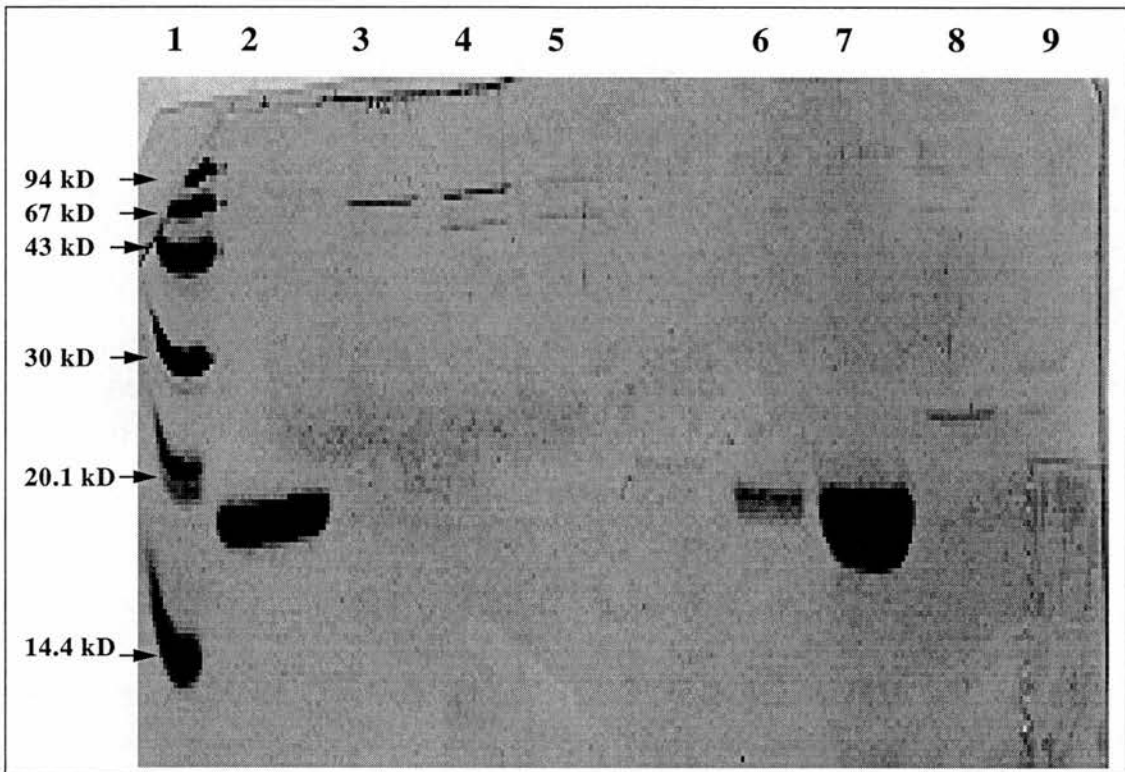


Fig. 3.4: SDS-PAGE (15 %). Eluted fractions from size exclusion column.

Lane 1: MW standards. Lane 2: Cyp-A standard. Lane 3, 4 and 5: Fractions contained high MW proteins. Lane 6 and 7: Fractions contained pure Cyp-A. Lane 8 and 9: Fractions contained low MW proteins.

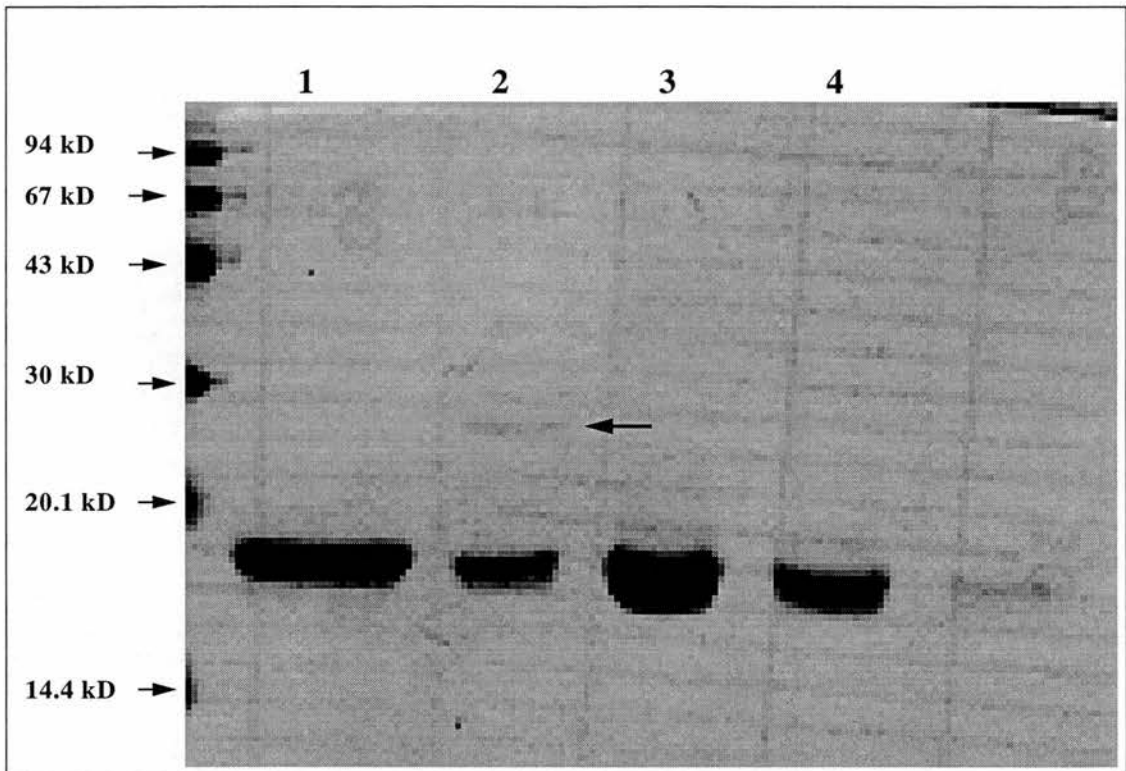


Fig. 3.5: SDS-PAGE (15 %). Eluted fractions from size exclusion column.

Lane 1: MW standards. Lane 2: Cyp-A standard. Lane 2: Fractions contained Cyp-A contaminated with low MW protein (25 kDa indicated with the arrow). Lane 2 and 4: Fractions contained pure Cyp-A.

The size exclusion column completely separated the Cyp-A (Fig.3.4 lane 6 and 7) from the high molecular weight proteins (Fig.3.3 lane 3, 4 and 5). The low MW proteins were also separated from Cyp-A using the same size exclusion column. Fractions containing these proteins can be seen in Fig. 3.4 (lane 8 and 9). Fractions eluted from the column in the following order: lane 8 (Fig. 3.4), lane 9 (Fig. 3.4), lane 2 (Fig. 3.5), lane 3 (Fig. 3.5), lane 4 (Fig. 3.5). Fraction 2 (Fig. 3.4) contained a lot of Cyp-A and a trace of 25 kDa protein and were not used further. The next pool (lane 3 and 4 Fig. 3.4) contained pure Cyp-A and they were used further. The high MW proteins were completely separated from Cyp-A as can be seen in Fig.3.5 lane 3,4 and 5. In a typical experiment the yield of Cyp-A was 1.6 mg purified Cyp-A for 1 l of culture broth.

2. Cyp-B

The first purification step used a mono-S column. An SDS-PAGE gel showing the purity of the eluted material from this column is given in Fig. 3.6. Only fraction no 1 was used for further purification. Fraction no 2 contained a lot of Cyp-B but was contaminated with a protein of similar MW (~20 kDa).

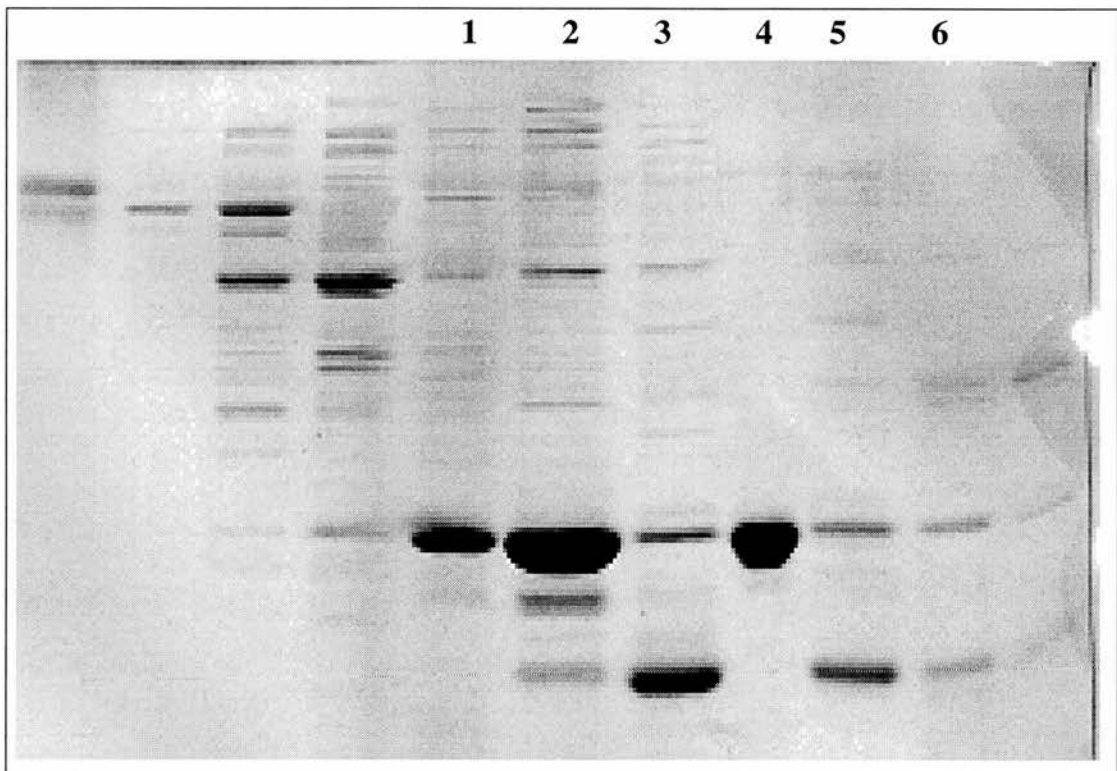


Fig. 3.6: SDS-PAGE (15 %) of eluted fractions containing Cyp-B from mono-S column: Lane 1: Fraction containing Cyp-B used for further purification (size exclusion). Lane 3, 5 and 6: Fractions containing Cyp-B. Lane 4: Cyp-B standard.

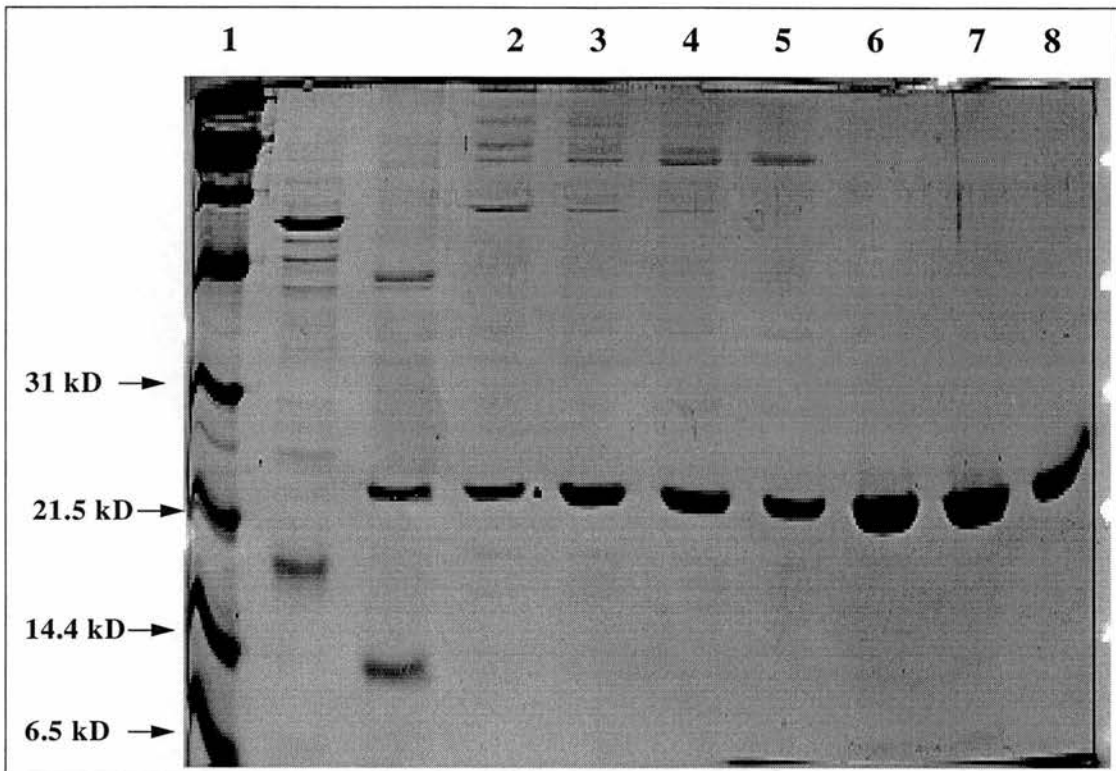


Fig. 3.7: SDS-PAGE (15 %) eluted fractions from size exclusion column: Lane 1: MW standards. Lane 2 to 5: Fractions containing Cyp-B. Lane 6 and 7: Pure Cyp-B fractions. Lane 8: Cyp-B standard.

The next purification step was size exclusion chromatography using a Sephacryl S-200 HR column. The eluted fraction can be seen in Fig. 3.7. Fractions 2 to 5 in Fig.3.7 contained Cyp-B but were contaminated with high MW proteins (66 to 100 MW) and discarded. Fraction 6 and 7 contained pure Cyp-B and those were used for further studies. In a typical experiment the yield of Cyp-B was 2 mg/l. purified Cyp-B for 1 l of culture broth.

3. BrCyp

The supplied material was dialyzed against 200 volumes of Tris 20 mM pH 8.0. The results of 12 hours cleavage is presented Fig.3.8. Initial material (fusion protein 65 kDa lane 1) has been broken down in lane 2 to 3 band (MW 43 kDa, 22 kDa and 17kDa).

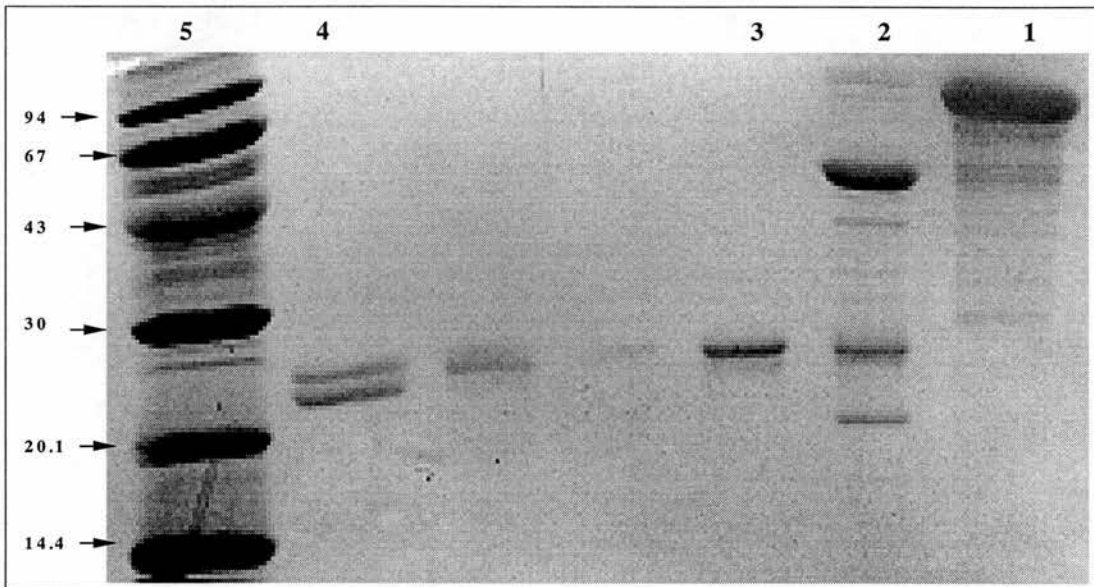


Fig. 3.8: SDS-PAGE (15 %) of eluted fractions from mono-Q column. Lane 1: Fusion protein. Lane 2: Cleaved fusion protein. The high molecular weight band (~65 kDa) was MBP protein, band in 22 kDa was recombined BrCyp. Lane 3: BrCyp after ultrafiltration step. Lane 4: BrCyp standard. Lane 5: Molecular weight standards.

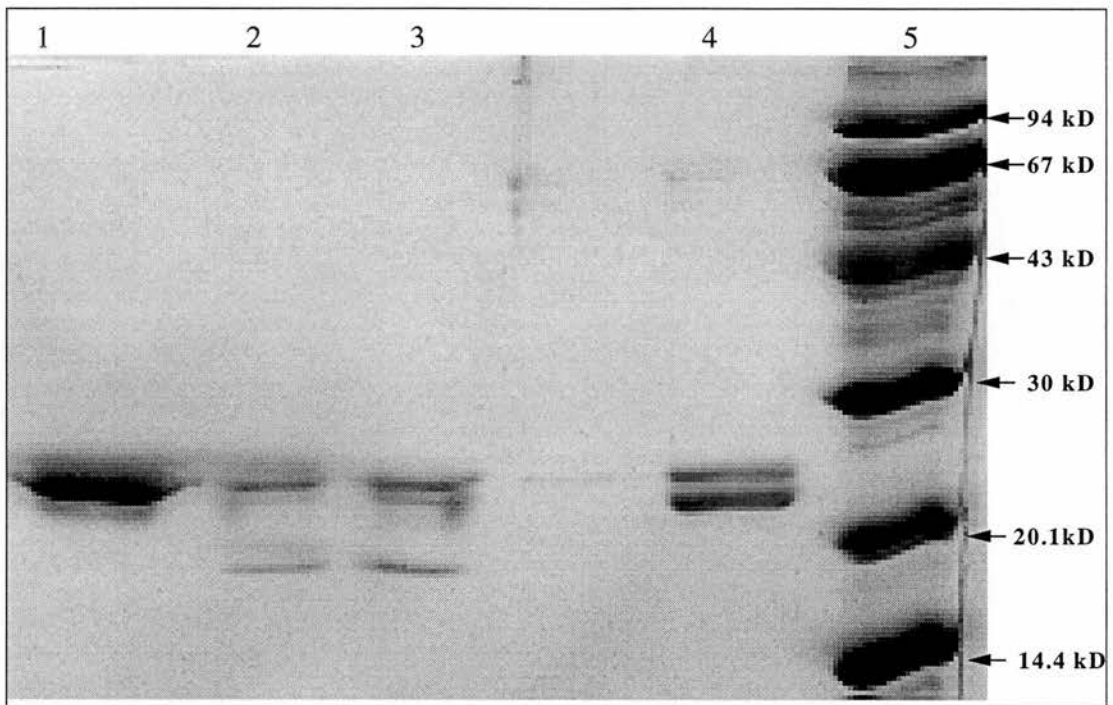


Fig. 3.9: SDS-PAGE (15 %) of past through of mono-Q column. Lane 1: Pure BrCyp after ultrafiltration. Lane 2 and 3: Passed through fractions of mono-Q. Lane 4: BrCyp standard. Lane 5: MW standards.

The cleaved material was loaded onto a mono-Q column. Cyclophilin and the 17kDa protein were passed through (Fig. 3.9 lane 2 and 3) and MBP bound. The final separation of BrCyp from the 17kDa fragment (Fig. 3.9 lane 2 and 3) was achieved by ultrafiltration. An Amicon YM 10 membrane was used (10 kDa cut-off).

3.5 Discussion

1. Cyp-A

Cyp-A required three purification steps from cell extract to pure protein. In the initial attempt only two purification steps were used. A mono-S column and a size exclusion column were not enough to give pure Cyp-A. An additional cation-exchange chromatography (SP sepharose column) step was introduced at the beginning of the procedure.

In Fig.3.1 it can be seen that most of the Cyp-A was released into the supernatant but some can be detected in cell extract. More protein could be released into the supernatant if its volume was increased. It was, however, difficult to handle such a large volume of cell extract.

In the first purification step a significant amount of Cyp-A did not bind to the Sepharose column. This was caused by high protein concentration in the eluted material or from intracellular salt from pellets. The intracellular salts concentration (potassium, sodium, calcium and magnesium) in *E.coli* could be up to 3 % of dry weight of the pellets (Stanier et al 1986 page 22). This amount of intracellular salt, taking account of the weight of the pellets and the volume of lysis buffer in which they were diluted, resulted in a concentration of 30 mM salt. More protein possibly could be recovered if the first purification step was repeated but this should be done as soon as possible since the cell extracted material was degraded fast. Cell extracted material after 3 days at 4°C was unusable. The yield of the pure Cyp-A was enough to carry out crystallization and enzymatic experiments.

2. Cyp-B

Cyp-B required two purification steps from cell extract to pure protein. In the first purification steps after elution there were four fractions that contained Cyp-B (Fig.3.6 1, 2, 3 and 5). Only fraction no 1 was used for further purification. Fraction no 2 contained a lot of Cyp-B but was contaminated with a protein of similar MW (~20 kDa) which could not be separated by size exclusion. Fractions 2,3 and 5 were contaminated with lysozyme. One way to over come this problem and increase the yield is the use of mechanical lysis (Cull and McHenry 1990). The yield was higher than Cyp-A probably because less purification steps were required and the higher MW.

3. BrCyp

In Fig.3.8 lane 2 it can be seen that the cleavage was working efficiently. The yield of pure BrCyp was only 15.8 % from that contained in the fusion protein. The factorXa was probably contaminated with another protease which resulted in further cleavage of BrCyp to a 17kDa protein (Fig. 3.8 lane 2 and Fig. 3.9 lane 2 and 3).

Globular solutes with MW of 10 kDa are retained at least 90 % by the YM 10 membrane. Separation of BrCyp and the 17kDa fragment (see Fig. 3.9) caused either because 17kDa fragment pass through the membrane, nevertheless that it much heavier than 10 kDa, or because it had a specific affinity and binds to the membrane material.

4 Protein Characterisation

4.1. Introduction

Before starting crystallization or enzymatic studies of a protein, the degree of purity, the concentration and the activity must be accurately determined. The purity of the protein can be estimated by polyacrylimide gel electrophoresis, which has been described (chapter 2.4).

Protein concentration can be assayed by variety of methods including ultraviolet absorption measurement, the Biuret method, the Lowry method and protein-dye binding using Coomassie Brilliant Blue G-250 method or BCA (bicinchoninic acid) method (Burkhard 1983). The determination of protein concentration is important to provide an accurate reference point for other measurements such a K_d (dissociation constant) or enzymatic activity.

The protein can be further characterised by determination of size, molecular weight, enzymatic activity and binding studies. In the current study the assay of peptidyl prolyl *cis-trans* isomerisation (PPIase) was used to test the enzymic activity of proteins purified 'in house' (Cyp-A, Cyp-B and CypBr) and to test ligand binding by Cyp-A. Fluorescence spectroscopy was used for characterisation of proteins with published ligands and for binding studies with novel ligands to the proteins FKBP and cyclophilin A.

The dissociation constant (K_d) for ligands can be obtained by fluorescence measurements. The enzymatic assay (PPIase) can also be used to calculate the concentration of the ligand resulting in 50 % inhibition (IC_{50}) which should related to the K_d for that ligand.

4.2 Material & Methods

A) Protein determination

The methods used in the current work were the BCA method (similar to the Lowry method) and the Coomassie Brilliant Blue G-250 method.

Both of the methods used in current work require standardisation. Ideally, the assay should be calibrated with the protein whose concentration is to be measured or with another protein which closely matches the behaviour of the test protein. Since this was impractical because of the price of pure CypA and FKBP-12 or similar to them proteins and because CypBr is not commercial available, bovine serum albumin (BSA) was used as the standard.

1. BCA method

The method is based on the reaction of Cu^{2+} ions in alkaline solution with the protein and the production of Cu^+ ions, which chelates two bicinchonic acids and forms a complex which absorbs at 562 nm.

The working range of the BCA Protein Assay Reagent is 10 $\mu\text{g}/\text{ml}$ to 2mg/ml.

The protocol used comes from Wiechelmann et al (1988) slightly modified.

1. Six standards of BSA (Pierce BSA 2 mg/ml) with concentration 20, 40, 60, 80, 100, and 120 $\mu\text{g}/\text{ml}$ were made from 2 mg/ml BSA (PIERCE) by dilution in NaN_3 0.02 % w/v.
2. 1 part of reagent B and 50 parts of reagent A both obtained from Pierce mixed together to form the solution C.
3. 50 μl of each of the above standards was added in a microfuge tube to 1 ml of the solution C, mixed and incubated for 30 min at 37°C.
4. The absorbance was read at 562 nm against the blank sample containing 50 μl of NaN_3 0.02 % w/v and 1ml of the solution C.

The sample consisted of 50 μ l protein in NaN_3 0.02 % w/v and was treated in the same way as the standards.

Results of the method and figure can be found in appendix 2.

2. Bradford or Coomassie Blue Method

The principle of the method is that a dye (in this case Coomassie Brilliant Blue G-250 from Pierce) binds to the protein. A shift of the absorption maximum of the dye from 465 to 595 nm occurs upon binding of the dye to protein in an acidic medium (Bradford 1976). The increase in absorption at 595 nm was monitored.

The Coomassie G (Coomassie Brilliant Blue G-250) seems to be bound to proteins by electrostatic attraction enhanced by hydrophobic bonding (Tal et al 1980). The molecules of Coomassie G interact differently with different proteins dependent upon that amino acid composition (Tal et al 1980). The protocol used was taken from Burkhard (1983) with a modification of the volumes used:

1. Seven standards of BSA (Pierce BSA 2mg/ml) with concentration 10, 20, 40, 60, 80, 100 and 120 μ g/ml were made from 2mg/ml BSA (Pierce) dilution in NaN_3 0.02 % w/v.
2. 20 μ l of each of the above standards were mixed in a microfuge tube with 1ml of the dye reagent solution (Pierce Coomassie Protein Assay Reagent) and incubated for 5 min at room temperature.
3. The absorbance was read at 595 nm against the blank sample containing 20 μ l of NaN_3 0.02 % w/v and 1 ml of the dye reagent solution.

The sample consisted of 20 μ l protein in NaN_3 0.02 % w/v and was treated in the same way as the standards.

Results of the method and figure can be found in appendix 2.

3. Extinction Coefficient ($A^{1\text{mg/ml}}_{1\text{cm}}$)

Most proteins absorb ultraviolet-light with an absorption maximal around 275-280 due to their tyrosine, tryptophan and phenylalanine content. If a pure protein is studied, the absorbance at 280 nm can be used for quantitation. The relationship between protein concentration and absorbance is linear (Stoscheck 1990).

The BCA and the Bradford methods were first used for the determination of the concentration of Cyp-A, FKBP-12, and BrCyp samples. The absorbance of the sample was then measured at 280 nm relative to the buffer in which the protein is dissolved. By dividing the absorbance at 280 nm with the concentration (mg/ml) the absorbance coefficient is obtained.

$$A^{1\text{mg/ml}}_{1\text{cm}} = \text{absorbance 280 nm} / \text{concentration (mg/ml)}$$

The numbers are given as $A^{1\text{mg/ml}}_{1\text{cm}}$ and represent the absorbance (280 nm) per 1mg/ml protein when using a cuvette with a path length of 1 cm. Because concentration values depend on the method which have been used (Bradford or BCA), the value of $A^{1\text{mg/ml}}_{1\text{cm}}$ reflected this difference. The concentration of a sample then can be determined by simple measurement of the absorbance at 280 nm, divided by the $A^{1\text{mg/ml}}_{1\text{cm}}$.

Table 4.1: Absorbance Coefficient ($A^{1\text{mg/ml}}_{1\text{cm}}$)

Method	Cyp-A	FKPB-12	BrCyp
<i>BCA</i>	0.749	1.69	-
<i>Bradford</i>	0.421	0.901	0.565

B) Fluorescence spectroscopy

Fluorescence spectroscopy is a powerful means of detecting interactions between proteins and other molecules. In the current work this technique was used to measure the binding of ligands to target proteins. A requirement is that the optical properties of the protein-ligand complex differ from those of free ligand and free protein (Bagshaw and Harris 1987). Aromatic residues such as phenylalanine, tyrosine and tryptophan are responsible both for fluorescence and the absorbance of proteins in the near ultraviolet region. In most proteins tryptophan fluorescence dominates at $\lambda_{\text{emit}}=340$ nm (Bagshaw and Harris 1987).

In this series of experiments the fluorescence of Cyp-A and FKBP-12 was examined, each protein having a tryptophan residue near to its binding site. FKBP-12 has only one tryptophan residue which sits at the bottom of the binding site and has no contact to the solvent other than via the active site. Cyclophilin A also has only one tryptophan, located about 8 Å from the center of the active site making a hydrogen bond to the inhibitor cyclosporin when bound.

Fluorescence titration in its simplest form involves fluorescence measurement on a solution of protein with successive additions of ligand. Typically, measurement (fig. 4.1) occurs at a single wavelength and continues until no further change is observed (apart from the dilution change due to addition of free ligand). The emission readings can be numerically evaluated and can be used to calculate a binding constant. This method has been used by Handschumacher *et al* (1984) for cyclophilin A.

After each addition of ligand, the portion of the protein bound is proportional to the fractional fluorescence change. When 50% of the binding sites are filled, the fractional fluorescence change is 50% when the protein ligand stoichiometry is 1:1. The K_d (dissociation constant) has been estimated by assuming a 50% occupancy of

the protein at fractional fluorescence change of 50%. At this point the concentration of the bound ligand equals the free protein (Husi and Zurini 1994). The mathematical basis of K_d calculation follows:



[P] = free protein concentration

[P]_b = bound protein concentration

[L] = free ligand concentration

[PL] = protein ligand complex concentration

[P]_o = total protein concentration

[L]_o = total ligand concentration

[L]_b = bound ligand concentration

$$K_d = \frac{[P] \cdot [L]}{[PL]}$$

when 50% fluorescence change occurred: [P] = [PL] = 1/2 [P]_o

$$[L]_o = [L]_b + [L]$$

$$[L]_b = [P]_b = 1/2 [P]_o$$

$$\begin{aligned} K_d &= [P] \cdot [L] / [PL] \\ &= 1/2 \cdot [P]_o \cdot ([L]_o - [L]_b) / (1/2 \cdot [P]_o) \\ &= [L]_o - [L]_b \\ &= [L]_o - 1/2 [P]_o \quad \text{(equation 4.1)} \end{aligned}$$

A typical plot of ligand concentration against fluorescence quenching is given in Fig 4.1. From that figure the [L]_o (0.09 mM) can be found and by using equation 4.1 the K_d can be calculated. The most meaningful values in a titration curve are those near to 50% of fractional fluorescence change because they allow more accurate determination of ligand concentration at that point.

50% of fractional fluorescence change because they allow more accurate determination of ligand concentration at that point.

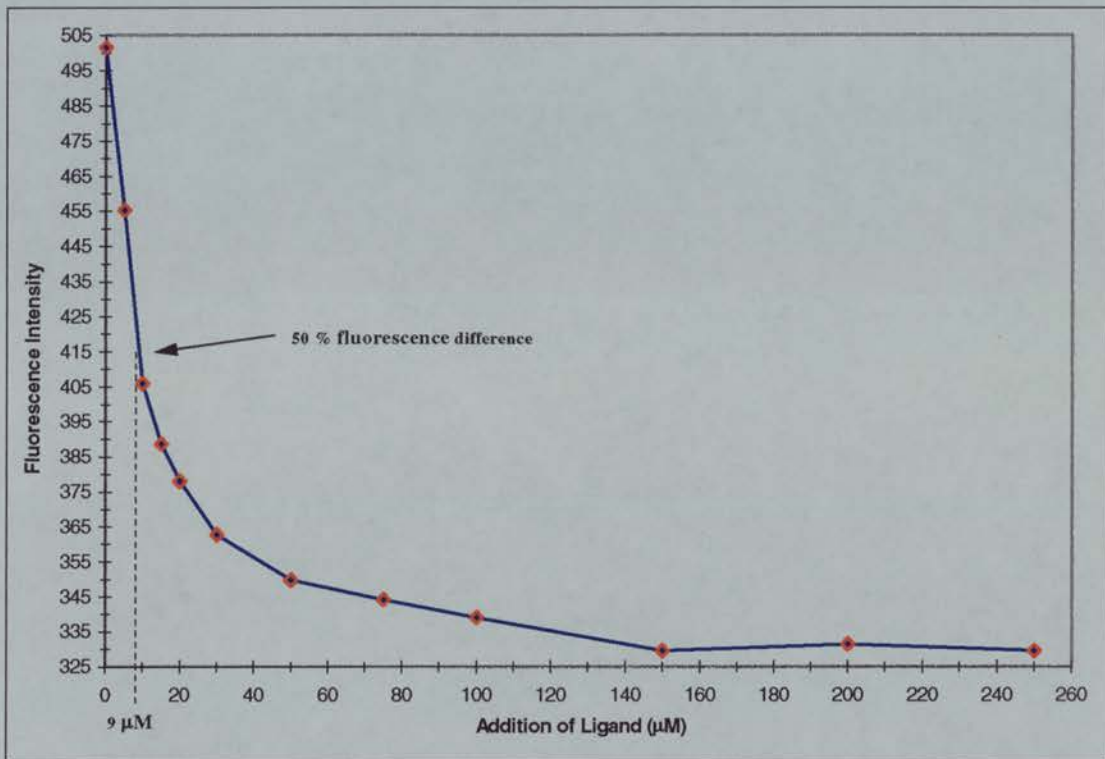


Fig. 4.1: Fluorescence emission titration of FKBP-12 with 5-Beta-Pregnane-3,20-dione. The point with 50 % signal is indicated with an arrow. The ligand concentration at 50 % of fractional fluorescence was 9 µM.

Two other reasons may cause fluorescence quenching when the ligand concentration becomes high and must be taken into account in every fluorescence titration.

- Inner filter effect. This can arise because the excitation or (and) the emitted light is (are) strongly absorbed by the solution containing the fluorophore. As a result less light can reach the detector, so there is apparent quenching of fluorescence.
- Scattering due to precipitation. Insoluble ligands can form precipitates which scatter the emission and the excitation light, so less quenching is recorded..

The first effect can be accounted for (Bagshaw and Harris 1987). To achieve this, measurements are taken with the same experimental set-up but with tryptophan (Trp)

instead of protein. By calculating the difference between the two measurements (fluorescence of protein and fluorescence of control, Fig. 4.2) the new corrected fluorescence values were calculated.

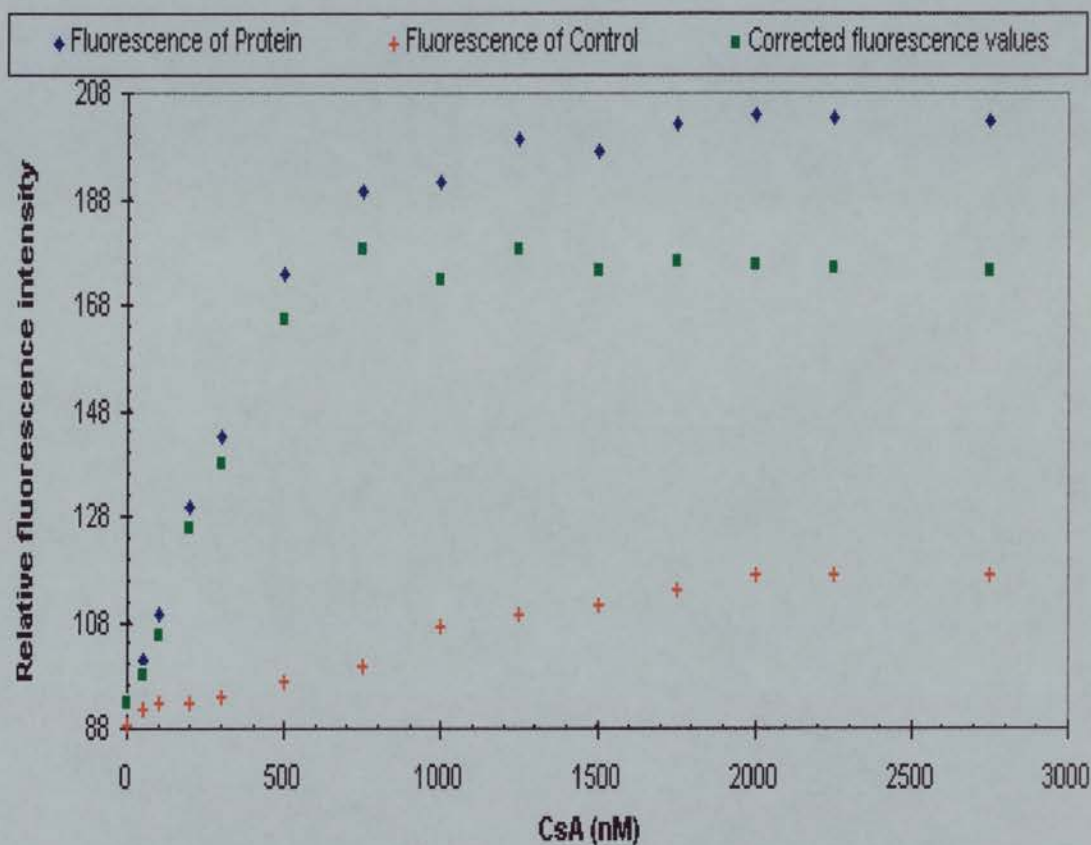


Fig. 4.2: Fluorescence emission titration of Cyp-A with CsA. Measurement starts at intensity 88. Cyp-A titration with CsA is one of few examples in which enhancement of fluorescence is observed.

- (◆) Original measured values
- (+) Values of the control measurement with Trp
- (■) New corrected values

The control experiment was done for all ligands to correct the inner filter effect. Additionally the control experiment can be used to correct for the dilution effect due to addition of ligand. After each addition of ligand the final volume of protein

solution increases, and the protein concentration decreases, resulting in a decrease in fluorescence intensity.

Measurements were carried out using a Perkin Elmer LS50B fluorescence spectrophotometer. The experiments took place at 20°C. Constant temperature was maintained within the cuvette by a temperature control. The protein solution was equilibrated until the signal was stable. A 1.4 ml fluorescence cuvette was used (Hellma 6140F). The excitation wavelength was 280 nm and the emission wavelength was varied from 330 to 345 nm according to protein and ligand. Emission and excitation slits varied from 2.5 to 10 nm, determined by experimental parameters.

For each ligand concentration one fluorescence value was measured, and at the same concentrations a reference emission value was taken. The difference between the two values was calculated and a new corrected value was used to determine the K_d . The fluorescence titration data were analysed graphically (Fig. 4.1) and the K_d was determined graphically.

For FKBP-12 titration, solution of 3 μ M FKBP-12 (determined with BCA method section 4.2.1) in 50mMTris, 100mM NaCl, pH=7.6 was used. Cyp-A solutions of 5 to 0.5 μ M in 50mMTris, 100mM NaCl, pH=7.4 were used. Protein concentration varied according to the ligand under test. Water soluble ligands were dissolved in the same buffer as the protein, the water insoluble in ethanol. The ligands tested with FKBP-12 and Cyp-A are given on Table 4.2 and 4.3.

Table 4.2: Ligands tested for binding to FKBP-12

Name	Ligand Abbrev.	Supplier
5 β Pregnane 3,20 dion*	PRG	Sigma
Prednisone	PRD	Sigma
Dimethylsulphoxide	DMSO	BDH

Cyclopentanone	PNT	ACROS
Cycloheptanone	HEPT	ACROS
1-Acetyl-3-methyl-1-piperidine	ACMPIP	Aldrich
Ethyl-1-Piperidineglyoxylate	ETPIPG	ACROS

Table 4.3: Ligands testing for binding to Cyp-A

Name	Ligand Abbrev.	Supplier
Cyclosporin A	CsA	Sandoz
Suc-ala-ala-pro-phe-pNA	Suc-ala-ala-pro-phe-pNA	BACHEM
ST3897	ST3897	MENAI
Dimethylsulphoxide	DMSO	BDH
E238	E298	MENAI
Cyclopentanone	PNT	ACROS
5,5 Dimethyl-1-,3-Cyclohexanedione	DCH	Aldrich
1-Acetyl-3-methyl-1-piperidine	ACMPIP	Aldrich
CBZ	CBZ	Chemistry Department University of Edinburgh
Pro-xydroxy-Pro	Pro-xydroxy-Pro	Sigma
Pro-Gly	Pro-Gly	Sigma
N-Benzoy-Phe-Ala-Pro	N-Benzoy-Phe-Ala-Pro	Sigma
Ethyl-1-Piperidineglyoxylate	ETPIPG	ACROS

C) PPIase assay

The enzymatic reaction of peptidyl prolyl *cis-trans* isomerase, also known as rotamase (Fig.4.3) was first described by Fischer and Bang at 1984. It catalyses prolyl isomerisation in both peptides (Harrison and Stein 1992) and proteins (Fischer and Bang 1984). The enzymatic reaction of peptidyl prolyl *cis-trans* isomerase can be used to characterise immunophilins as well as in testing binding of ligands.

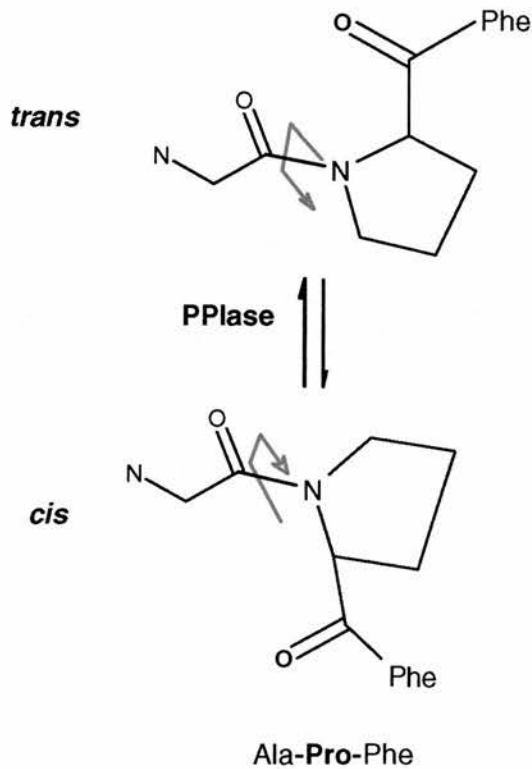


Fig. 4.3: Schematic representation of *cis*↔*trans* isomerisation of peptidyl-prolyl bonds

1. Rotamase activity assay

PPIase activity is usually assessed with the α -chymotrypsin-coupled enzymatic assay (Kofron et al 1991). α -chymotrypsin selectively hydrolyses the C-terminal p-nitroanilide bond of the substrate in the *trans* X-Pro conformer only (Fig. 4.3). This hydrolysis releases a chromophore 4-nitroaniline, the accumulation of which is recorded by measuring the absorbance at 400 nm as a function of time. The *trans* peptide is cleaved within the deadtime so this cleavage does not contribute to the total reaction time (Takahashi et al 1989).

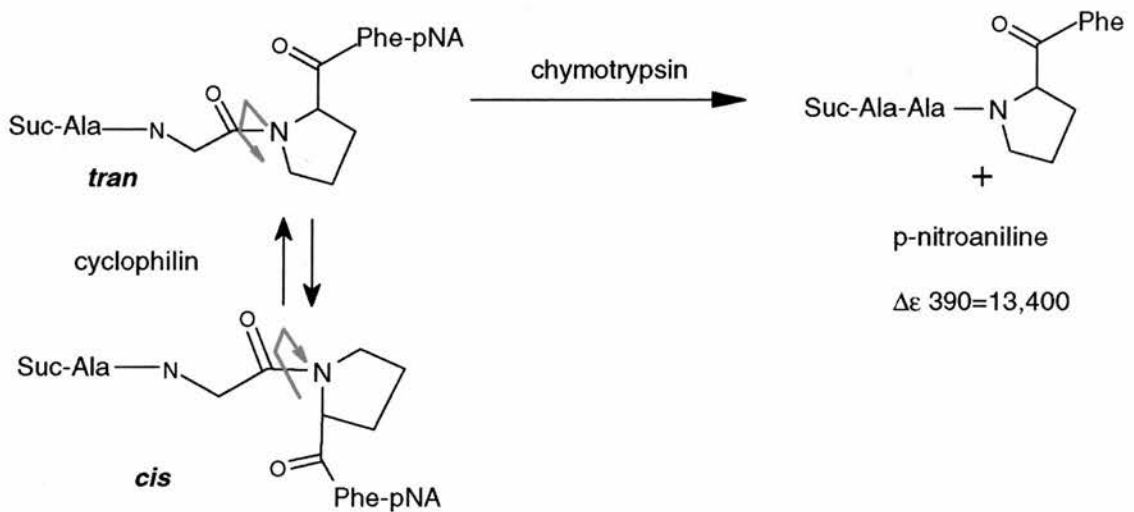


Fig. 4.4: PPIase assay: Cyclophilin catalyses *cis-trans* isomerisation of the substrate and chymotrypsin instantaneously cleaves off the C-terminal blocking group (pNA) of

experiment took place at 4°C. Constant temperature was maintained within the cuvette by a Peltier (PTP-1) temperature control unit. A mini magnetic stirring system (telemodule from Variomag) was used for mixing the solution in the cuvette after the addition of the substrate. A Perkin Elmer UV/VIS Lambda 20 spectrophotometer was used.

The following materials were used:

Substrate: Suc-Ala-Ala-Pro-pNA (Bachem AG) (N-succinyl-Ala-Ala-Pro-Phe-p-nitroanilide)

Proteins: Cyp-A, Cyp-B and CypBr purified in house. The protein solution was freshly prepared before the experiment from frozen stock solution, at the appropriate concentration (see result section 3.B), by dilution in buffer 50 mM Hepes, 100 mM NaCl pH=8.0.

50 mg/ml (of α -chymotrypsin (Sigma)

In a typical experiment 90 μ l of 2.5-30 nM cyclophilin (plus the inhibitor when the IC_{50} has to be determined) was made up to 2520 μ l with buffer A in a 3 ml glass cuvette. The cuvette then was preincubated for 30 min on ice. Immediately before the assay, 300 μ l of chymotrypsin solution (6 mg/ml in 10 mM HCl) was added, followed by 90 μ l of a 3.7 μ M stock solution of Suc-Ala-Ala-Pro-PNA in LiCl (470mM)/TFE. The reaction progress was monitored by the absorbance change at 400 nm that accompanies the hydrolysis of the amide bond and the release of 4-nitroaniline product.

2. IC_{50} determination

The method will be described together with the results section (4.3 B).

The following materials were used:

Substrate: as in rotamase assay

Proteins: as in rotamase assay.

Table 4.4: Ligands testing for inhibition activity with Cyp-A

Name	Ligand Abbrev.	Supplier
Cyclosporin A	CsA	Sandoz
Ala-Pro	Ala-Pro	SIGMA
Dimethylsulphoxide	DMSO	BDH
Tetramethylene sulfoxide	TMSO	ACROS
5,5 Dimethyl-1-,3-Cyclohexanedione	DCH	Aldrich
1-Acetyl-3-methy-1- piperidine	ACMPIP	Aldrich
Ethyl-1-Piperidineglyoxylate	ETPIPG	ACROS

Full chemical names and chemical formulas of the inhibitors can be seen in results section Table 4.5 and 4.6.

4.3 Results

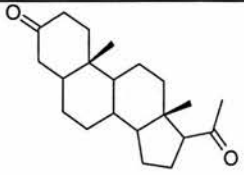
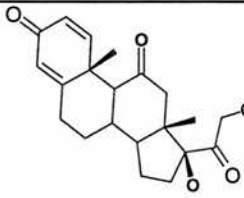
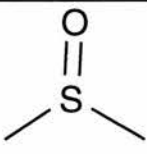
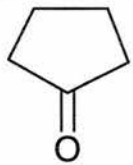
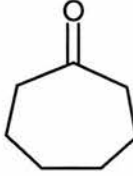
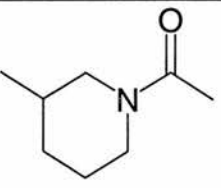
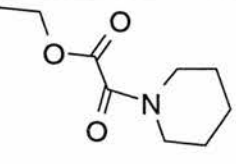
A) Fluorescence spectroscopy

A fluorescence assay was the first method used for ligand testing since was simpler than the PPIase assay, did not require additional substances e.g substrate was used in the PPIase and the K_d can be determined directly from the data without additional calculations.

1. FKBP-12

Some of compounds tested during this work have been reported to bind to FKBP-12 (Peter Burkhard Thesis Basel University 1995). The compounds proposed by Burkhard were tested by fluorescence spectroscopy assay along with other compounds which were suggested during this work. The suggestions are based on structural similarities with Burkhard's compounds or on structural similarities with Ala-Pro which is a substrate for FKBP-12.

Table 4.5: Ligands had been tested by fluorescence assay with FKBP12

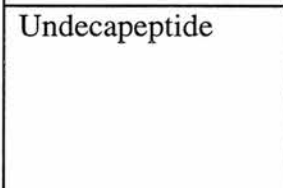
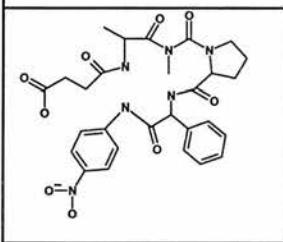
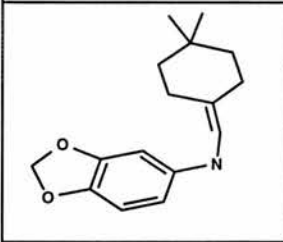
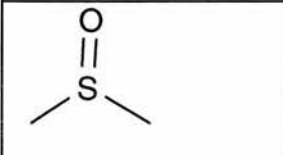
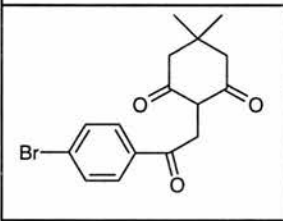
Formula	Abbrev.	Name	K_d (This work)	Comments
	PRG	5 β Pregnan-3,20-dione*	7.5 μ M	K_d = 7 μ M determined by Burkhard
	PRD	Prednisone	not determined	shares structural similarities with PRG
	DMSO	Dimethylsulphoxide*	10 mM	K_d = 20mM determined by Burkhard
	PNT	Cyclopentanone	not determined	shares structural similarities with HEPT
	HEPT	Cycloheptanone*	not determined	K_d = 30 μ M determined by Burkhard
	ACMPIP	1-Acetyl-3-methyl-1-piperidine	not determined	shares structural similarities with Ala-Pro
	ETPIPG	Ethyl-1-Piperidineglyoxylate	not determined	shares structural similarities with Ala-Pro

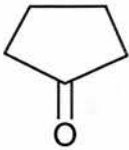
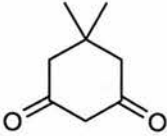
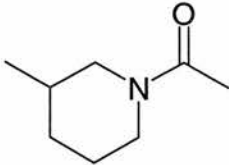
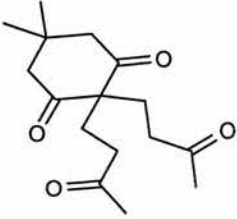
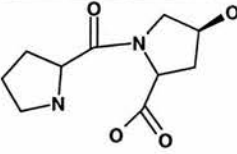
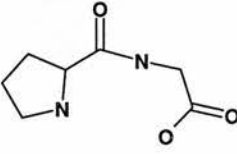
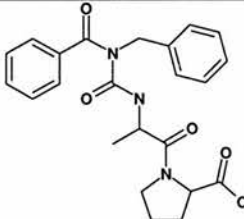
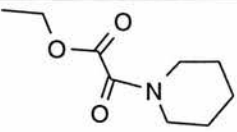
* Compounds found to bind by Burkhard

2. Cyp-A

The compounds tested share structural similarities to the natural substrate Ala-Pro or to DMSO or to 5,5 Dimethyl-1-,3-Cyclohexanedione. 5,5 Dimethyl-1-3-Cyclohexanedione was suggested to bind to the active site of Cyp-A by the docking program LIDAEUS. CsA was the first ligand was tested, since it has been observed to bind to Cyp-A by fluorescence spectroscopy (Handschumacher et al 1984). The ligands tested by fluorescence spectroscopy are given in Table 4.6.

Table 4.6: Ligands had been tested by fluorescence assay with Cyp-A

Formula	Abbrev.	Name	K_d	Comments
	CsA	Cyclosporin A	40 nM	K_d 36.8 nM reported by Husi and Zurini (1994)
	PRG	Suc-ala-ala-pro-phe-pNA	not determined	Substrate for Cyp-A
	ST3897	ST3897	not determined	shares structural similarities with DCH
	DMSO	Dimethylsulphoxide	not determined	
	E298	E238	not determined	shares structural similarities with DCH

	PNT	Cyclopentanone	not determined	shares structural similarities with DMSO
	DCH	5,5 Dimethyl-1,3-Cyclohexanedione	not determined	fraction of the molecule suggested to bind by docking program
	ACMPIP	1-Acetyl-3-methy-1-piperidine	not determined	shares structural similarities with Ala-Pro
	CBZ	CBZ	not determined	shares structural similarities with DCH
	PHP	Pro-xydroxy-Pro	not determined	shares structural similarities with Ala
	PG	Pro-Gly	not determined	shares structural similarities with Ala-Pro
	NBPAP	N-Benzoy-Phe-Ala-Pro	not determined	shares structural similarities with Ala-Pro
	ETPIPG	Ethyl-1-Piperidineglyoxylate	not determined	shares structural similarities with Ala-Pro

The only ligand shown to bind by fluorescence measurements was CsA. Suc-ala-ala-pro-phe-pNA also shown some binding but solubility problems prevented a further investigation.

B) PPIase assay

1. PPIase activity

The rotamase activity assay was performed on three proteins purified in house, Cyp-A, Cyp-B and CypBr (see chapter 3). The characterisation confirmed that the protein was enzymatically active. Variation of the amounts of the enzyme used gives a family of curves in each experiment. The initial velocities were used for the calculation of the k_{obs} (for definition of k_{obs} see section 4.3 B 2) according to the method described by Liu et al (1990). Then the value of k_{cat}/K_m was calculated from k_{obs} ($k_{\text{obs}}=v/[S]$, where v is the velocity and $[S]$ is the substrate concentration) by plotting the ratio $v/[S]$ for different protein concentration traces against the respective protein concentration. A linear plot can be obtained and the slope of the plot is k_{cat}/K_m (Liu et al 1990). The value of k_{cat}/K_m is an indication of the PPIase activity.

Cyp-A

Three concentrations of Cyp-A were used 22.5 nM, 17.5 nM and 10.0 nM. The results are shown in Fig 4.5.

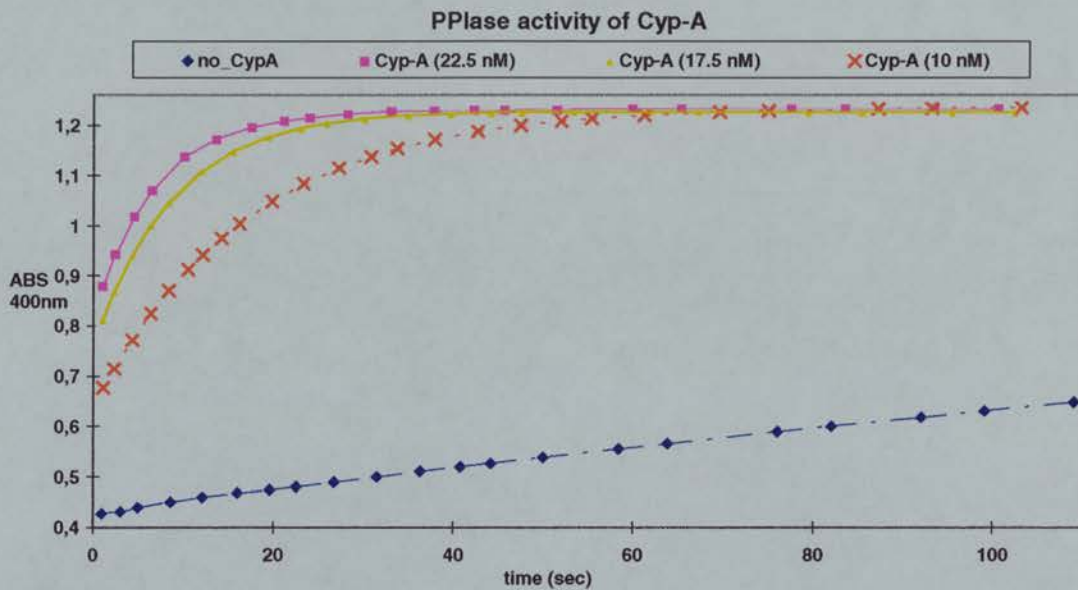


Fig.4.5: Chymotrypsin-coupled assay of rotamase activity with various amounts of Cyp-A.

From Fig.4.5 it can be seen that recorded absorbance values for 22.5 nM Cyp-A start at 0.93 and the reaction is complete when $A_{400\text{nm}}=1.2$. The fact that the trace with no protein starts from 0.43 which is only 35.8 % of the end absorbance shows that about 64 % of the substrate was *cis* at the beginning of the reaction.

A value of $k_{\text{cat}}/K_m=1.2 \times 10^7 \text{M}^{-1} \text{s}^{-1}$ for Cyp-A was calculated from the Cyp-A traces according to Liu et al (1990).

Cyp-B

The experiment was repeated with three concentrations of Cyp-B: 21.8 nM, 16.3 nM and 5.45 nM. The results are shown in Fig 4.6.

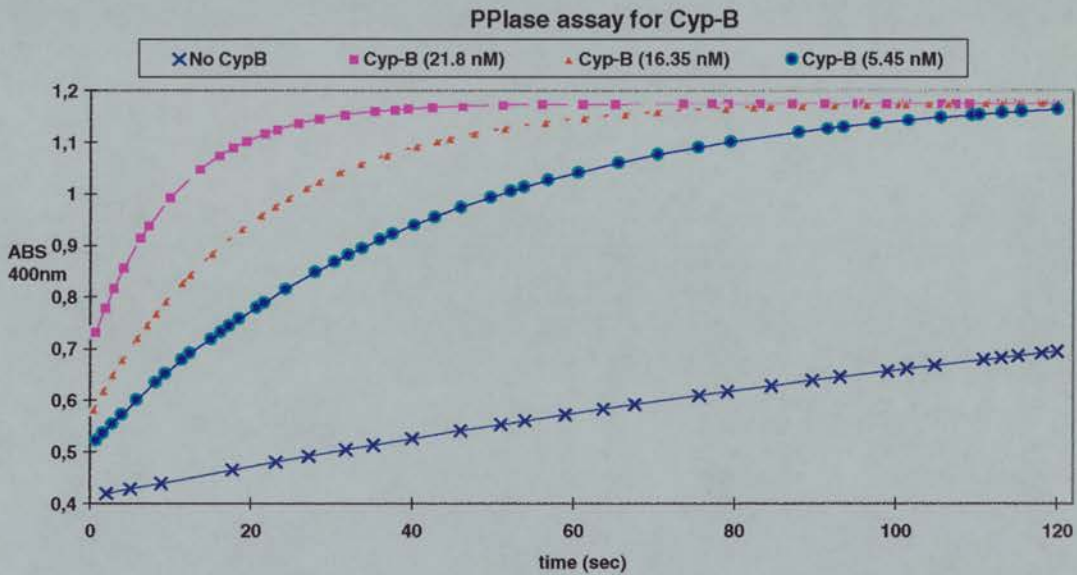


Fig. 4.6:Chymotrypsin-coupled assay of rotamase activity with various amounts of Cyp-B purified in house.

A value of $k_{cat}/K_m=8 \cdot 10^6 M^{-1} s^{-1}$ for Cyp-B was calculated using the three Cyp-B traces from above.

BrCyp

The experiment was repeated with three concentrations of BrCyp: 80 nM, 40 nM and 16 nM. The results are shown in Fig 4.7.

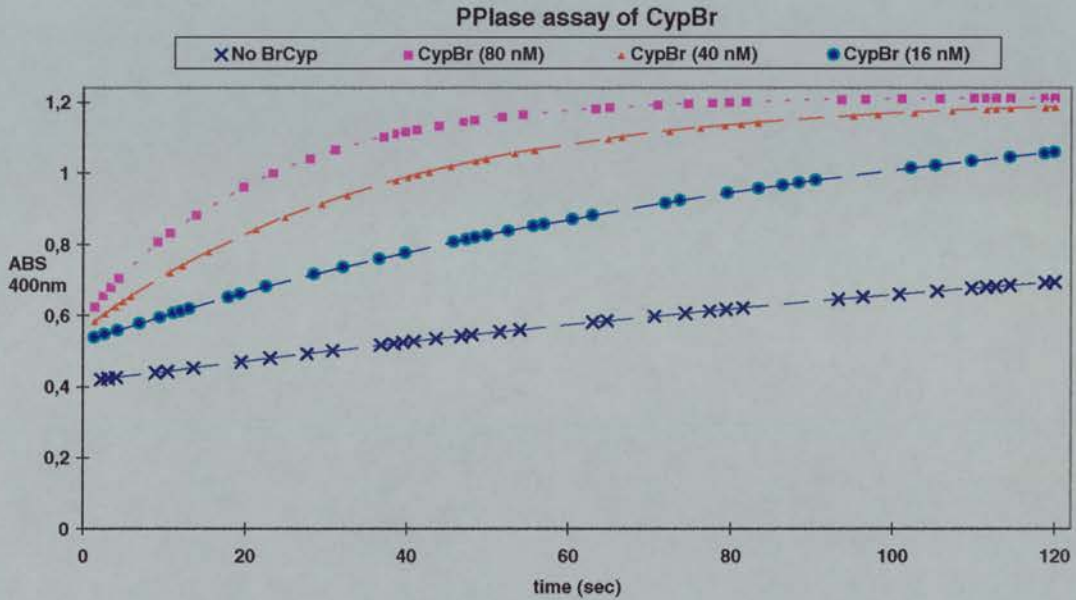


Fig. 4.7: Chymotrypsin-coupled assay of rotamase activity with various amounts of BrCyp purified in house.

A value of $k_{cat}/K_m = 10^6 M^{-1} s^{-1}$ for BrCyp was calculated from the above result.

2. Determination of IC_{50} for Cyp-A ligands

The reaction rate at low substrate concentrations where $[S] \ll K_m$ can be expressed as a second-order rate equation (Fersht 1984).

$$v = (k_{cat}/K_m) \cdot [E]_T \cdot [S] \quad \text{equation 4.2}$$

[E]=free enzyme concentration

[S]=substrate concentration

$[E]_T$ =total enzyme concentration

v=velocity of the reaction

At low substrate concentration $[S] \ll K_m$ the enzyme is largely unbound and $[E] \approx [E]_T$ (Fersht 1984). The method used for the determination of IC_{50} (Fischer et al 1989, Liu et al 1990 and Rinfret et al 1994) requires the calculation of k_{obs} , where $k_{obs} = (k_{cat}/K_m) \cdot [E]$. The next step is the calculation of k_{obs} in the presence of various amounts of inhibitor.

The method required the determination of k_{obs} for total inhibition. Total inhibition means saturation of the protein in the presence of high inhibitor concentration. The above applied when $[S] \ll K_m$ (Rinfret et al 1994). Many ligands tested in this work were poorly soluble in aqueous solution. The novel ligands that were found bound weakly to Cyp-A. Together these two features made it impossible to determine total inhibition, as many ligands formed precipitates at high concentrations. A different approach was followed to determine IC_{50} values.

In general an enzymic reaction can be described by the following scheme:



The dissociation constant of the enzymic-substrate complex is:

$K_s = [E][S]/[ES]$ (equation 4.4) and the velocity of the enzymatic reaction is $v = k_{cat}[ES]$ (equation 4.5) (Fersht 1984). This equation for the velocity of the enzymatic reaction can be applied from the beginning till the end of the reaction and not only in the initial stage. Also the total enzyme concentration $[E]_T$ the bound enzyme concentration $[ES]$ and the free enzyme concentration $[E]$ are related by

$$[E] = [E]_T - [ES] \quad \text{equation 4.6}$$

Thus from equation 4.4

$$[ES] = [E]_T[S] / K_s + [S] \quad \text{equation 4.7}$$

and from equation 4.5

$$v = [E]_T[S] k_{cat} / (K_s + [S]) \quad \text{equation 4.8}$$

At low substrate concentration ($[S] \ll K_m$) Equation 4.8 becomes:

$$v = [E][S] \frac{k_{cat}}{K_s + [S]} \quad \text{equation 4.9}$$

For the substrate used in this method a $K_m = 870 \mu\text{M}$ has been reported (Kofron et al 1991) for Cyp-A. The substrate concentration in this experimental series was less than $60 \mu\text{M}$.

Equation 4.9 applies throughout the enzymatic reaction and not only to the initial rate. The velocity (equation 4.9) at constant substrate concentration changes linearly with the free enzyme concentration $[E]$. This means that by performing a series of experiments varying the protein concentration and keeping the substrate concentration constant the velocity v should fit to a linear plot.

An example of how the IC_{50} of CsA was determined follows. The same method was used to determine the IC_{50} of the rest of the ligands.

Initially, Cyp-A was assayed at a range of dilutions (Fig. 4.8). The added amount of substrate was the same in all of this series of assays. This means that at the same absorbance, the substrate concentration is the same for each curve. Absorbance readings around 0.76 Abs units of each curve in Fig. 4.8 were used for the determination of velocity.

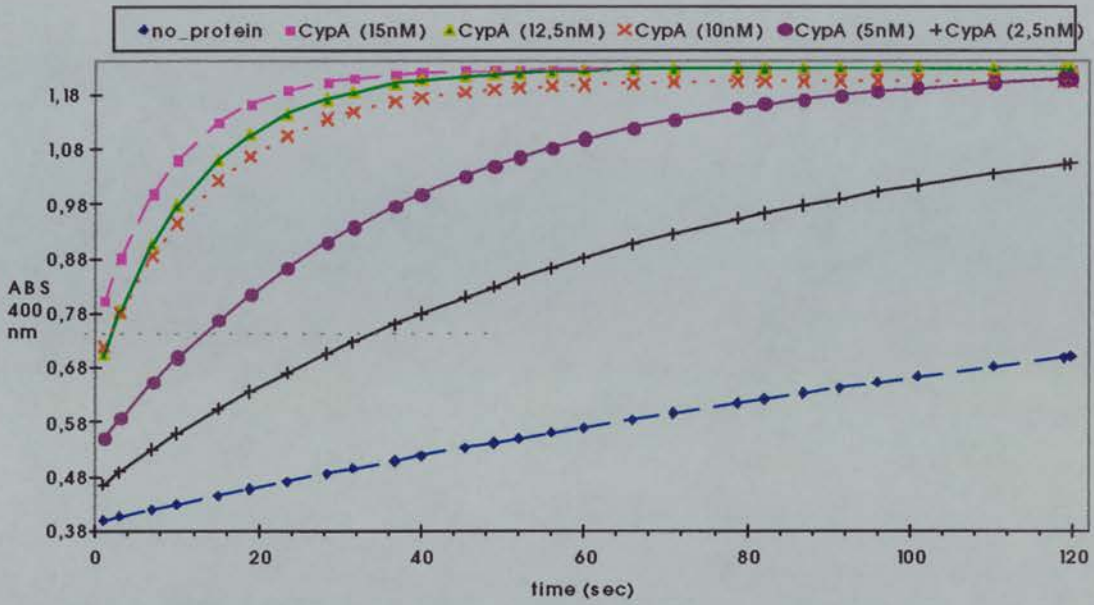


Fig. 4.8: PPIase assay with various amounts of Cyp-A. Sample (♦) nonenzymatic thermal isomerisation.

The substrate concentration during the time used for the calculation of the slope (Fig. 4.9) changes less than 3 % ($A_{400} = 0.762$ to 0.776 Fig. 4.9) and the assumption that substrate concentration is constant can be made. During that time the absorbance changes linearly with time and the points fit very well to the equation $y = a \cdot x + b$ where y is absorbance and x is the time. “ a ” is the slope of the equation and has dimensions y/x which is equal to the rate of the change of absorbance $d(\text{Abs})/dt$ (velocity).

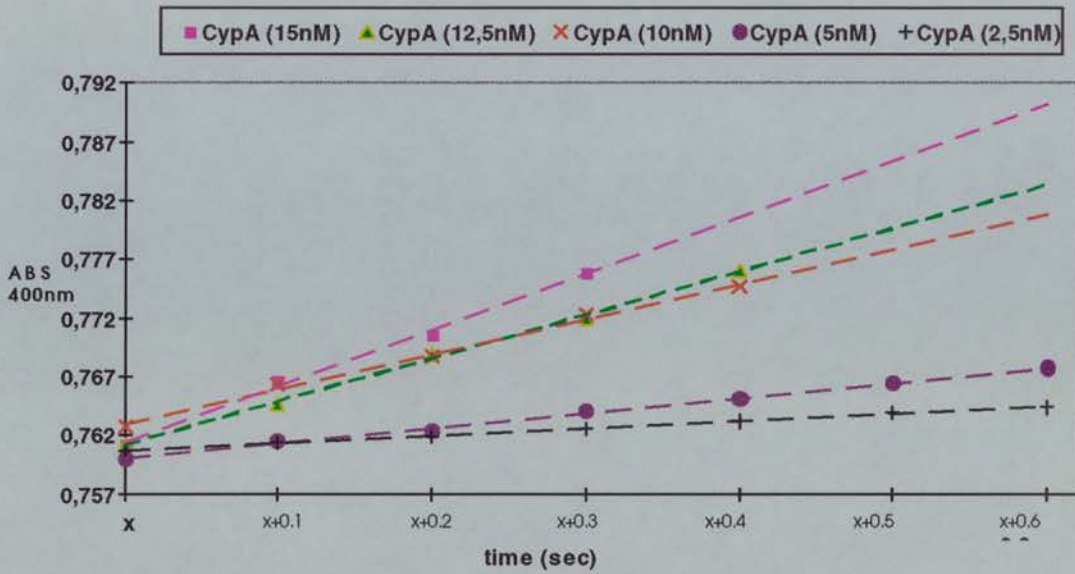


Fig. 4.9: Expression of readings at absorbance units around 0.76 from Fig.4.8.

The time at which the slope of each curve is determined (point x) is different for each of the above curves. X corresponds to 1.5 sec, 2.3 sec, 2.5 sec, 14.8 sec and 41.8 sec for Cyp 15nM, 12.5nM, 10nM, 5nM and 2.5nM respectively.

Using the least square method, each series of points in Fig. 4.9 is fitted to a linear equation.

15 nM ■	Abs=0.0481t+ 0.7614
15nM ▲	Abs=0.037t+ 0.7612
10 nM ×	Abs=0.0298t+ 0.763
5 nM ●	Abs=0.0128t+ 0.7601
2.5 nM +	Abs=0.0062t+ 0.7607

By plotting the slopes of the above equation against the respective protein concentrations the relationship between protein concentration and velocity can be found (Fig. 4.10). The X axis is [P] (free protein concentration). Using Fig.4.10 the protein concentration corresponding to velocity in the range 6×10^3 to 4.8×10^4 can be determined graphically.

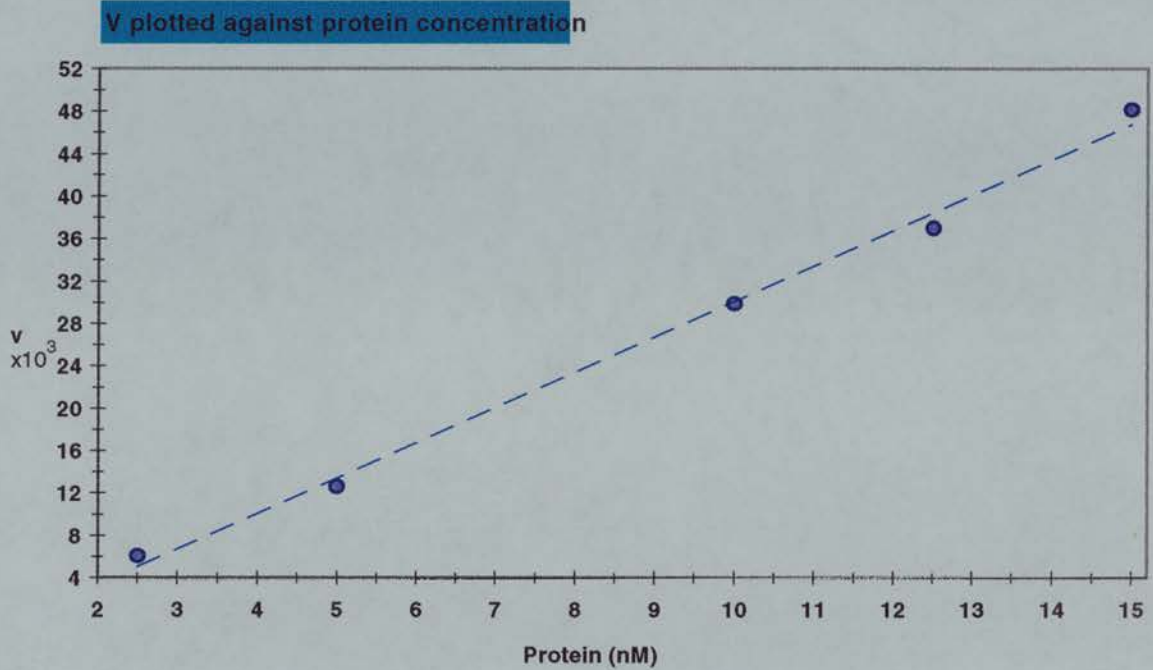


Fig. 4.10: Protein concentration plotted against velocity (v)

Under the conditions of this experiment ($[S] \ll K_M$) the velocity reduces to a second order rate equation $v = \frac{[S]k_{cat}}{K_S + [S]}[E]$ (equation 4.9). With constant $[S]$ (since the velocities are all calculated at the same absorbance of 0.76) the previous equation reduces to a first order rate equation $v = K[P]$ when $K = \frac{[S]k_{cat}}{K_S + [S]}$. The calculated velocities of the reaction should therefore be proportional to the protein concentration as can be seen in Fig.4.10.

The same assay protocol was followed except that various amounts of ligand CsA (5-40 nM) were added. The protein concentration was 15 nM. Upon addition of ligand the free protein concentration $[E]$ was decreased so the velocity of the reaction v . The results are presented in Fig.4.11 from which it can be seen that inhibition of the reaction follows the addition of CsA.

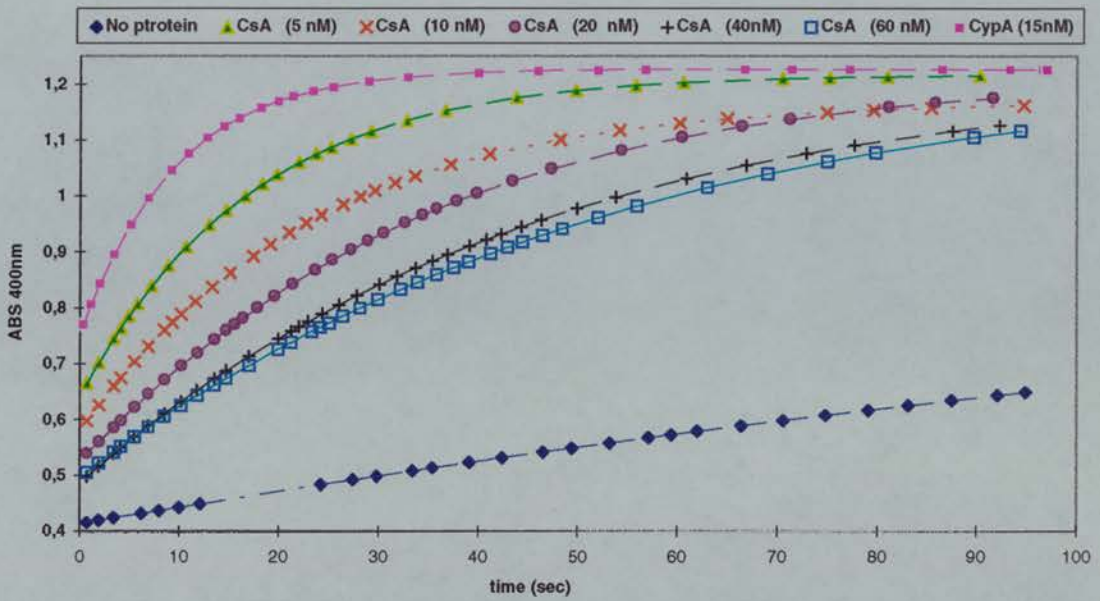


Fig. 4.11: PPIase assay with various amounts of CsA. Sample (♦) contains protein only.

The absorbance readings around 0.76 Abs units of each curve in Fig. 4.11 were used for the determination of velocity. Using the least square method each series of points in Fig. 4.12 conform to a linear equation.

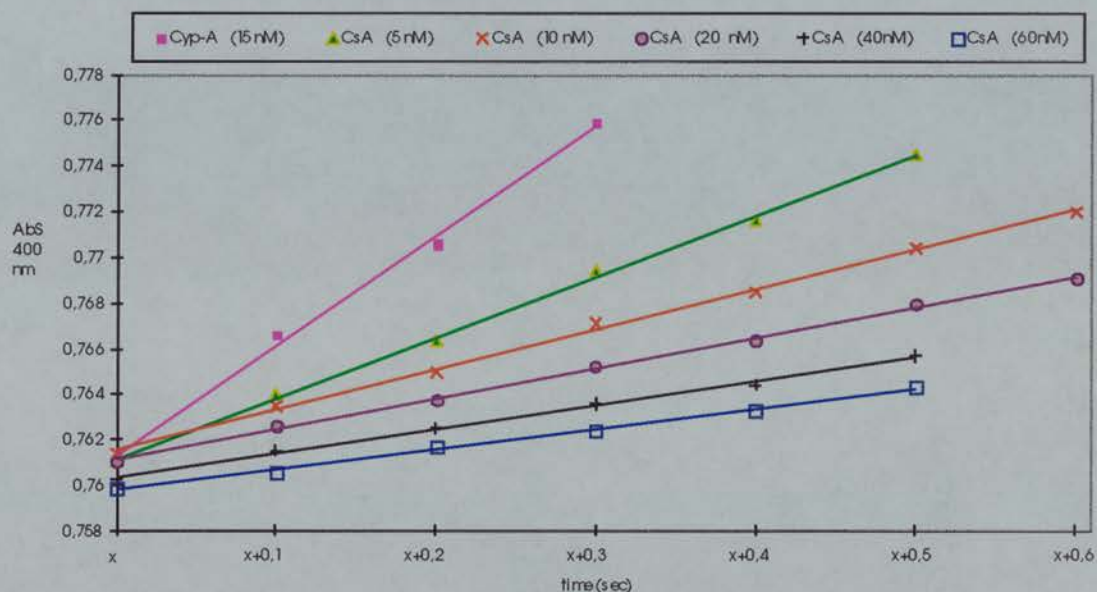


Fig. 4.12: Readings at absorbance units around 0.76 from Fig.4.11. The observed change (point x) in Fig.4.9 is different for each of the above time curves. X corresponds to the time point at which Cyp15nM, CsA 5nM, CsA 10nM, CsA 20nM, CsA 40nM and CsA 60nM, CsA 5nM, have an absorbance of 0.762 in Fig.4.6.

15 nM ■	$Abs=0.0481t+ 0.7614$
5 nM ▲	$Abs=0.0267t+ 0.7558$
10 nM ×	$Abs=0.0175t+ 0.7545$
20 nM ●	$Abs=0.0134t+ 0.7557$
40 nM +	$Abs=0.0105t+ 0.7553$
60 nM □	$Abs=0.0088t+ 0.7552$

By plotting the slopes of the above equation against the respective protein concentrations the relation between CsA concentration and velocity can be found (Fig. 4.13).

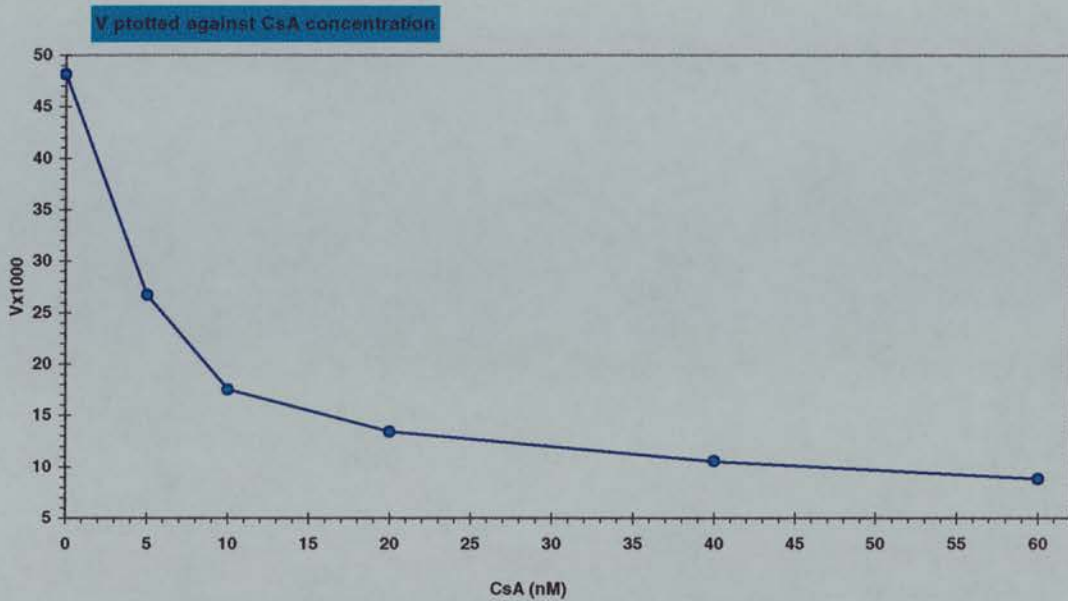
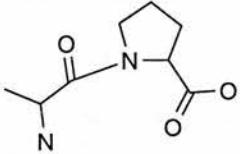
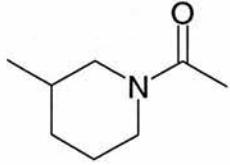
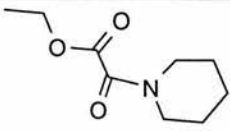
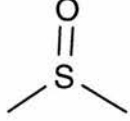
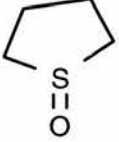
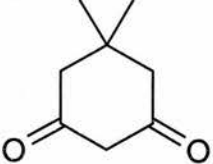


Fig. 4.13: Plot of velocity of enzymatic *cis-trans* isomerisation against CsA concentration.

Using Fig.4.8 the ligand concentration corresponding to velocity in the range 8800 to 48000 can be determined graphically. From Fig.4.11 it can be found that for velocity=22000 the free [E] is 7.5 nM. Using Fig.4.8 the CsA concentration at which velocity=22, is around 9 nM. Also $[E]_T = [E] + [EL]$. $[E]_T$ is the total protein concentration which is 15 nM, and the [E] is the free protein concentration. This means that the concentration of the CsA in which half inhibition occurs is 9 nM. CsA was the only ligand which was shown to bind by both assays (fluorescence and PPIase). The same method was followed for the other ligands. The results are given in the Table 4.7:

Table 4.7: IC₅₀ values for inhibitors of CypA is determined by PPIase assay

Ligand	Abbrev.	Formula	IC ₅₀
	CsA		9 nM
	Ala-Pro		18 mM
	ACMPIP		335 mM
	ETPIPG		25 mM
	DMSO		45 mM
	TMSO		33 mM
	DCH		22 mM

3. Determination of K_d

The concentration of the free protein [P] after the addition of the inhibitor for low substrate concentrations ($[S] \ll K_m$) can be calculated after determination of the velocity according to the method previously described (section 4.3.B.2). The bound protein concentration [EL] after addition of the inhibitor L, is $[PL] = [L]_T - [L]$ (where $[L]_T$ = total inhibitor concentration). The free inhibitor concentration $[L] = [L]_T - [PL]$. The dissociation constant of an inhibitor can be determined by replacing the above terms to give the following equation:

$$K_d = \frac{[P] \cdot [L]}{[PL]} \quad (\text{equation 4.10})$$

When an inhibitor binds weakly a high concentration of the inhibitor is required in order to achieve 50% inhibition (in this work under weak inhibitors the concentration $[L]_T$ was 10^6 times higher than the total protein concentration $[P]_T$ at half maximal inhibition). The free inhibitor concentration to give half inhibition, $[L]_{IC50}$, is much higher than the bound [PL] ($[PL] = 1/2[P]_T$ at half inhibition). With such an excess of ligand, the assumption $[L]_{IC50} = [L] \approx [L]_T$ can be made. At the point at which half maximal inhibition occurs $[PL] = [P]$ and equation 4.10 reduces to $K_d = [L]_T$.

Using equation 4.10 the K_d for the CsA can be calculated. From section 4.3.B.2 the total concentration of the CsA in which half inhibition occurred is 9 nM (Fig. 4.8), the free [E] is 7.5 nM and the concentration of E-CsA protein concentration is also 7.5 nM which means that the free inhibitor concentration is 2.5 nM. Replacing these values in equation 4.10, the calculated K_d is 2.5 nM. This value is the same as that determined by Fischer et al (1989) for Cyp-A with the same inhibitor.

4.4 Discussion

A) Protein determination

The BCA assay depends on the number of peptide bonds of the protein rather than individual amino acid residues. Therefore, the method is independent of the standard samples and was used wherever an accurate estimate of the concentration was required, for example calculation of K_d .

Bradford results are more dependent upon the standard, but it was the method of choice when a quick result was required (e.g eluted sample from chromatography). The difference between the Absorbance Coefficients obtained by BCA and Bradford method (Table 4.1) reflected the fact that each method is based on a different principle for determination of the concentration.

The Bradford protein assay has been reported to overestimate the actual quantity of FKBP-12 by 3-fold (Siekierka et al 1989) and of Cyp-A by 1.7-fold (Harding et al 1985). The above overestimates fit with the observed values for FKBP-12 and Cyp-A. It can be seen that Absorbance Coefficients, which are inversely proportional to concentration, are much lower when calculated using the Bradford assay.

B) Fluorescence spectroscopy

The value of K_d calculated from fluorescence results for CypA-CsA was similar to that reported in the literature (Husi and Zurini 1994 Table 4.6) and the same was true for the K_d of FKBP12-PRG (Table 4.5). The determination of K_d values similar to those already published suggests that the method and the procedure were correct.

The lack of results from fluorescence titration of Cyp-A with small ligands could be explained by structural results. Many ligands found to bind in the active site of Cyp-A by X-ray crystallography showed no effect when tested in fluorescence. The measurement of ligand binding by fluorescence spectroscopy requires that the optical properties of the protein-ligand complex differ from those of the free ligand and free protein (Bagshaw and Harris 1987). The optical properties of Trp would change when the surrounding environment of Trp changes. This environment is solvent molecules or residues which make contact with Trp. In fact the only compound which clearly gave results in the fluorescence assay was CsA. Cyclophilin's tryptophan residue makes a hydrogen bond with CsA. None of the other ligands used during this work make contact with the tryptophan. Also the tryptophan and the residues with which it comes into contact remain practically unchanged on binding. All the ligands used in the current work apparently do not effect the Trp environment when they bind.

C) PPIase assay

The method introduced for the determination of IC_{50} is based on the determination of velocity of the enzymatic reaction for a series of protein dilutions not at $t=0$ but at the same substrate concentration. The reproducibility of the method is highly dependent on the protein and the substrate concentration. The determined velocity of the reaction depends on protein and substrate concentration (section 4.3.B.2) so accurate determination of substrate and protein concentration is required. The substrate concentration can be easily determined by the absorbance during the experiment. The protein concentration could be determined accurately but the amount of active protein could not be determined. As active protein concentration is involved in the calculation of IC_{50} the protein solution should be freshly prepared before the experiment (to prevent any denaturation).

The enzymatic results for Cyp-A, Cyp-B and BrCyp confirmed that all the proteins are active. The k_{cat}/K_m values found during this work are similar to those reported in the literature. The activity of Cyp-A ($k_{\text{cat}}/K_m=1.2 \times 10^7 \text{M}^{-1} \text{s}^{-1}$) is similar to that reported by Liu et al (1990) for the same protein ($k_{\text{cat}}/K_m=1.37 \times 10^7 \text{M}^{-1} \text{s}^{-1}$). Also the activity of BrCyp ($k_{\text{cat}}/K_m=1 \times 10^6 \text{M}^{-1} \text{s}^{-1}$) is close to that reported by Page et al (1995) for the same protein ($k_{\text{cat}}/K_m=7.9 \times 10^6 \text{M}^{-1} \text{s}^{-1}$). Cyp-A seems to have the highest activity of all.

The enzymic assay was used mainly because no results were obtained from fluorescence titration or dynamic light scattering, for Cyp-A and small ligands. The ligands used during this work are relatively small compounds, from 4 up to 13 atoms (non-hydrogen). Also the natural substrate Ala-Pro has a similar size (13 atoms). It was expected this dipeptide would act as an alternate substrate inhibitor (Harrison and Stein 1990) and an attempt was made to determine its dissociation constant.

Even after clear evidence that this dipeptide bound in the active site of Cyp-A (Ke et al 1993) the binding affinity of this dipeptide has not been reported. The only indication was given by Harrison and Stein (1990) who placed a conservative lower limit on K_i of 20 mM. The same applied to all other oligopeptide-cyclophilin complexes which have been studied by X-ray (Zhao and Ke 1996). The K_d of 18 mM found during this work was very close to the value suggested by Harrison and Stein. The K_d was calculated using the total concentration of the Ala-Pro in the solution (*cis* and *trans* isomers) since was not able to determine the concentration of each individual isomer.

All non-peptide ligands found during this work bound with similar strength (K_d values 22-35 mM) except AMPIP (K_d 335 mM). ETPIPG and ACMPIPG are very similar molecules and both fit the same way into the binding site (crystallographic results), nevertheless their K_d values are significantly different. Further investigation using crystallographic results (chapter 7) may clear up this point.

5. Crystallization

5.1 Introduction

Crystal growth is perhaps the most crucial step in protein crystallography. There is no clear way to predict the conditions that will cause protein crystallization which can be one of the most time consuming steps in protein crystallography. Many different methods to crystallize proteins have been developed like vapour diffusion and dialysis methods (Ducruix, A. and Giegé, R., 1990), all of which aim at bringing the solution of protein to a supersaturated state.

Several techniques have been developed to improve the quality of the crystal as well as the size. Screening procedures (McPherson 1985) are the most common. The screening first starts with crystallization conditions to obtain the first crystal and then optimisation of these conditions to improve crystal size and quality. Also seeding has often been used as a method to improve size and quality. Seeding requires crystals as a starting point to generate nucleation. This has often been used as a method of last resort rather than a standard practice for crystal growth. There are three different methods, streak seeding , macroseeding and microseeding (McRee, 1993). The streak seeding can be used to carry out a search quickly over a wide range of growth conditions and later the use of macro and micro seeding could be used to grow larger crystals with good degree of reproducibility.

Re-chromatography has also been proposed (Ducruix, A. and Giegé, R., 1990) before crystallization trials in order to increase the chance for crystal growth. Trace contaminants and denatured forms, which are not detectable by SDS-gels, of the protein may prevent crystallization of the native form. These could be removed by chromatographic methods.

The quality of the crystals affects the resolution, survival during fast freezing, and the time of survival in soaking solution as well as crystal parameters like mosaicity. The size of the crystal can also affect the resolution, larger crystals tend to diffract better but on the other hand tend to crack during flash freezing.

5.2 Methods and Materials

A) Proteins

1. Cyp-A

Cyp-A was obtained from two different sources. Initial protein kindly provided by Sandoz and later on when the cell line for this protein was available the protein was produced and purified in house.

2. Cyp-B

Cyp-B was obtained from two different sources. Initial protein kindly provided by Sandoz and later on when the cell line for this protein was available the protein was produced and purified in house.

3. BrCyp

BrCyp was obtained from two different sources. Initial protein kindly provided by Dr Page (Glasgow University). Also was provided as fusion protein (from the same source) which was then cleaved and purified in house.

4. FKBP-12

FKBP-12 was obtained from two different sources. Initial protein provided by Sandoz and later on from Dr. Villafranca (Agouron pharmaceuticals INC USA).

B) Crystallization and crystal handling

1. Crystallization by vapour diffusion

The principle of vapour diffusion crystallization is that a droplet containing protein, buffer, crystallizing agent, and additives, is equilibrated against a reservoir (mother liquor) containing a solution of crystallizing agent at higher concentration than the droplet. Equilibration takes place by diffusion of the volatile contents (water or organic substance) until vapour pressure in the droplet reaches that of the reservoir.

The hanging drop technique was used in all crystallization experiments in this work. A 1:1 ratio between the mother liquor and the protein solution was used to set up the drop. The volume of the reservoir was 0.5 or 1 ml and the droplet between 2 to 10 μ l. Commercially available Linbro boxes are used in all experiments for crystallization.

2. Screening

Three different approach have been used

1. Screening with common precipitants like PEG (polyethylene glycol) 4000 PEG 8000 and AS (ammonium sulphate).
2. Published conditions
3. Using Hampton Research screening solutions. Crystal screen formulation kit (Jancarik & Kim 1991) and crystal screen 2 formulation kit (Cudney et al 1994) were used. The protocols utilized in these two kits evaluates 98 unique

combinations of pH, additives, precipitant.

The initial drop volume was usually 2 μ l (or even less when not much protein was available). Once crystallization conditions were found, the drop size was increased (6 to 10 μ l) to obtain larger crystals.

3. Seeding

A seed crystal provides the nucleation for the assembly of molecules to form a crystal with the same characteristics as the crystal from which the seed originated.

Streak seeding was performed with a glass needle. The end of the needle was used to touch an existing crystal and dislodge seeds from it. A glass needle was then used immediately to introduce seeds into several (3 to 5) other pre-equilibrated drops by running the probe across the drops.

In macroseeding a single crystal, which was free from twinning or any other crystallites, was picked up into a glass capillary. The crystal then was washed in mother liquor twice to insure that any microseeds or unwanted nuclei has been washed out. Finally the crystal was transferred to a suitably pre-equilibrated solution.

4. Soaking

A native, well diffracting crystal is introduced to a solution containing the appropriate ligand concentration.

There are three requirements for this operation.

- The crystal can stand in the soaking solution without cracking or dissolving
- The ligand should be small enough to go through solvent channels in the crystal lattice and access the active site.
- The binding site is unoccupied.

The soaking technique has the advantage of reducing the complexity of the crystallographic problem to that of determining the position of the newly introduced atoms by difference Fourier methods. Also screening for crystallization conditions for the protein-ligand complex is not required unlike co-crystallization.

A) Soaking ligands into Cyp-A crystals

The crystal was picked up using a glass capillary (0.3-0.5 mm diameter). As the crystals were grown in presence of DMSO, which binds in the active site of the protein (see chapter 5), the DMSO was soaked out before any soaking experiment. In a typical experiment a single crystal of CyP-A was soaked for 30 min in a solution which was the same as the precipitating solution in the well but less DMSO (4 % v/v) and including 5 mM ligand (substance). This soaking procedure was repeated a total of 6 times. In each soaking step the DMSO concentration was decreased eventually to 0 % (v/v) and the ligand concentration was gradually increased to the maximum allowed by solubility.

The crystal was soaked for approximately 30 min in each step. For example when ACMPIP ligand (see Table 5.3) was soaked into a Cyp-A crystal the soaking took place in six steps as follows:

Steps	Time of soaking in hours	Soaking Solution (mM)	
		Concentration of ACMPIP	DMSO
1	0.5	5	560
2	0.5	10	230
3	0.5	20	100
4	0.5	40	40
5	0.5	100	20
6	1.5	150	0
Final solution			

The time in the final solution (DMSO 0 %) ranged from 30 min to 2 days and depended on how well the crystal behaved in the soaking conditions. The ligand concentrations ranged between 40mM and 400mM.

Finally the crystal was soaked in cryoprotectant solution before mounting. The ligand concentration was kept the same in cryoprotectant solution as in its final soaking solution in order to eliminate any chance of the ligand being washed out (despite the fact that the crystal was soaked in cryoprotectant solution only for couple of seconds). The cryoprotectant solution had the same composition as the final soaking solution plus glycerol (see chapter 5 Table 5.1). All ligand complexes in this work were made by soaking except the Cyp-A DMSO complex which was made by co-crystallization.

B) Soaking ligands into FKBP-12 crystals

The same procedure for the cyclophilin crystals was followed with FKBP-12 crystals.

C) Soaking ligands into BrCyp crystals

Since the BrCyp binding site is occupied only by water two soaking steps were used which gradually increased the concentration of the ligand to 200 mM.

5. Co-crystallization

The size and the configuration of the channels within the crystalline lattice determine the maximum size of the solute molecules that may diffuse into the crystal. In the case where a complex with a relatively 'big' molecule is required, co-crystallisation is the only method to obtain it.

In co-crystallization, the formation of the complex does not have to contend with lattice forces, but the solubility and the conformation of the complex may be sufficiently different from that of the native molecule to prevent the formation of isomorphous crystals. As a result, the conditions for crystal growth of a protein-ligand complex need not necessarily be the same as the native one and screening of crystallization conditions is indispensable. This was the main reason that the method was not used as much as soaking in order to make protein-ligand complexes. Nevertheless complexes can however grow crystals that are isomorphous with the native crystals (Stura et al 1987). The conditions in which native Cyp-A, FKBP-12 and BrCyp crystallize were known and were the first conditions tried out in every co-crystallization trial.

In the co-crystallization of protein ligand complexes, the droplet contains additionally a ligand which binds, or is expected to bind, to the protein. The ligand concentration in the drop was 3 times more than the K_d value. If the ligand is volatile the mother liquor contains the ligand in a concentration double that in the drop. If the K_d was unknown then a concentration in the range of mM was used, provided the ligand was sufficiently soluble. If the ligand could not be dissolved to mM concentration then a saturated solution was used.

5.3 Results

TABLE 5.1 Crystals forms of FKBP, Cyp-A, and BrCyp

Protein	FKBP-12	Cyp-A	BrCyp	
Precipitants	AS	PEG8000	PEG4000	AS
Buffer pH	Tris pH 8.0	Tris pH 8.0	Tris pH 7.4	imidazole pH 6.5
Space group	C2	P2 ₁ 2 ₁ 2 ₁	P3 ₁ 2 ₁ 2.	P4 ₁ 2 ₁ 2.
a, b, c (Å)	102.7, 36.4 55.7	36.2, 57.6, 70.2	88.9, 88.9, 106.4	58.1, 58.1, 141.7
α , β , γ (deg)	90, 96.2, 90	90, 90, 90	90, 90, 120	90, 90, 90

1. Crystallization of native cyclophilin A, cyclophilin B, FKBP-12 in forms suitable for soaking experiments with novel ligands

A) Cyclophilin A

1. Crystallization

The vapour diffusion method was used to grow crystals of CyP A (Ducruix and Giegé, 1990). The precipitating solution in the well consisted of 100mM Tris HCl (pH 8.0), 19 % (w/v) PEG 8000, 5% (v/v) DMSO, 0.02% NaN₃. The hanging drop consisted of 50mM Tris HCl (pH 8.0), 9.5% (w/v) PEG 8000, 2.50% DMSO, 40 mM NaCl, 0.02% NaN₃, and 8.9mg/ml cyclophilin (Mikol, et al. 1993). The 1 ml precipitating solution was prepared by addition of 100 µl of Tris HCl 1 M (pH 8.0), 475 µl of 40 % (w/v) PEG 8000, 50 µl 100 % DMSO and 375 µl 0.02% (w/v) NaN₃. The initial 4µl drop consisted of 2 µl of the precipitant solution plus 2 µl of 17.8 mg/ml cyclophilin in 80 mM NaCl, Hepes 20 mM pH (7.4).

With the above conditions, crystals only grow at 25°C in in the drop solution (Mikol and Duc 1994). However our procedure (without the presence of CsA) yielded large, well formed, orthorhombic single crystals of native CyP A at 17 °C with dimensions of about 0.4mm x 0.2mm x 0.2mm (Fig 5.1 A to D). The drops that did not give crystals after 10 days were seeded by streak seeding which was found to give single crystals suitable for data collection but not reproducibly. By increasing the hanging drop size from 4 µl to 8 µl the crystal dimension could be increased to about 0.65 mm x 0.25 mm x 0.25 mm (Fig.5.1). The cell dimensions are a=36.2 Å, b=57.6 Å, c=70.2 Å, the space group is P2₁2₁2₁.

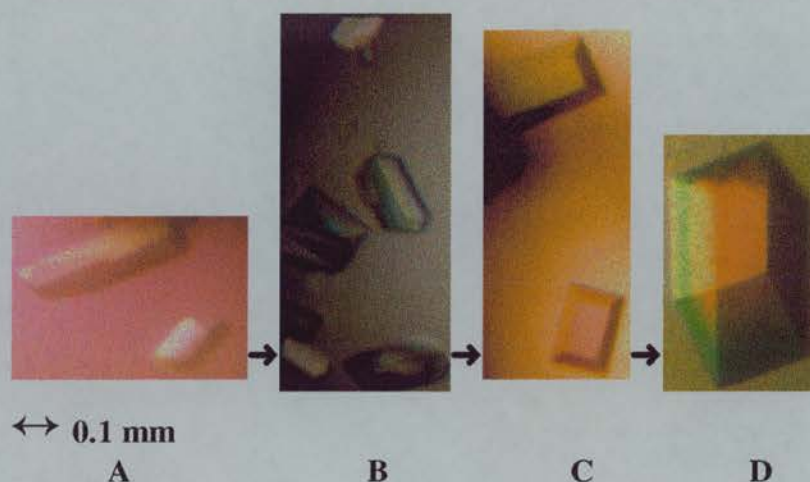


Fig 5.1: Improvement of quality and size in Cyp-A crystal during this work. Crystallization conditions shown in Table 5.2.

TABLE 5.2 Crystallization conditions for crystals shown in Figure 5.1. All crystal grow in 6, at 17 °C, Tris 100 mM pH 8.0, 2.5 % v/v DMSO, 40 mM NaCl and 7.8 protein and in PEG 8000 from 9.5 % to 11.5 % w/v as shown below.

Crystal	Protein (mg/ml)	Drop size (μ l)	PEG 8000 (w/v)
A	7.8	6	9.5
B	7.8	6	11.5
C	7.8	6	10.5
D	11	8	11

2. Co-crystallization

Co-crystallization was also used as a technique for crystallizing Cyp A/ligand complexes when large ligands were employed. The two novel ligands were N-CBZ-Ala-Pro (43 atoms MW=320) and N-Benzoyl-Phe-Ala-Pro (59 atoms MW=437.5). The crystallization conditions were the same as the native plus 1 mM N-CBZ-Ala-Pro or N-Benzoyl-Phe-Ala-Pro in the drop solution.

The above co-crystallization experiments however did not yield any crystals even after streak seeding with native crystals.

B) Cyclophilin B

1. Crystallization

The hanging drop method was used to grow crystal of CyP B (Ducruix and Giegé, 1990). The reported (Mikol, et al., 1994) conditions were used to grow crystal of CypB/CsA. The precipitating solution in the well consisted of 100mM Tris HCl (pH 8.0), 16 to 14 % (w/v) PEG 8000, 4 to 2%(v/v) DMSO, 0.02% NaN₃. The initial 4µl drop consisted of 50mM Tris HCl (pH 8.0), 8 to 9%(w/v) PEG 8000, 1 to 2 % DMSO, 0.02% NaN₃, and 8.9 mg/ml cyclophilin B. The 1 ml precipitating solution was prepared by addition of 100 µl of Tris HCl 1 M (pH 8.0), 375 µl to 400 µl of 40 % (w/v) PEG 8000, 40 µl 100 % DMSO and the volume made up to 1 ml with 0.02% (w/v) NaN₃ solution. The initial 6µl drop made up of 3 µl of 100mM Tris HCl (pH 8.0), 16 to 14 % (w/v) PEG 8000, in 0.02% NaN₃ solution plus 3 µl of 17.8 mg/ml cyclophilin, 0.5 mM CsA in 4% DMSO and Hepes 20 mM pH (7.4).

Crystals of CypB/CsA grew in the above conditions and were used for seeding. Seeding, however did not yield any crystals. A number of other crystallization trials were used, including screening in different PEG 8000 concentrations 14 to 25% w/v, pH from 7,4 to 8,2 and the variation of DMSO from 5 to 7% v/v. The crystal screen from Hamilton Research, containing fifty unique reagents, did not yield any crystals.

C) FKBP-12

1. Crystallization

The crystallization conditions for FKBP-12 were adopted from Burkhard, P., Ph.D Thesis (1995). The precipitating solution in the well consisted of 100mM Tris HCl (pH 8.0), 58 to 61% (w/v) AS_{sat} , 4 %(v/v) DMSO, 0.02% NaN₃. The initial 4µl drop

consisted of 50mM Tris HCl (pH 8.0), 29 to 30.5%(w/v) AS_{sat}, 2% DMSO, 0.02% NaN₃ and 7 to 9 mg/ml FKBP-12. The 1 ml precipitating solution was prepared by addition of 100 μ l of Tris HCl 1 M (pH 8.0), 580 μ l to 610 μ l of AS_{sat}, 40 μ l 100 % DMSO and the volume made up to 1 ml with 0.02% (w/v) NaN₃ solution. The initial 6 μ l drop consisted of 2 μ l of the precipitant solution plus 2 μ l of 14 to 18 mg/ml FKBP-12 in 0.02% (w/v) NaN₃.

Crystals grew within a week. This procedure yielded large, well formed crystals with space group C2 and dimensions of about 0.8mm x 0.22mm x 0.22mm. Increasing the size of the hanging drop from 6 μ l to 10 μ l gave crystal dimensions of about 1.0mm x 0.25mm x 0.25mm. The drops which did not grow crystals after 4 days were seeded by streak seeding but the technique produced only small crystals. Macroseeding was however successful. A single crystal (0.6mm x 0.2mm x 0.2mm) was transferred to another pre-equilibrated drop and the crystal size increased to 1.22mm x 0.25mm.

During the course of this work, other reported conditions for the growth of FKBP-12/ligands crystals were tried out. Screening took place in sodium citrate-cocodylate conditions (Tatlock et al 1995) and ammonium sulfate-hexanedion (Babine et al 1995). The above co-crystallization experiments did not however yield any crystals



Fig 5.2 .Results of streak seeding technique in FKBP-12



Fig 5.3. Crystal of FKBP-12 grew after macroseeing

2. Soaking

Cyclooctanone was shown to bind to FKBP by fluorescence studies (Burkhard, P., Ph.D Thesis). This ligand was added to a hanging drop containing crystals of FKBP to a concentration of 7.6 mM (maximum solubility). A single crystal (0.85mm x 0.22mm x 0.22mm) from this drop was selected after 2 hours. After 2 hours soaking, the crystals developed cracks. After two unsuccessful experiments it was decided that the soaking technique must be divided in two parts i) soaking in the same solution as the original drop but without DMSO (in order to remove DMSO from the crystal) and ii) soaking again in a new solution containing no DMSO, and 7.6mM cyclooctanone.

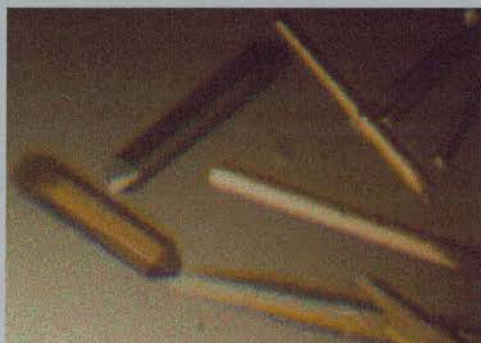
D) *Brugia malayi* Cyclophilin (BrCyp)

1. Crystallization

Two crystal forms of BrCyp were grown using the hanging drop method.

Trigonal form: The 4 μ l hanging drop consisted of 50 mM Tris/HCl at pH 7.4, 6.5 % w/v PEG 4000, 50mM ammonium acetate, 25 mM sodium acetate, 0.02 w/v NaN_3 , 0.4 mM BrCyp. The drop was suspended over a well containing 100mM Tris/HCl at pH 7.4, 13 % w/v PEG 4000, 100 mM ammonium acetate, 50mM sodium acetate, 0.02 w/v NaN_3 . The 1 ml precipitating solution was prepared by

addition of 200 μl of Tris/HCl 0.5 M (pH 7.4), 260 μl of 50 % (w/v) PEG 4000, 100 μl of 1 M ammonium acetate, 50 μl of 1 M sodium acetate and 390 μl of 0.02% (w/v) NaN_3 solution. The initial 6 μl drop was made up of 3 μl of well solution plus 3 μl of 0.8 mM BrCyp in Tris 20 mM pH (7.4). The crystals are trigonal with $a=b=88.9 \text{ \AA}$ and $c=106.4 \text{ \AA}$ and space group $P3_12_12$.



↔ 0.1 mm

Fig. 5.4: Crystals of BrCyp Trigonal form

Tetragonal form: The 3 μl hanging drop consisted of 50 mM imidazole at pH 6.5, 15% saturated ammonium sulphate, 0.02% w/v NaN_3 , and 0.38 mM BrCyp. The drop was suspended over a well containing 100 mM imidazole at pH 6.5, 30 % saturated ammonium sulphate, 0.02% w/v NaN_3 . The 1 ml precipitating solution was prepared by addition of 100 μl of imidazole 1 M (pH 6.5), 300 μl of saturated ammonium sulphate and 600 μl of 0.02% (w/v) NaN_3 solution. The initial 3 μl drop was made up of 1.5 μl of well solution plus 1.5 μl of 0.76 mM BrCyp in Tris 20 mM pH (7.4).

The crystals are tetragonal with $a=b=57.2 \text{ \AA}$ and $c=141.9 \text{ \AA}$ and space group $P4_12_12$.

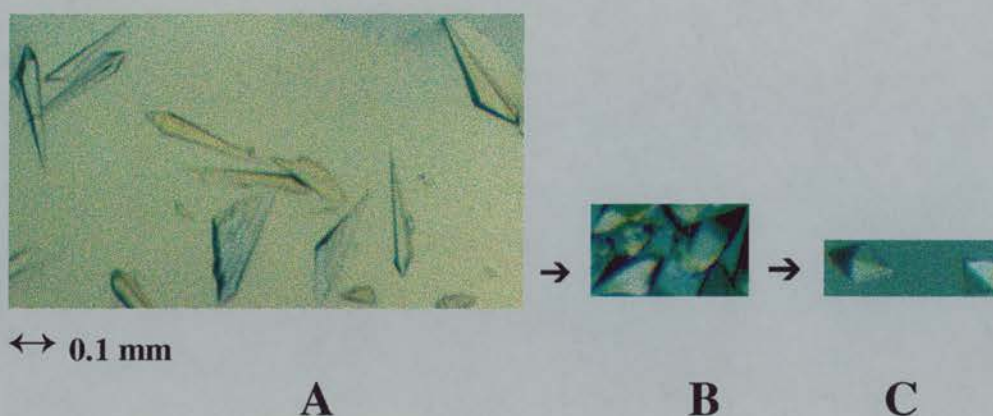


Fig. 5.5. Improvement of quality in BrCyp crystals Tetragonal form.

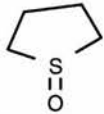

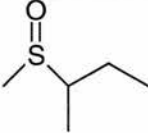

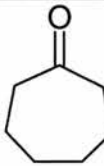
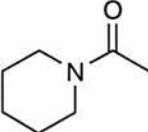
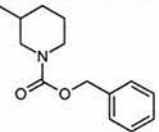
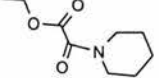
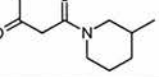
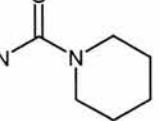
Crystals in Figure 5.5 **A** grew in a 3 μ l drop consisting of 50 mM imidazole at pH 6.5, 15% saturated ammonium sulphate, 0.02% w/v NaN_3 , and 0.38 mM BrCyp. Crystals in Figure 5.5 **B** grew in a 3 μ l drop consisting of 50 mM HEPES at pH 7.5, 15% saturated ammonium sulphate, 0.02% w/v NaN_3 , and 0.38 mM BrCyp. Crystals in Figure 5.5 **C** grew in a 3 μ l drop consisting of 50 mM Bis-Tris at pH 6.8, 15% saturated ammonium sulphate, 0.02% w/v NaN_3 , and 0.38 mM BrCyp.

2. Soaking

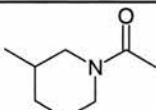
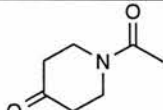
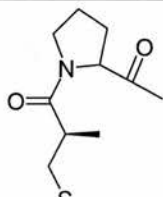
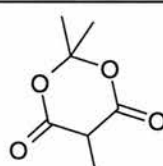
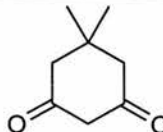
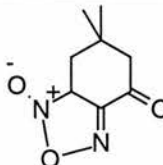
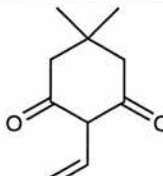
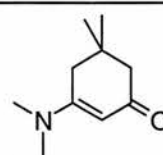
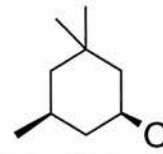
A) Soaking Cyclophilin A crystals

The last soaking step continued for 0.5 to 48 hours depending on how long the crystal can survive in the soaking solution. The above procedure was necessary because the DMSO bound in the active site of the Cyp-A. To introduce a new molecule in this binding site DMSO must first be washed out. The reason that the procedure was carried out gradually (6 steps) was to keep the ionic strength for each soaking solution about the same and this helped prevent the crystals from cracking.

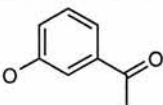
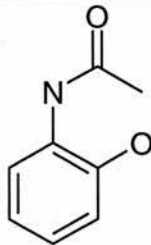
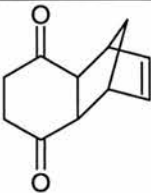
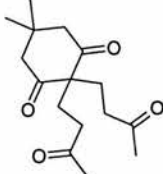
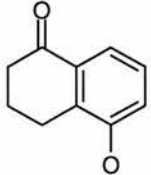
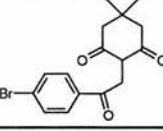
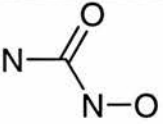
Table 5.3: List of ligands soaked into Cyclophilin A crystals

No	Ligand	Abbrev.	Formula	Final soaking conc. (mM)	Time of soaking in final conc. (h)
1	Tetramethylene sulfoxide	TMSO		180	24
2	Acetone	ACET		680	24
3	Sec-Butyl-methyl-sulfoxide	SBMS		600	20
4	Cyclopentanone	PNT		450	5
5	Cycloheptanone	CHPN		500	48
6	1-Acetyl-piperidine	ACPIP		800	20
7	3N-PMP	3N-PMP		200	24
8	Ethyl-1-Piperidineglyoxylate	ETPIPG		180	3
9	1-Acetoacetyl-3-methylpiperidine	AAMP		300	40
10	1-Piperidinecarboxamide	PCA		350	20

Crystallization

11	1-Acetyl-3-methyl-1- piperidine	ACMPIP		300	1.5
12	1-Acetyl-4-piperidone	APD		300	24
13	captopril [2S]-1-3[mercapto-2-methyl propionyl]-l-proline	CAP		150	3
14	2,2,5 trimethyl-1,1-dioxane-4,6-dione	TDD		30	1
15	5,5 Dimethyl-1,3-Cyclohexanedione	DCH		60	0.5
16	MENAI ST3567,3	ST3567		350	10
17	MENAI ST3267	ST3267		50	15
18	5,5 Dimethyl-3-aminodimethyl-2-cyclohexen-1-one	DAMC		350	24
19	cis-3,3,5-trimethyl-cyclohexanol	TCH		50	6

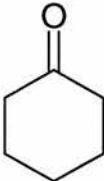
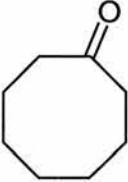
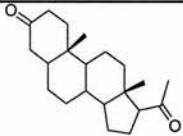
Crystallization

20	3-Hydroxyacetophenone	HAP		100	2
21	2-Acetamidophenol	AAP		60	4
22	1,4,4a,8a-Tetrahydro-endo-1,4-methanonaphthalene-5,8-dione	hmpd		50	3
23	CBZ	CBZ		40	30
24	5-hydroxy-1-tetralone	HTL		15	2
25	MENAI E298	E298		50	15
26	Hydroxyurea	HDUR		680	24

B) Soaking FKBP-12 crystals

The same technique as for Cyp-A was used. The soaking in pregnane took place in a solution containing 5 % v/v ethanol.

Table 5.4: List of ligands soaked into FKBP-12 crystals

No	Ligand	Abbrev.	Formula	Final soaking conc. (mM)	Time of soaking in final conc. (h)
1	Cyclohexanone	hex		10	2
	Cyclooctanone	oct_1		3.5	1
		oct_2		7	1
2	5-Beta-Pregnane-3,20-dione	prg_1		2	1
		prg_2		4	1

C) Soaking BrCyp crystals

The tetragonal crystal form was used. The crystal was transferred from the mother drop to a soaking solution containing 50 mM imidazole at pH 6.5, 15% saturated ammonium sulphate, 100mM ACMPIP (1-Acetyl-3-methyl piperidine) 0.02% w/v NaN₃. The soaking time was 1/2 hour after which the crystal started showing visible damage.

5.4 Discussion

Conditions under which a given protein is likely to crystallize can be found experimentally. These conditions then can be tested by screening in order to improve the size and the quality of the crystal. Further improvement can be carried out by different techniques like streak seeding and macroseeding.

FKBP crystals can be increased in size by macroseeding (Fig.5.3). Also the streak seeding technique seems to work well for this crystal form. Nevertheless the particular crystal form did not withstand different environments. As a result a lot of crystals were lost during soaking experiments. This was one of the reasons for screening different crystallization conditions.

The macroseeding technique did not seem to work so well for Cyp-A. Streak seeding worked quite well but not always. This could be explained by the fact that the surface of old crystals, specially when grown from polyethylene glycol, tends to become cross-linked (McRee 1993 page 6) and it is difficult to dislodge seeds from it.

The real improvement in crystal quality came after screening around starting conditions (Fig 5.1). As a result Cyp-A crystals (0.1 x 0.1 x 0.05 mm) collected at the home source diffracted to 1.7 Å (see X-ray diffraction data). Also the quality of the crystals allowed us to try different ligands at high concentration. This was one of main reasons for the success of the project. This also relates to the age of the crystal since old crystals may be more stable due to cross-linking (McRee 1993 page 6). Age of the protein may be an important factor in the success of cryoprotectant experiments also.

The starting conditions (crystallization results D1), for BrCyp trigonal form, yielded good quality crystals (Fig. 5.4). Streak seeding then was used to grow crystals in equilibrated drops around those conditions. This technique was used for all proteins

in the current work. Equilibrated drops which did not yield any crystals around the starting conditions, provided crystals after streak seeding.

The trigonal form of crystals turned into a gel after a period of four months. These crystals did not diffract any more and were unable to be used for seeding. It has been reported that light causes free radical chain reactions which cross-link and eventually destroy the crystal (McRee 1993) specially in polyethylene glycol solution. That was probably the case in trigonal form of BrCyp since the crystals were exposed to light and high polyethylene glycol concentration.

The conditions in which made tetragonal BrCyp crystals form were repeated on two occasions. The first attempt did not yield any crystals while on the second attempt crystals grew (Fig.5.5 A). The only difference between those two trials, was that the second time, the protein was used 3 to 4 days after purification. In the first crystallization trial the protein was used two weeks after purification.

6. X-ray Diffraction Data

6.1 Introduction

The home X-ray source (rotating anode) was used for most of the data collected during this work. A number of data sets were collected at the Synchrotron radiation source in Daresbury. The main advantage of the synchrotron source is, the higher intensity beam. An image plate was used in all data set as detector device during this work.

Since X-rays damage crystals, a flash-freezing technique had to be employed. Flash freezing is the technique of freezing crystals and data collection at cryogenic temperatures. The main advantages of the technique are minimisation of radiation damage (increase of lifetime of the crystal), reduction of background scatter (crystals mounted in capillaries scatter X-rays due to excess mother liquor and glass/quartz), often an increase in resolution limit (Garman, E. and Schneider, T., 1997) and long-term storage.

6.2 Material & Methods

1. Data Collection Strategy

High exposure time enables higher resolution data to be collected, but on the other hand may overload the low resolution data. A compromise between different parameters has to be made. The approach used was to collect a few images with different setting parameters and analyse the preliminary data. Two or three images were processed to determine crystal mosaicity. The parameters changed were size of the collimator, crystal distance from the detector, exposure time and rotation step size. The parameters are discussed further in section 2.C.

Reflections which are measured on different images, are called “partials,” in contrast to reflections fully recorded on a single image. Mosaicity is a measure of the order within a crystal. The DENZO (Otwinowski 1993) program used for processing the data can estimate this value using information about partially recorded reflections. Nevertheless the partially recorded reflections rely on scaling for accurate determination of the intensity. Therefore the rotation step was chosen such that it was slightly bigger than the mosaicity of the crystal in order to observe fully recorded reflections.

2. X-ray source

X-rays for diffraction analysis are typically produced either by a generator bombarding an anode with electrons from the cathode or by a synchrotron. Data sets were collected at the home source and at Daresbury SRS (Synchrotron Radiation Source).

The rotating anode generator is a widely used example of the first type of X-ray source. When in an evacuated chamber electrons travelling at high speeds from the cathode hit the outer edge of a fast rotating anode, a continuum of radiation (white radiation) is emitted due to collision of the electrons with the target. Anodes are made of metal and an incoming electron can ionise metal atoms of the anode by smashing through the outer electron shell and expelling an inner shell electron. When an electron from the outer shell moves to the inner shell to fill the gap, a “characteristic” radiation is emitted, depending on the initial and the final energy state of the electron. This radiation is anode material specific and presents itself as a few intense peaks in the emission spectrum at the wavelengths equivalent to the energy state difference between which the electron moved. To obtain a monochromatic beam all wavelengths save one of the characteristic wavelengths are removed by one or more monochromator crystals and the beam is focused by mirrors. The home source was a

CuK α rotating anode generator FR571 (Enraf Nonius) of the Department of Biochemistry (The University of Edinburgh) which emits at 1.5418 Å wavelength. The setup of the generator was as followed:

- The voltage was always set to 40kV
- The current was always set to 80mA
- Bias was 25 to 30 V
- Focal spot size was set to 0.3 x 3 mm

For X-ray diffraction experiments synchrotron radiation is far superior to the radiation generated by a rotating anode generator. Synchrotron radiation is far more intense, has a high degree of polarisation, and a wide range of wavelengths can be selected. It is emitted when very high-energy electrons travelling in an electron storage ring are accelerated. X-rays are emitted tangentially to the ring as nanosecond pulses with very high intensity and a continuous spectral distribution. The desired wavelength can be selected with similar tools as for the rotating anode radiation. Those data collected in Daresbury SRS came from stations 7.2 and 9.5 which had different wavelength. The wavelength used is given in Tables 6.2, 6.3 and 6.4 for each data set.

3. X-ray Detector

The requirements for X-ray area detectors become more strict when the molecular weights of the specimen of interest become larger and/or the crystal sizes available become smaller.

The most fundamental of the requirements for an X-ray area detector are high detective quantum efficiency, wide dynamic range, linearity of response, high spatial resolution, large active area and uniformity of response.

Developing technology has allowed fast and accurate data collection using an image plate. It has been shown experimentally that the image plate meets the above

requirements for X-ray detector in macromolecular crystallography (Amemiya, 1997).

All data were collected using a MAR 300 image plate (radius: 150mm, pixel size: 150x150 μ m). The image plate works in the following way:

- X-ray photons cause a chemical change in the plate coating.
- Image plate is scanned with light of a proper wavelength.
- Plate coating releases a fluorescence (due to the previous step) that is detected by a photomultiplier.

The output of the photomultiplier is amplified and converted to a digital image which can be processed by a computer. Image plates are erased by exposing to white light (and be ready for another exposure) so they must be protected from light after exposure.

4. Cryoprotection and Mounting

Cryoprotectants are employed to prevent the crystallization of water both within the crystal and within the surrounding solvent during freezing. A large number of compounds have been used successfully (Rodgers D., 1997) for the cryoprotection of macromolecular crystals. Glycerol was used in all flash freezing experiments in the present work. High glycerol concentration prevents formation of ice but can result in cracking or dissolution of the crystal.

For crystal mounting, a suitable loop (Cryoloops Hampton Research) is first selected. The size of the loop depends on the size, and the shape of the crystal. Loops were produced from fine fibres which are supported by a fine wire, which is itself attached to a steel base. The crystal is picked-up using the loop and transferred to the cryoprotectant solution where it is held for a few seconds. It is then picked up using the loop and plunged into liquid nitrogen. Immersed in liquid nitrogen the crystal

was taken to the mounting device in front of the detector and mounted on the goniometer head keeping the crystal in a stream of gaseous nitrogen cooled to 100K by the Cryostream cooler (Oxford Cryosystems).

For data collected at room temperature the crystal was mounted in a glass capillary.

5. Data reduction

The data were processed by the program Denzo (Otwinowski 1993). The program takes X-ray diffraction data and reduces it to a file containing the hkl index and background and LP corrected intensity of the spots (Gewirth 1995). The analysis and reduction of the diffraction data of a single crystal, takes place through seven major steps (Otwinowski and Minor1997):

- Visualisation and preliminary analysis of the original, unprocessed detector data.
- Indexing of the diffraction pattern.
- Refinement of the crystal and detector parameters.
- Integration of the diffraction maxima.
- Finding the relative scale factors between measurements.
- Precise refinement of crystal parameters using the whole data set.
- Merging and statistical analysis of the measurements related by space-group symmetry.

A) Visualisation of diffraction image

Before data processing, the first diffraction image is visualised, in order to accurately check that the detector is correctly positioned, check if spots are overlapping, measure the spot maxima and view the spot shape. The high resolution limit of

diffraction can also be estimated. If the spots are overlapping the rotation step may have to be changed or this indicates a twinned crystal. The spot maxima, should be always less than the saturation value of the pixels, and the exposure time should be reduced if they are not. Problems with the detector, spots overlapping and spots maxima should be discovered and corrected before the whole data set is collected.

B) Indexing of the diffraction pattern

The indexing program requires the crystal detector distance and the rotation step. The spot size was evaluated, at this stage, to be slightly bigger than the actual reflection size without overlapping the neighbouring reflection. The background size was chosen 0.1 mm larger than the spot size.

The indexing starts with a peak search. The peaks found are used for autoindexing the image. The results of autoindexing is a table containing the 14 Bravais lattices along with the amount of distortion the unit cell would suffer in order to fit the lattice. The lattice of higher symmetry and minimal distortion was chosen.

C) Refinement of the crystal and detector parameters

The crystal detector distance, unit cell dimensions, unit cell angles, Bravais lattice, detector centre respective to the X-ray beam and crystal orientation parameters determined from the indexing step above are used in this process. At this stage the crystal and detector parameters were refined in order to get accurate prediction of spot position and measurement of intensities. Both detector and crystal parameters can be fitted simultaneously by a fast-converging least squares method which minimises the deviation of the reflection centroids from their predicted position.

A good estimate of the crystal mosaicity can be evaluated at this stage. If the mosaicity value in the command file was lower, than that estimated from the

program, the new higher value was set and the processing program run again. Also if the number of rejected reflections was high the spot size was re-evaluated in this stage, in order to minimise this number.

DENZO also integrates the reflection intensity. Strong reflections can be used to determine profiles which are then applied to weak reflections. The average profile was fitted to the reflection as closely as possible and the area under the profile was counted as intensity. The area outside the profile was considered as background. The background was subtracted from the intensity to get the correct measurement. The output of the above process is a list of indices (hkl) for each reflection, an unscaled integrated intensity and an estimated standard deviation for the intensity.

D) Scale and merge of the integrated reflections

The scaling procedure puts all the reflections on the same intensity scale and a merging procedure finds reflections with symmetry related indices and merges their intensities together. Scaling and merging of the reflections is done by the program SCALEPACK. The χ^2 output values from the SCALEPACK were examined after each iteration. The χ^2 values should be close to 1 for all resolution shells. This was achieved by adjusting the estimated errors in the command file. A value of χ^2 close to 1 improves the accuracy of the estimated standard deviations for the intensities.

The mosaicity is determined accurately for each frame. The maximum mosaicity value was compared with that one used during data processing. If the determined value, was higher than the one used in the command file in processing program, the data were processed again using the new value.

A criterion of how well symmetry related reflections merge is the R_{merge} number.

$$R_{\text{merge}} = \frac{\sum_h |I - \langle I \rangle|}{\sum_h I}$$

I = the intensity of hkl reflection

$\langle I \rangle$ = average intensity of all reflections with same hkl

An $R_{\text{merge}} < 5\%$ reflects good data, values from 5% to 10% are regarded as acceptable, values above 10% required further investigation before use.

SCALEPACK is also used for space group determination when this was not known. The primary space group of that lattice type determined by DENZO was used first to scale the data. The next higher symmetry Laue group of the same Bravais lattice class was used and data scaled again. The χ^2 output values from the SCALEPACK was examined after each iteration. The χ^2 values and the systematic absences of each candidate space group was used for the determination of the space group. The candidate space group with the best χ^2 values and with appropriate systematic absences was chosen.

6. Ice removal

Crystals which during data collection developed ice were taken off the cryostream, plunged into liquid nitrogen and then transferred to the cryoprotectant solution, where they are held for a few seconds. They were then picked up using the loop and plunged into liquid nitrogen and mounted again. The data collection was continued. The above technique cleaned the crystal from any ice particles without destroying it.

7. Data Collection set-up

Size of collimator

The best results can be obtained when the whole crystal volume is illuminated. The size was chosen according to the largest crystal dimension, which was measured using a microscope. The size of the slits was varied between 0.1 and 0.4 mm.

Crystal distance from detector

The smaller detector to crystal distance allowed us to collect higher resolution data. The distance was chosen after visual inspection to be as short as possible to obtain the maximum resolution. Visual inspection determined the resolution limits and the distance at which overlap of the spots occurs.

Exposure time

Longer exposure times enable higher resolution data to be collected, but this also increases the background scatter. The exposure time was chosen depending on the crystal size, quality, and varied between 20 min to 30 min per rotation step for data which were collected in house. Data collected at the SRS had exposure times which varied between 60 to 120 seconds.

Rotation step

If the rotation increases, the spots at some point will start overlapping. This will affect first the high resolution spots at the edge of the image. The maximum rotation angle in degrees can be estimated from the formula $\Delta\phi=57.3\cdot(d/a)$ where d is the resolution limit and a is the cell dimension (Dauter 1997). This formula does not take into account the effect of crystal mosaicity and beam divergence. Another limit to the rotation is the amount of background that can be tolerated.

A small step size allows the reflection profile to be determined more exactly (McRee

1990). The minimum rotation step size was chosen regardless of mosaicity of the crystal and the available beam time. The rotation step was each time slightly bigger than the mosaicity of the crystal. The rotation step was from 1° to 2° degrees.

6.3 Results

1. Cryoprotection

High glycerol concentration prevents formation of ice rings but can result in cracking or dissolution of the crystal. The correct concentration of glycerol for each particular system was found by trial and error. All the cryoprotectant solutions contained between 26 and 30 % v/v glycerol. The cryoprotectant solution contained the ligand in the same concentration as the last soaking solution (see crystallization chapter). The cryoprotectant solutions were as follows:

Table 6.1: Cryoprotectan solutions used in the current work.

Protein	Cryoprotectan solutions
FKBP-12	61% (w/v) AS _{sat} 29 % (v/v) glycerol ligand in X concentration * 0.02% NaN ₃
Cyp-A	100mM Tris HCl (pH 8.0) 21 %(w/v) PEG 8000 26 % (v/v) glycerol ligand in X concentration * 0.02% NaN ₃ .
Cyp-B	100mM Tris HCl (pH 8.0) 16 %(w/v) PEG 8000 26 % (v/v) glycerol 0.02% NaN ₃ .
BrCyp (trigonal form)	100mM Tris/HCl pH 7.4 13 % w/v PEG 4000 100mM ammonium acetate 50mM sodium acetate 30 % (v/v) glycerol 0.02 w/v NaN ₃ .
BrCyp (tetrgonal form)	100 mM imidazone pH 6.5 30% AS _{sat} 30 % (v/v) glycerol 0.02% w/v NaN ₃

* For ligand concentrations see Table 4.3 and 4.4.

2. Data collection

The following tables contain statistics for the different data sets. In total 45 data sets have been collected of three different proteins (CypA, FKPB12 and BrCyp). Where data sets were collected in Daresbury (SRS) the wavelength is given. The low resolution limits vary from 17 to 24 Å. The last column of each of the following tables contains mosaicity values which were obtained after scaling the data.

A) CypA

All cyclophilin data sets were collected at 100°K except PG data which collected at room temperature. In total 36 data sets have been collected (Table 6.2), in Daresbury SRS or in home source and all belonging to space group $P2_12_12_1$. Some data were collected from the same crystal at the home source and in Daresbury therefore a comparison between them is more reliable.

DMSO data sets of resolutions 1.8 Å, 1.8 Å and 1.7 Å, were collected from different crystals. The DMSO data at 1.8 Å resolution collected in Daresbury SRS ($\lambda=0.9$ Å) had a very low R_{merge} and relatively high completeness. This data set should be considered as the best.

Table 6.2: Statistics for the cyclophilin A data collection. All crystals belong to space group $P2_12_12_1$ with $\alpha=90^\circ$ $\beta=90^\circ$ and $\gamma=90^\circ$.

Ligand Resol.	Total Refl.	Unique Refl	Source	a b c (Å)	Dist. (mm) D θ (deg)	R _{mer}	Completeness	Mosaic.
DMSO 1.8 Å	76436	12909	Daresbury SRS (0.9 Å)	36.22 56.65 70.05	270 1.5	4.5	92.7	0.25°
1.8 Å	105536	13951	Daresbury SRS (1.488 Å)	36.16 56.54 70.33	120 1	5.4	98.8	0.85°
1.73 Å	109648	15672	home	36.23 56.60 70.07	110 1	6.9	99.5	0.4°
PG 2.25 Å	43662	10170	home	42.83 52.65 89.08	175 2	10. 6	95.2	0.8°
TMSO 1.78 Å	72135	14433	home	36.24 56.65 70.00	120 1	5.4	94.2	0.4°
ACET 1.7 Å	117109	16376	home	36.13 56.43 69.98	105 1	5.3	95.2	0.37°
SBMS 1.9 Å	106733	11806	home	36.04 56.44 70.03	130 1	7.8	99.1	0.73°
PNT 1.8 Å	127103	13931	home	36.16 56.76 69.94	120 1	6.3	98.7	0.59°
CHPN 1.8 Å	104446	14072	home	36.25 56.84 70.18	120 1.25	6.1	97.4	0.5°
3N-PMP 1.79 Å	150829	14256	home	36.23 56.80 70.16	120 1	7.1	99	0.35°
ETPIPG 2.05 Å	116400	9327	home	36.26 54.54 70.90	150 1	5.1	98.9	0.84°
ETPIPGd1 1.65 Å	56745	17735	Daresbury SRS	36.26 54.54	109	3.5	53.7	0.7°

X-ray Diffraction Data

			(1.488 Å)	71.10	2.0			
ETPIPGdl2 1.65 Å	68571	17641	Daresbury SRS (1.488 Å)	36.26 54.54 71.10	109 1.5	3.9	75	0.5°
AAMP 1.8 Å	92660	13886	home	36.09 56.41 70.05	120 1.25	6	99	0.5°
ACMPIP 1.8 Å	103411	13522	home	36.08 54.31 70.97	120 1	5.9	98.7	0.5°
PCA 1.8 Å	63373	13837	home	36.12 56.30 70.10	120 1.5	9.5	83.2	1.02°
APD 1.8 Å	60468	14149	Daresbury SRS (0.9 Å)	36.36 56.87 70.39	270 1.5	11. 1	87.1	0.47°
CAP 1.79 Å	129344	14177	home	36.18 56.60 70.07	120 1	4.7	99.7	0.37°
1.8 Å	157286	13816	home	36.39 55.07 70.93	120 1.25	4.9	97.1	1.14°
TDD 1.78 Å	94720	14523	home	36.26 57.06 69.89	120 1.25	5.0	98.6	0.3°
DCH 1.78 Å	141509	14540	home	36.24 57.20 69.86	120 1.5	5.7	94.6	1.02°
ST3567 1.8 Å	101747	14024	home	36.23 56.79 70.16	120 1	7.9	97.7	0.38°
DAMC 1.7 Å	126301	16511	home	36.17 56.56 70.28	105 1.25	5.0	99.5	0.5°
TCH 1.8 Å	124633	14046	home	36.34 56.58 70.32	105 1.25	7.2	92.9	0.85°
1.86 Å	65942	12788	Daresbury SRS (1.488 Å)	36.28 56.62 70.47	138 2	6.1	94.3	0.43°
ST3267 1.7 Å	133583	12043	home	35.98 55.77 70.07	130 1.25	10. 2	98.1	1.09°
HDUR 1.8 Å	134190	13975	home	36.22 56.57 70.24	120 1.25	6.9	98.1	0.75°

ACPIP 1.75 Å	124098	15143	home	36.11 56.60 70.20	110 1	5.2	99.2	0.64°
CHX 2.05 Å	106534	9326	home	35.92 56.00 69.66	150 1.5	5.7	80.5	1.8°
HTL 1.8 Å	157382	13851	home	36.18 56.36 69.96	120 1	6.6	99.8	0.73°
HAP 1.79 Å	109415	14374	home	36.30 56.81 70.52	120 1	3.3	92.2	0.85°
AAP 1.79 Å	114708	14275	home	36.30 56.70 70.17	120 1	5	96.9	0.8°
hmpd 1.82 Å	93224	13537	home	36.23 56.59 70.16	125 1	8.5	97.3	0.54°
CBZ 1.8 Å	49050	14029	home	36.19 56.84 70.18	110 1	5.5	73.3	0.75°
E298 1.8 Å	88190	13908	home	36.14 56.48 70.15	120 1.25	7.8	94.3	0.51°
E298dl 1.8 Å	101492	13988	Daresbury SRS (1.488)	36.23 56.54 70.35	119 2	9.7	94.8	0.91°

TCH data to 1.8 and 1.86 Å from Table 6.2 were collected from the same crystal so any comparison can be regarded as reliable. Even when the TCH data was collected on the home source processed and scaled to 1.86 Å resolution the R_{merge} was 7.0 % compared to 6.1 % for the synchrotron using all data. Clearly from those data sets, the one that was collected in Daresbury SRS (1.488 Å) was better.

The TCH crystal developed ice during data collection and was taken off and the ice removal method was performed (see material and method in this chapter). The ice was removed and the mosaicity was improved after the procedure. The technique was repeated a further two times during data collection. The reduction of the mosaicity is given in Table 6.3.

Table 6.3. Changes of the crystal mosaicity after numbers of flash cooling in TCH crystal.

Times of flash cooling	1	2	3
Average mosaicity	0.85	0.63	0.41

Data set ETPIPG was collected to 2.05 Å. The resolution of the data was improved when the same crystal was collected at Daresbury SRS ($\lambda=1.488$ Å). Two data sets were collected, ETPIPGd11 (110 degrees rotation) and ETPIPGd12 (90 degrees rotation). The first data set in Daresbury (ETPIPGd11) was collected at 2 degrees per image due to lack of time. Later during data processing it was found that lot of spots overlapped so another data set was collected (ETPIPGd12) at 1.5 degrees per image. Both data sets had low completeness due to ice developing in the crystal. The completeness, calculated by program SCALEPACK, in resolution zone 1.78 to 1.74 Å for example was 89 % for ETPIPGd12 nevertheless the total completeness was 75 %. The completeness of ETPIPGd11 was worse than that of ETPIPGd12, despite the fact that 110 degrees data set were collected compared with 90 degrees in ETPIPGd12.

Since none of the data collected in Daresbury SRS was complete enough to use for structure determination, data sets of ETPIPG, ETPIPGd11 and ETPIPGd12 were merged together using the program Scalepack. The completeness of the merged data was 90.4 % for the whole data set of 24 to 1.65 Å and the R_{merge} was 4 % for the whole data set in the same range.

B) FKBP

In total five data sets of FKBP-12 crystals have been collected. Data oct_1 and oct_2 in Table 6.4 were collected at room temperature. All other FKBP-12 data sets were collected at 100°K. The R_{merge} of the data collected at room temperature appeared to be worse than those collected at 100°K. The unit cell volume of **oct_1** was 205519 (Å)³ when for **hex it** was 200631 (Å)³.

Table 6.4: Statistics for the FKBP-12 data collection. (see also Table 5.3 in chapter 5 for details about soaking time)

Ligand	Total Refl.	Unique Refl	Source	Distance (mm)	R_{merge} (%)	Comple. (%)	Mosaic.
Resol.				Dθ (deg)			
oct_2 2.05 Å	76172	13104	home	150 1.5	7.8	96.8	0.78°
oct_1 1.8 Å	103721	19441	home	120 1	8.3	97.2	0.67°
prg1 2.05 Å	63951	12611	home	125 2	5.6	86.1	2.02°
hex 1.8 Å	138921	18980	home	110 1	6.9	83.3	1.13°

C) BrCyp

Four data sets of BrCyp crystal have been collected belonging to two different space groups (Table 6.5). Any comparison of trigonal data sets in Table 6.5 collected at home and at Daresbury SRS (1.488 Å) can be reliable since both came from the same crystal. The same applied to the tetragonal form. The mosaicity from data sets collected in Daresbury was lower than that from home for both tetragonal and trigonal forms as shown in Table 6.4. The R_{merge} also was lower for both data sets from

Daresbury.

Table 6.5: Statistics for the Cyclophilin *Brugia* data collections

Crystal Form	Total Refl.	Unique Refl	Source	Distance (mm)	R_{merge} (%)	Compet. (%)	Mosaicity
Resolution				Dθ (deg)			
Tetragonal 2.8 Å	37494	6508	Home	200	10.2	95.2	0.54°
				1.5			
Tetragonal 1.95 Å	103228	18657	Daresbury SRS (1.488 Å)	138	9.2	96.9	0.46°
				1.5			
Trigonal 2.57 Å	117993	15883	Home	210	9.9	98.4	0.45°
				1			
Trigonal 1.9 Å	206863	38706	Daresbury SRS (1.488 Å)	240	6.3	99.7	0.4°
				2.0			

6.4 Discussion

From the statistics given in Tables 6.2 it is clear that crystal parameters (R_{merge} , Mosaicity), of the same protein, grown in the same conditions can vary significantly. Comparison of data sets collected from the same crystal are more similar compared to those derived from different crystals. Thus only data collected on the home and at SRS from the same crystal, are compared and discussed in this chapter.

Data sets collected on the home source and at Daresbury SRS of BrCyp crystals confirms that those collected in Daresbury SRS have better R_{merge} and mosaicity (Table 6.4). The smaller mosaicity reflects the smaller beam divergence of Daresbury SRS beam. When the mosaicity is low, more spots can be collected in one image without overlapping. Also the more intense synchrotron beam results in a higher

intensity of the recorded spots, which affect the accuracy of the measurements. Accurate measurement of spots gives better R_{merge} for the same crystal. The data set collected on the home source had an $R_{\text{merge}}=10.2$ and 9.9, when the SRS data had $R_{\text{merge}}=9.2$ and 6.3 for the tetragonal and the trigonal forms respectively.

In Cyp-A, data sets of TCH (Table 6.2) exhibited better R_{merge} values from the data sets collected in Daresbury SRS. The difference in the mosaicity of the data sets was partially because of the beam source and also because of the number of flash cooling cycles (Table 6.3) which took place. At the time which these results were observed no publication was available about the reduction of mosaicity due to rapid cycles of thawing and refreezing. The technique was reported for the first time as flash-annealing technique to improve diffraction limits and lower mosaicity on August of 1998 by Yeh and Hol (1998). Crystals of glycerol kinase were used by Yeh and Hol (1998) for studying the flash-annealing technique. In all of the crystals, resolution increased by 0.5 Å to 0.9 Å and mosaicity values decreased by between 0.4° to more than 1° in the best case. The mosaicity of the Cyp-A crystal decreased by 0.44° after two freeze-thaw cycles (0.22° after each cycle) tests to check whether increasing the annealing time and number of the cycles further affected the mosaicity were not performed. Nevertheless it has been reported by Yeh and Hol (1998) that optimizing the timing and the number of freeze-thaw cycles affects the result obtained.

Data sets ETPIPG, ETPIPGd11 and ETPIPGd12 (Table 6.2) were collected from the same crystal. These data sets are not directly comparable since the number of multiple observations between them is significantly different and this effects the R_{merge} .

7 Structure Determination

7.1 Introduction

Crystals are defined as solids with a regular repeated internal arrangement of atoms contained in a unit cell. The unit cell is a box defined by width, height and length and the three interaxial angles. Usually the longest axis is called c and the shortest a . The angle α is defined as the angle between b and c , β as the angle between a and c , and γ as the angle between a and b .

If each unit cell is replaced by a point, disregarding the actual atomic content of the unit cell, the crystal lattice is formed. The crystal lattice describes the repeated translations of unit cells in all dimensions to form the crystal. Another way to consider the crystal lattice is to see it as three intersecting sets of parallel planes. The three sets of plane can simply be defined by the Miller indices $h k l$. The number of times a set of parallel planes intersects unit cell axis a is the value of h . The value of k is the number of times this same set intersects b , and l is the number of times it intersects c . The three sets of planes describing the crystal lattice are therefore $(1 0 0)$, $(0 1 0)$, and $(0 0 1)$.

The crystal structure can also be described in terms of symmetry. The asymmetric unit is the smallest collection of atoms of a crystal structure from which the complete structure can be derived, first by use of point group symmetry operations, then by translational symmetry operations. Point groups are sets of symmetry elements which leave at least one point of the object, which they are applied to, unmoved. Examples are rotation axes, inversion centres, and mirror planes, which pass through or lie within the object.

The structure of a crystal can be determined from X-ray diffraction data. Each diffraction maximum has associated with it both an amplitude and a phase. The

phases are not directly measurable in a typical diffraction experiment and must therefore be estimated by indirect means. Three different methods can be used for phase determination, depending on knowledge of the protein structure:

- Multiple isomorphous replacement (MIR)
- Multiple wavelength anomalous diffraction (MAD)
- Molecular replacement (MR)

If nothing is known about the protein structure, the isomorphous replacement or the multiple wavelength anomalous diffraction method has to be used (Blundell and Johnson 1976). The MIR method depends on making isomorphous derivative crystals (with a heavy atom) of the macromolecule under investigation and estimation of phases from the differences between the amplitudes of native and derivative. The heavy atoms can be located in the unit cell, using the difference data of the native and the heavy atom crystals. At least two, and often more, derivatives are required for successful phase determination.

Isomorphous derivatives are also required for multiple wavelength anomalous diffraction (Wayne et al 1997) for reliable phase determination. The phase is determined using anomalous diffraction information which involves the measurement of diffraction data at different wavelengths and estimation of phases from the differences between the amplitudes of each wavelength.

When the structure of the protein or a similar structure exists, then the molecular replacement method (Brünger 1997) can be used to solve the phase problem. In this method, the homologous protein structure is fitted into the unit cell of the unknown structure and the phases are used as an initial guess of the unknown structure phases.

In this work the molecular replacement method was used to determine the structures of BrCyp and mainly difference Fourier techniques for the structures of Cyp-A and

FKBP-12. Structures with protein-ligand complexed are isomorphous with the native and difference Fourier techniques were used to solve the structures. The structure of BrCyp is homologous to Cyp-A, which was used as a probe during molecular replacement to solve the BrCyp structure.

The study of protein complex structures with “small molecules” requires high resolution data. At low resolution the configuration and the conformation of the ligand can not be determined accurately. Also at low resolution, electron density from water molecules could be mistaken for ligand density. All the protein complex structures that have been determined during this work had a resolution better than 1.9 Å.

7.2 Material & Methods

1. Molecular replacement

A frequent crystallographic problem arises when a known molecule exists in an unknown orientation in a crystal. Object A1 (protein target) and A2 a protein model (model), can be related by six rigid body parameters; three angles of rotation and three translational components.

In principle the correct position of the model (protein), in the new unit cell can be found by a trial and error using a six dimensional search. Every orientation and position of the previous molecule can be used. These positions then can be compared by calculating R factors.

The R factor is the agreement between the observed and the calculated amplitudes and can be used for estimating the error in the structure. It is usually the sum of the

difference between observed structure amplitudes $|F(hkl)|_o$, and calculated structure amplitudes $|F(hkl)|_c$ over the sum of the observed structure amplitudes (Glusker et al 1994).

$$R = \frac{\sum_{\text{all } hkl} \left| |F(hkl)|_o - |F(hkl)|_c \right|}{\sum_{\text{all } hkl} |F(hkl)|_o}$$

$|F(hkl)|$ is the structure factor amplitude of the scattered X-ray beam caused by $h k l$ set of planes.

If the positions of all atoms in the unit cell are known, e.g. from a model structure and the asymmetric unit content and spacegroup is known, then the structure factor amplitudes $|F_c(hkl)|$ and the corresponding phase angle α_{hkl} can be calculated:

$$|F_c(hkl)| = \left(\left(\sum_j [f_j \cos 2\pi(hx_j + ky_j + lz_j)] \right)^2 + \left(\sum_j [f_j \sin 2\pi(hx_j + ky_j + lz_j)] \right)^2 \right)^{1/2}$$

$$\alpha_{hkl} = \tan^{-1} \left[\frac{\sum_j [f_j \sin 2\pi(hx_j + ky_j + lz_j)]}{\sum_j [f_j \cos 2\pi(hx_j + ky_j + lz_j)]} \right]$$

f_j is the atomic scattering factor which gives the scattering power of an atom of an element j relative to the scattering power of a single electron modified by a factor describing the disorder or vibration the atom experiences in the crystal structure.

$$f_j = f_{j0} * e^{-B_j(\sin^2\theta/\lambda)}$$

f_{j0} atomic scattering factor for a stationary atom j

λ wavelength

θ scattering angle

$B_j = 8\pi^2 \langle u^2 \rangle$ the displacement parameter (B-factor)

$\langle u^2 \rangle$ isotropic mean square amplitude of atomic vibration

The Patterson function is

$$P(uvw) = 1/V \cdot \sum_h \sum_k \sum_l [|F_{hkl}|^2 \cdot \cos 2\pi(hu + kv + lw)]$$

The interatomic vectors which can be identified in the Patterson map (Glusker et al 1994) do not allow a localisation of atoms in the unit cell but the shorter intramolecular vectors can be used to find all orientations of the model structure in the unit cell. When the space group of the crystal is taken into account, the results of the *rotation search* can be narrowed down to the orientations to be found in the asymmetric unit.

Using only the longer interatomic vectors of the Patterson map the positions of the model in the unit cell can be identified in a *translation search*. The model atom coordinates thus obtained can then be used to calculate an electron density (F_o) map (Stout & Jensen):

$$\rho(x,y,z) = 1/V \cdot \sum_h \sum_k \sum_l [|F_o(hkl)| \cdot e^{-2\pi i \cdot (hx + ky + lz - \alpha' hkl)}$$

$|F_o(hkl)|$ structure factor amplitudes calculated from the
observed diffraction intensities

$$\alpha'_{hkl} = \{ \tan^{-1} [\sum_j [f_j \cdot \sin 2\pi(hx_j + ky_j + lz_j)] / \sum_j [f_j \cdot \cos 2\pi(hx_j + ky_j + lz_j)]] \} / 2\pi$$

x_j, y_j, z_j co-ordinates of model atom j

f_j atomic scattering factor of model atom j

2. Refinement

A) Adding water molecules

The water molecules can be located using difference Fourier, (Fo-Fc) maps which will show unaccounted density. The addition should be started with the largest peaks in the difference map. It is better to avoid adding too many waters too quickly (McRee 1993). The last place where water molecules were added was the binding site, and only if the shape of the difference electron density map indicated water molecules. The potential water molecule should make a hydrogen-bond with the protein with interatomic distance greater than 2.2 Å. The addition of water molecules was carried out by the program XPLOR (Bruenger 1992) or by SHELX (Sheldrick and Schneider 1997). Between one half and two ordered water molecules are found per residue in protein crystal structures (Levitt and Park 1993).

The addition procedure was as follows:

1. Calculation of a difference Fourier map (Fo-Fc)
2. Examination of local maxima with peaks higher than 3σ of the main electron density.
3. Addition of up to 15 water molecules if the electron density peaks were closer than 4 Å to the protein hydrogen bonding atom (N, O) but not closer than 2.2 Å.
4. Refinement of position and temperature factor of the new water molecules. If the temperature factor was higher than 70 \AA^2 the water molecule was removed from the model.

The occupancies of the water molecules were not refined. The addition of the water molecules was carried until the free R factor started to increase.

B) Addition of Ligands

When a ligand has been found to bind to the protein the correct conformation of the ligand has to be found and modelled into the density contour found for the ligand. Usually protein crystals do not diffract to such a high resolution and it is useful to have information about the conformation of the ligand from other sources. The conformation of small molecules can be found by experimental high resolution data which have been deposited in the CSD. Databases also were used for searching of available molecules which share structural similarities with ligands bound in proteins.

The databases used in the current work are described in chapter 1.

3. Evaluating errors of the model

When a structure has been solved by x-ray crystallography the geometry of the structure has to be examined. There are geometrical restraints on the possible values of torsion angles of proteins, so that many combinations are not possible (Glusker et al 1994). The same is also true for all angles between three atoms and bonds lengths. The structure must not only have a good R factor but a good geometry compared with other structures. The program PROCHECK (Laskowsky et al 1993) was used for the stereochemical parameter evaluation which was derived by Morris et al (1992). 118 protein reference structures were used to derive mean bond length and angle values with a resolution higher than 2.0 Å and an R factor less than 20 %.

A) Ramachandran Plot

The torsion angles of Φ (torsion angle about the C α -N bond) and Ψ (torsion angle about the C α -C(=O) bond) can not take all possible values. One evaluation criteria is

the plot of Φ against Ψ angles for each amino acid to give the Ramachandran Plot. Only certain combinations of Φ and Ψ angles are allowed. Glycine, which has only a hydrogen atom as the side chain, has more conformational flexibility, and hence variability in its torsional parameters. For a good quality model it is expected that 90 % of the residues have a conformation lying in the most favoured region of the Ramachandran Plot (Fig 7.2).

B) Ω , ζ and χ angles

The ω angle describes rotation about the peptide bond C(=O)-N. This angle should be near 180° for a normal *trans* peptide or 0° for a *cis* peptide. The ζ angle is a “virtual” torsion angle of C α -N-C-C β with a mean value around 34 degrees (Morris et al 1992). The χ is the torsion angle of the side chains (χ^1 is the torsion angle of N-C α -C β -C γ). These are denoted by χ^1 to χ^n working along the chain away from C α . The distribution of these angles are clustered and standard deviations could be calculated for the same 118 proteins structures (Laskowsky et al 1993). The standard deviations of the χ angles decrease with resolution, whereas standard deviations of ω and ζ angles are independent of the resolution (Fig 7.3).

C) Bad contacts and hydrogen bond energies

Bad contacts are defined as contacts where the distance of closest approach violates the van der Waals close contact criteria (Laskowsky et al 1993). When atoms are very close, this will give rise to high repulsive forces and this part of the structure should be re-examined. The hydrogen bond energies were calculated by the Kabsch and Sander (1983) method. The mean value of hydrogen bond energy is -2.03 (Kcal/mol) with standard deviation varying according to resolution of the model.

7. 3 Results

A) Cyp-A

1. Introduction

Three dimensional structures have been determined for the unligated human T cell CyP A (Ke et al., 1991; Ke, 1992) and for CyP A complexed with a proline-containing tetrapeptide (Kallen et al., 1991). CyP-A (165 residues) has 64% overall sequence identity with CyP-B (184 residues) and the overall structures of CyP-B and of CyP-A are similar; however significant differences occur in two loops and at the N and C termini (Mikol et al., 1994).

Human T cell CyP A is a water-soluble protein with a molecular weight of about 18,000 dalton (Harding et al. 1986). The main structural feature is an eight-stranded antiparallel β -barrel, which consists of two roughly perpendicular four-stranded β -sheets connected by short loops (Fig 7.1). The binding site for CsA is in a cleft on the surface of the barrel (Pflügl et al., 1994).

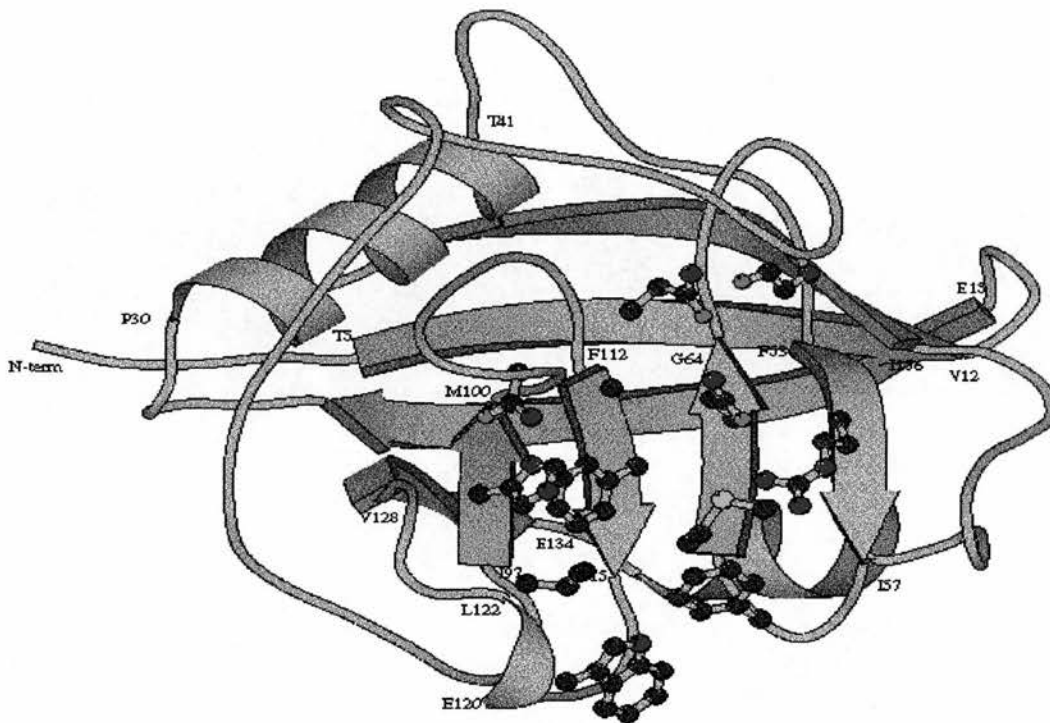


Fig. 7.1: X-ray structure of Cyp-A. Residues which interact with CsA are highlighted.

The three-dimensional structures of CsA by NMR showed that the bound CsA has a *trans* amide bond between MeLeu 9 and MeLeu10 (Fesik et al., 1990; Weber et al., 1991; Fesik et al., 1991), in comparison to *cis* configuration in the free crystal or in solution stage (Loosli et al., 1985). However, both structures of CyP A complexed with Ala-Pro (Ke et al., 1993) or with the tetrapeptide N-acetyl-Ala-Ala-Pro-Ala-amidomethylcoumarin (Kallen and Walkinshaw, 1992) showed that only the *cis* form of the substrate, binds to the enzyme. Both Ala-Pro and N-acetyl-Ala-Ala-Pro-Ala-amidomethylcoumarin bind to the same site and form either hydrophilic or hydrophobic interactions with Arg 55, Phe 60, Met 61, Gly 63, Ala 101, Asn 102, Phe 113, and Leu 122 (Ke et al, 1993; Kallen and Walkinshaw, 1992).

The structural comparison between CyPA-CsA and CyP-Ala-Pro suggests that CsA probably is not a transition state analogue of substrate. Also the two features of cyclophilin, its abilities to participate in immunosuppression and to catalyse peptidyl-

prolyl *cis*↔*trans* isomerization, are not structurally related and probably functionally unrelated.

The first non-peptide ligand for Cyp-A was found during this work. All the reported Cyp-A ligands before this work were peptides (Taylor et al 1997a). Of ligands found to bind to Cyp-A in this work some share structural similarities with the natural substrate of Cyp-A, Ala-Pro (piperidine family), another with the immunosuppressive drug CsA (dimedone) and some (DMSO family) have no similarity with known Cyp-A ligands.

2. Overview

Crystals grown in PEG8000 and DMSO were used for soaking in all ligands. The DMSO was soaked out of a crystal and this refined structure is referred to as native. The native structure was compared with the liganded and to the published structures. Evidence of ligand binding was the difference map made from the observed data and the native model.

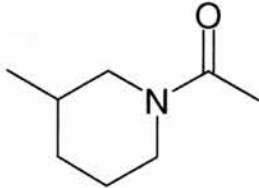
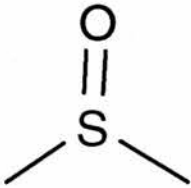
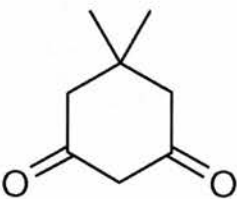
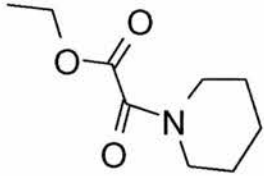
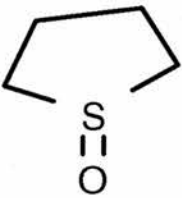
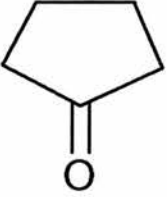
Six small ligands showed clear electron density in the binding site during refinement. The rest of the ligands, (see list of ligands soaked into Cyclophilin A crystal in Table 7.2) did not show any electron density in the binding site consistent with a bound ligand. So all those ligands are not discussed in the current work.

The six novel non-peptide cyclophilin ligands found during this work have been classified into 3 different families (Table 7.1). 3-Acetyl-1 methyl piperidine and ethyl-piperidine glyoxylate belong to the piperidine family and share structural similarities with a natural substrate of Cyp-A, the dipeptide Ala-Pro. Dimethyl sulfoxide (DMSO), tetramethylene sulfoxide and cyclopentanone form the DMSO family and they do not share any similarities with known Cyp-A ligands. Only one compound has been discovered in the third family. This compound 5,5-dimethyl-1,3-

cyclohexanedione also known as dimedone shows some structural similarities with the Val 11 residue of the Cyp-A ligand cyclosporin.

The refined structures of this work were compared to the published structures of CypA-CsA complex (**1cwa**) from Mikol et al (1993), cyclophilin Ala-Pro complex (**1cyh**) from Ke et al (1993) and unliganded Cyp-A (**2cpl**) from Ke (1992). The structure of the cyclophilin complex with Ala-Pro (1cyh) has been solved to a resolution 1.64 Å with an R factor of 19.6 %, the Cyp-CsA, complex (1cwa) has been solved to 2.1 Å with an R factor of 16.7 % and the native CypA from Ke et al (2cpl) to 1.63 Å with an R factor of 18 %. The Ala-Pro is a ligand similar in size with most of the ligands found during this work and is bound in the same active site. The CypA-CsA complex crystal was crystallized under the same conditions as used during this work. Also the Cyp-A structure of CypA-CsA complex was the one used initially during this work as a starting model.

Table 7.1: Families and members of novel cyclophilin A ligands

Piperidine family	DMSO family	Dimedone family
3-Acetyl-1 methyl piperidine (ACMPIP) 	Dimethyl sulfoxide (DMSO) 	5,5-dimethyl-1,3- cyclohexanedione (DCH) 
Ethyl-piperidine glyoxylate (ETPIPG) 	Tetramethylene sulfoxide (TMSO) 	
	Cyclopentanone (PNT) 	

The crystal form of Cyp-A in PEG8000 (space group $P2_12_12_1$, see chapter 5 Table 5.1) was used in all crystal structure determinations. Only the first structure solved during this work (DMSO) required a rotation and translation search and afterward the

Cyp-A coordinates of this structure were used as a model for the following data sets. The unit cell dimensions changed slightly from data set to data set and a translation search was necessary to locate exactly the molecule in the unit cell. Mainly the refinement was carried out with the program XPLOR and when no reference is given then XPLOR was used.

The structures of Cyp-A complexes have been solved with R factors less than 19 % for all of them (Table 7.2). The resolution of all structures is considered as high (<1.9 Å) which was essential for accurate determination of the configuration and the conformation of the ligand.

No sigma cut offs were applied and all the reflections were used for the refinement of the models except for 10 % of the reflections which were chosen randomly and not used in the refinement. These reflections were used for calculation of the free R factor.

Table 7.2: Refinement results for the Cyp-A complex structures

Cyp-A complex Structure	R factor	free R factor	Resolution range	water molecules per protein
Native	17.4	21.9	1.7-24 Å	192
DMSO	17.8	21.3	1.73-24 Å	187
TMSO	17.7	26.1	1.88-24 Å	266
PNT	18.6	24.3	1.8-24 Å	243
ETPIPG	18.8	22.8	1.65-24 Å	244
ACMPIP	17.8	23.1	1.8-24 Å	189
DCH	18.4	23.6	1.9-24 Å	231

3. Stereochemical quality of CypA-ligand complexes and comparison

The structures refined during this work were compared with published structures (1cwa, 1cyh and 2cpl see above). The Φ and Ψ angles of the above structures can be seen in Table 7.3. The disallowed residues in the 1cwa structure in Table 7.3 belong to CsA.

Table 7.3: Ramachandran plot values. Numbers show the percentage of Φ and Ψ angles found in each region defined in Figure 7.2.

Region	1cwa	1cyh	2cpl
most favoured (%)	83.9	88.0	87.2
additional allowed (%)	14.7	12.0	12.8
generously allowed (%)	0	0	0
disallowed (%)	1.4	0	0

The root mean square deviation (rmsd) from ideal bond lengths is between 0.006 and 0.007 Å and the rmsd from ideal angles is between 1.25° and 1.57° (Table 7.4). The conformation of the cyclophilin molecules in all the CypA/small-ligand structures are in general very similar with the native structure. A least squares fit on to the 562 C, N, C α and O main chain atoms of residues 2 to 164 of the native (unliganded) structure was carried out for all CypA/ small-ligand structures (Table 7.5).

Table 7.4: The root mean square deviation least (rmsd) from ideal bond lengths and angles for CypA complexes structures

Struct.	Native	DMSO	TMSO	PNT	ETPIPG	ACMPIP	DCH
bond lengths (rmsd) Å	0.007	0.006	0.006	0.007	0.007	0.007	0.007
angles (rmsd) °	1.321	1.279	1.291	1.567	1.302	1.252	1.306

An overlay of the native CypA (this work) with the 1cwa structure on C,N, C α and O main chain atoms of residues 2 to 67 and 76 to 164 was also carried out by least squares fit. The two structures are very similar with a (rmsd) of 0.271 Å. The “70 loop” was excluded because it has been reported to show atomic displacements of up to 1.7 Å for main-chain atoms for different cyclophilin structures (Kallen et al 1997).

Table 7.5: rmsd fit of CypA structures. Each structure was fitted onto the native structure. A least-squares fit was carried out using the C α , C, N and O atoms of the main chain of the cyclophilin residues 1 through 164.

Struct.	DMSO	TMSO	PNT	ETPIPG	ACMPIP	DCH
(rmsd) Å	0.097	0.314	0.088	0.188	0.175	0.149

A comparison of all cyclophilin structures solved during this work and those selected from the literature can be seen in Table 7.4. More, than 82 % of the Φ and Ψ angles, of the structures solved during this work, lay in the most favoured region and the rest in the additional allowed (Table 7.6). In Fig 7.2 the Ramachandran plot of the cyclophilin PNT complex is shown as a representative example.

PROCHECK

Ramachandran Plot

PNT

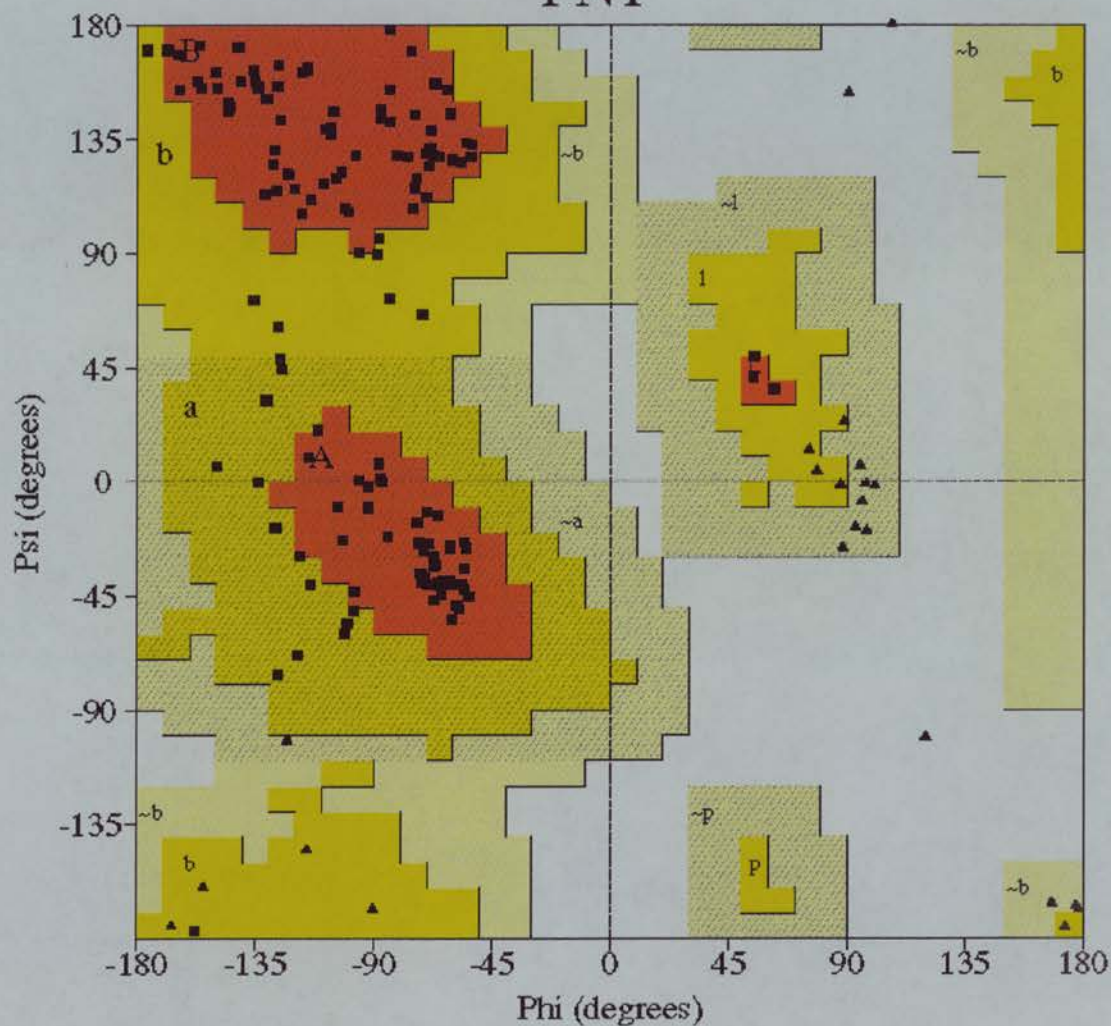


Fig.7.2: Ramachandan plot for Cyp-A complexed with PNT.

Glycine residues shows as ▲, non-glycine and non-proline residues shows as ■.

Plot statistics

	Residues	
Residues in the most favoured regions (A, B, C)	113	84.3%
Residues in additional allowed regions (a, b, l, p)	21	15.7 %
Residues in generously allowed regions (~a, ~b, ~l, ~p)	0	0.0 %
Residues in disallowed regions (white colour)	0	0.0 %

No generously allowed or disallowed values of Φ and Ψ angles were found for any structure. The values of Φ and Ψ angles have the same distribution (Table 7.4) for all structures with the best example the cyclophilin-ETPIPG complex. Comparing the structures in Table 7.3 with those of Table 7.4, the structures solved during this work have a comparable geometry with the 1cwa structure.

Table 7.6: Ramachandran plot values. Numbers shows the percentage of Φ and Ψ angles found in each region defined in Figure 7.2.

Region	Native	DMSO	TMSO	PNT	ETPIPG	ACMPIP	DCH
most favoured	83.6	84.3	85.1	84.3	85.8	84.3	82.8
additional allowed	16.4	14.9	16.4	15.7	14.2	15.7	17.2
generously allowed	0	0	0	0	0	0	0
disallowed	0	0	0	0	0	0	0

The main chain parameter values of refined structures and those from the published structures are given in Table 7.7. As a representative example of the geometric parameters of the main chain the CypA-PNT complex is shown (Fig 7.3). The bad contacts of TMSO and ACMPIP are genuine, due to the alternative conformations adopted by side chains of residue Glu₆₉ and Arg₅₅.

Table 7.7: Main chain parameter values. The typical value is the value (standard deviation) for all 118 protein reference structures. 1cwa is the CypA-CsA complex, 1cpl is the native and 1cyh the CypA complex with Ala-Pro.

Cyp-A complex Structure	Omega angle	Bad contacts	Zeta angle	H-bond energy
Typical value	6	RD	3.1	RD
Native	1.5	0	1.3	0.8
DMSO	1.5	0	1.3	0.7
TMSO	1.5	0.5	1.3	0.7
PNT	1.4	0	1.3	0.7
ETPIPG	1.7	0	1.4	0.8
ACMPIP	1.5	0.3	1.3	0.7
DCH	1.5	0	1.3	0.8
1cwa	4.2	8	5.8	0.7
1cyh	4.1	0	0.6	0.7
2cpl	4.3	2.4	0.6	0.7

RD = resolution dependant value (see Fig.7.3).

The bad contact is the contact of the side chain with itself in both cases and not with another residue. In general the small non-peptide ligand complexes have better stereochemistry of the main chain parameters than the three reference structures. The ω angle standard deviations are much better.

PROCHECK

Main-chain parameters

PNT

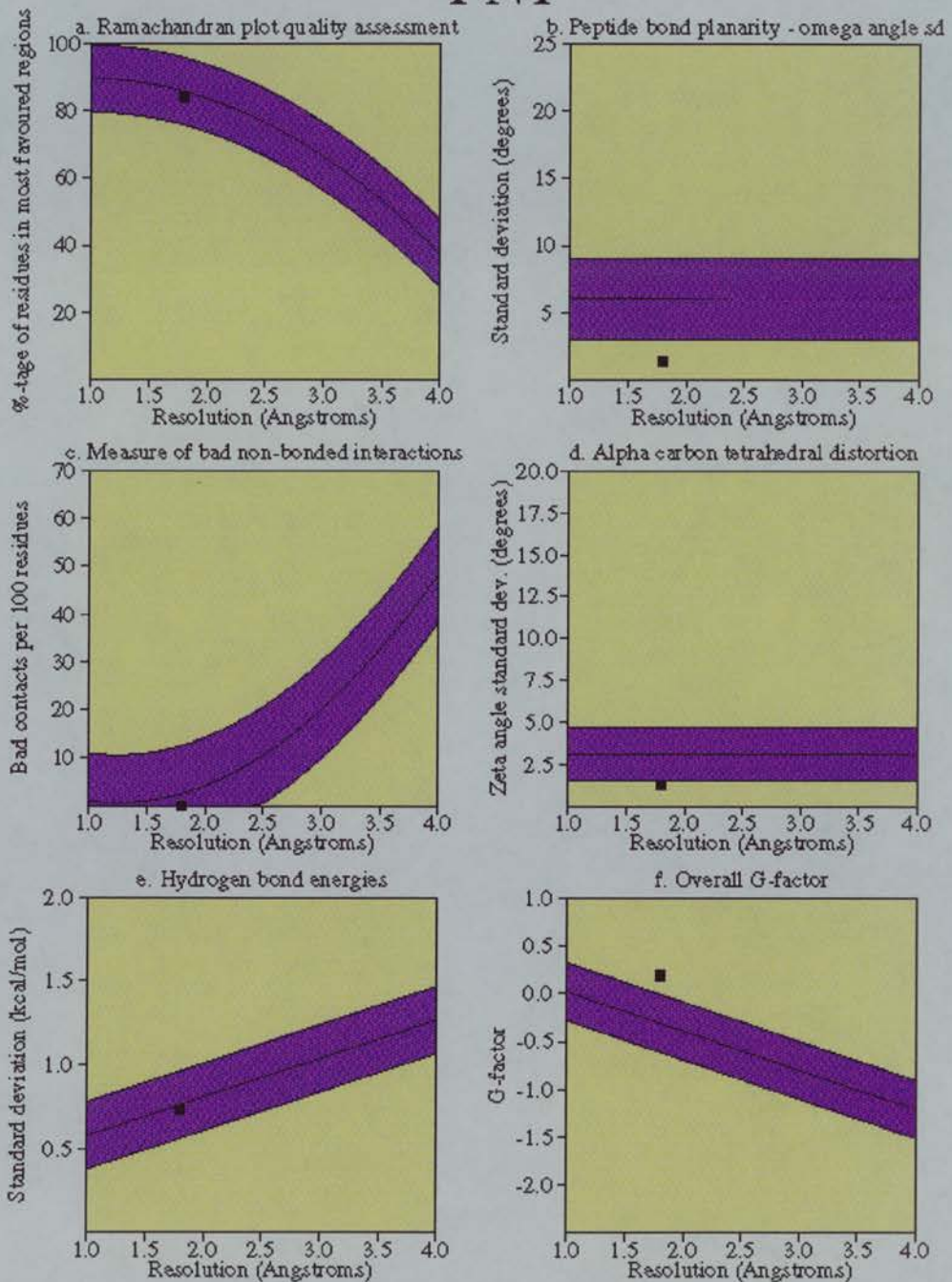


Fig 7.3: Statistical values of the main chain parameters for Cyp-A complexed with PNT. The typical value (magenta colour) is the value with band showing standard deviation for all 118 protein reference structures.

The quality of the side chains are given as standard deviations of the dihedral angles χ^1 and χ^2 (for definition of χ^1 and χ^2 see section 3). The structure of the cyclophilin PNT complex is shown as a representative example (Fig 7.3) of the structures refined during this work. In general the seven structures solved during this work have better stereochemistry of the side chain parameters than the three reference structures.

Table 7.8: Side chain parameter values. 1cwa is the CypA-CsA complex, 1cpl is the native and 1cyh the CypA complex with Ala-Pro.

Cyp-A complex Structure	Chi-1 gauche minus	Chi-1 trans	Chi-gauche plus	Chi-1 pooled	Chi-2 trans
Native	7.7	6.8	9.2	8.3	12.5
DMSO	7.4	9.3	9.7	9.1	10
TMSO	7.9	9.9	10.1	9.5	14.8
PNT	7.8	9.9	10.1	9.5	14.8
ETPIPG	8.2	10.9	9.9	9.9	14.6
ACMPIP	8.0	8.0	8.9	8.7	12.6
DCH	7.6	9.4	11.8	10.1	12.5
1cwa	8.5	12.1	10.5	10.7	14.6
1cyh	8	11.6	12.1	11.0	14.1
2cpl	6.3	10.1	10.5	9.2	14.1

4. Temperature factor evaluation and comparison

The mean values for the temperature factors of CypA complexes with the small ligands are summarised in Table 7.9. The temperature factor for the protein molecule are in the range from 10 Å² to 16 Å² in all small ligand complex structures and significant higher in the 1cyh and 2cpl structures (Table 7.9). This difference in the overall temperature factors could be an effect of the crystal packing, or the effect of cooling during data collection, or/and the effect of different refining procedures and programs.

Table 7.9: Overall temperature factors for CypA complexes (Å²). 1cwa is the CypA-CsA complex, 1cpl is the native and 1cyh the CypA complex with Ala-Pro.

In ETPIPG and TMSO structures the ligand adopts an alternate conformation.

Structure	Protein	Ligand	Solvent
Native	12.83	-	31.26
DMSO	10.85	32.87	23.91
TMSO	11.35	ALT1 37.6 ALT2 49.5	29.23
PNT	15.14	22.79	31.85
ETPIPG	15.93	ALT1 20.21 ALT2 23.27	29.11
ACMPIP	14.35	25.91	30.84
DCH	15.37	27.4	31.36
1cwa	13.11	15.88	29.65
1cyh	26.49	25.47	39.75
2cpl	27.13	-	47.51

The structure of CypA complexes with the small ligands were refined with the same program (XPLOR) following the same protocol. The first obvious explanation of the difference of the average temperature factor of protein atoms between CypA complexes with the small ligands and 1cyh and 2cpl structures is the effect of the cooling during the data collection (1cyh and 2cpl 293°K, CypA-small ligand 100°K).

The values of $V_M[\text{\AA}^3/\text{Da}]$ for 1cyh, 2cpl, 1cwa, and DMSO are 2.82, 2.12, 2.08 and 2.01 respectively. According to the above values the DMSO (all the small molecule CypA complexes have the same packing) has the closest packing followed by 1cwa 1cyh and 2cpl. Closer packing causes the atoms to be less mobile. The overall temperature factor of protein atoms for the above structures (Table 7.9) follows the same order was the V_M values.

The binding of a big ligand (1cwa) could be an additional explanation of the difference between overall temperature factor of protein atoms between 1cwa and 1cyh and 2cpl. 1cwa is the CypA-CsA complex, 1cpl is the native and 1cyh the CypA complex with Ala-Pro. The surrounding residues in the liganded structure are less mobile than the unliganded due to the contacts with the ligand. This is something observed also during this work (see section 4). Such an effect will be dependent on the size of the ligand and will be unlikely in a small size ligand (Ala-Pro, 1cyh) to have the same effect as a big ligand (CsA, 1cwa structure) in the overall temperature factor of protein atoms.

The overall temperature factor of protein atoms for the native structure (Table 7.9) is lower than the DCH complex. Nevertheless the binding site is more rigid due to ligand binding i.e the overall temperature factor for NH1, NH2, CZ and NE of Arg_55 for the native structure and DCH are 42.3 \AA^2 and 36.2 \AA^2 respectively. The same effect is observed in the DMSO structure where again the ligand makes contacts with Arg_55. The overall temperature factor of protein atoms in the DMSO structure is about 20 %

lower than the native but the overall temperature factor for NH1, NH2, CZ and NE of Arg_55 is about 26.9 \AA^2 , 60 % lower than the native.

5. Native structure (unliganded)

In the original conditions used to obtain cyclophilin crystals, the binding site was occupied by DMSO and all crystals used in the current work were crystallized in the presence of DMSO (crystallization conditions given in chapter 5). By soaking out the DMSO the binding site should be occupied only by water molecules. The availability of a good unliganded structure was essential since any indication of side chain movement and replaced water molecules due to the ligand binding was based on the comparison of the unliganded and liganded structures.

The coordinates of Cyp-A complexed with DMSO found in this work (R factor 17.8 %) were used as a starting model for a translation search in the native data. All atoms (except the ligand and the solvent) from the model structure were used in the search since the homology is 100%.

A translation search using XPLOR (Brünger 1992) was enough to locate the molecule in the unit cell. Data from 4 to 15 \AA were used during the translation search. The R factor for the model generated after the translation search was 33 %. The refinement proceeded with rigid body refinement as well as positional and individual B-factor refinement and the R factor dropped to 27 %. At that point the first difference electron density map ($1F_o - 1F_c$) was calculated and the binding site was inspected (Fig. 7.5). The electron density convincingly showed that only water molecules occupied the binding site and no trace of DMSO was present.

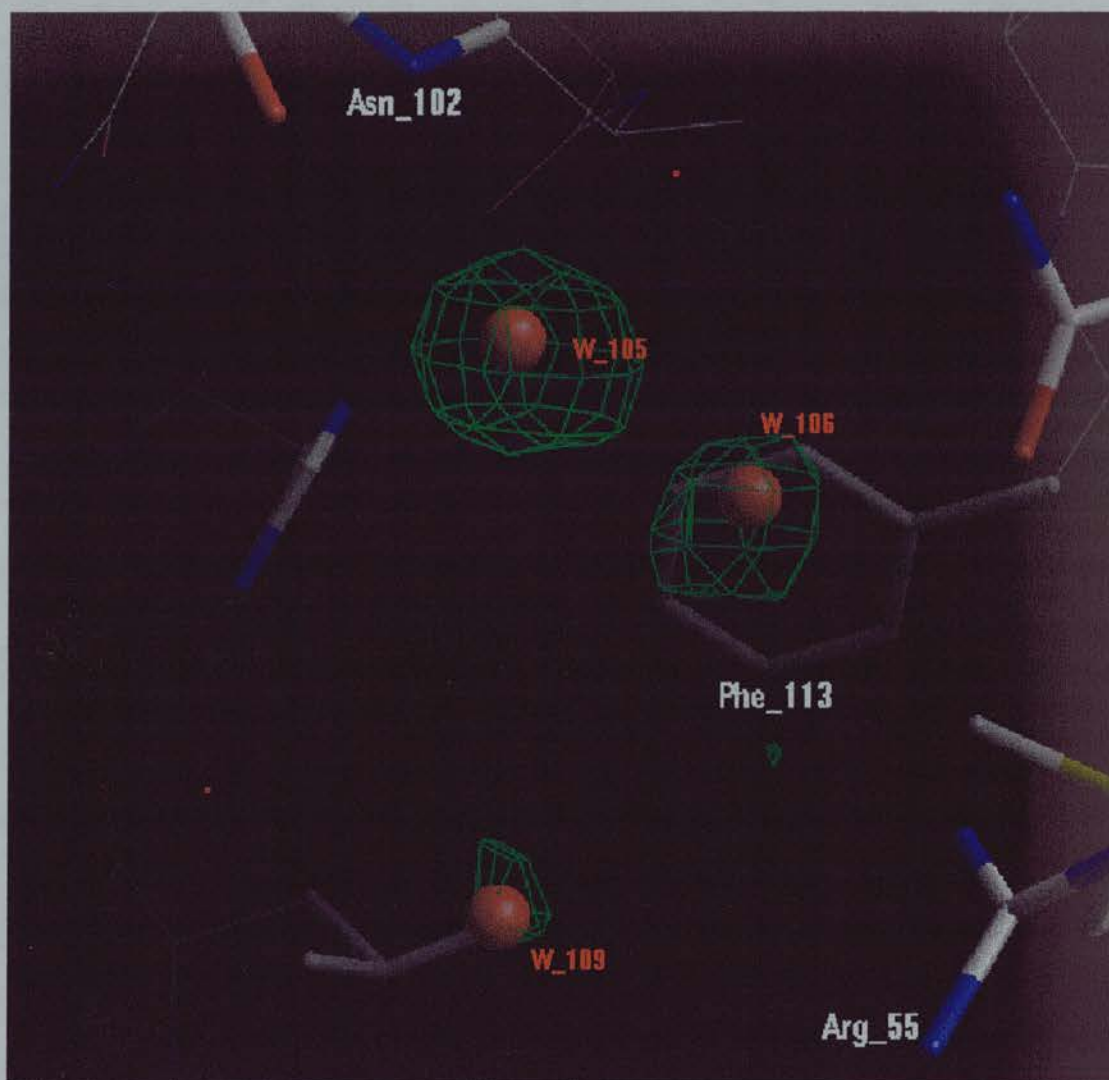


Fig. 7.5: Difference electron density map ($1F_o-1F_c$) of the water molecules in the binding site of unliganded Cyp-A. The difference electron density was calculated before including the water molecules in the model. The water molecules shown in the figure were taken from the final refined structure.

The refinement procedure was continued with addition of water molecules in cycles. In each cycle 10 to 15 water molecules were added followed by positional and temperature factor refinement. 196 water molecules were added in total. The binding site was occupied by six water molecules (Fig 7.6) W_105, W_106 W_109, W_121, W_198 and W_208. The water molecules W_121 and W_198 did not show up in the

first difference electron density map (Fig. 7.5) because they diffracted weakly but as the model improved their electron density became visible.

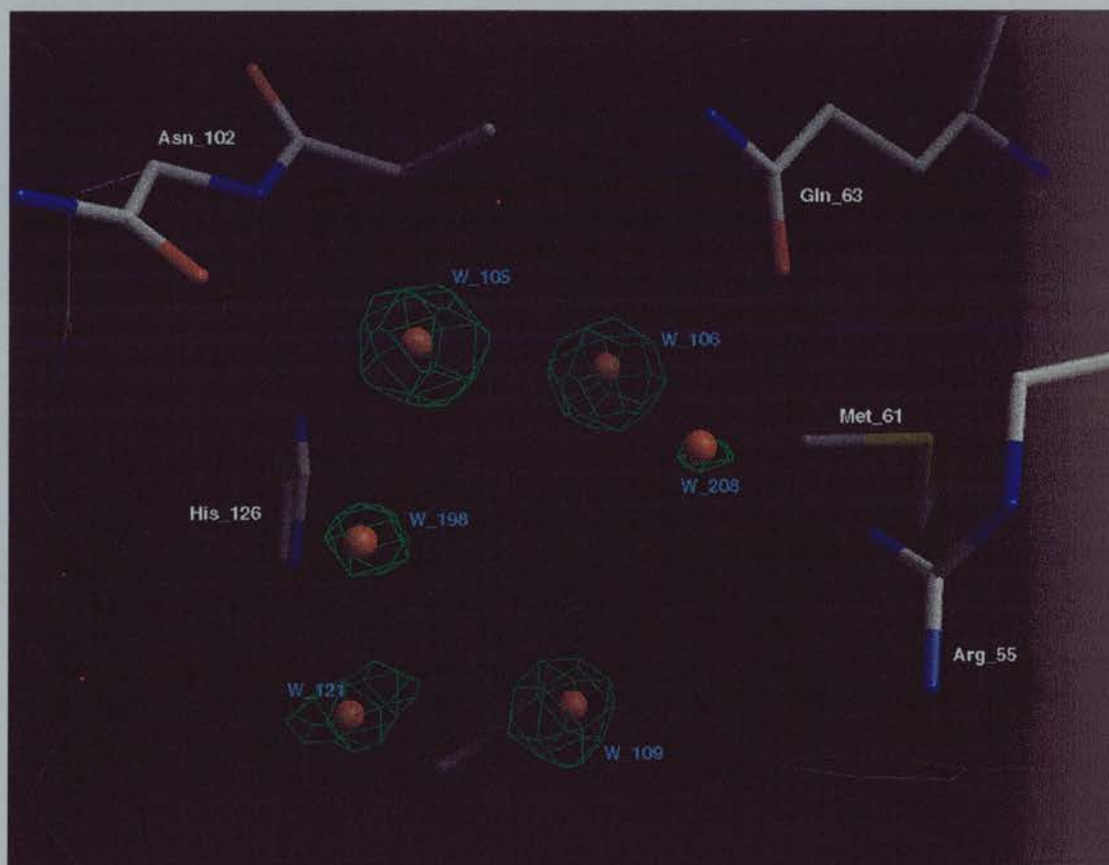


Fig. 7.6: Difference electron density map (2Fo-1Fc) of the water molecules in the binding site of unliganded Cyp-A. The water molecules were included in the model used for the calculation of the phases. The map was contoured only around the water molecules.

The solvent molecules make a number of contacts with the protein (Fig. 7.7) in the binding site. Waters 105, 106 and 121 form hydrogen bonds to Asn102/N, Gln63/OE1 and His126/NE2 (Table 7.10) respectively.

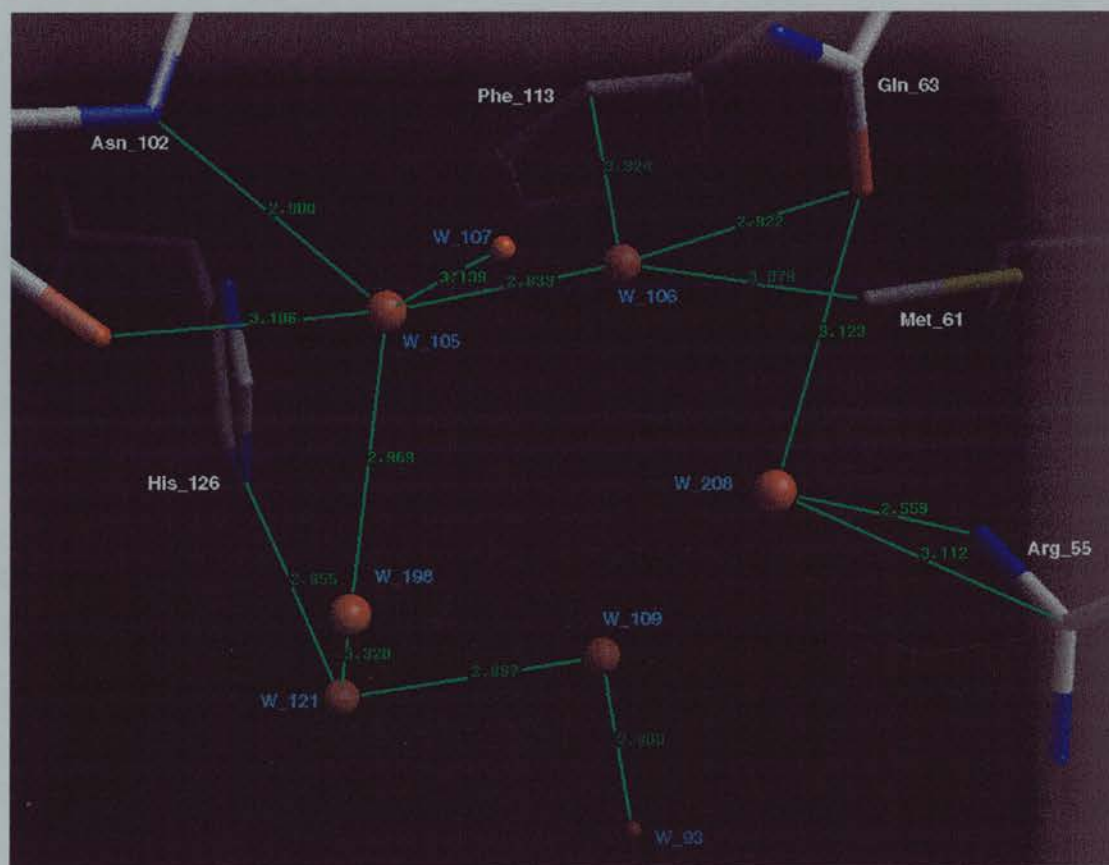


Fig. 7.7: Contacts of solvent molecules in the cyclophilin binding site. The temperature factors of these six water molecules presented in Table 7.10 are related to the number of contacts which each water makes and to the location of each water. Water molecule 105 makes five contacts and has the lowest temperature factor of 12.7 \AA^2 followed by W_106 (four contacts $B=24 \text{ \AA}^2$). Further from the binding site are, W_121 which makes three contacts and has a temperature factor of 34.5 \AA^2 and W_109 which makes two contacts has a temperature factor of 34.8 \AA^2 . W_208 and W_198 are even further than the previous two water molecules from the binding site and have temperature factors of 60.5 \AA^2 and 63.1 \AA^2 respectively.

Table 7.10: Contacts of solvent molecules in the binding site with surrounding atoms of the protein and the solvent as shown in Fig. 7.7.

B factor (\AA^2)	Water	Distance (\AA)	Residue/Atom
12.7	W_105	2.90	Asn_102/N
“	“	3.14	W_107
“	“	2.97	W_198
“	“	3.11	Asn_102/O
“	“	2.83	W_106
24.0	W_106	2.92	Gln_63/OE1
“	“	3.08	Met_61/CE
“	“	3.32	Phe_113/CD1
“	“	2.83	W_105
34.5	W_121	2.86	His_126/NE2
“	“	3.32	W_198
“	“	2.9	W_109
34.8	W_109	2.9	W_121
“	“	2.8	W_93
60.5	W_208	2.6	Arg_55/NH2
“	“	3.11	Arg_55/CZ
“	“	3.12	Gln_63/OE1
63.1	W_198	2.97	W_105
“	“	3.32	W_121

The temperature factors of these six water molecules present in Table 7.10 are related to the number of contacts which each water makes and to the location which each water has. W_105 and W_106 are deep inside the binding pocket and form hydrogen

bonds with the protein as well as other contacts (Fig. 7.7). This makes them more rigid. As a result of this the temperature factor of those waters is lower than for W_198, W_121, W_109 and W_208 (Table 7.10).

Water molecule 105 makes five contacts and has the lowest temperature factor of 12.7 \AA^2 followed by W_106 (four contacts $B=24 \text{ \AA}^2$). Further out of the binding site are, W_121 which makes three contacts and has a temperature factor of 34.5 \AA^2 and W_109 which makes two contacts has a temperature factor of 34.8 \AA^2 . W_208 and W_198 are even further than the previous two water molecules from the binding site and have temperature factors of 60.5 \AA^2 and 63.1 \AA^2 respectively. Also the contact atoms of W_208 have high temperature factors, 44.7 \AA^2 and 41.1 \AA^2 for NH1 and CZ atoms of Arg 55 respectively.

Water molecules 198 and 109 do not make any contact with protein residues but only with other water molecules in the binding site (W_105, W_106 and W_121). Those water molecules could be replaced by hydrophilic or hydrophobic atoms depending upon the nature of the substitution replacement seen in the neighbouring water molecule. The water molecules which form hydrogen bonds (W_105, W_106 and W_121) are more likely to be replaced by hydrophilic atoms.

The native structure of Cyp-A, refined during this work was compared with the native CypA structure (2cpl) from Ke (1992). An overlay of the two structures has an rmsd fit of 1.68 \AA for the main chain atoms (Fig. 7.7A). Water molecules 198, 106, 121 and 109 were not observed in the 2cpl structure (Fig. 7.7A).

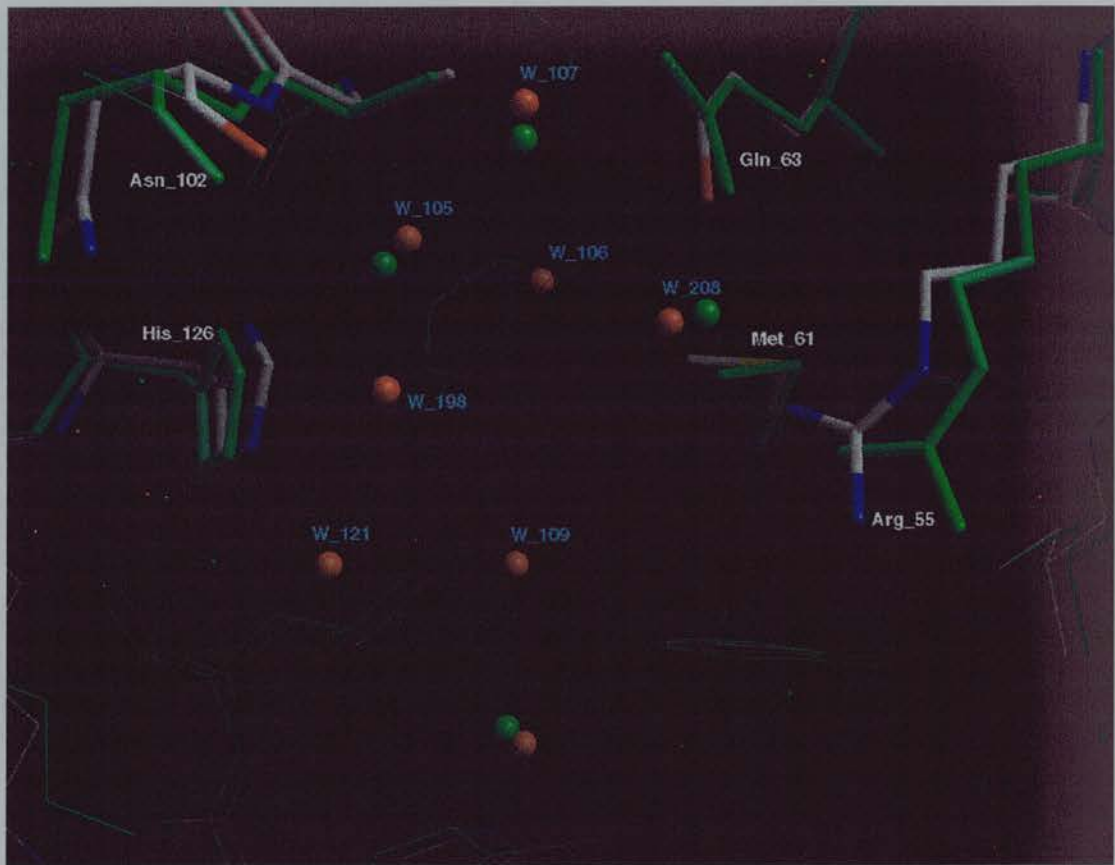


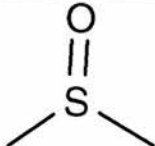
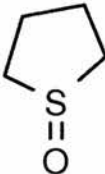
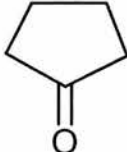
Fig. 7.7A: Overlay of native CypA (this work, with data sets collected at 100 K^o) with the 2cpl (Ke 1992) native structure (data sets collected at room temperature). The 2cpl structure is in green. The two structures have an rmsd fit of 1.68 Å for the main chain atoms. Water molecules 198, 106, 121 and 109 were not observed in the 2cpl structure

An inspection of the binding (Fig. 7.7A) shows that the side chains of Gln 63, Met 61 and Arg 55 adopt almost the same positions in both structures. The side chains of these residues can apparently adopt a range of conformations and make contacts with the ligands in all small molecule structures of CypA. Also these side chains have different conformations when the binding site is occupied by water molecules or by small ligands. The other side chains in the binding site did not show any significant movement when the binding site is occupied by water molecules as opposed to by small ligands.

6. DMSO family

The DMSO family are named after the first ligand found during this work; dimethylsulphoxide. The family consists of three members DMSO, TMSO and PENT (Table 7.11). All members of the family are of similar size and also have one hydrogen group acceptor (sulfoxy group or carbonyl group). DMSO was the first and smallest ligand found during this work and the only one which was co-crystallised with CypA.

Table 8.11: Members of Cyp-A ligands belonging to DMSO family

DMSO family		
DMSO	TMSO	PENT
Dimethylsulfoxide	Tetramethylene sulfoxide	Cyclopentanone
		

1. DMSO

Dimethylsulfoxide was found to bind to Cyp-A by chance. DMSO was an additive in the crystallization solution which was used for growth of Cyp-A crystals (see chapter 5 section 2). At that time nothing was known about its binding with Cyp-A.

The structure of Cyp-A complexed with CsA (1cwa see section 2.2) from Mikol et al (1993) was used as a starting model for rotation and translation search of DMSO

data. All atoms (except the ligand and the solvent) from the model structure were used in the search since the homology is 100%.

The rotation search was carried out using the program XPLOR. The rotation function search was performed by maximising the function: $RF = \langle P_{obs} * P_{model}(\Omega) \rangle$

P_{obs} Patterson vectors calculated from the observed data

P_{model} Patterson vectors calculated from the model structure at orientation Ω

First a rotation search was carried out using data from 10 to 4 Å and with an angular grid step with an interval of 2.5° degrees. The highest value of the standard deviation of the rotation function was 2.22 and corresponds to a rotation of $\theta_1=0$, $\theta_2=2.5$ and $\theta_3=0$ degrees from the original Cyp-A model (1cwa). The second rotation solution had a much lower value of 1.25. The first and the second rotation solution was tried out with a translation search to locate the molecule in the unit cell of space group $P2_12_12_1$. Data from 4 to 15 Å were used during translation search. The R factor for the model generated after the translation search was 39.2 % for the first rotation solution and 62.34 % for the second. The first rotation solution was used and the refinement proceeded with rigid body refinement, positional and B factor refinement and the R factor dropped to 34 %. At this point the first difference electron density map (1Fo-1Fc) was calculated and the binding site was inspected (Fig. 7.8).

The electron density map of the active site was compared with that of the native. In the native structure (unliganded) the binding site is occupied only by water molecules (Fig.7.6). The difference electron density map for DMSO data indicated a molecule with the shape of DMSO in the active site of Cyp-A (Fig. 7.8).

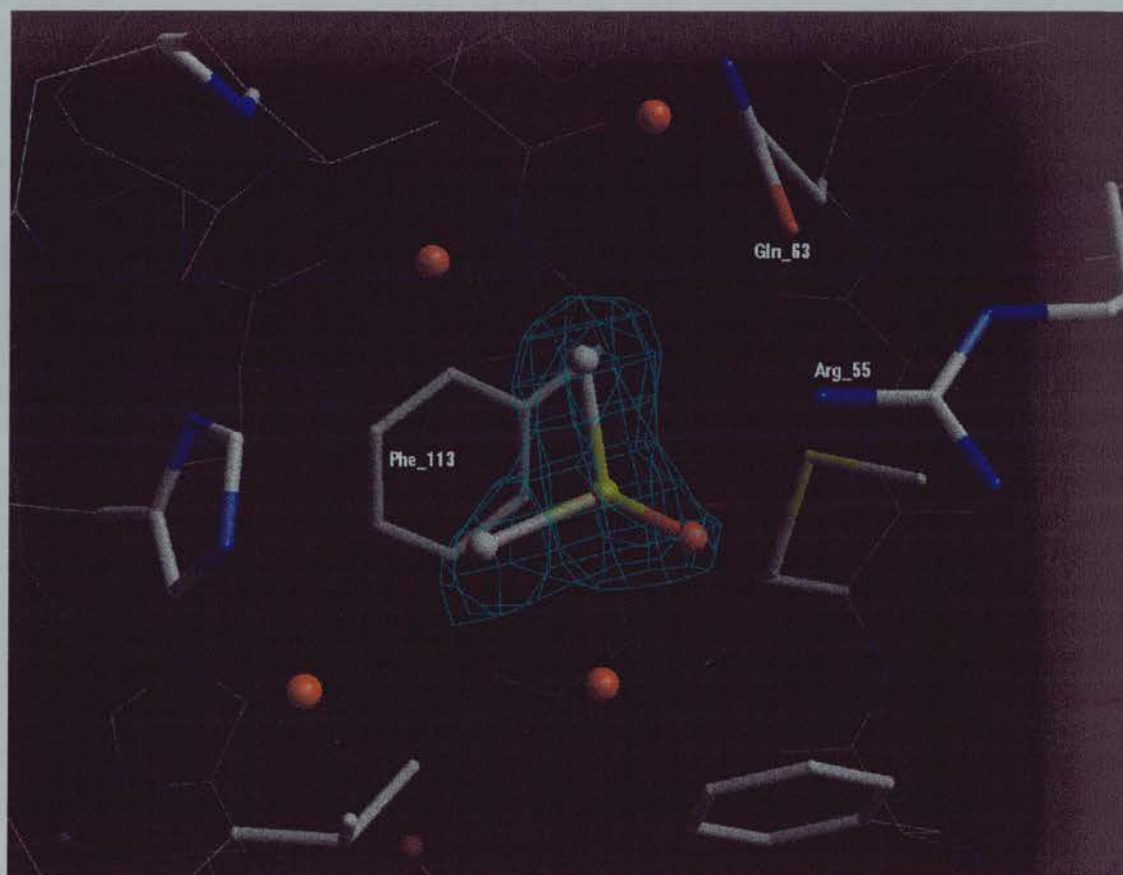


Fig. 7.8: Difference electron density map (1Fo-1Fc) for the ligand DMSO. The difference electron density was calculated before including the ligand and the water molecules in the model. The position of the water molecules and ligands are taken from the final refined structure.

The conformation and charges of the DMSO molecule were calculated by the program SYBYL using force field minimisation (SYBYL a molecular modeling program, Tripos Inc., University of Georgia, St. Louis Missouri). The DMSO molecule as it is generated from the program SYBYL has a dipole. The positive charge is on the carbons (0.15 partial charge each carbon atom) and sulfur (0.25 partial charge) and the negative (-0.55 partial charge) on the oxygen, the total charge of the whole molecule is zero.

The refinement proceeded with the addition of water molecules. After the addition of 187 water molecules and with an R factor less than 20 % the addition of the DMSO molecule followed. The R factor of the final model was 17.8 % and the free Rfactor 21.3 %. The root-mean-squared deviations were 0.007 Å and 1.28° from the ideal bond and angle geometries. This model was used for the calculation of a 2Fo-1Fc electron density map (Fig 7.9). All the atoms of the DMSO molecule were covered by the electron density contour as can be seen in Figure 7.9.

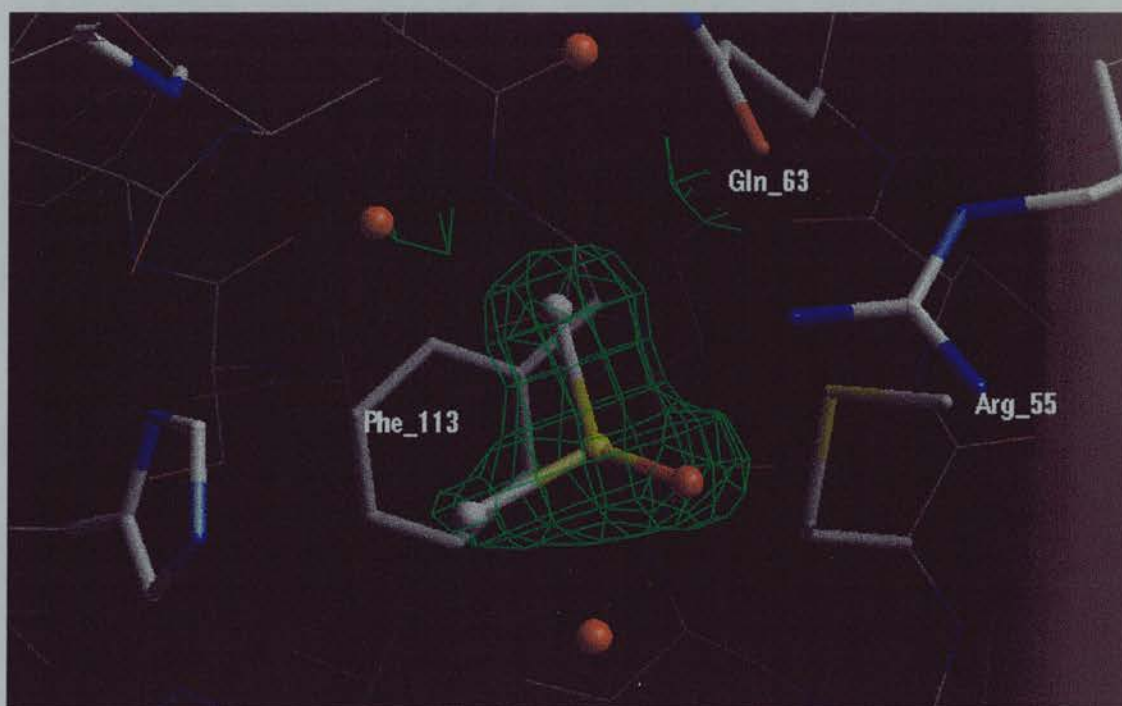


Fig. 7.9: Difference electron density map (2Fo-1Fc contoured around DMSO molecule) for the ligand DMSO from final refined model. Both water and ligand were included in the phases calculation. The ligand electron density was well defined in the first difference electron density map (Fig. 7.8) and did not change significantly as can be seen from Figure 7.8 to 7.9.

DMSO has an approximate three fold symmetry around the sulfur atom and can be fitted into electron density contour in three different ways. One given in Fig. 7.10. The alternative positions have the O atom overlapping with C1 (position 1) or C2 (position 2). Crystallographically position 2 and the current position of DMSO molecule are equivalent since the sigma level of electron density around C2 and O atom are almost the same (carbon atom C1 has much less). The reason that the DMSO molecule was put in the current position was to prevent a bad contact between Arg_55/NH1 and C1 or C2.

The DMSO molecule makes a number of contacts with protein and the solvent (Fig. 7.10). The O of the DMSO forms hydrogen bonds to the guanidinium group of Arg 55 and to W_176 (Fig. 7.10). The contacts of DMSO with the protein and surrounding water molecules are listed in Table 7.12.

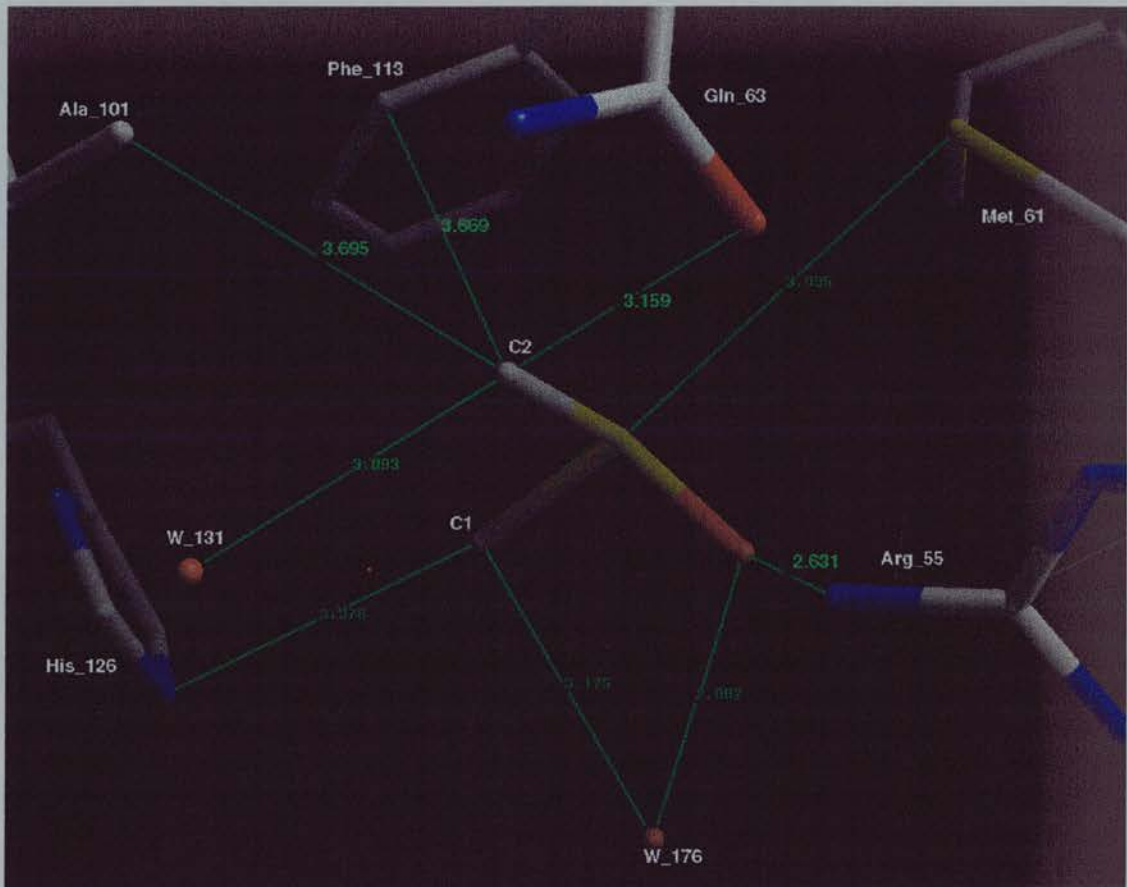


Fig. 7.10: Contacts of DMSO ligand with surrounding atoms of the protein and the solvent. The sulfoxy group of DMSO hydrogen bonds with Arg 55/NH1 and W_176. The carbon atoms of DMSO have partial positive charges and could form hydrophobic and hydrophilic contacts.

Table 7.12: Contacts of DMSO ligand with surrounding atoms of the protein and the solvent as shown in Fig. 7.10.

Ligand atom	Distance (Å)	Residue/Atom
S	3.6	Arg_55/NH1
C2	3.16	Gln_63/OE1
C2	3.44	Arg_55/NH1
C2	3.09	W_131
C1	3.18	W_176
C1	3.48	His_126/CE1
C1	3.38	His_126/NH2
O	2.63	Arg_55/NH1
O	3.56	Arg_55/CZ
O	2.88	W_176

2. TMSO

A) Structural similarities and selection of TMSO ligand

Structural similarity provides a method of selecting new ligands. The principle is that compounds with similar structure are going to have similar conformation and thus bind the same 3D template. The method is schematically described in Figure 7.11. The DMSO structure was used as a template for selection of new ligands.

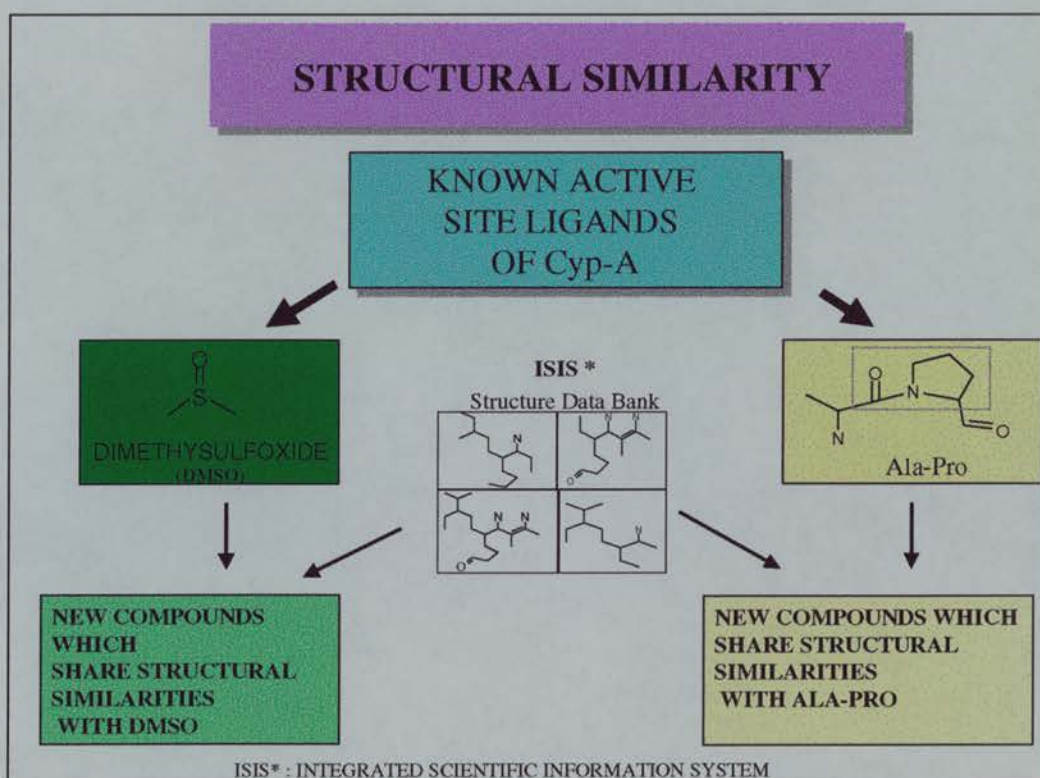


Fig. 7.11: Selection of compounds based in structural similarities

TMSO was chosen because of its similarity with DMSO (see Table 7.11). After study of the active site it was found to be large enough to accommodate the two extra carbons of TMSO (see Table 7.8). TMSO was the closest structurally similar molecule to DMSO, which was found running the structural similarity search in the

program ISIS (see material and methods section 2). The conformation of TMSO was found in CSD (Cambridge Structure Database). TMSO was part of the structure of tetra (μ -trifluoroacetato)-bis (trifluoroacetato) tetrakis (tetramethylenesulfoxide) dineodymium (III) (Castellano et al 1985) found in that database.

Modelling in the binding site followed using the TMSO structure found from above. TMSO was fitted over DMSO using common atoms of the two molecules (see Table 7.11). The active site was found to be large enough to accommodate the two extra carbons of TMSO. The picture of the ligand in the binding site will give an idea of what kind of interaction could be formed. The first step is a careful inspection of the residues around the candidate ligand (TMSO). At this point the possibility of hydrogen bonding, electrostatic, hydrophobic and van der Waals interactions should be examined. Since the binding site is very hydrophobic, the addition of two extra carbons (from DMSO to TMSO) was expected to increase the binding strength.

The next important step is the comparison of the native (unbound) structure with the bound one. This will give a clear view of the rigid and flexible domains of the binding site. Furthermore the water molecules which have been replaced by the ligand (if any) can be marked. The water molecules in the native structure (Fig. 7.6) are very important since they give us an idea which part of the ligand could be modified by extension, replacing one or more of these water molecules. The release of the water when it is replaced by a ligand, leads to a net increase in entropy. It has been estimated that by replacing a water molecule with a part of a ligand with exactly the same binding enthalpy (van der Waals interaction, hydrogen bonding interaction), this increases binding strength by -2 kcal/mol (Burkhard 1995). The water molecules also indicate favoured sites for hydrophilic interaction or hydrogen bonding.

B) Refinement of TMSO data

The refinement procedure was started with a translation search and followed by a rigid body refinement and finally positional and individual B-factor refinement. At that point the first difference electron density map (1Fo-1Fc) was calculated and the binding site was inspected (Fig. 7.11). The electron density map around the active site was compared with that of the native (unliganded, Fig.7.6). The electron density showed convincingly that the binding site was not occupied by water molecules but by a molecule of the size of TMSO.

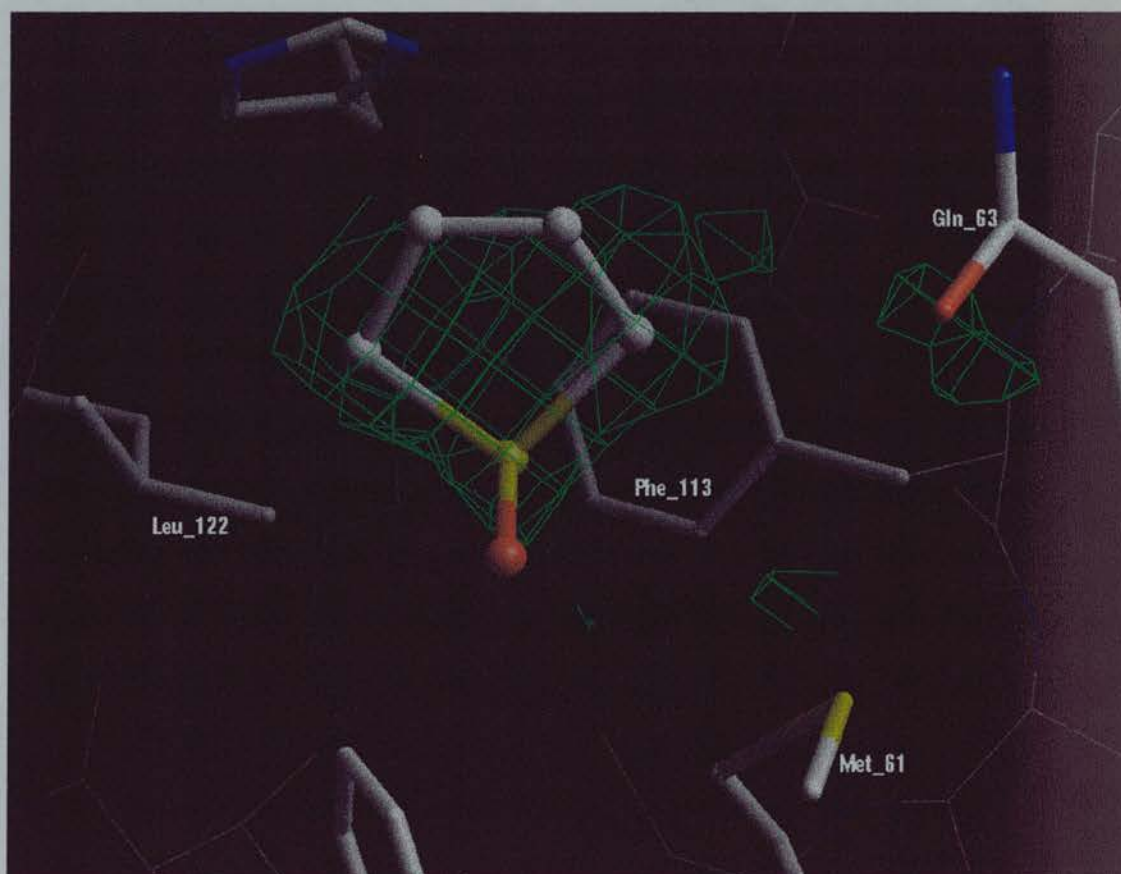


Fig. 7.11: Difference electron density map (1Fo-1Fc at 2.3-sigma level) for the ligand TMSO. The difference electron density was calculated before including the ligand and the water molecules in the model.

The refinement proceeded with addition of water molecules. The first attempt to model the ligand was after the addition of 243 water molecules and with the R factor of the model at 21.1 %. The ligand was introduced into the model and the refinement was continued with positional and individual B-factor refinement. From the electron density map (2Fo-1Fc) the ligand fits very well to the contour except the area between carbons C2 and C3. A difference electron density map (1Fo-1Fc) calculated around carbons C2 and C3 showed positive density in that area (Fig. 7.12).

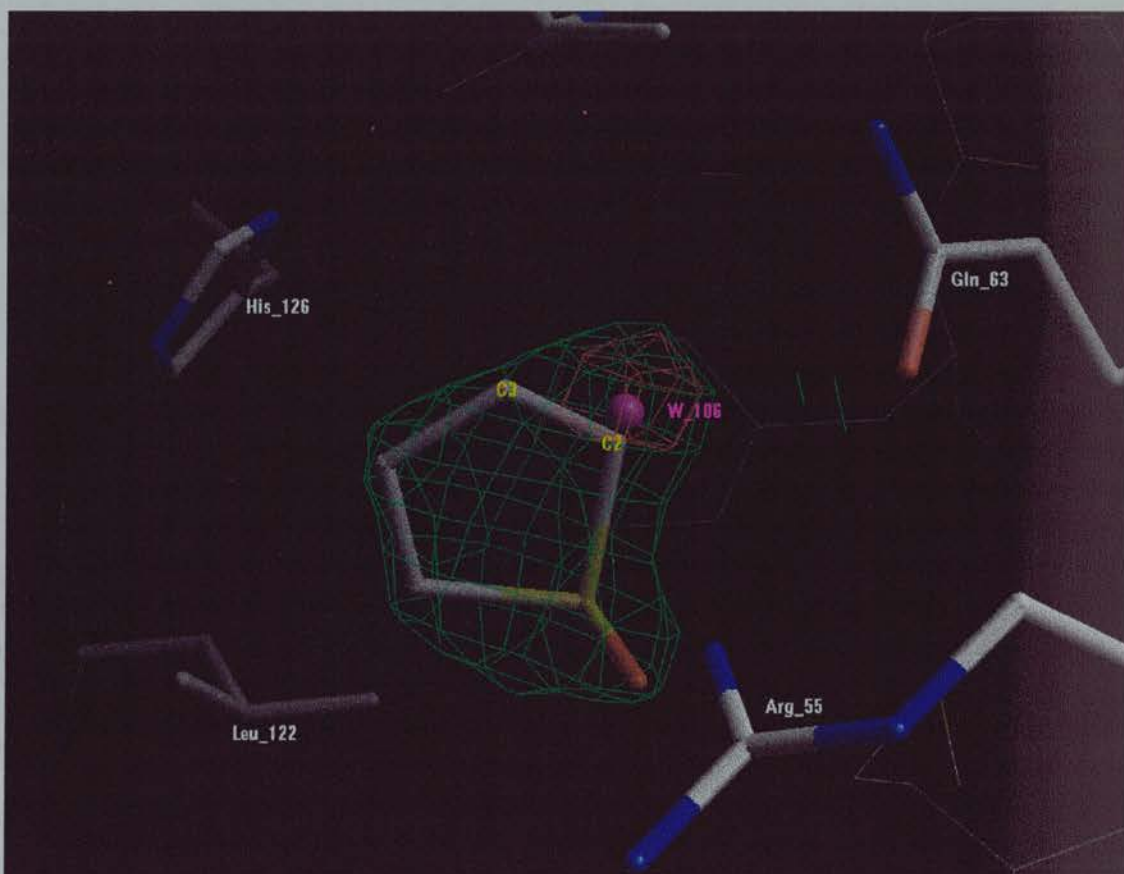


Fig. 7.12: Difference electron density map (2Fo-1Fc) for the ligand TMSO (green color). W₁₀₆ was not used in the calculation of the phases. The red contour (1Fo-1Fc) is positive difference electron density. The map was contoured only around the TMSO molecule.

Three different models (1, 2 and 3) were developed to explain the additional unfilled density around carbons C2 and C3 in Fig. 7.12. This density was overlapped with the W_106 of the native structure. In all models the binding site is occupied (not 100%) at least by one TMSO molecule. In **model 1** an additional water molecule is added, in **model 2** there is an extra TMSO molecule and finally in **model 3** there is one TMSO molecule plus a water molecule. Partial occupancy refinement was carried out by program XPLOR.

Model 1

In model 1 W_106 from the native structure was renamed W_310. W_310 was added to the model and the refinement was continued with positional, individual B-factor and occupancy refinement. The occupancy was refined to 80 % for the TMSO and 20 % for W_310 (the sum of the occupancy was constrained to 100 %) and the average B factor to 40 and 2 respectively. Model 1 containing TMSO and W_310 in the binding site (Fig.7.13) has an R factor of 17.6 % and a free R factor of 23.5 %.

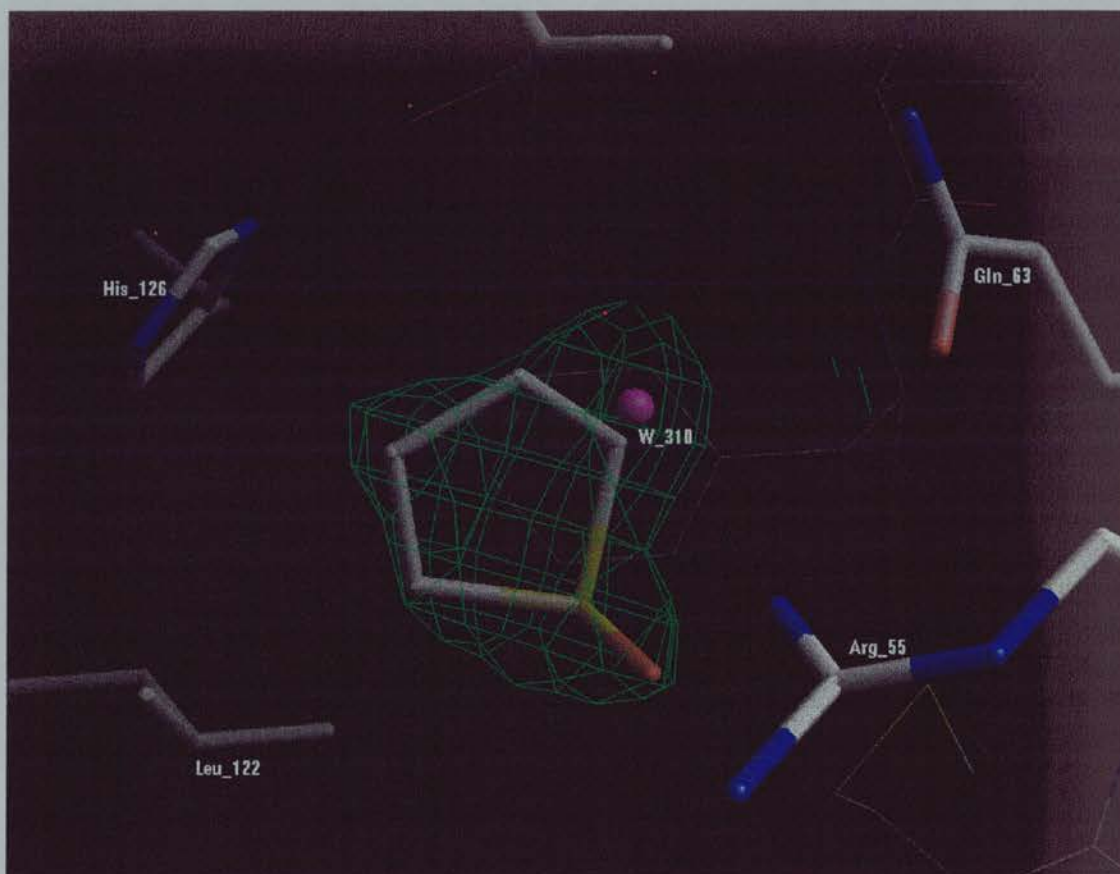


Fig 7.13: Difference electron density map (2Fo-1Fc) for the ligand TMSO and W_310 (**model 1**). Occupancy was 80 % and 20 % for TMSO and W_310 respectively. Both water and ligand were included in the phases calculation.

Model 2

The B factor of W_106 (W_310 in the TMSO structure of model 1) in the native structure was refined to 23.4. In the TMSO structure, the same water even when the occupancy was set to 100 %, has a B factor of 21.0. During refinement of model 1 it was found that a minimum occupancy of 70 % was required for the TMSO molecule in order to eliminate any positive electron density (1Fo-1Fc) around it. When the occupancy of W_310 was set to 30 % the B factor dropped to 4.5. A low temperature factor of W_310 could mean that something heavier than O (8 electrons) occupied that area, and the only heavier atom in the structure is the S (16 electrons). This area can be occupied by an S atom only if the position of the TMSO ligand changes. Since

the initial position of TMSO (Fig. 7.13) fits well to the contour of the density and makes good chemical sense (with hydrogen bonding between Arg_55/NH1 and O atom of TMSO). An alternate position was given (Fig. 7.14) in which the sulfoxy group of the TMSO 2 fits into the positive electron density found around W_106 (see Figure 7.12). The model was refined with these two alternatives of the TMSO ligand (Fig. 7.14).

The occupancies were refined to 52 % and 32 % for alternative sites 1 and 2 respectively. The restraint that occupancy of site 1 plus occupancy of site 2 should sum up to 100% was set (the above values sum up to 84 %). Because of that restraint the original values of occupancies were multiplied by 100/84 in order that they sum to 100 %. In the final model the average temperature factor for site 1 and site 2 was 37.6, 49.5 respectively with occupancies 62 % and 38 %. When TMSO binds then the side chain (Gln_63) has to adopt an alternative position also (Fig. 7.13) in order to form a hydrogen bond with the O of the TMSO (Gln_63/ALT2/NE2---O/TMSO/ALT2). A total of 243 water molecules were added into the final model and the R factor was 17.7 % with free R factor being 23.6 %. Model 2 contains two positions of TMSO in the binding site.

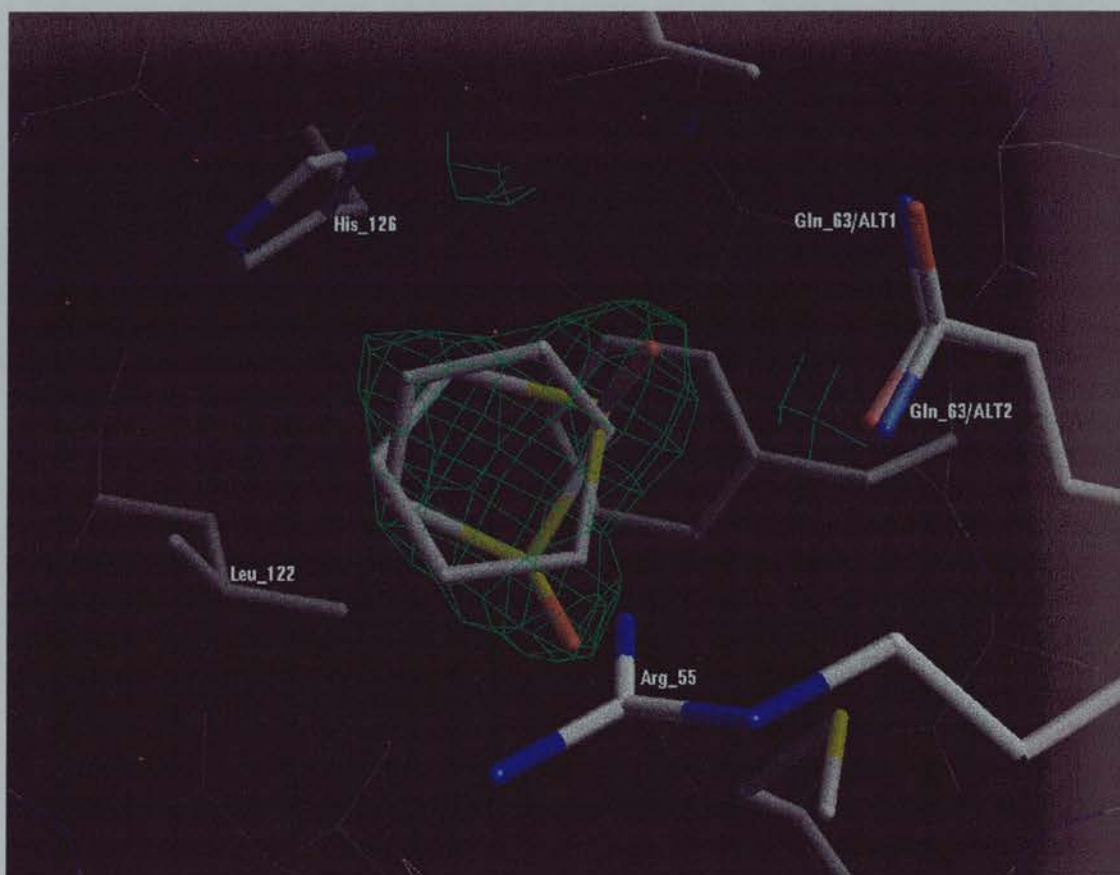


Fig. 7.14: Difference electron density map (2Fo-1Fc contoured around TMSO molecule) for the ligand TMSO. The ligand can adopt two alternative positions 1 and 2 (**model 2**). Both sites were included in calculation of the phases. Also the side chain of Gln_63 can adopt two alternate positions according to TMSO ALT1 and ALT2.

Model 3

In a last attempt at refinement of TMSO data, a model (Fig. 7.15) containing the two sites of TMSO (see Fig. 7.14) plus W_310 (see Fig. 7.13) was used. This trial was based on the fact that during refinement of model 2 (see above) the occupancy of TMSO/ALT1 was refined to 52 % and TMSO/ALT2 to 32 % respectively. The remaining 16 % (in order to reach 100 % occupancy) of the binding sites should be occupied by water. The refinement was run by fixing the occupancies of TMSO/ALT1 to 52 %, TMSO/ALT2 to 32 % and W_310 to 16 %. Positional and individual B-factor refinement was run on that model. The R factor was refined to 17.7 % and the

free R factor to 23.6 %. The average B factors were 30.3 for the TMSO/ALT1, 48.5 for the TMSO/ALT2 and 6.1 for the W_310.

All the models used for the refinement of the TMSO data set are summarised in Table 7.13. The TMSO molecule in model 1 has practically the same position as TMSO/ALT1 in models 2 and 3. TMSO/ALT2 occupies almost the same position in model 2 and 3. Also model 1 has the lowest free R factor which is probably an indication that models 2 and 3 are overrefined.

Table 7.13: Refinement results for the three models used for the refinement of TMSO data set. The binding site is partial occupied of TMSO and W_310 in **model 1**, of two alternates in **model 2** and of two alternates and W_310 in **model 3**.

	Model 1	Model 2	Model 3
R factor	17.6 %	17.7 %	17.7 %
free R factor	23.5 %	23.6 %	23.6 %
B factor TMSO (average)	39.4		
Occupancy	80 %		
B factor TMSO ALT1 (average)		37.6	30.3
Occupancy		62 %	52 %
B factor TMSO ALT2 (average)		49.5	48.5
Occupancy		38 %	32 %
B factor W_310	2		6.1
Occupancy	20 %		16 %

The TMSO molecule makes a number of contacts with protein and the solvent (Fig. 7.15). The O of the TMSO forms a hydrogen bond to the guanidinium group of Arg 55 in model 1, 2 and 3 and a hydrogen bond to Gln_63/OE1, when it adopts the second position. The contacts of TMSO with the protein and surrounding water molecules are listed in Table 7.14.

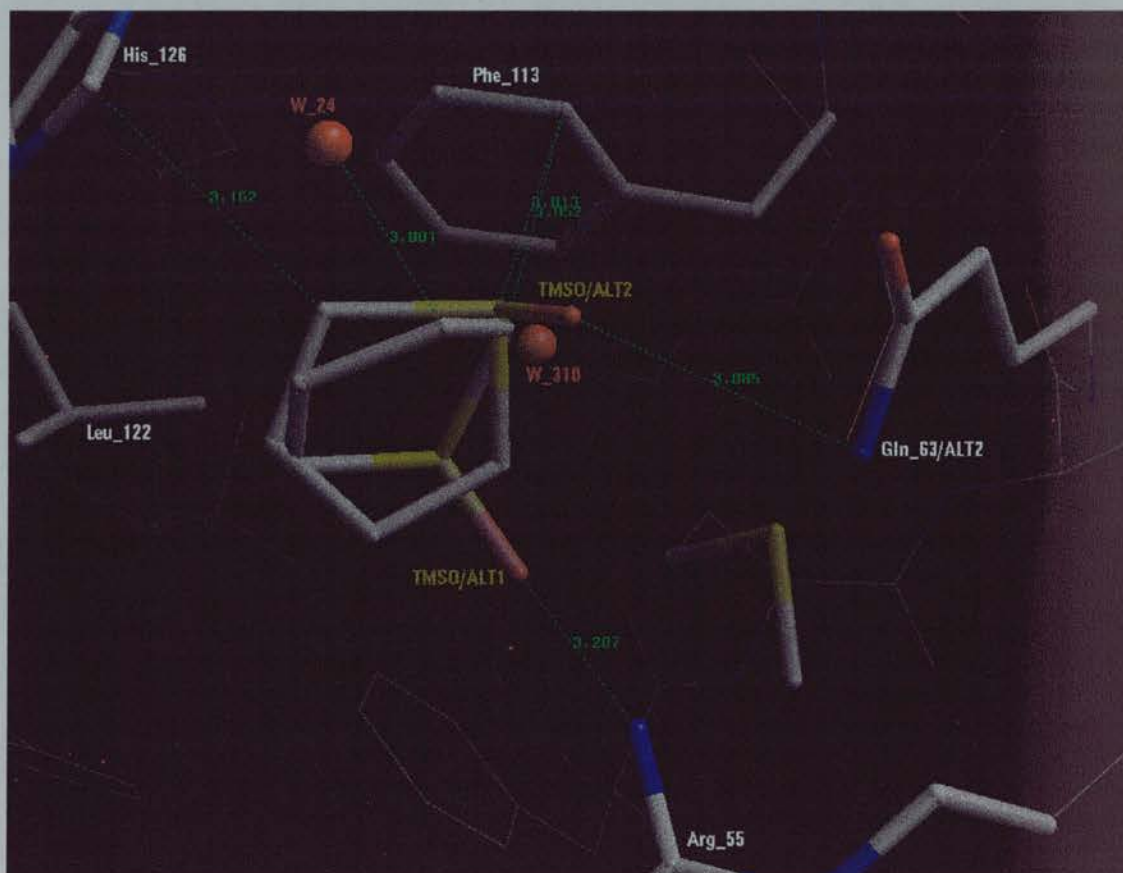


Fig. 7.15: Contacts of sites 1 and 2 of the TMSO ligand with surrounding atoms of the protein and the solvent of model 3. The O of the TMSO makes a hydrogen bond to the guanidinium group of Arg 55 in model 1, 2 and 3. When TMSO adopts the second position (ALT2) it makes a hydrogen bond to Gln_63/OE1.

Table 7.14: Contacts of sites 1 and 2 of TMSO ligand with surrounding atoms of the protein and the solvent of model 3 as shown in Fig. 7.15.

Ligand atom	Distance (Å)	Residue/Atom
O/ALT1	3.21	Arg_55/NH1
O/ALT1	3.20	Met_61/SD
O/ALT1	3.30	Met_61/CE
C2/ALT1	3.05	Phe_113/CD1
C3/ALT1	3.00	W_24 (W_105 in native)
C4/ALT1	3.29	W_24 (W_105 in native)
O/ALT2	3.08	Gln_63/ALT2/NE2
O/ALT2	3.22	Gln_63/ALT2/CD
S/ALT2	3.01	Phe_113/CD1
S/ALT2	3.24	Phe_113/CE1
C1/ALT2	3.48	His_126/CE1

3. PNT

The selection of the ligand was based on the structural similarities as described in the TMSO section above. PNT shares high structural similarities with TMSO (Table 7.11). The conformation of the PNT was found in CSD as part of the methacryloul chloride structure (Fischer et al 1985).

The refinement procedure was as described for TMSO. The first difference electron density map was calculated at that stage of refinement and showed the clear presence of a ligand (initial electron density map Fig. 7.16). The refinement proceeded by addition of water molecules. 204 water molecules were added before the ligand was

introduced into the model. The difference electron density map (1Fo-1Fc) in the binding site clearly indicated a molecule with size and shape to fit to PNT (Fig. 7.16).



Fig. 7.16: Difference electron density map (1Fo-1Fc at 2.5-sigma level) for the ligand PNT. The difference electron density was calculated before including the ligand and the water molecules in the model.

The ligand was introduced into the model and the refinement was continued with positional and individual B-factor refinement. The ligand fits very well to the contour of the electron density (Fig. 7.16). A total of 243 water molecules were added into the final model and the R factor was 18.6 %.

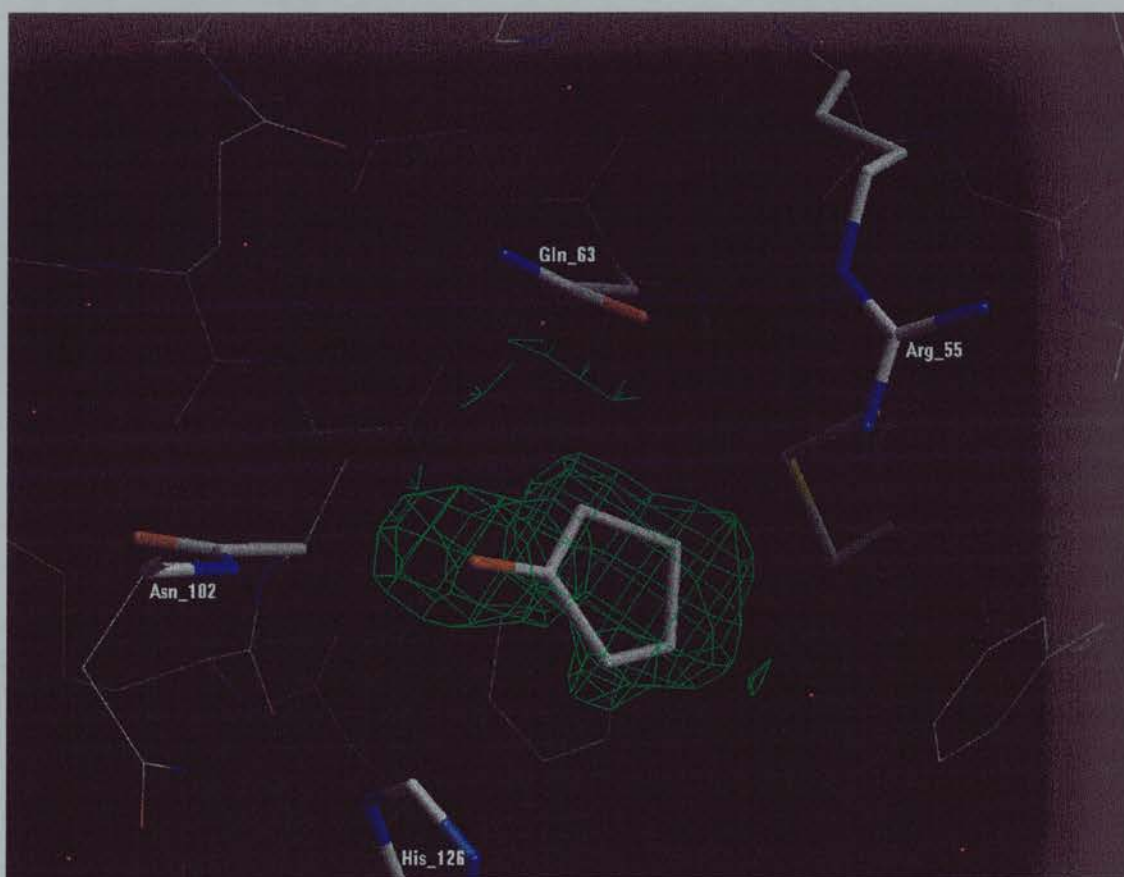


Fig. 7.17: Difference electron density map ($2F_o - 1F_c$ contoured around PNT molecule) for the ligand PNT. A total of 243 water molecules and the ligand were included in the phase calculation.

The PNT molecule makes a number of contacts with protein and the solvent (Fig. 7.17). The O of the PNT forms a hydrogen bond to Asn_102/N. The contacts of PNT with the protein and surrounding water molecules are listed in Table 7.15. One hydrogen bond forms between O1 of PNT and Asn_102/N.

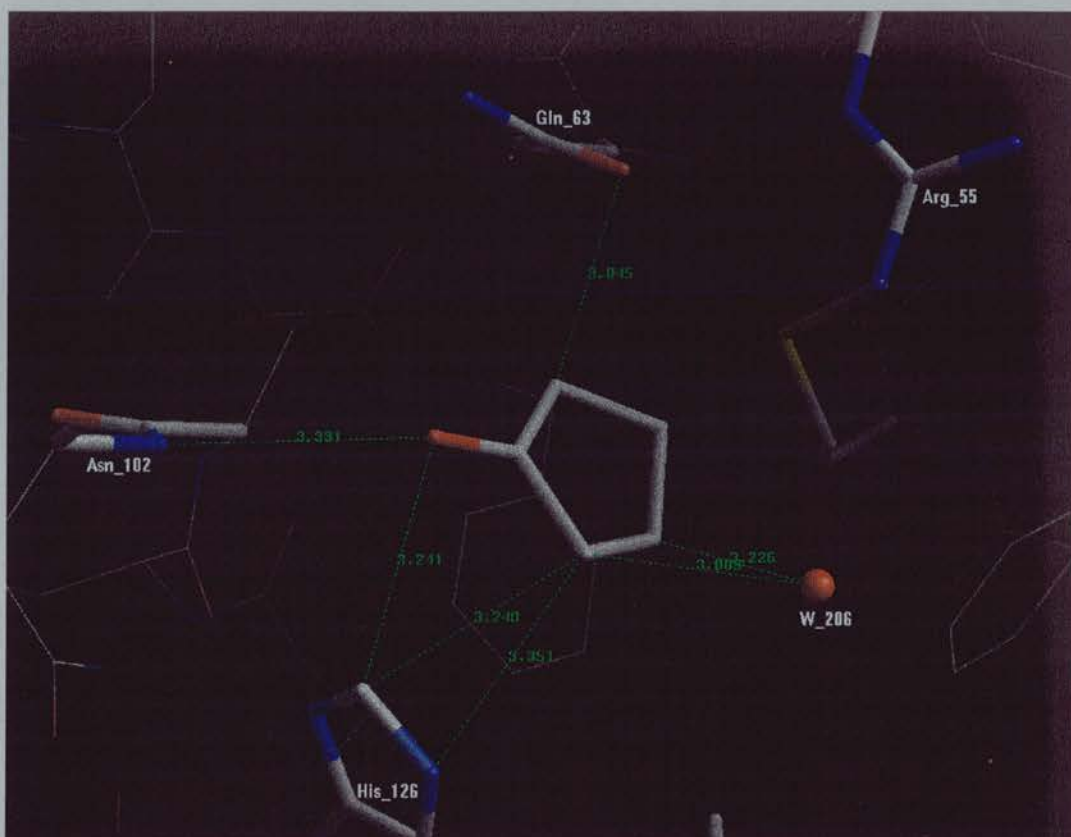


Fig. 7.18: Contacts of PNT ligand with surrounding atoms of the protein and the solvent. The O of the PNT makes a hydrogen bond (3.3 Å) to Asn_102/N and a number of contacts with side chain of His_126 and Gln_63.

Table 7.15: Contacts of PNT ligand with surrounding atoms of the protein and the solvent as shown in Fig. 7.18.

Ligand atom	Distance (Å)	Residue/Atom
O1	3.33	Asn_102/N
O1	3.24	His_126/CE1
C2	3.24	His_126/CE1
C2	3.35	His_126/NE2
C2	3.09	W_206 (W_106 in native)
C3	3.23	W_206 (W_106 in native)
C5	3.04	Gln_63/OE1

7. Piperidine family

Members of this family are derivatives of piperidine. Piperidine shares structural similarity with the proline ring (Fig.7.19). Dipeptides containing proline are well known to bind to Cyp-A (Ke et al 1993, Zhao and Ke 1996). Piperidine derivatives were chosen as putative ligands for that reason. Also both ligands of the piperidine family (table 7.13) share an amide group. The oxygen of that amide group always forms a hydrogen bond with Asn₁₀₂ in all CypA-XPro complexes (Ke et al 1993, Zhao and Ke 1996).

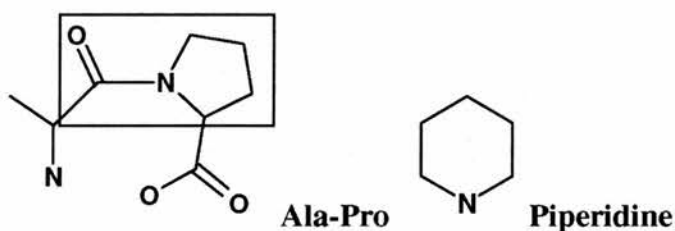
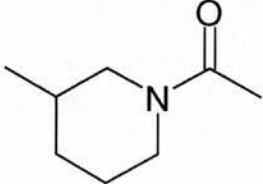
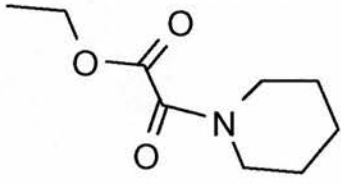


Fig. 7.19: Structure of Ala-Pro and piperidine. The partial structure of the dipeptide shown in the box was used as a guide to search for putative ligands of Cyp-A.

The search for putative ligands sharing the above features was carried out using the ISIS data base using the structure of 1-Acetyl piperidine as a template. A number of molecules were found including ACMPIP and ETPIP (Table 7.16).

Table 7.16: Cyp-A ligands belonging to the piperidine family

Piperidine family	
ACMPIP 1-Acetyl-3-methyl piperidine	ETPIPG Ethyl-piperidine glyoxylate
	

1. ETPIPG

The refinement procedure started with a translation search and proceeded on with rigid body refinement, positional and individual B-factor refinement using as a model the co-ordinates of the CypA/DMSO structure. The first difference electron density map ($1F_o-1F_c$) was calculated and the binding site was inspected (Fig. 7.19A). The electron density map in the active site was compared with that one of the native (unliganded, Fig.7.5). The electron density convincingly showed that the binding site was not occupied by water molecules but by a molecule of the size of ETPIPG. An initial conformation of the ETPIPG molecule was calculated by the program WITNOTP using force field minimisation (Widmer 1997). ETPIPG has many rotational degrees of freedom and can adopt many different conformations.

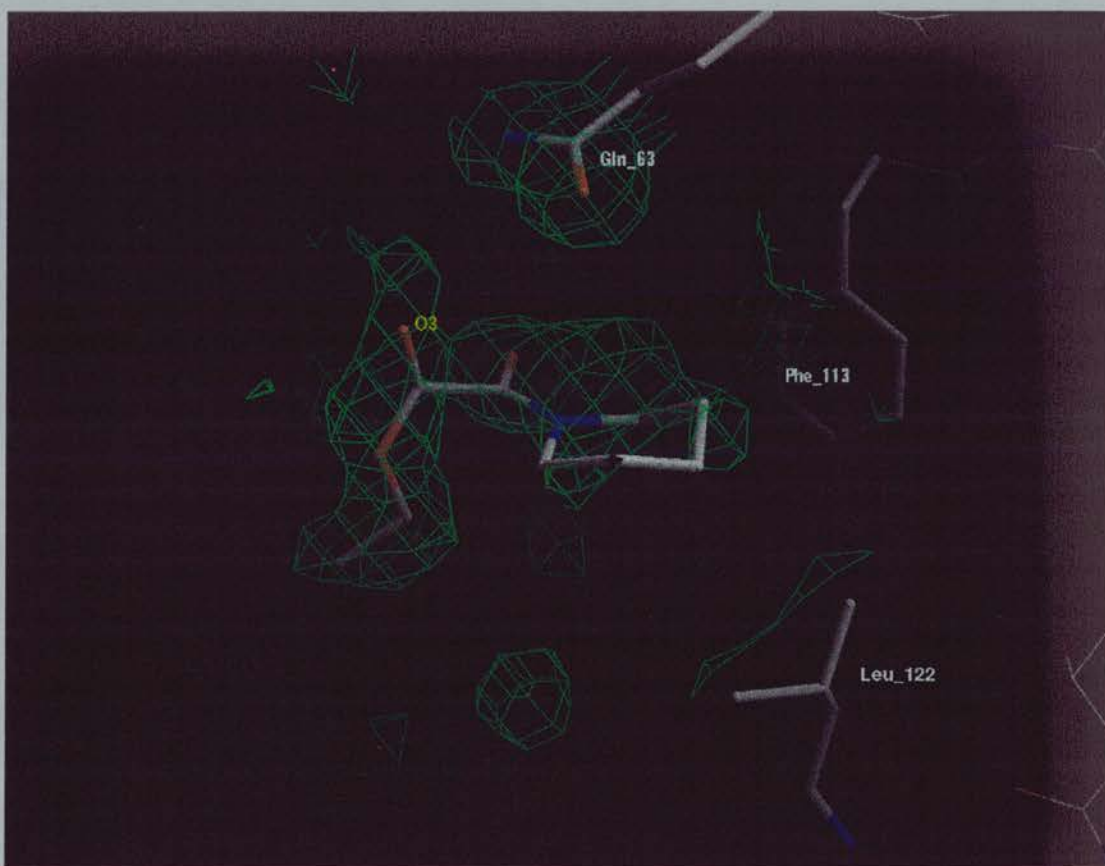


Fig. 7.19A: Difference electron density map (1Fo-1Fc) for the ligand ETPIPG. The difference electron density was calculated before including the ligand and the water molecules in the model. The water molecules and ligands shown were taken from the refined structure.

Refinement of ETPIPG using data to 2.05 Å

The refinement proceeded by addition of water molecules. The first attempt to model the ligand was after the addition of 161 water molecules and with a R factor about 19 %. The ligand was introduced into the model and the refinement was continued with positional and individual B-factor refinement. From the electron density map (2Fo-1Fc) the ligand's atoms fit very well to the contours of the electron density except two carbon atoms of the piperidine ring and the area around carbonyl oxygen O3 (Fig. 7.20). The six-membered ring can adopt more than one conformation

(Glusker et al 1994) and as a result the electron density of the ring could become weak. The electron density which extended from atom O3 of the ligand suggests an alternative conformation of the ligand tail. The ligand was modeled into the electron density with its tail (after O2) adopting two conformations ALT1 and ALT2 (Fig. 7.21). All the above results derive from the 24 to 2.05 Å resolution data set.

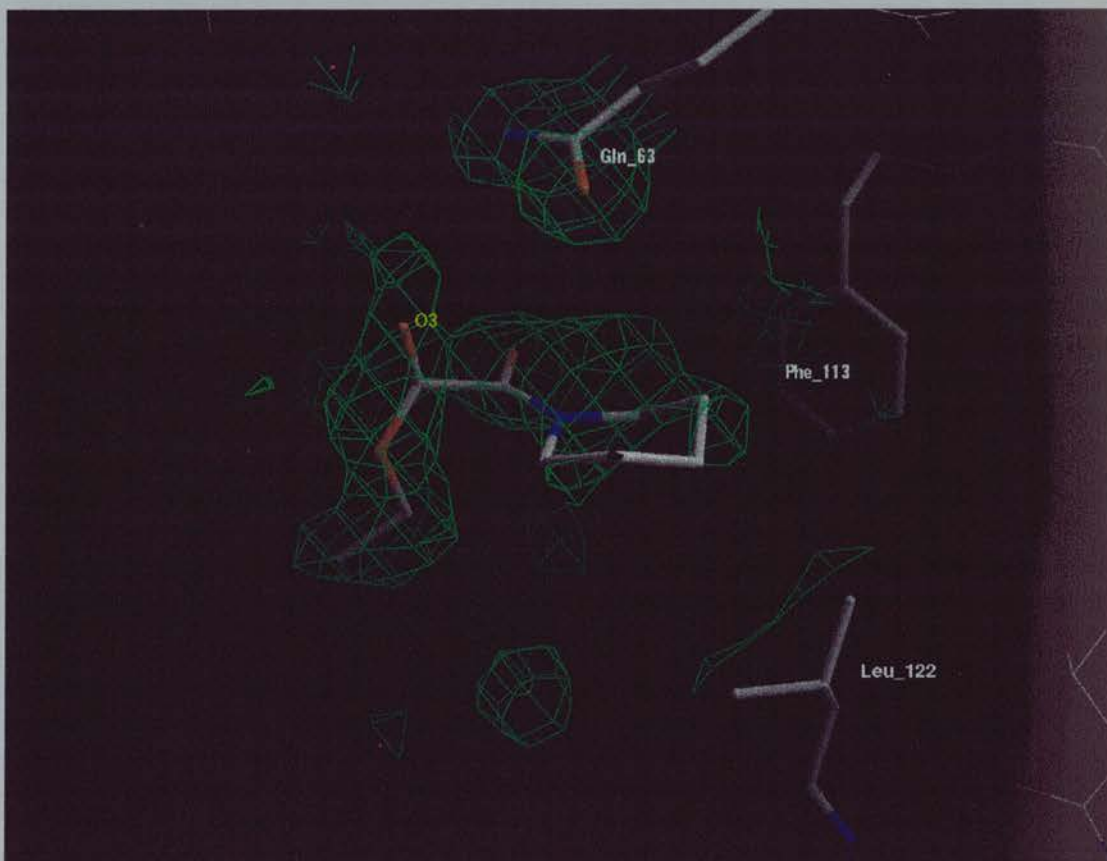


Fig. 7.20: Difference electron density map (2Fo-1Fc) for the ligand ETPIPG. The extension of electron density from atom O3 could be explained by an alternate conformation of the tail of the ligand. The ligand was included in the phase calculation.

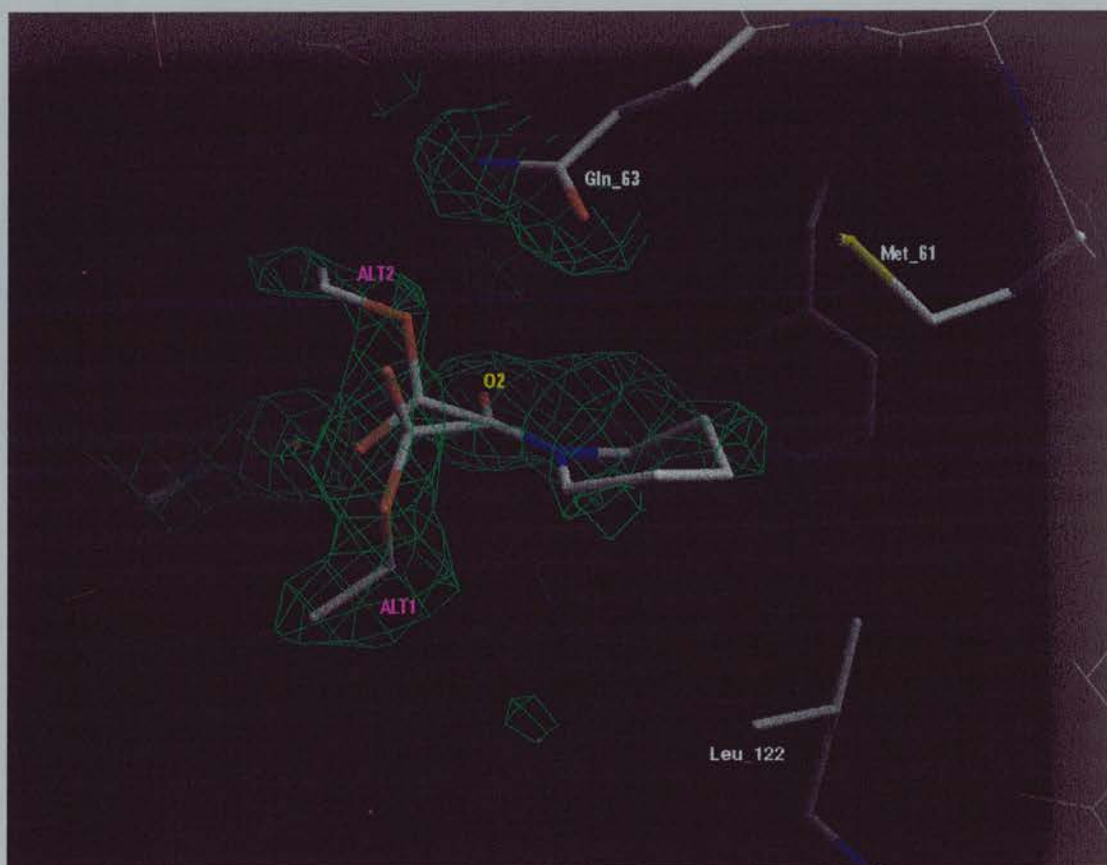


Fig. 7.21: Difference electron density map (2Fo-1Fc) for the ligand ETPIPG when its tail (3 atoms) adopts two alternate conformations ALT1 and ALT2. The model was refined against data from 24 Å to 2.05 Å. The atoms of both alternate conformations of the ligand were included in the phase calculation.

Refinement of ETPIPG using Synchrotron data to 1.65 Å

A high resolution data set was collected at the SRS (Daresbury see chapter 6) to 1.65 Å from the same crystal. The new high resolution data were refined against the model of the CypA-ETPIPG complex where ETPIPG adopted two conformations (Fig.7.22). This showed continuous density extending from from O4 (Fig. 7.22). Two carbon atoms (C1 and C2 Fig. 7.23) of the piperidine ring are not covered by the density contour. The ring can adopt two different twist conformations. (see Fig. 7.23). This results in a weaker electron density in that area (see Fig. 7.22). The atoms of the two conformers (ALT1 and ALT2 Fig. 7.23) almost overlap except the atoms

C8, C9 at the tail and atoms C1, C2 in the piperidine ring. The result from the refinement for low resolution data (24 Å to 2.05 Å) and for high resolution data are given in the Table 7.17.

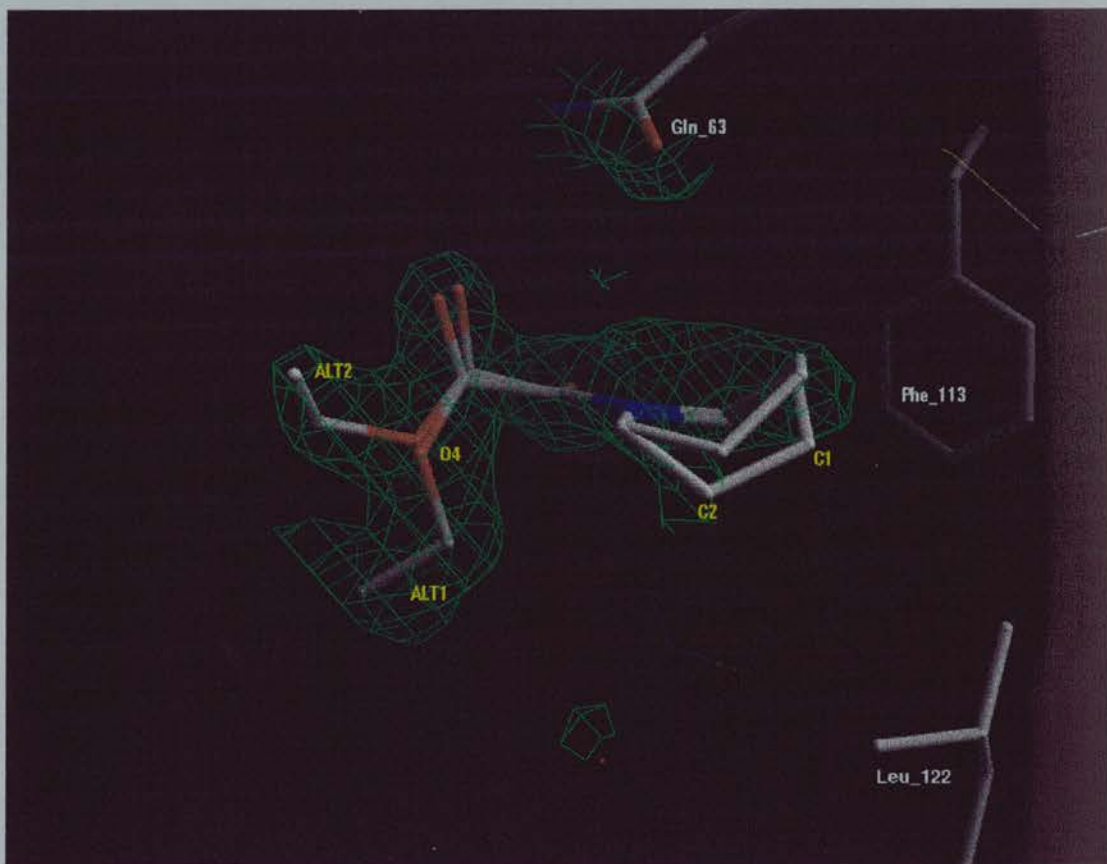


Fig. 7.22: Difference electron density map (2Fo-1Fc) for the ligand ETPIPG when its tail (2 atoms) and piperidine ring (2 atoms) adopts alternative conformations. The model was refined against data from 24 Å to 1.65 Å. Two molecules of the ligand (ALT1 and ALT2) were included in the phase calculation with an occupancy of 50% for each.

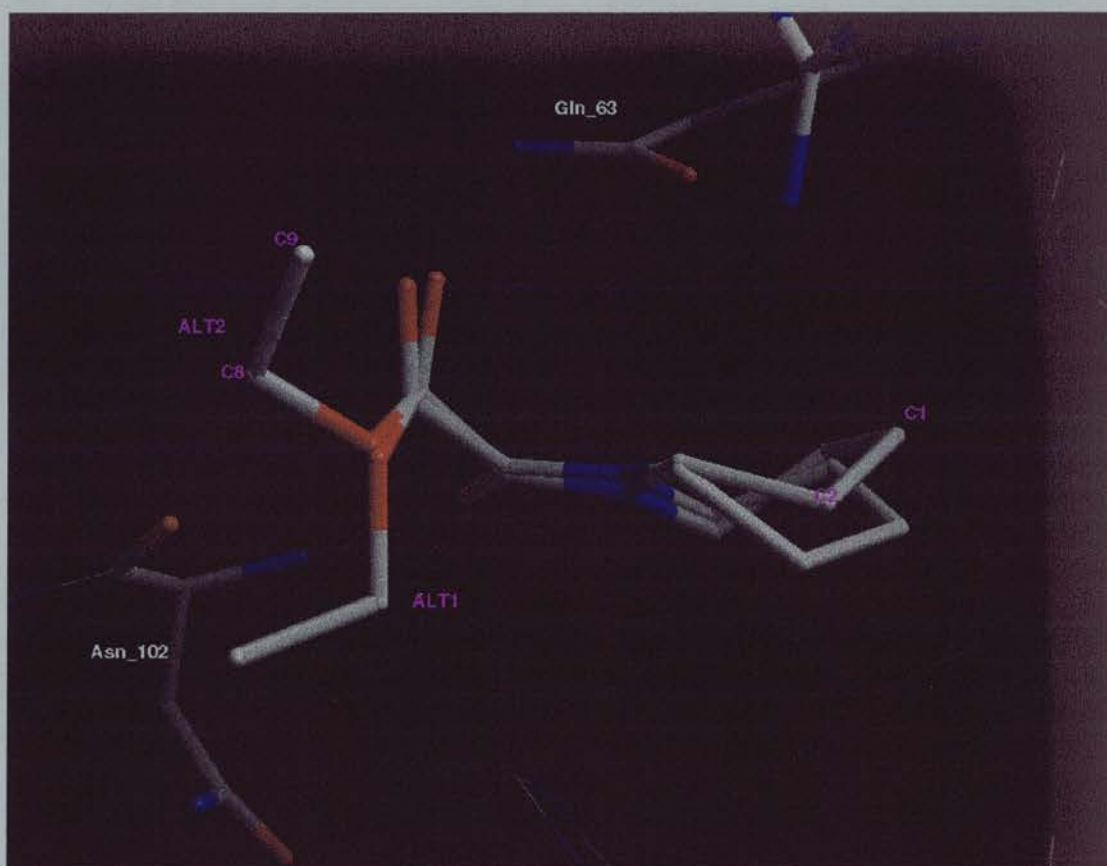


Fig. 7.23: ALT1 and ALT2 of ETPIPG in the binding site of CypA. The main differences between the two molecules are in carbons C1, C2 of the piperidine ring and C8, C9 of the tail of the molecule.

Table 7.17: The model of ETPIPG bound with two alternative conformations (Fig. 7.21 and 7.22) in the active site of Cyp-A was refined against two data sets one low resolution and one high resolution.

Data sets	24 Å to 2.05 Å.	24 Å to 1.65 Å.
R factor	17.9 %	18.8 %
R free	24.3 %	22.8 %
Water molecules	163	244
Average B factor of ligand	ALT1 21.4 ALT2 23.7	ALT1 21.8 ALT2 18.9

The ETPIPG molecule makes one hydrogen bond (Fig. 7.23 A and B) as well as contacts with the surrounding residues. The piperidine ring of ETPIPG (Fig. 7.23 A and B) makes hydrophobic contacts with the phenalanine side chain of residues 60, 113 and histidine 126. Also it makes contacts with the side chain of residues Met 61 and Arg 55.

Table 7.18: Contacts of ETPIPG ligand ALT1 and ALT2 with surrounding atoms of the protein as shown in Fig. 7.23A and 7.23B. The closest contacts of each residue are presented.

Ligand atom ALT1	Distance (Å)	Residue Atom	Ligand atom ALT2	Distance (Å)	Residue Atom
C1	3.23	Phe_60/CZ	C6	3.56	His_126/CE1
C1	3.63	Phe_60/CE1	O3	3.32	Gln_63/NE2
C4	2.95	Arg_55/NH1	O2	3.26	His_126/CE1
C3	3.66	His_126/CE1	O2	2.98	Ala_101/CA
C3	3.66	Phe_113/CE1	O2	2.79	Asn_102/N
C6	3.64	His_126/CE1	C4	3.56	His_126/CE1
O2	3.24	His_126/CE1	C4	3.61	Phe_113/CE1
O2	3.06	Ala_101/CA	C3	2.88	Arg_55/NH1
O2	2.80	Asn_102/N	C5	3.68	Phe_113/CD1
O3	3.54	Gln_63/NE2	C5	3.58	Met_61/SD
			C1	3.56	Phe_60/CZ
			C1	3.62	Phe_60/CE1

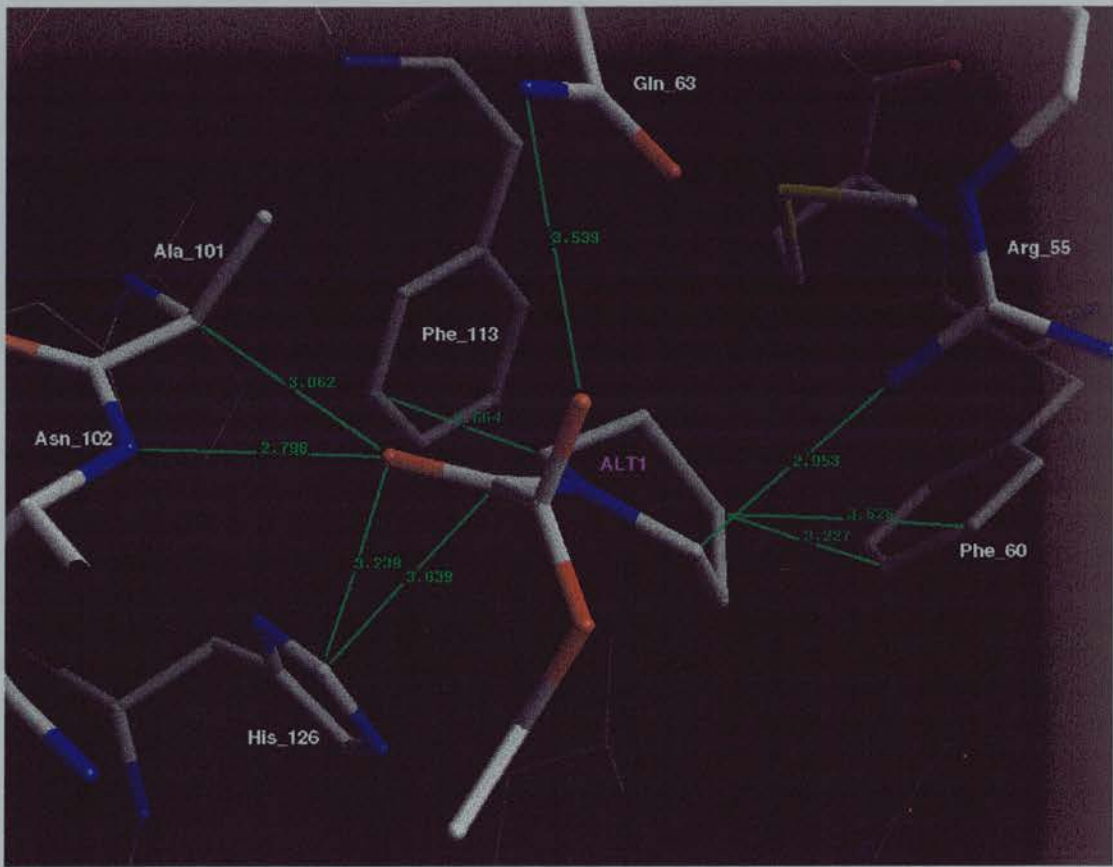


Fig. 7.23A: Contacts of conformer 1 of ETPIPG ligand with surrounding atoms of the protein. ETPIPG (ALT1) makes a hydrogen bond to the N/Asn102 (2.80 Å) and to NE1/Gln63 (3.3 Å). The most hydrophobic part of the ETPIPG (ALT1) molecule (piperidine ring) fits into the hydrophobic pocket and forms a number of contacts with side chains of Phe_60 and Phe_113. The hydrophilic part of the ligand faces the solvent.

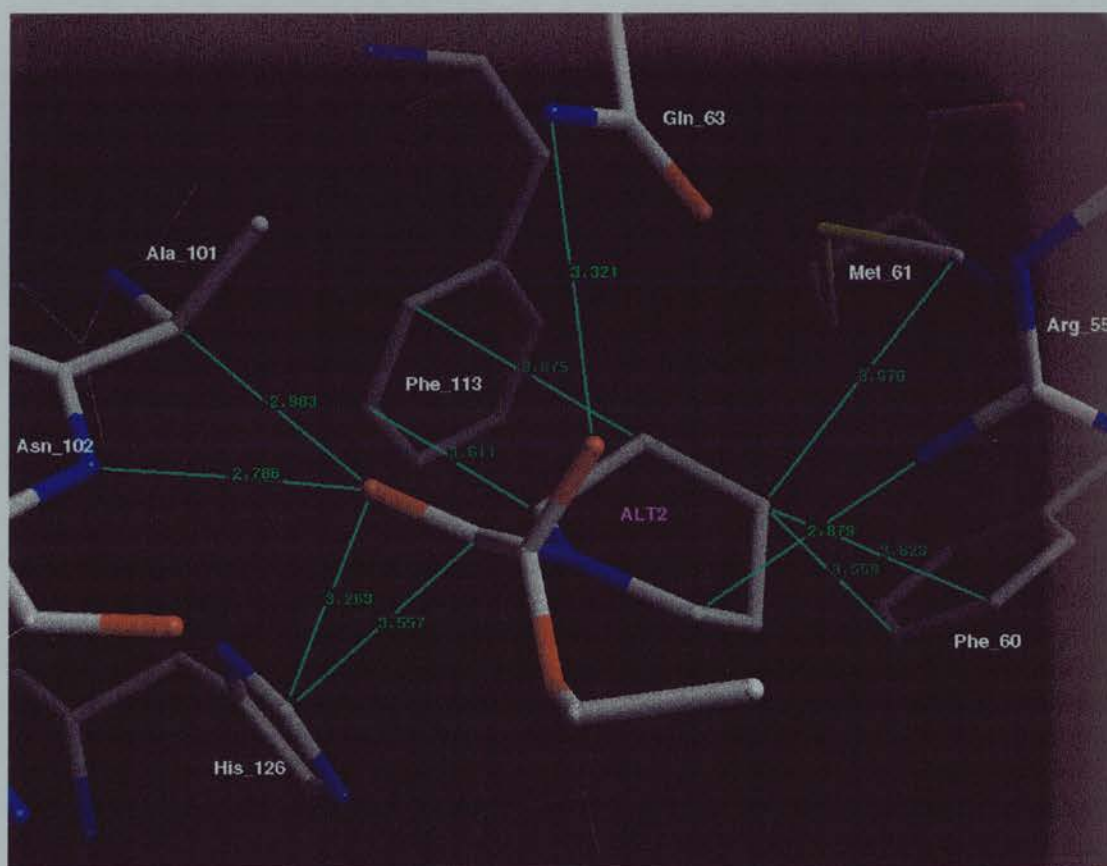


Fig. 7.23B: Contacts of conformer 2 of ETPIPG ligand with surrounding atoms of the protein. ETPIPG (ALT2) makes a hydrogen bond to the N/Asn102 (2.8 Å) and to NE1/Gln63 (3.3 Å). The most hydrophobic part of the ETPIPG (ALT2) molecule (piperidine ring) fits into the hydrophobic pocket and forms a number of contacts with side chains of Phe_60, Phe_113 and Met_61. The hydrophilic part of the ligand faces the solvent.

2. ACMPIP

The same refinement procedure as in ethyl-piperidine glyoxylate was used at the beginning of the refinement. The first difference electron density map (1Fo-1Fc) was calculated and the binding site was inspected (Fig. 7.24). The electron density map in the active site was compared with that of the native (unliganded, Fig. 7.5). The electron density showed convincingly that the binding site was not occupied by water

molecules but by a molecule the size of ACMPIP. An initial conformation of ACMPIP was calculated by the program WITNOTP using force field minimisation (Widmer 1997).

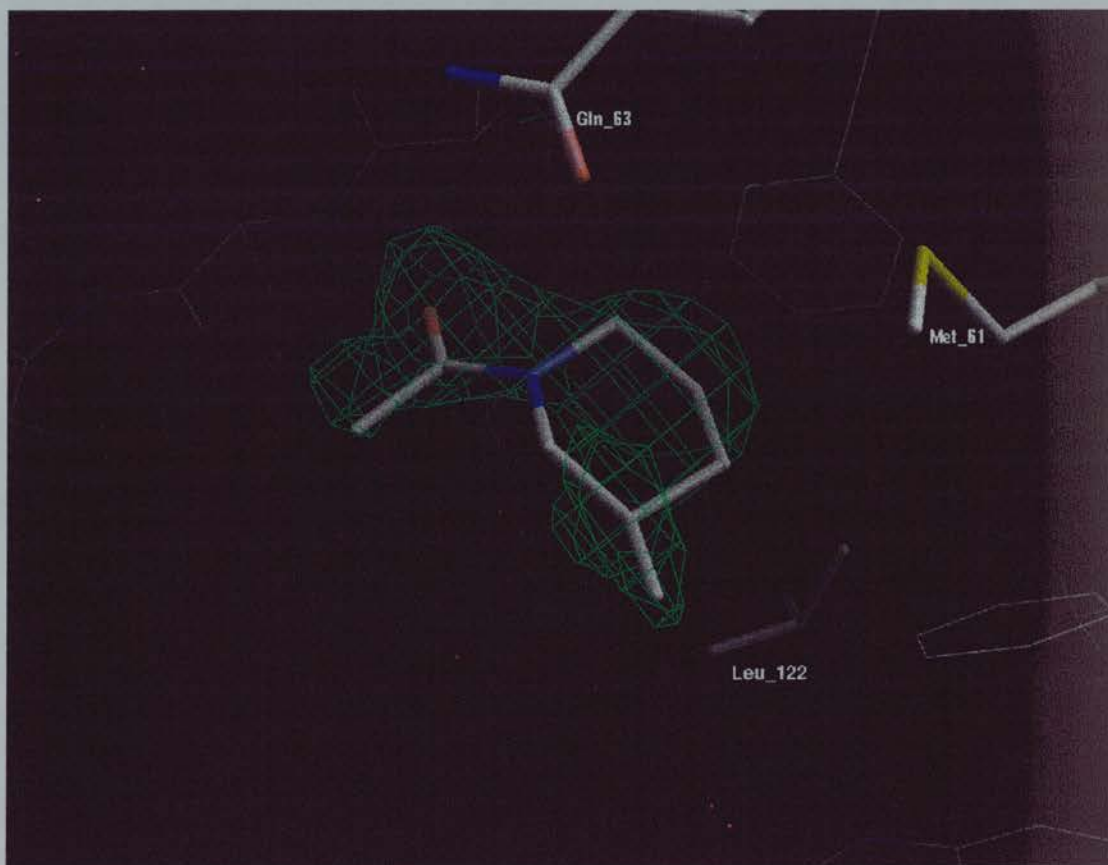


Fig. 7.24: Difference electron density map ($1F_o-1F_c$) for the ligand ACMPIP. The difference electron density was calculated before including the ligand and the water molecules in the model. The water molecules and ligands were taken from the refined structure.

The refinement proceeded by addition of water molecules. The first attempt to model the ligand was after the addition of 169 water molecules and with an R factor of about 20 %. The ligand was introduced into the model and the refinement was continued with positional and individual B-factor refinement. From the ($2F_o-1F_c$) electron

density map it is clear that the ligand fits very well to the contour of the electron density (Fig. 7.25).

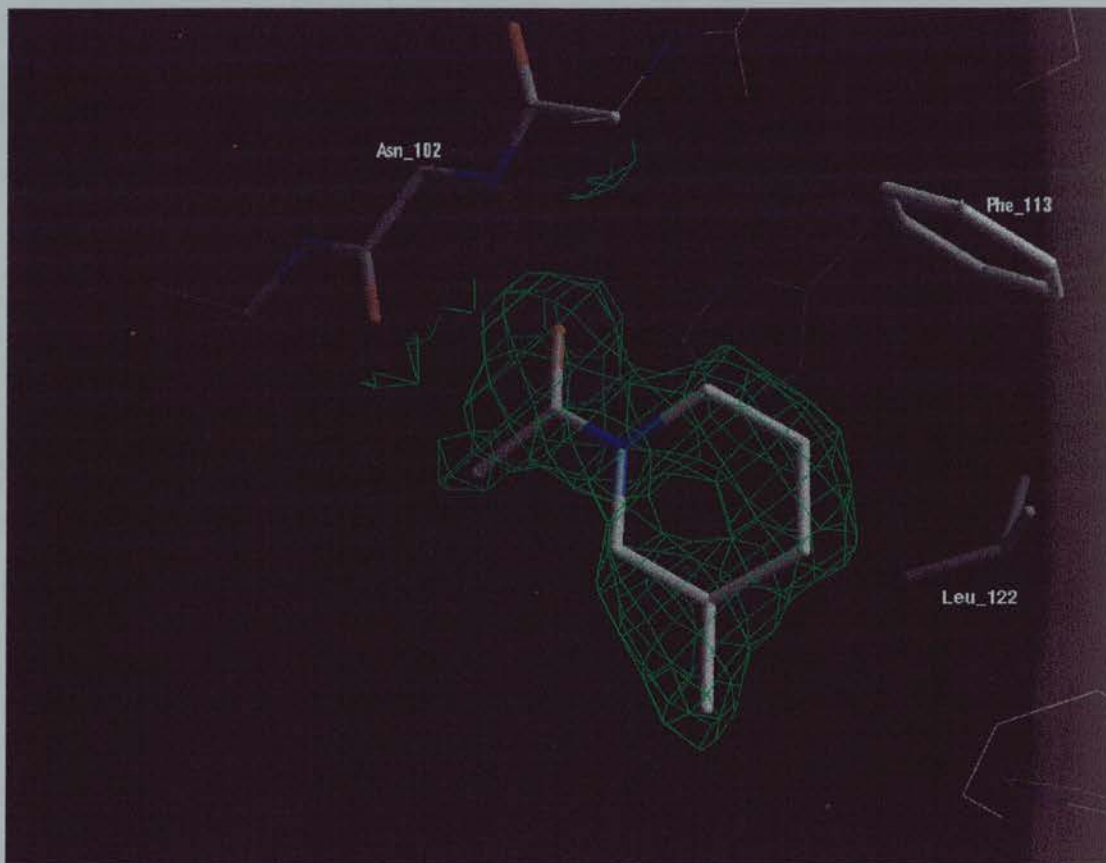


Fig. 7.25: Difference electron density map (2Fo-1Fc) for the ligand ACMPIP. Both water molecules and ligand were included in the phase calculation. The map was contoured only around ACMPIP molecule.

The (2Fo-1Fc) electron density map around residue Arg 55 shows that the side chain adopts two different positions (Fig. 7.26). These two alternative conformations refined to 50 % for ALT1 and 50 % for ALT2 with the program XPLOR. Both alternative conformations of Arg₅₅ form hydrogen bonds; ALT1 with Asn 164 and ALT2 with Gln 63 and water 164.



Fig. 7.26: (2Fo-1Fc) difference electron density map for the side chain of Arg 55. The side chain adopts two conformations and both of them form hydrogen bonds with surrounding residues and the solvent. These two alternative conformations refined to 50 % for ALT1 and 50 % for ALT2 with the program XPLOR.

The ACMPIP molecule makes a number of contacts with the protein (Fig. 7.27). The amide O of ACMPIP forms a hydrogen bond to N of Asn 102 similar to that formed to the amide O2 of ETPIPG (see Fig. 7.23A and 7.23B). The piperidine ring makes a number of hydrophobic contacts with the side chains of Phe 133 and Phe 60.

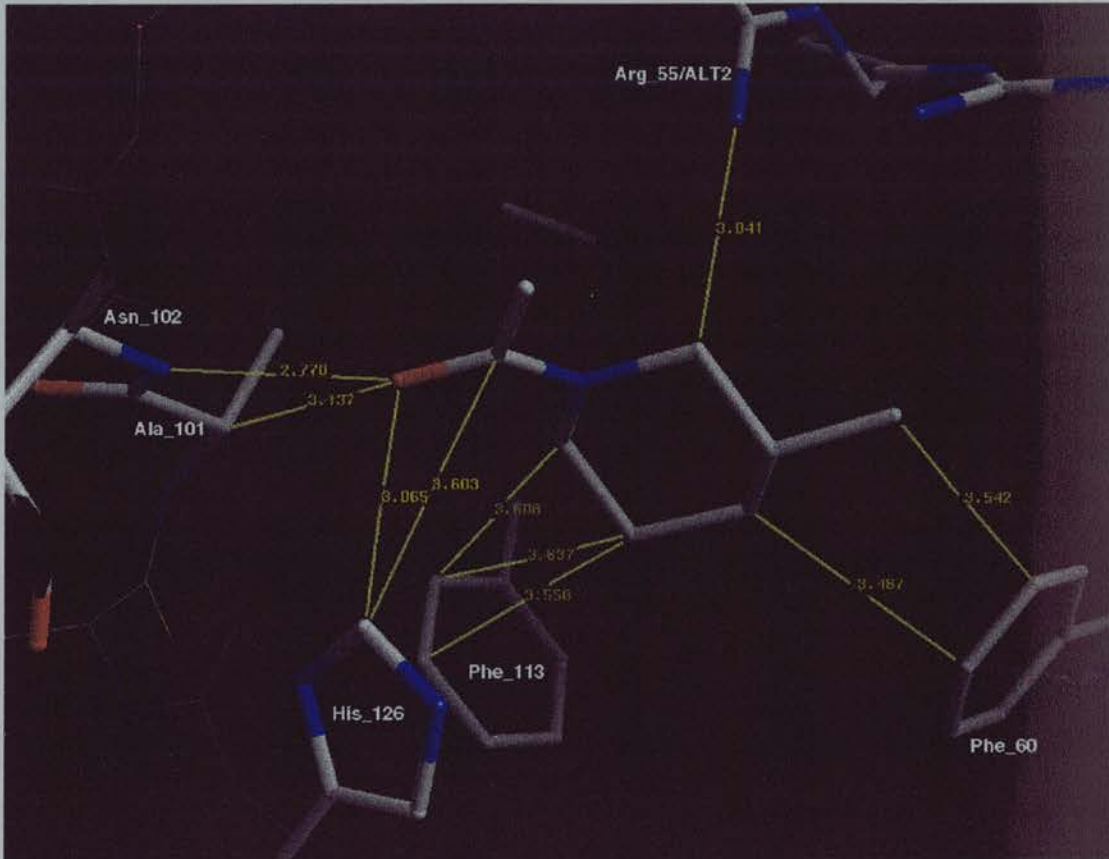


Fig. 7.27: Contacts of ACMPIP ligand with surrounding atoms of the protein. ACMPIP makes one hydrogen bond to the N/Asn102 (2.8 Å). The most hydrophobic part of the ACMPIP molecule (methyl-piperidine ring) fits into the hydrophobic pocket and makes a number of contacts with side chains of Phe_60 and Phe_113.

8. Dimedone

A) Selection and modification of the putative ligands

Selection of the putative ligand was based on molecular weight and hydrophobicity. The most hydrophilic ligands were selected from the list generated by LIDAEUS (see chapter 1 section 1.B). Small molecules can easily go through crystal channels and reach the binding site so molecules with molecular weight larger than 300 were not used for soaking.

The putative ligand found by the LIDAEUS program was the 2,2,5-trimethyl-1,3-dioxane-4,6-dione (Fig. 7.29). A Cyp-A crystal was soaked in a solution containing 20 mM of this ligand and a data set collected. The model was refined following the same procedure as in ETPIPG. The electron density ($1F_o-1F_c$) showed convincingly that the binding site was occupied only by water molecules. The R factor of the model was 25.4 % when the electron density in the binding site was inspected.

The 2,2,5 trimethyl-1,3-dioxane-4,6-dione (TDD) molecule was partially modified (Fig. 7.29). The modifications were based on crystallographic results from other ligands and from modelling. Previous studies (crystallographic results) had shown that the side of the molecule which faces the binding site should be hydrophobic. This theory was based on the fact that 1-acetyl-methyl piperidine binds (see section 3.6) to Cyp-A while 1-acetyl-piperidone does not bind (Fig. 7.29). The main difference between the two molecules is that the 1-acetyl-piperidone is hydrophilic on the piperidine ring side. The piperidine ring of ACMPIP goes into the binding site and is surrounded by hydrophobic residues (Fig. 7.26).

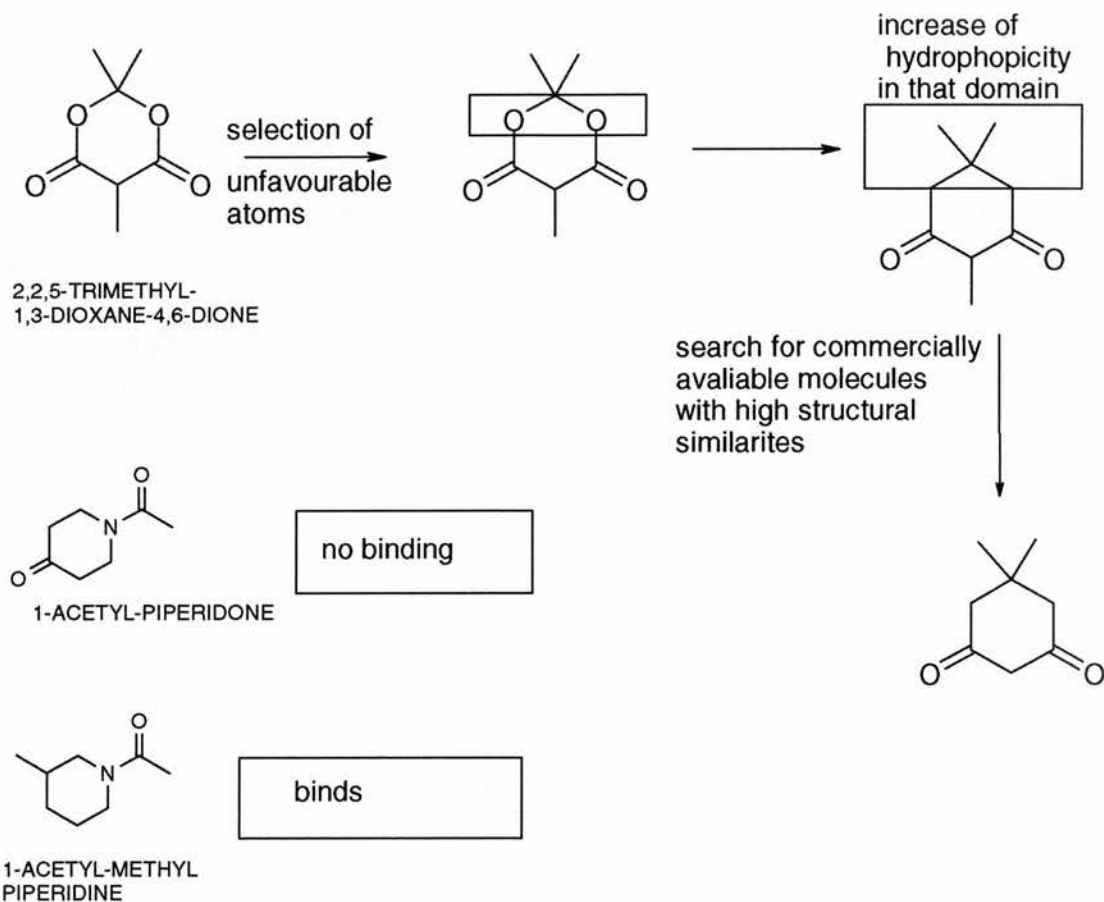


Fig. 7.29: Modifications applied in the ligand (TDD) found by the docking program, based on crystallographic data from ligands APD and ACMPIP. The result of these modifications was the DCH molecule.

The TDD molecule was modelled by the LIDAEUS program to bind with the two methyl groups and two ether oxygens going into the binding site. Since it was known that the binding surface of the ligand should be hydrophobic, the two ether oxygens were replaced by carbon atoms (Fig. 7.28). That molecule was used as a template to search for structurally similar molecules in ISIS. The most similar molecule found by this search was the dimedone (Fig. 7.29).

B) Refinement of DCH data

The refinement procedure was started with a translation search (protein model from DMSO structure) and proceeded with rigid body refinement, positional and individual B-factor refinement. At that point the first difference electron density map (1Fo-1Fc) was calculated and the binding site was inspected (Fig. 7.30). The electron density map on the active site was compared with that of the native (unliganded, Fig.7.6). The electron density showed convincingly that the binding site was not occupied by water molecules but by a molecule of the size of DCH. The R factor was about 28 %.

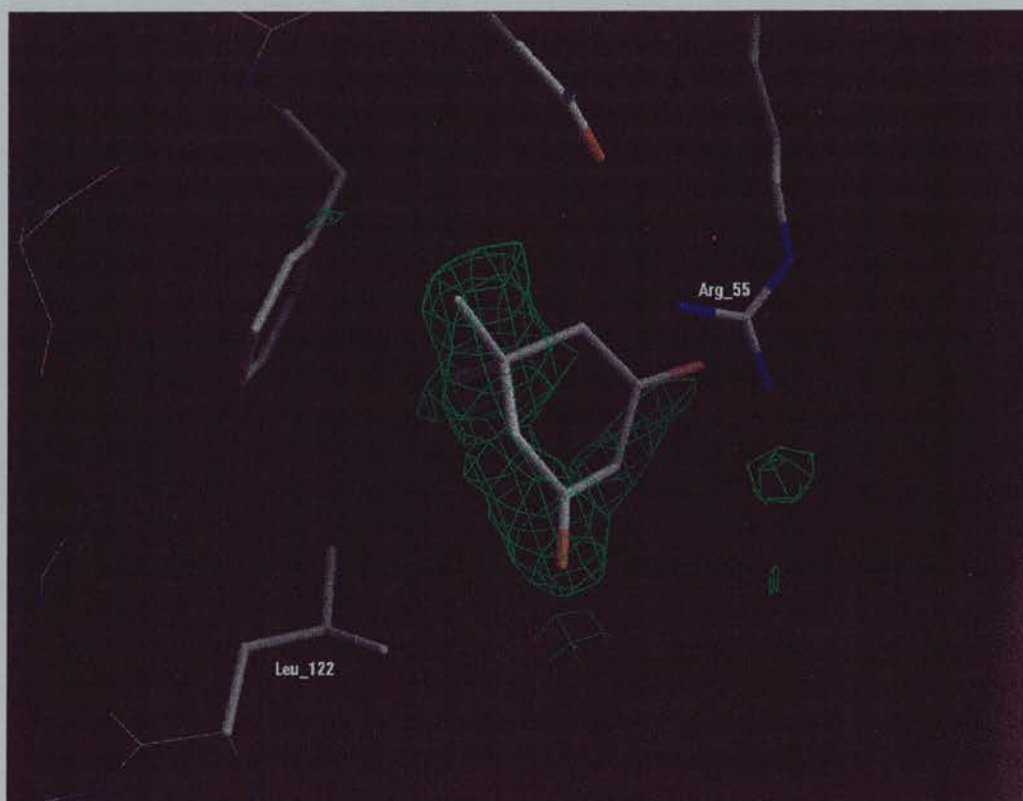


Fig. 7.30: Difference electron density map (1Fo-1Fc) for the ligand DCH. The difference electron density was calculated before including the ligand and the water molecules in the model. The water molecules and ligands were taken from the refined structure.

The refinement proceeded by addition of water molecules. The first attempt to model the ligand was after the addition of 147 water molecules and with the R factor of the model at 21.8 %. The side chain of Arg 55 adopts a different position compared to the DMSO complex (the DMSO structure of Cyp-A was used as a starting model)

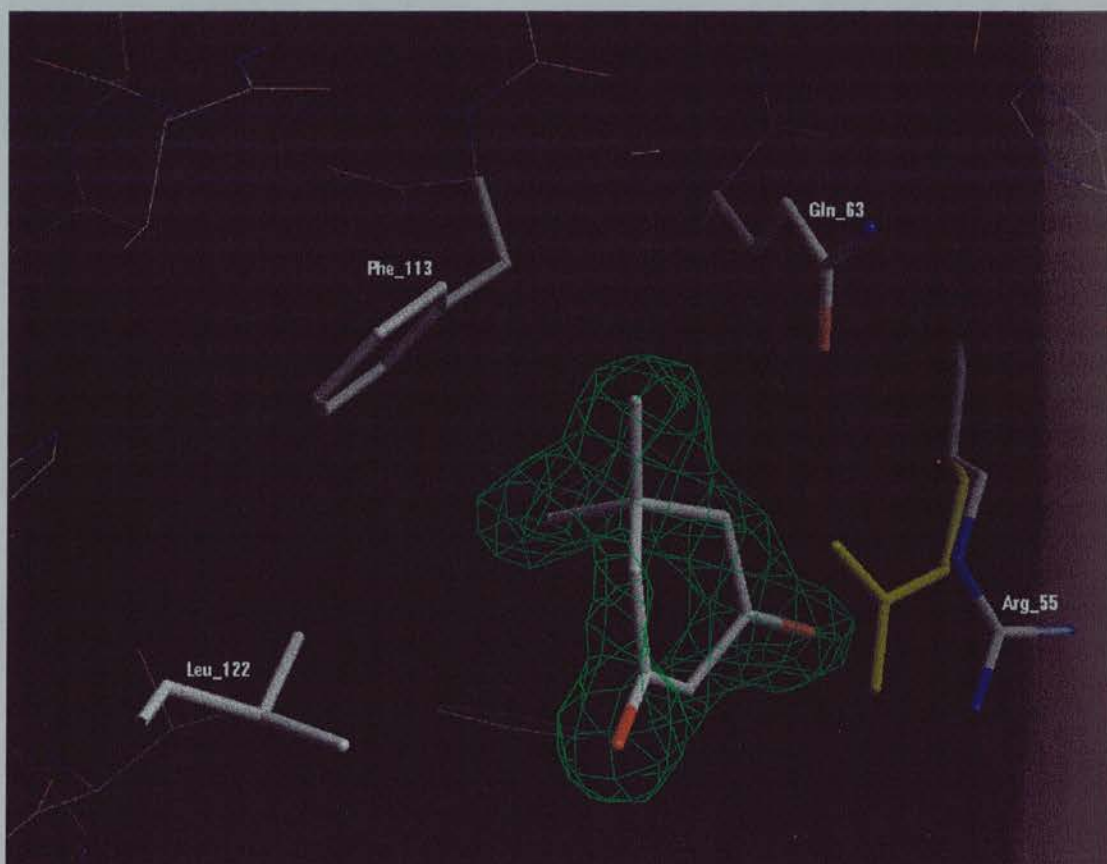


Fig. 7.31: Difference electron density map (1Fo-1Fc) for the ligand DCH. The difference electron density was calculated before including the ligand in the model. The ligand was taken from the refined structure. The side chain of Arg 55 moved further back in order to allow the ligand to bind. The yellow colour shows the position of the side chain of Arg 55 in the starting model (DMSO structure).

The ligand was introduced into the model and the refinement was continued with positional and individual B-factor refinement. From the electron density map (2Fo-

1Fc) the ligand fits very well to the contour of the electron density (Fig. 7.32). The DCH molecule makes a number of contacts with protein and the solvent (Fig. 7.33).

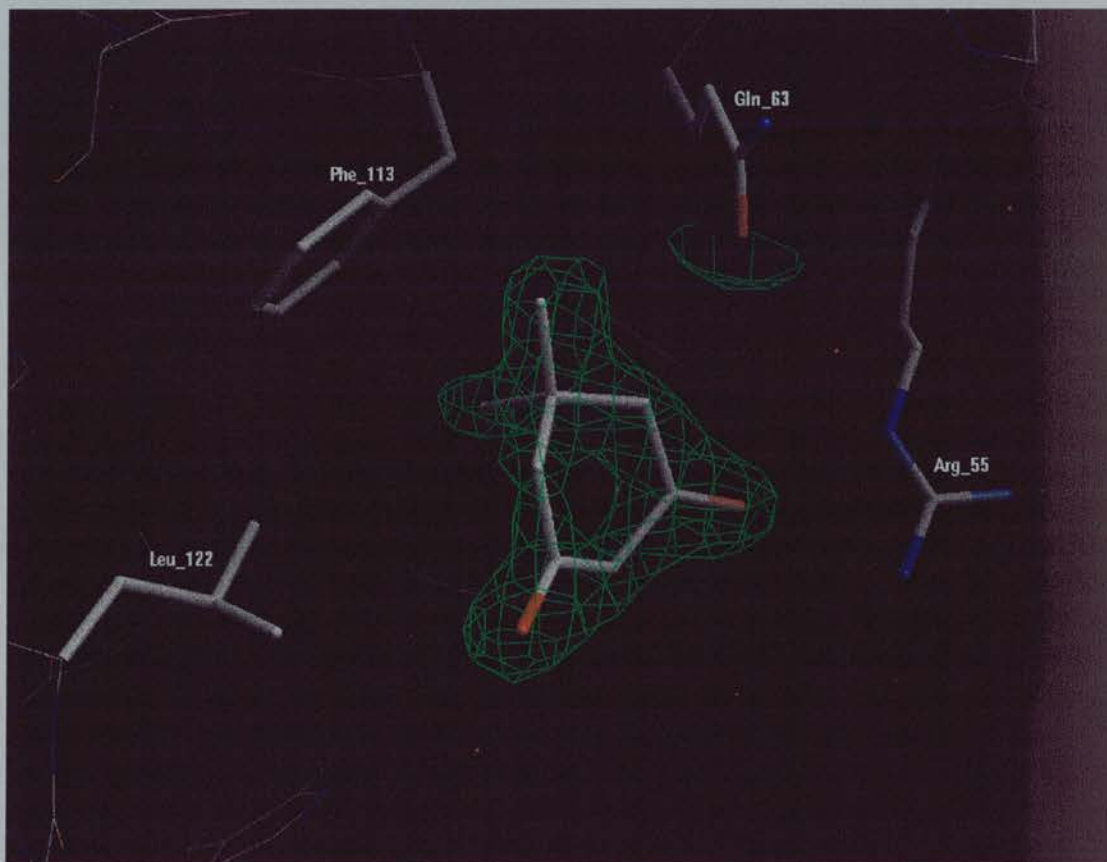


Fig. 7.32: Difference electron density map ($2F_o-1F_c$) for the ligand DCH. Both water and ligand were included in the phases calculation. The map was contoured only around DCH.

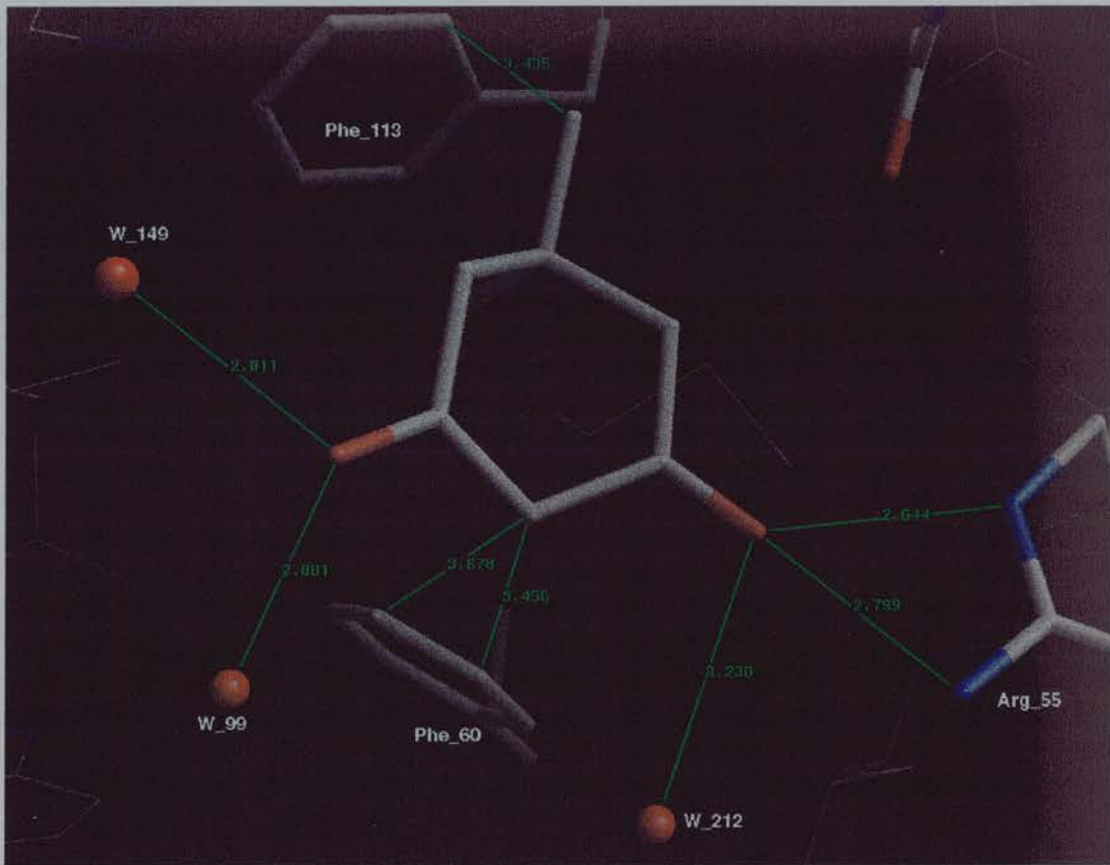


Fig. 7.33: Contacts of DCH ligand with surrounding atoms of the protein and the solvent. DCH makes five hydrogen bonds, two with the side chain of Arg₅₅ and three with W₉₉, W₁₄₉ and W₂₁₂. Also it forms hydrophobic contacts with side chains of Phe₆₀ and Phe₁₁₃.

B) FKBP-12

1. Introduction

As with CyP, several classes of FKBP have been found: one is cytosolic with a molecular weight of 12,000 daltons (FKBP-12, Maki et al., 1990). Another is membrane-associated with a molecular weight of 13,000 daltons (FKBP-13, Jin et al., 1991) with 43% sequence identity to FKBP-12 and exact identity for all amino acids lining the FK506 binding pocket. There is also a rapamycin-selective immunophilin, FKBP-25 (215 amino acids, Galat et al., 1992).

Although CyP and FKBP share some common properties such as immunosuppressant binding and rotamase activity, FK506 does not bind to CyP nor inhibit its rotamase activity, and similarly CsA does not bind to FKBP(Siekierka, et al., 1989; Harding et al., 1989).

Three-dimensional structures of FKBP have been solved for the unligated form (NMR, Michnick et al., 1991; Moore et al., 1991), for the FK506-FKBP complex (X-ray, Van Duyne et al., 1991a), and for the rapamycin-FKBP complex (Van Duyne et al., 1991b). Overall, the structure of FKBP is different from CyP (Ke et al., 1991).

FK506 has a *trans* configuration around the N7-O8 bond (Fig. 33A) in the bound state (Van Duyne et al., 1991) and *cis* in the unbound state (Tanaka et al., 1987). It is striking that FK506 changes its configuration from *cis* to *trans* upon binding to the FKBP-12. The overall FKBP-12 structure observed for all new FKBP-12 inhibitor complexes was not significantly different from that found in the uncomplexed protein or in the FKBP12 -FK506 or FKBP12-rapamycin crystal structures (Lepre et al., 1994; Michnick et al., 1991; Wilson et al., 1995; Van Duyne et al., 1991).

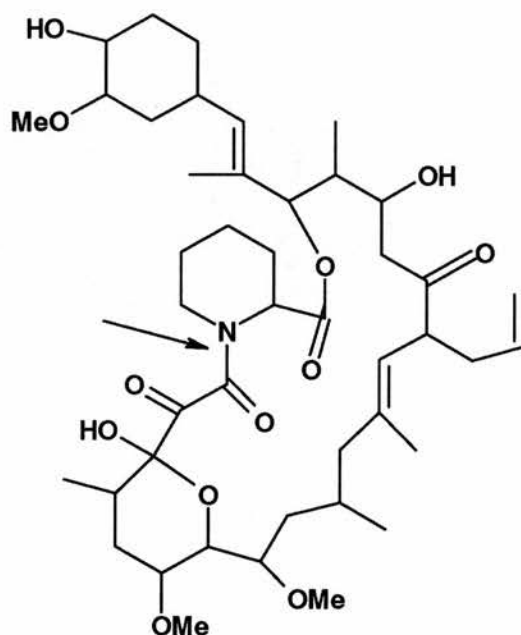


Fig. 7.33A: Structure of FK506 the arrow indicates the N7-O8 bond which changes from *cis* to *trans* when FK506 binds to the FKBP-12.

High affinity FKBP ligands, which bind to the active site of FKBP interact with: Phe 36, Asp 37, Arg 42, Phe 46, Glu 54, Val 55, Ile 56, Tyr 82, His 87, Ile 90, and Ile 91 (Holt et al., 1993). Another series of smaller FKBP ligands bind to the same pocket and form bonds with Asp 37, Ile 56, Tyr 82 (Burkhard, 1995). These three residues (Asp 37, Ile 56, Tyr 82) were principally responsible for the binding of eight small compounds in the FKBP-12 binding pocket.

The ligands tested by x-ray crystallography were cyclooctanone, cyclohexanone, and 5-beta-pregnane-3,20-dione. All of these ligands showed binding activity by fluorescence assay.

2. Overview

Crystals grown in AS and DMSO were used for soaking in all ligands (see chapter 6.3.C). DMSO binds in the active site of FKBP-12 and before introduction of any new ligands DMSO must be soaked out of the binding site.

The structure of FKBP complexed with DMSO (Burkhard 1995) was used as a starting model for rotation and translation searches. All atoms (except the ligand and the solvent) from the model structure were used in the search since the homology is 100%. A translation search using the program XPLOR, was enough to locate the molecules in the unit cell since the unit cell dimensions are similar to that of the model. The refinement and the addition of water molecules was done using SHELX (Sheldrick et al 1997).

3. Cyclooctanone

Two cyclooctanone data sets were refined during this work, one with data to 1.8 Å (oct_1) and one with data to 2.05 Å (oct_2) (see table 5.4 chapter 5). Data from 3.5 to 15 Å were used during the translation search. The R factor for the model generated after the translation search using data oct_1 was 36.2 % (program XPLOR). The refinement procedure was continued with rigid body refinement, positional and individual B-factor refinement and the R factor dropped to 35.9 %. At this point the first difference electron density map (1Fo-1Fc) was calculated and the binding site was inspected (Fig. 7.34).

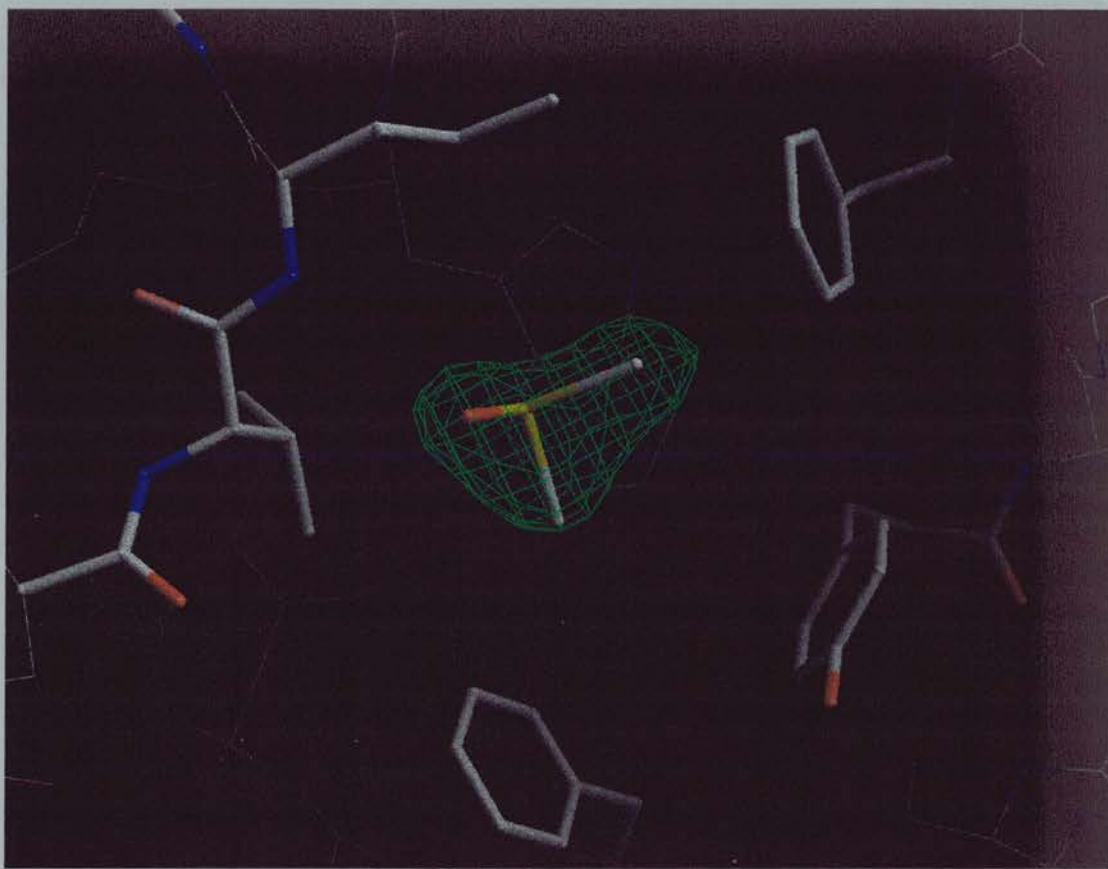


Fig. 7.34: Difference electron density map (1Fo-1Fc). The electron density has the shape and size of DMSO. The difference electron density was calculated before including the ligand and the water molecules in the model.

A trace of DMSO was present in the binding site of FKBP (Fig. 7.34). The refinement did not proceed further since the cyclooctanone was not present.

The second data set (see Table 6.4 chapter 6) was refined as described for the first one. The first difference electron density map (1Fo-1Fc) was calculated with an R factor of 35.5 % and the binding site was inspected (Fig. 7.35). The electron density in the binding site was different than that obtained from the first data set (Fig. 7.34). The refinement proceeded with addition of water molecules. After the addition of 62 water molecules the R factor dropped to 23.8 %.



Fig. 7.35: Difference electron density map (1Fo-1Fc) in the binding site of FKBP-12. The electron density is different from that in Figure 7.34. The difference electron density was calculated before including the ligand and the water molecules in the model.

The ligand was introduced into the model and refinement continued with positional and individual B-factor refinement. The R factor of the model was 21.5 % and the free R factor 29.7 % (SHELX for all reflections). The root-mean-squared deviations were 0.005 Å and 1.67° from the ideal geometries. This model consisted of the protein molecules A and B, 57 water molecules and the two cyclooctanone molecules one for each protein molecule. This model was used for the calculation of a 2Fo-1Fc electron density map (Fig 7.36). All the atoms of the cyclooctanone molecule were covered by the electron density contour as can be seen in Figure 7.35. It is known that cyclooctanone can adopt more than one conformation and this can be seen also from

the electron density. The refinement did not proceed further since it was clear that the ligand (cyclooctanone) occupied the binding site and was covered completely by electron density.

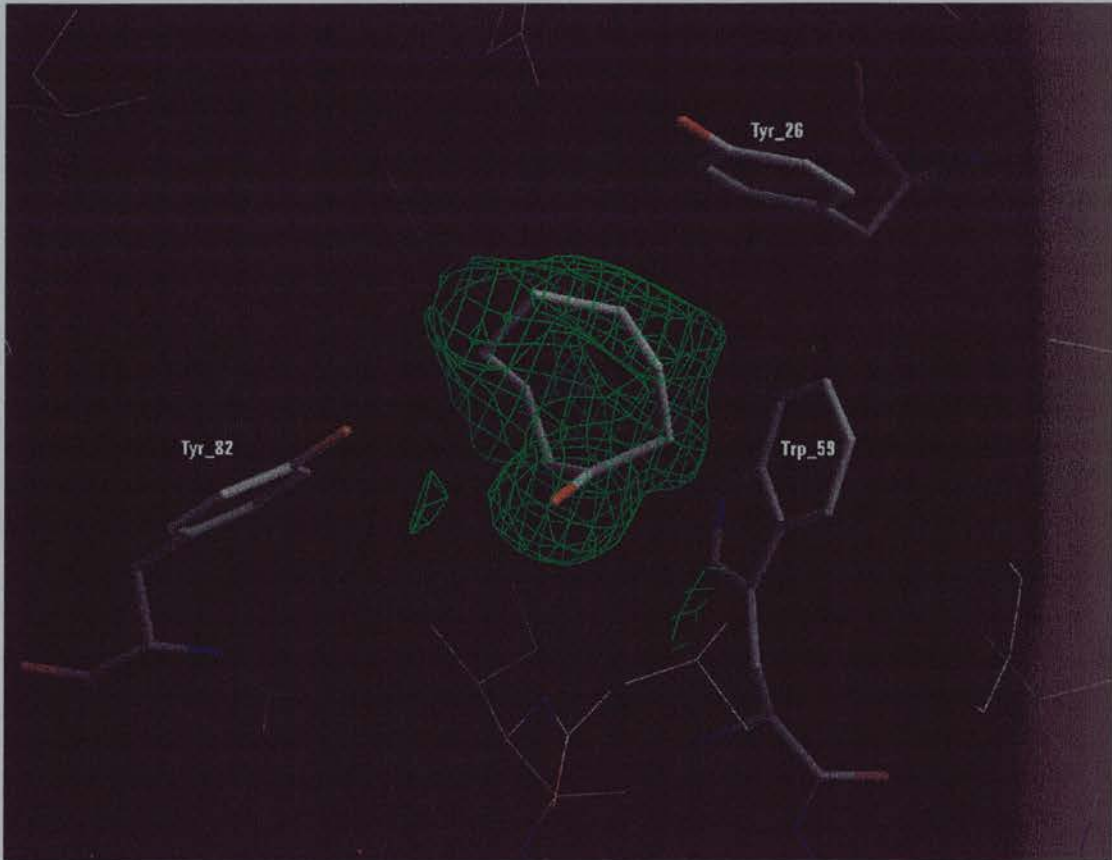


Fig. 7.36: Difference electron density map (2Fo-1Fc) for the ligand cyclooctanone. Both water and ligand were included in the phases calculation. The map was contoured only around cyclooctanone molecule.

3. Cyclohexanone

The refinement procedure was as described for cyclooctanone. The first difference electron density map (1Fo-1Fc) was calculated with a R factor of 31.8 % and the binding site was inspected (Fig. 7.37). From the first electron density map it was

difficult to decide if the density was DMSO or cyclohexanone since the difference in shape and size between them is not great. The refinement proceeded by addition of water molecules. With an R factor of 27.9 % and 105 water molecules added into the model an electron density map (1Fo-1Fc) was calculated (Fig. 7.38).

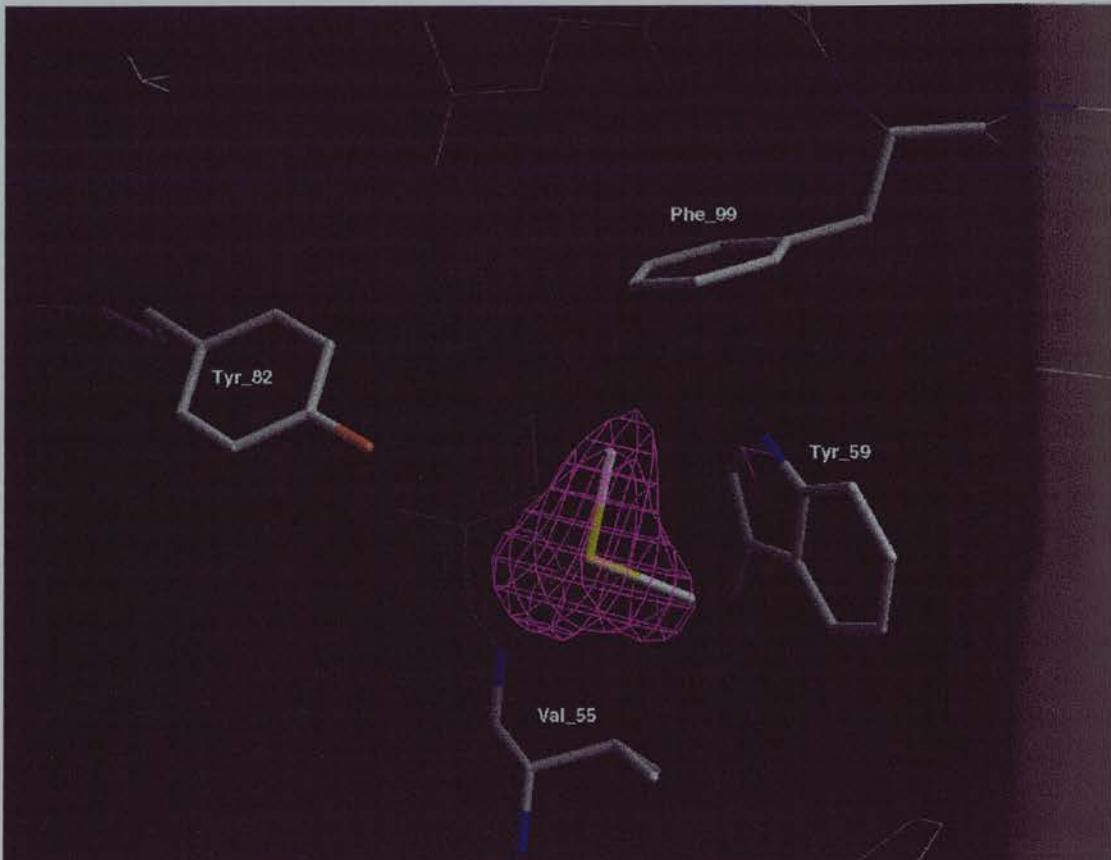


Fig. 7.37: Difference electron density map (1Fo-1Fc). The electron density has the shape and size of DMSO. The difference electron density was calculated using only the coordinates of the protein without the ligand and water molecules.

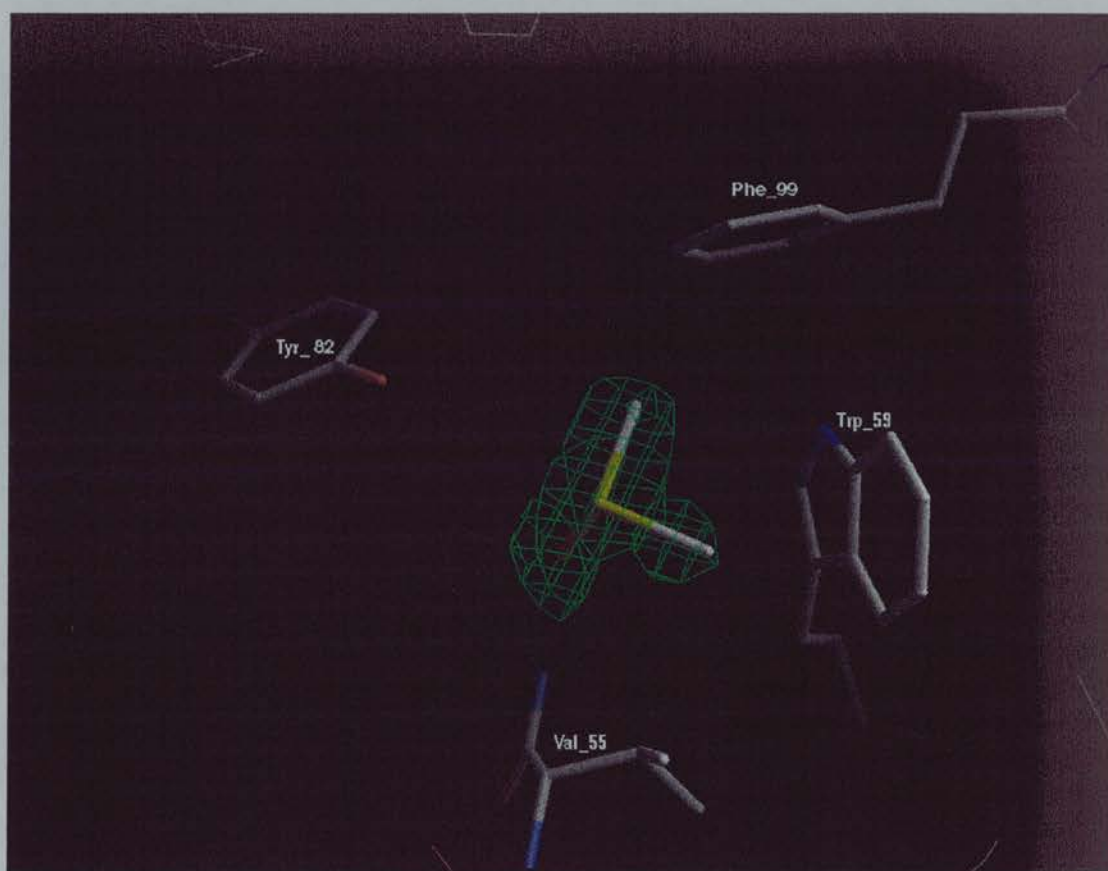


Fig. 7.38: Difference electron density map (1Fo-1Fc). The difference electron density was calculated after addition of 105 water molecules in the model. The DMSO molecule fitted into the density and was not used for the calculation of the phases.

The refinement did not proceed further since only DMSO was present in the binding site.

3. Pregnane

The refinement procedure was as described for cyclooctanone. The first difference electron density map (1Fo-1Fc) was calculated with a R factor of 34.8 % and the binding site was inspected (Fig. 7.39). The refinement did not proceed further since only DMSO was present in the binding site.

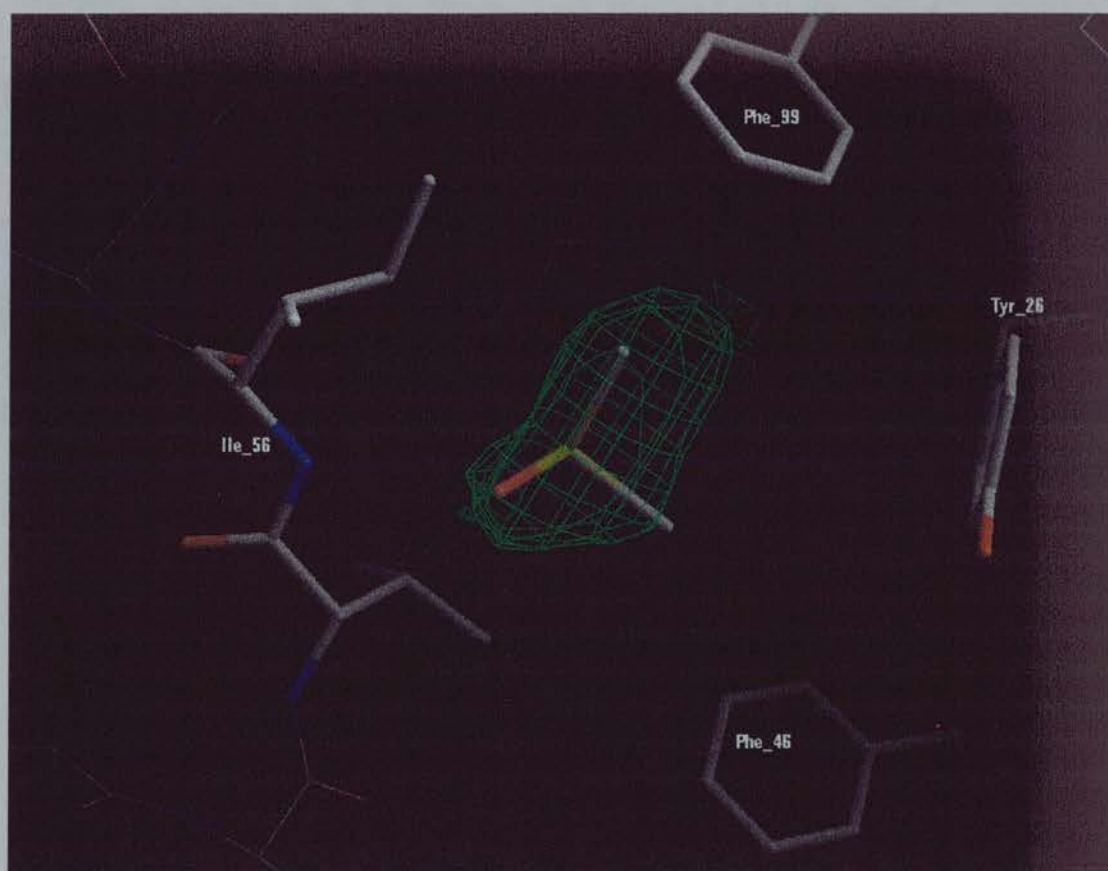


Fig. 7.39: Difference electron density map (1Fo-1Fc). The electron density has the shape and size of DMSO. The difference electron density was calculated without including the DMSO in the model.

C) BrCyp

1. Introduction

Cyclophilins have been found in numerous parasites, including the human filarial nematode *Brugia malayi*. *B. malayi* is a medically important parasite found in tropical countries, and infection is transmitted via mosquito vectors and can result in chronic debilitating filarial disease symptoms, which can include elephantiasis (Page et al 1995). BrCyp is a protein of the cyclophilin family from *Brugia malayi* nematode parasite with a molecular weight about 22kD (the sequence of BrCyp can be seen in appendix 1).

The protein has been characterised biochemically and has been shown to possess PPIase activity which can be inhibited by CsA (Page et al 1995a). Independent of its immunosuppressive activity CsA has powerful killing properties against a wide range of infectious organisms including large multicellular helminth parasites (Page et al 1995b). The precise mode of action of CsA, or its derivatives, against protozoan and helminth parasites is presently unknown and may involve an interruption of an essential signal transduction pathway, or inhibition of PPIase activity resulting in improper protein folding of a vital parasite molecule(s). BrCyp was purified (chapter 3) and crystallized (chapter 4) in the current work and the structure determination of the protein is described here.

2. Refinement of BrCyp data

A) Trigonal form

The space group $P3_12_12$ was indicated as the best candidate for this data set (trigonal 1.9 Å, see chapter 6, section 3.2.C) from SCALEPACK program (see chapter 6, section 5.D). A rotation search was run in XPLOR for data in the resolution range 10 to 2.6 Å with the search model consisting of CypA from the CypA/CsA complex

(Mikol et al 1993). Only one peak was found in the rotation function search. The translation function (XPLOR) showed a solution consistent with two molecules in the asymmetric unit related by an almost exact translation of $c/2$. The same results were observed by using the molecular replacement protocol from AMORE (Navaza & Saludjian 1997) by Dr P. Taylor (Taylor et al 1998). 10 % of the reflections were chosen randomly and not used in the refinement. These reflections were used for calculation of the free R factor. The structure was refined further by Dr P. Taylor using alternating rounds of positional and B factor refinement using the data in resolution range 5-1.9 Å, with water molecules added to the model. Refinement stuck at 32 % and the packing arrangement suggested that the crystal may be composed of an intimate twin.

It was possible to refine the structure using half of the data set with a unit cell of $a = b = 88.9$ Å, $c = 53.2$ Å, and space group $P3_22_12$. The above suggest that one possible twin may be a mixture of this small unit cell with one molecule per asymmetric unit overlapped with a larger cell with two molecules per asymmetric unit. No further attempt was made to refine the trigonal structure and an effort was put in crystallization trials into order to get a different crystal form.

B) Tetragonal form

A second crystal form grown from ammonium sulphate was found to have space group $P4_12_12$ (see chapter 6, section 3.2.C) from SCALEPACK program (see chapter 5, section 5.D). A rotation and translation search was carried out by Dr P. Taylor (see Taylor et al 1998) as well as most of the building of the protein model. Further refinement proceeded with addition of water molecules followed by positional and B factor refinement (XPLOR). The final structure has an R factor of 19.9 % and R free 23.4 %. RMS deviation from ideality in bond length, bond angle and torsion angle are 0.008 Å, 1.426° and 26.02° respectively. The mean temperature factor for the protein

and water molecules are 27.2 Å² and 43 Å² respectively. The parameter values of stereochemical quality of the refined BrCyp structure can be seen in Table 7.19.

Table 7.19: Stereochemical quality values of BrCyp structure.

Region	most favoured	additional allowed	generously allowed	disallowed
BrCyp	84.5 %	15 %	0 %	0 %

Main Chain Parameters	Omega angle	Bad contacts	Zeta angle	H-bond energy
Typical value	6	3.7	3.1	0.8
BrCyp	1.6	0	1.6	0.7

Side Chain Parameters	Chi-1 gauche minus	Chi-1 trans	Chi-gauche plus	Chi-1 pooled	Chi-2 trans
Typical value	17.7	18.6	17.2	17.8	20.1
BrCyp	15.9	18.0	11.9	14.8	12.5

The amino acid N-terminal fusion derived from the vector multiple cloning site (ile-ser-glu-phe-gly-ser the sequence of BrCyp can be seen in appendix 3.1) was not visible in the final electron density map. Mass spectrometry was used to measure the molecular weight of the protein at 20095Da (major peak Fig.7.41). This compares with a calculated weight of 20100Da for the 183 aa total protein and confirmed that no N-terminal cleavage had occurred. The mass spectrum was performed by Ms Violet R. Anderson. Electrospray ionisation spectra were acquired on a Micromass

Platform II mass spectrometer with an atmospheric pressure electrospray ion source and a maximum range of 4000 m/z. The sample was at 20pmoles/microlitre in 50% acetonitrile with 0.05% acetic acid was introduced via an infusion pump. Data was collected from 500-3000m/z at a cone voltage of 70V. The data was collected and processed using MassLynx software and deconvoluted using the MaxEnt algorithm.

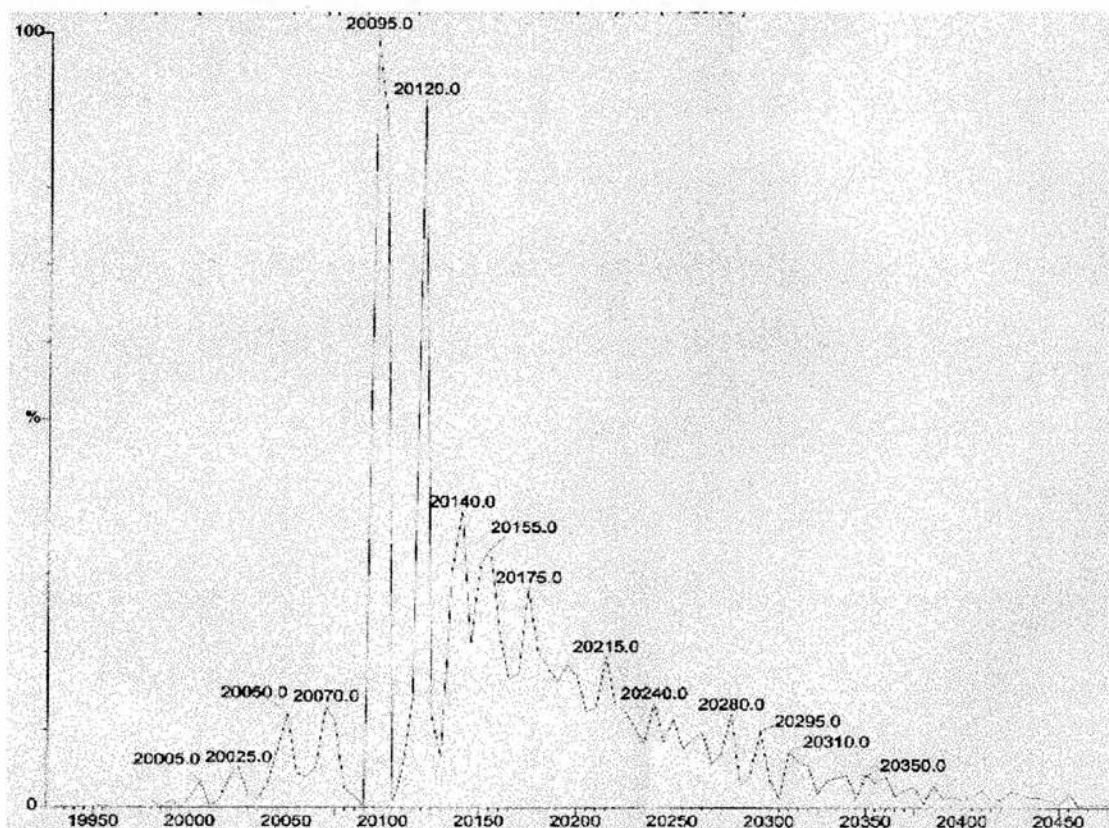


Fig. 7.41: Mass spectrum of BrCyp. The major peak 20095 Da is practically the same as the calculated weight of 20100Da for the 183 aa.

The divergent family of cyclophilins contain two cysteines (see sequence of BrCyp in appendix 1). The sulphur atoms of C-43 and C-173 are well defined in the difference electron density map (Fig. 7.42) and are separated by 5.43Å. Those two cysteines could form a disulphide bond by a small adjustment in the χ_1 torsion angles. This crystal is apparently composed of the reduced cysteine form.

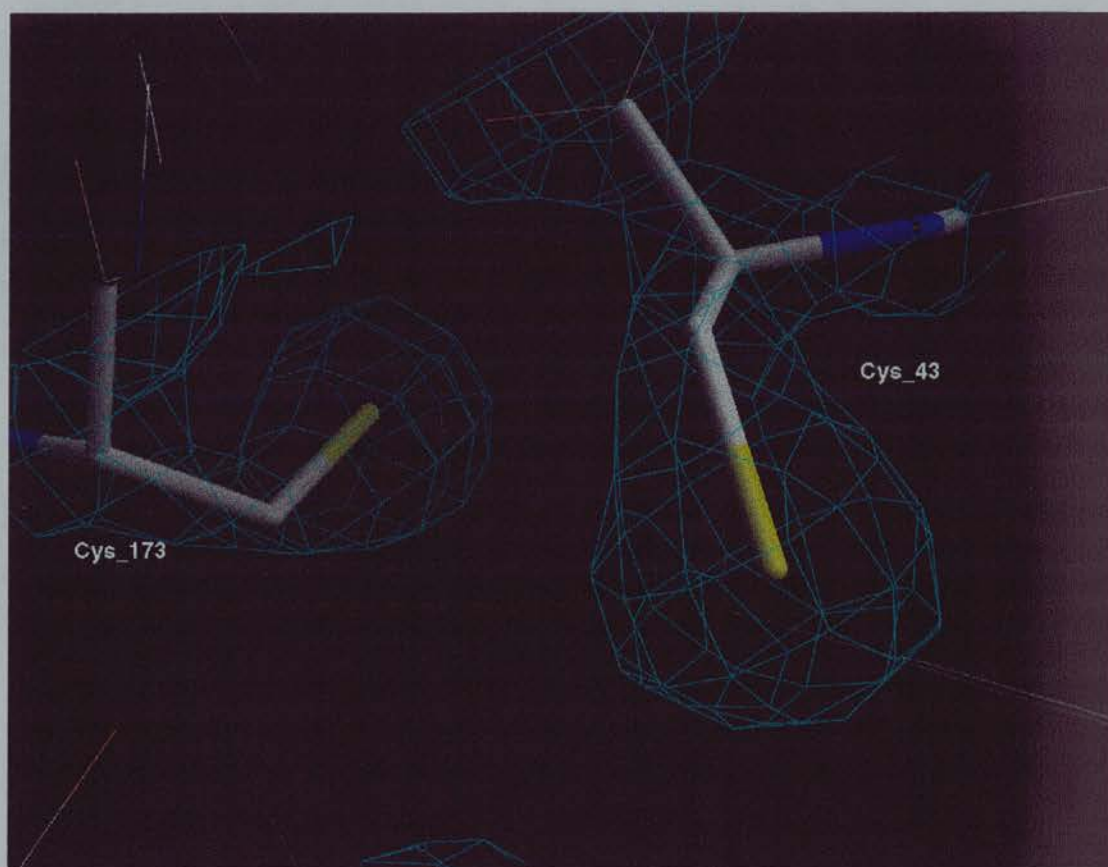


Fig. 7.42: Difference electron density map ($2F_o-1F_c$) for the side chains of the two cysteines (Cys 43 and 173) of BrCyp. The electron density map shows that no disulphide bond is present.

7. 4 Discussion

A) Cyp-A

The small ligand/CypA complexes and the native structure refined during this work were compared with published structures 1cwa, 2cpl, 1cyh of CypA (see section 2.2).

All small molecule complex structures have a similar rmsd when overlaid with the native structure refined during this work (Table 7.20). All protein atoms were used except residues 1 to 4, 67 to 76 and 162 to 165. The loop Phe/67 to Lys/76 also known as “70 loop” was excluded. It has been shown to adopt a different conformation and has significant atom displacements (1.7 Å for main chain atoms) when different CypA-CsA structures are overlaid (Kallen et al 1998).

Table 7.20: Rms differences between native CypA atom position and small ligand complexes [Å], using all protein atoms except residues 1 to 4, 67 to 76 and 162 to 165.

Structure	main chain
DMSO	0.151
TMSO	0.384
PNT	0.108
ACMPIP	0.286
ETPIPG	0.367
DCH	0.211

1. Native

The active site of the native CypA structure is occupied by six water molecules. W 105, W 106, W 109, W 121 W 198 and W 208 (Fig. 7.7). Depending upon which ligand is bound, a number of these water molecules are replaced. It may also be possible to incorporate some of these water molecules into the design of a ligand.

Water molecules 198, 106, 121 and 109 (Fig. 7.7A) were not observed in the 2cpl structure (native structure of Cyp-A, Ke 1992). In the current work 192 water molecules have been found compared to only 119 in the 2cpl structure. This was not as a result of overrefining the structure as the R factor (17.4%) is very close to the Rfree (21.9%) the Rfree was not reported for the 2cpl structure.

Water molecules in the 2cpl structure have an overall temperature factor much higher (47.5 \AA^2) than the native structure reported in this work (31.2 \AA^2). Some of the water molecules in the Ke structure have a temperature factor higher than 70 \AA^2 whereas in the current structure all water molecules have temperature factors below 70 \AA^2 . The high temperature factor of water molecules in the 2cpl structure means that water molecules are less well defined. This was probably the effect of the temperature at which the data was collected. The current structure comes from data collected at 100K° while the 2cpl structure is derived from data collected at room temperature.

The additional water molecules seen in the active site in this work (198, 106, 121 and 109) are important because they occupy the ligand binding site and make contacts to side chain of residues involved in the mechanism of the *cis-trans* isomerisation (Zhao and Ke 1996 b), as well as to residues which make contacts to CsA (Mikol et al 1993).

2. DMSO

DMSO is the smallest ligand found during this work and the only one which binds both Cyp-A and FKBP-12 (Burkhard 1995). The DMSO dissociation constant with Cyp-A was around 45 mM, the second worst interaction seen with all small ligands tested. The most hydrophobic part of the DMSO molecule fits into the hydrophobic pocket, the hydrophilic part faces the solvent (Fig. 7.10).

The main difference between the native protein structure and the structure with DMSO in the binding site is seen in the movement of the side chain of Met 61, replacement of W_106 and a slight movement of the Arg 55 side chain (Fig. 7.43). The rest of the side chains in the binding site are practically the same including the water molecules (W_105, W_109, W_121 W_208 and W_198 see section 4.1).

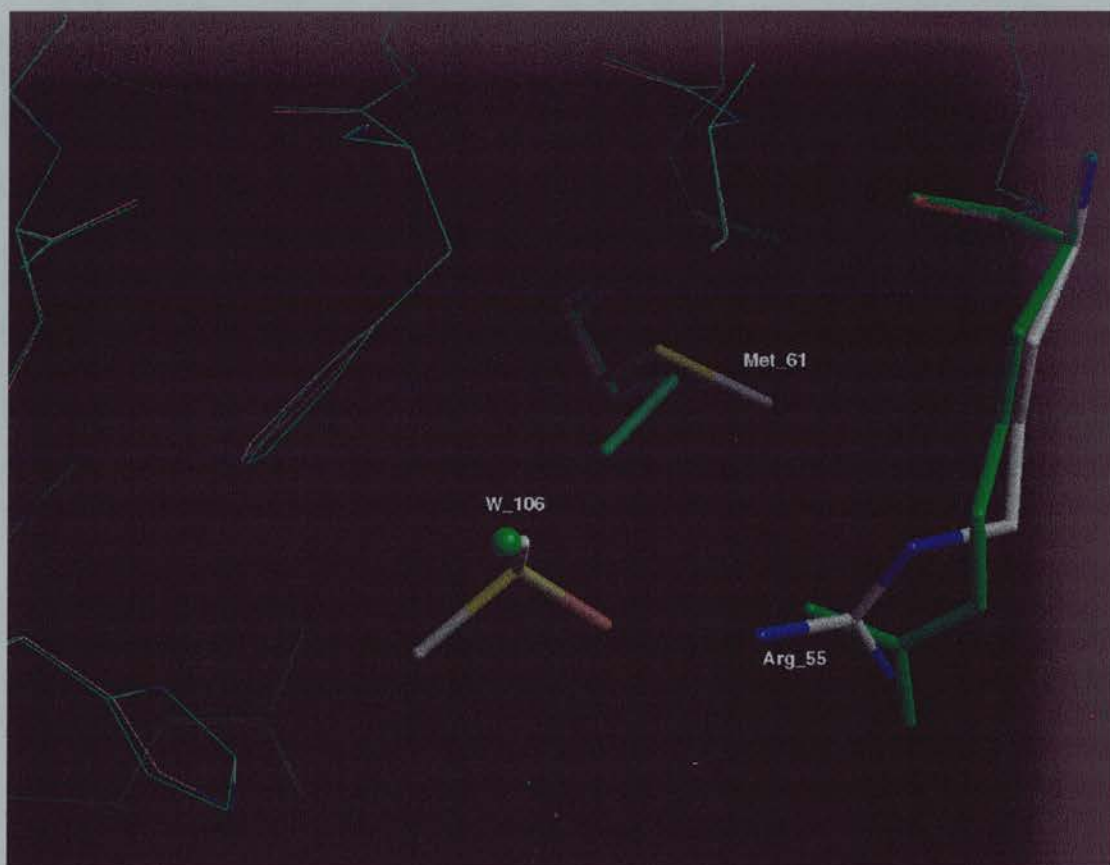


Fig. 7.43: Overlay of native CypA with the CypA-DMSO complex. The CypA native structure is in green. The main difference between the native protein structure and the structure with DMSO in the binding site is seen in the movement of the side chain of Met 61, replacement of W_106 and a slight movement of the Arg 55 side chain.

As a result of DMSO binding the CE carbon of Met 61 is pushed away from the centre of the binding site. The side chain of Met 61 was very mobile in the native structure and the mean temperature factor for CG, SD and CE was 17.4 \AA^2 which dropped to 9.42 \AA^2 in the DMSO structure. A similar effect happened to the Arg_55 where, because of the hydrogen bond (2.63 \AA) between sulfoxy group of DMSO and Arg 55/NH1 (Fig. 7.42) the side chain becomes more rigid. The overall temperature factor for NH1, NH2, CZ and NE of Arg 55 is 26.9 \AA^2 compared with 41.37 \AA^2 in the native structure. The difference in the overall temperature factor of protein atoms

between native and DMSO structure is very small (15.6 %) when compared to that for the side chain of Met 61 and Arg 55 referred to earlier.

Water molecule 106 in the native structure was replaced by atom C2 of the DMSO ligand (see Fig. 7.43). Initially this was a surprising result, the replacement of a hydrophilic atom by a hydrophobic one. In the native structure (Fig. 7.40) this particular water makes one hydrogen bond and two hydrophobic contacts. Therefore this water could be replaced by an amphiphilic atom (an atom which can make hydrophobic as well as hydrophilic contacts). The carbon atoms of DMSO satisfy the above conditions because the methyl groups have partial positive charges (see chapter 7 section 3.A.6.1). This explains the hydrophobic and hydrophilic contacts which both carbon atoms make (Fig. 7.10).

The distance between the sulfur atom of the DMSO and Met 61 (3.99 Å) is long but nevertheless represents a genuine contact because of the high van der Waals radii of sulfur atoms. The interaction is electrostatic since the sulfur of the DMSO has a positive charge and sulfur of the Met 61 is electronegative. A calculation of the partial charge for DMSO using the SYBYL program (see section 3.6) gave -0.55 for the O, 0.25 for the S and 0.15 for each carbon atom.

3. TMSO

TMSO was chosen because of the high similarity with DMSO (see Table 7.8). The active site was examined and seen to be large enough to accommodate the two extra carbons of TMSO (see Table 7.11). The structure of TMSO (Model 1 section 3.6.2) reveals that the prediction was correct. TMSO molecule (ALT1) binds almost in the same position as DMSO and makes the same contacts with the common atoms of DMSO (Fig. 7.44). The only significant difference in the binding site is the movement

of the Arg 55 side chain. The side chains of His 126 and Phe 60 move slightly to accommodate the two extra carbons of TMSO. Both side chains make contacts with the two extra carbon atoms of TMSO. The movement of the Gln 63 side chain is as a result of the hydrogen bond made with the O of TMSO ALT2 (Fig. 7.45).



Fig. 7.44: Overlay of CypA with TMSO and DMSO bound in binding site. The DMSO structure is in green. TMSO molecule (ALT1) binds almost in the same position as DMSO and makes the same contacts with the common atoms of DMSO.

An overlay of the native structure with the TMSO bound structure (Model 3 see section 3.A.6.1) shows similar features to that seen with DMSO. As a result of ligand binding, the side chain of Met 61 was pushed away (Fig. 7.44). Also W₁₀₆ was replaced by the ligand (Fig. 7.45) but not 100% (about 80% based on the occupancy of TMSO see section 3.6.2). W₁₀₆ in the native structure is equivalent to W₃₁₀ in

the TMSO structure. The explanation how the hydrophobic part from a ligand can replace W_106 is the same given for DMSO and has been discussed in section 4.A.2.

W_109 was also displaced by the ligand. Since the occupancy of the ligand is around 80% it might therefore be expected that W_109 might contribute towards the remaining 20% of the electron density seen in the native structure in this position. Nevertheless no electron density was seen around that position. This can be explained by the fact that W_109 diffracts more weakly than W_106 as can be seen in Table 7.10 (the temperature factors of water molecules).

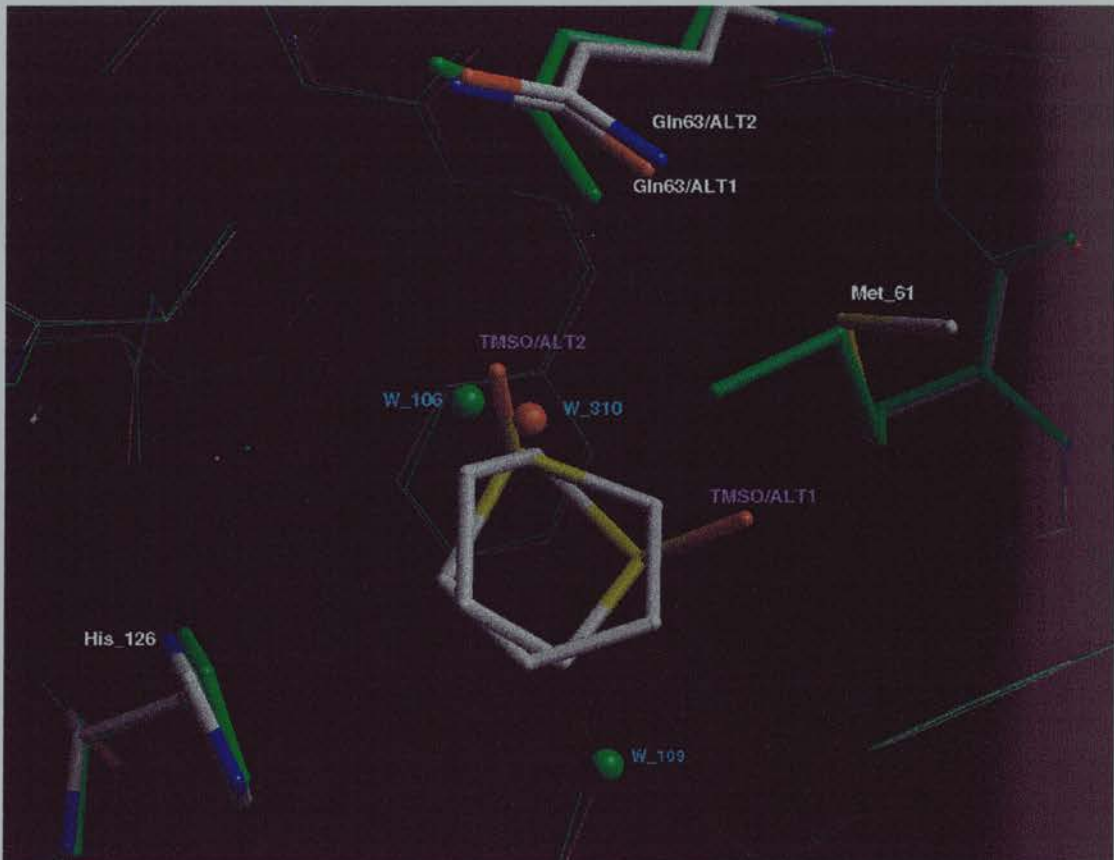


Fig. 7.45: Overlay of CypA with TMSO (Model 3) bound in binding site and native structure in binding site. Native structure is in green. The movement of the Met 61 side chain is the result of ligand binding. Water molecule 106 of the native is equivalent to W_310 in the TMSO structure.

The difference in mean temperature factor of all protein atoms between the native and the TMSO structure is only 11.5%. However the difference is much greater in the side chains which make contacts with the ligand. The mean temperature factor for CG, SD and CE of Met 61 is 17.4 \AA^2 in the native which dropped to 11.5 \AA^2 (34 % difference, 3-times higher compares to the 11.5% difference for all protein atoms) in the TMSO structure. A similar result is seen with Arg 55 due to hydrogen bonding between the sulfoxy group of TMSO and Arg 55/NH1 (Fig. 7.15) the side chain becomes more rigid. The overall temperature factor for NH1, NH2, CZ and NE of Arg 55 becomes 30.8 \AA^2 (27 % difference) from 42.3 \AA^2 in the native structure.

With a K_d of 33 mM (determined by PPIase assay Table 4.7) and a soaking solution of TMSO of 180 mM (see Table 6.2) the calculated occupancy is 86% which is very close to that calculated by the refinement program XPLOR (82% for Model 3 and 80% for Model 1 section 3.6.2). The agreement seen between the solution studies (PPIase) and crystallographic (XPLOR) values of occupancy, mean that the crystallographic results provide an estimate of K_d .

Three models (1, 2 and 3) have been proposed for the binding of TMSO in the active site of CypA in section 3.6.2. When the TMSO molecule is bound to the active site of Cyp-A the side chain of Gln 63 adopts two different positions (ALT1 and ALT2). The ALT1 position of the side chain of Gln 63 is similar to the position found in the native structure and it is adopted when TMSO in its (ALT1) position occupies the binding site (Fig. 7.45). As a result of binding of TMSO (ALT2) molecule, the Gln 63 side chain is adopted position ALT2. Crystallographically it is not possible to discriminate between the position ALT1 and position ALT2 of the side chain of Gln 63 side chain, since both OE2 and NE2 of Gln have the same scattering power. The conclusion that the Gln 63 side chain adopts two positions is based on the fact that the position ALT2 can explain the contact of O/TMSO with the Gln 63 side chain (Fig. 7.45).

TMSO (ALT1) makes similar contacts to DMSO (Fig. 7.46) with a hydrogen bond to Arg 55/NH1 and a S \cdots S contact (Fig. 7.45) to the sulfur atom of Met 61. This is an electrostatic interaction since both sulfur atoms are partially charged (see section 4.A.2 DMSO).

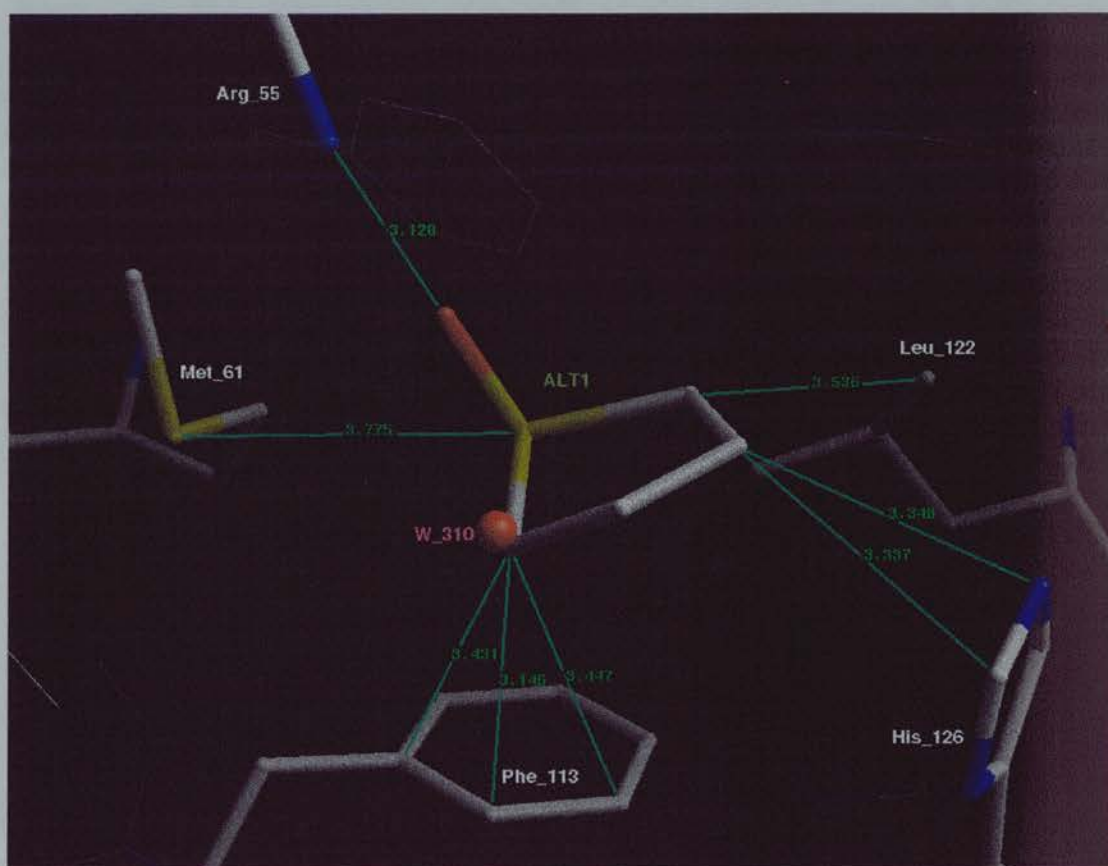


Fig. 7.46: Contacts of site 1 of TMSO ligand with surrounding atoms of the protein. DMSO makes the same contacts with the side chains of Arg 55 and Met 61. The O of the TMSO(ALT1) forms a hydrogen bond to the guanidinium group of Arg and a number of hydrophobic contacts to the side chains of Phe₁₁₃, His₁₂₆ and Leu₁₂₂. The occupancy was refined to 80 % for the TMSO and 20 % for W₃₁₀.

TMSO (ALT2) binding causes a rotation of the C γ -C δ bond of Gln 63 (Fig. 7.45) and generates a new hydrogen bond with NE1/Gln63 (Fig. 7.47). The contact of SD/Met61 to a carbon of TMSO/ALT2 (Fig. 7.47) is an electrostatic interaction, both

atoms are partially positively and negatively charged respectively. The partial positive charge of the sulfur atom of TMSO also explains the interaction seen with the ring of Phe 113. The sulfur atom of TMSO is partially positively charged when the π -electrons of the Phe ring induce a partial negative charge above and below the ring. The remaining contacts of TMSO (ALT2) with surrounding residues (Fig. 7.47) are hydrophobic interactions.

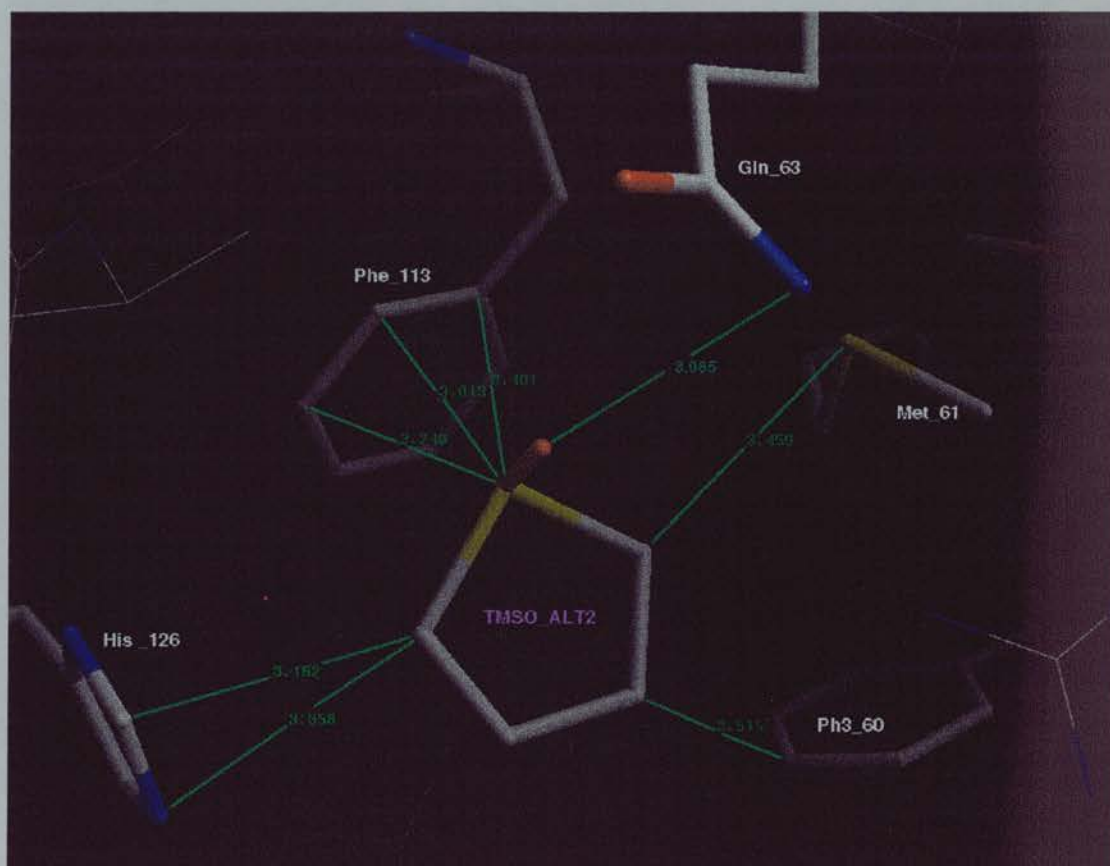


Fig. 7.47: Contacts of site 2 of TMSO ligand with surrounding atoms of the protein. The O of the TMSO (ALT2) forms a hydrogen bond to Gln_63/OE1 Arg and a number of contacts to the side chains of Phe_113, His_126, Phe_60 and Met_61. The occupancy was refined to 38 % for the TMSO (ALT2).

Three models have been proposed for the binding of TMSO in the active site of CypA. Comparison of these three models shows no significant difference (0.1%) in both the R factors and the R free (see Table 7.13). This means that the addition of an extra TMSO molecule (ALT2 seen in model 2) can account for the additional density in the difference (1Fo-1Fc) map around carbons C2 and C3 (Fig. 7.12), but does not actually improve the model (in fact both R factors increase by 0.1%). By comparing only the R factors (free and working) of model 1, 2 and 3 of the TMSO structures model 1 is the best. Nevertheless the B factor of water 310 failed to refine to a reasonable value therefore models 2 and 3 were proposed. With a total of 8 electrons and an occupancy of not more than 20% the B factor of W_310 has practically no effect on the R factor of a model containing 1539 atoms of a similar size. This also applied to the second TMSO molecule (ALT2) which has an occupancy of only 20%. One thing that is revealed in all models (1, 2 and 3) is that the binding site is not fully occupied by TMSO. Higher resolution data will be required to provide a more detailed picture of TMSO binding.

4. PNT

PNT belongs to the DMSO family of ligands and shares structural similarities with the other two members but surprisingly binds in a different position in the binding site of Cyp-A. PNT was chosen because of its high similarity seen with TMSO (see Table 7.8). The only difference between these two molecules is one atom (carbon replaced by sulfur). Carbon atoms have different chemistry to that of sulfur resulting in an effect seen on the binding of PNT. The PNT is almost a flat molecule while in DMSO and TMSO the torsion angle of O-S-C1-C2 (see Fig. 7.44) is around 105°. This seems to be the reason that PNT binds in a different place in the binding site of Cyp-A. The PNT binding site is similar to ACMPIP and ETPIPG (Fig. 7.48). The common feature

of those ligands (PNT, ACMPIP and ETPIP) is the carbonyl group. In all these ligands the carbonyl group forms a strong hydrogen bond with the N of Asn102.

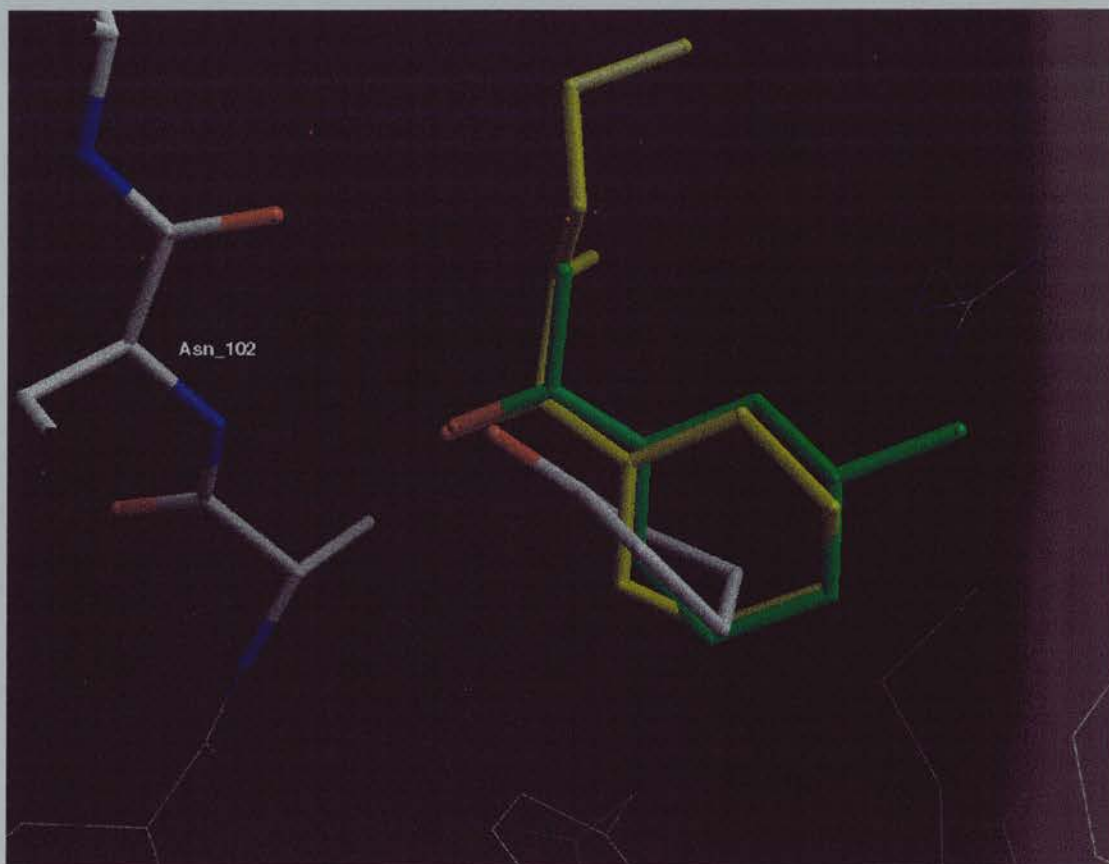


Fig. 7.48: Overlay of PNT, ACMPIP and ETPIP structures bound in the binding site of CypA. ACMPIP is in green, ETPIP is in yellow. The common feature of those ligands (PNT, ACMPIP and ETPIP) is the carbonyl group. The common oxygen which forms a hydrogen bond with N/Asn102 is coloured red.

An overlay of both native and PNT structures show similar features to that seen with DMSO. The side chain of Met 61 was pushed away due to binding and W_106 and W_105 were replaced by the ligand (Fig. 7.49). W_208 was not included in the model

of CypA complexed with PNT since the electron density of this water was very weak and the temperature factor was refined to a number greater than 70 \AA^2 (see section 2.2.A addition of water molecule). The rest of the side chains in the binding site are practically the same including the water molecules (W_109, W_121 and W_198 see section 4.1).

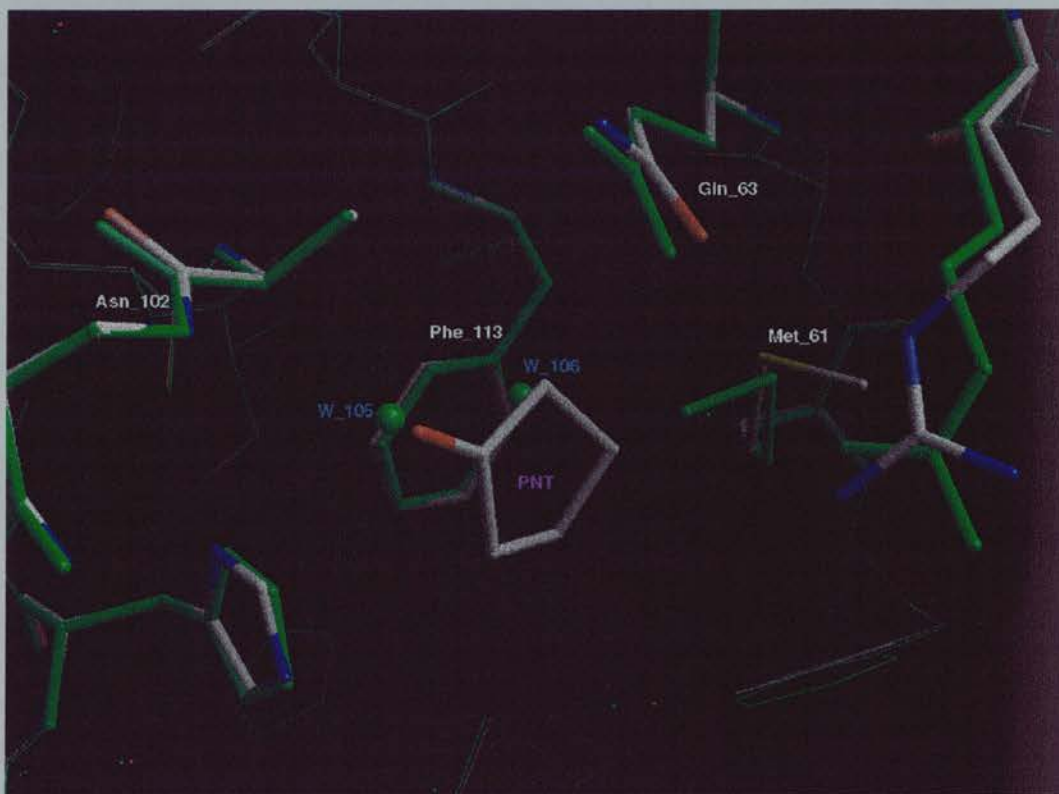


Fig. 7.49: An overlay of native and PNT structures show similar features to that seen with DMSO. The side chain of Met 61 was pushed away due to binding and W_106 and W_105 were replaced by the ligand. CypA native structure is in green.

W_106 is placed in an amphophilic environment (close to hydrophobic as well as hydrophilic atoms see contacts in chapter 7 section 3.A.5) and was replaced by carbon atom in the PNT structure (Fig. 7.49). W_105 was replaced by the oxygen atom of PNT which again it makes similar contacts as W_105 with surrounding residues (see Fig. 7.10).

5. ETPIPG

The ETPIPG ligand binds as predicted in the proline binding pocket with a conserved hydrogen bond between N/Asn102 and the carbonyl oxygen atom (Fig. 7.49). An rmsd value of 0.54 Å was obtained after least squares fit on to the N, C, O and CA atoms of residues 4 to 67 and 76 to 160 of the two structures. The side chain of Arg_55 of ETPIPG moved further into the binding site and the Gln_63 side chain moved closer to the ETPIPG molecule making a hydrogen bond with O3 of the ETPIPG. The rest of the binding site did not show any significant difference.

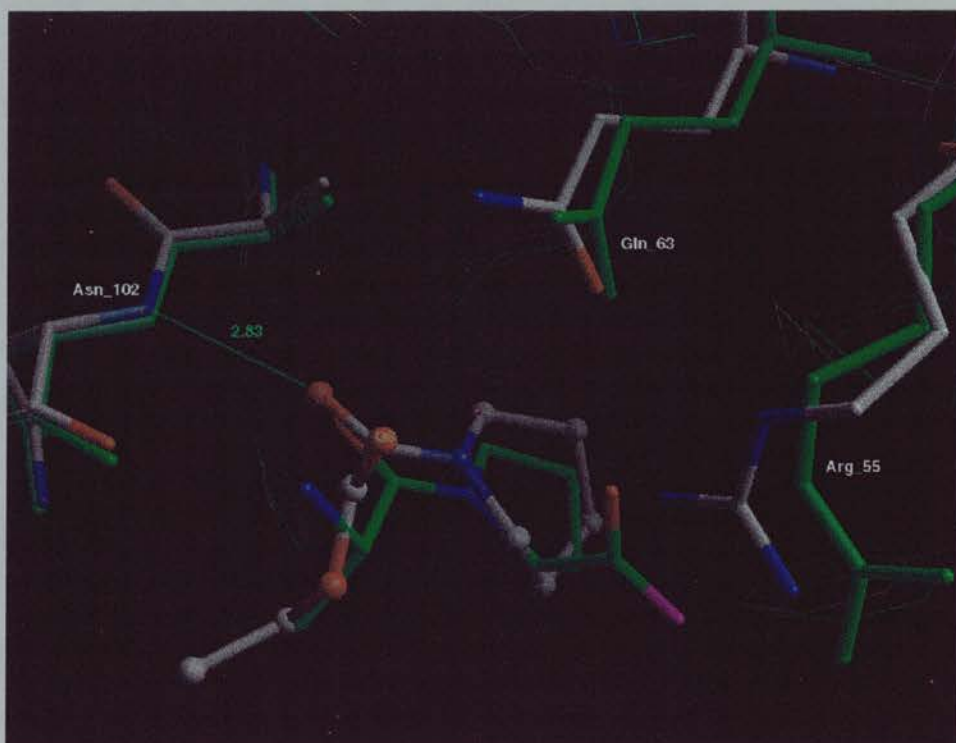


Fig. 7.50: Overlay of ETPIPG and CypA-AlaPro (1cyh) complex structures. The ETPIPG ligand binds as predicted in the proline binding pocket with a conserved hydrogen bond between N/Asn102 and the carbonyl oxygen atom. In green is the CypA-Ala Pro structure.

The main difference between the native protein structure and the structure with ETPIPG in the binding site is the movement of the side chain of Met 61, replacement

of six water molecules by ETPIPG and a slight movement of the Arg 55 side chain (Fig. 7.51). The rest of the side chains in the binding site are practically the same.

W_105 was replaced by an oxygen atom of ETPIPG. This is comparable to the situation in the PNT structure. W_106 has always been replaced by a carbon atom in previous structures (DMSO, TMSO, PNT) because it is placed in an amphiphilic environment and this is true for the ETPIPG structure also. In the native structure, W_107 makes a hydrogen bond with NE1/Gln63 (3.2 Å). This has been replaced by O3 (see Fig. 7.50) of ETPIPG which also makes a hydrogen bond to NE1/Gln63 (3.3 Å). W_198 was replaced by a carbon atom of ETPIPG. This is not an unfavourable replacement since W_105 which makes a strong hydrogen bond with W_198 in the native structure, has now been replaced by ETPIPG. W_208 are displaced due to bad contacts with the ligand and the side chain of Arg 55.

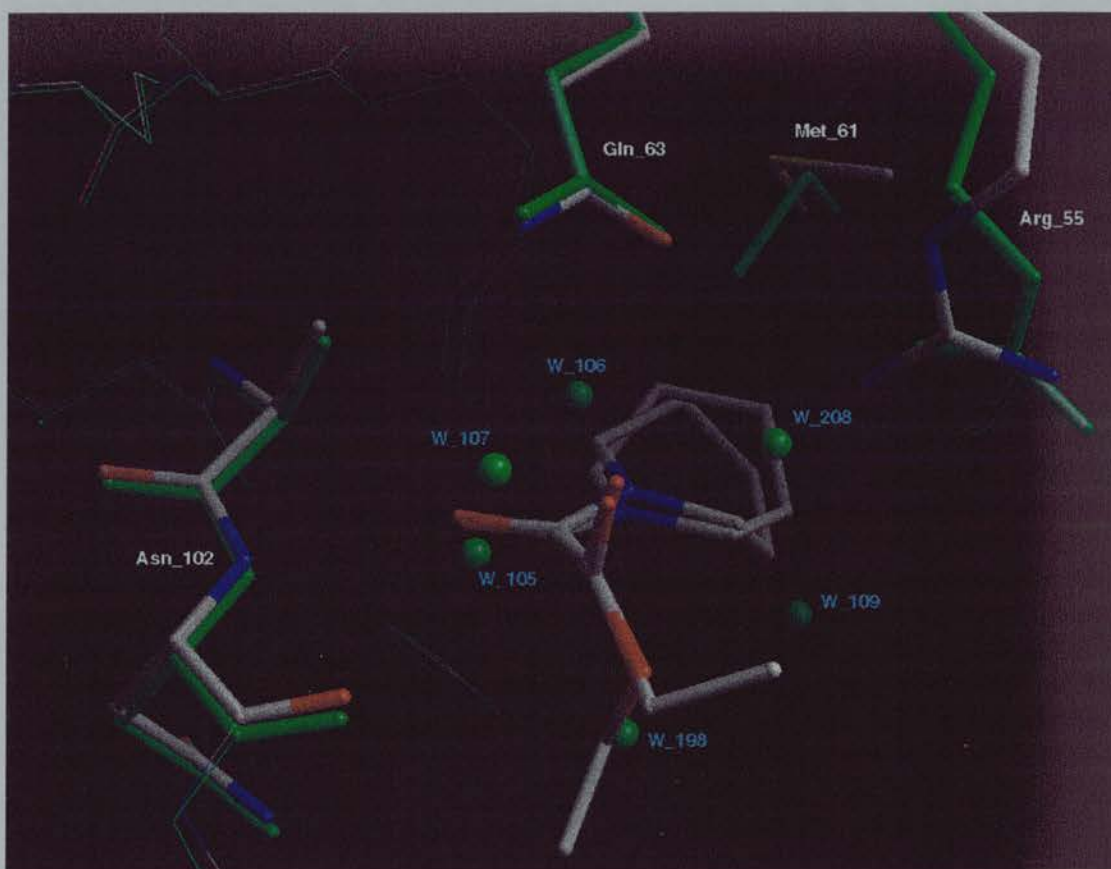


Fig. 7.51: Overlays of native CypA with the CypA-ETPIP-G complex. The main difference between the native protein structure and the structure with ETPIP-G in the binding site is the movement of the side chain of Met 61, replacement of six water molecules by ETPIP-G and a slight movement of the Arg 55 side chain. CypA native structure is in green.

As a result of ETPIP-G binding, side chains in the binding site of Cyp-A become more rigid than in the unliganded structure. The overall temperature factor of protein atoms in the ETPIP-G structure is about 24 % higher than in the native structure. However, the active site of the native structure tends to have higher B factors. The side chain of Arg 55 was very mobile. In the native structure the mean temperature factor for NH1, NH2, CZ and NE was 41.37 \AA^2 and dropped to 35.49 \AA^2 (38 % difference) in the ETPIP-G structure. Similar effects were obtained at His 126 where, because of the

contacts between ETPIPG (ALT1) and His 126 (see Fig. 7.52) the side chain becomes more rigid. The average overall temperature factor for the five ring atoms is 9.81 \AA^2 compared with 10.47 \AA^2 in the native structure.



Fig. 7.52: Contacts of ETPIPG (ALT1) with side chain of His 126. The contacts results is a more rigid side chain in CypA-ETPIPG structure compared with the native unliganded structure. The average overall temperature factor for the five ring atoms is 9.81 \AA^2 compared with 10.47 \AA^2 in the native structure.

6. ACMPIP

ACMPIP was chosen because of the high similarity with ETPIPG (see Table 7.16). The tail of ETPIPG was very mobile and adopts two conformations in the active site of CypA. Also it does not form favourable contacts (Fig. 7.23A and 7.23B). This tail was the first target for modification when the new ligand was designed. The tail (two carbon atoms and one oxygen atom) was removed and a search by structural similarity was carried out using the remaining fraction of the ETPIPG molecule. ACMPIP was the closest structural similar molecule found at that time and binds as predicted in the same position as the ETPIPG (Fig. 7.53).

The active site of CypA does not change when ACMPIP binds instead of ETPIPG except the side chain of Arg 55. The Arg 55 side chain was pushed away from the piperidine ring of ACMPIP. If the Arg 55 side chain adopted the same position as in the ETPIPG structure it would make a bad contact of 2.2 Å with the piperidine ring of ACMPIP. In all other structures of Cyp-A the Arg 55 side chain adopts one position. The resulting two alternative conformations for the Arg 55 side chain seems to be the explanation of the large difference observed in K_d (chapter 4 section 3.3.B) between two structurally similar ligands like ACMPIP ($K_d=335$ mM)of and ETPIPG ($K_d=25$ mM).

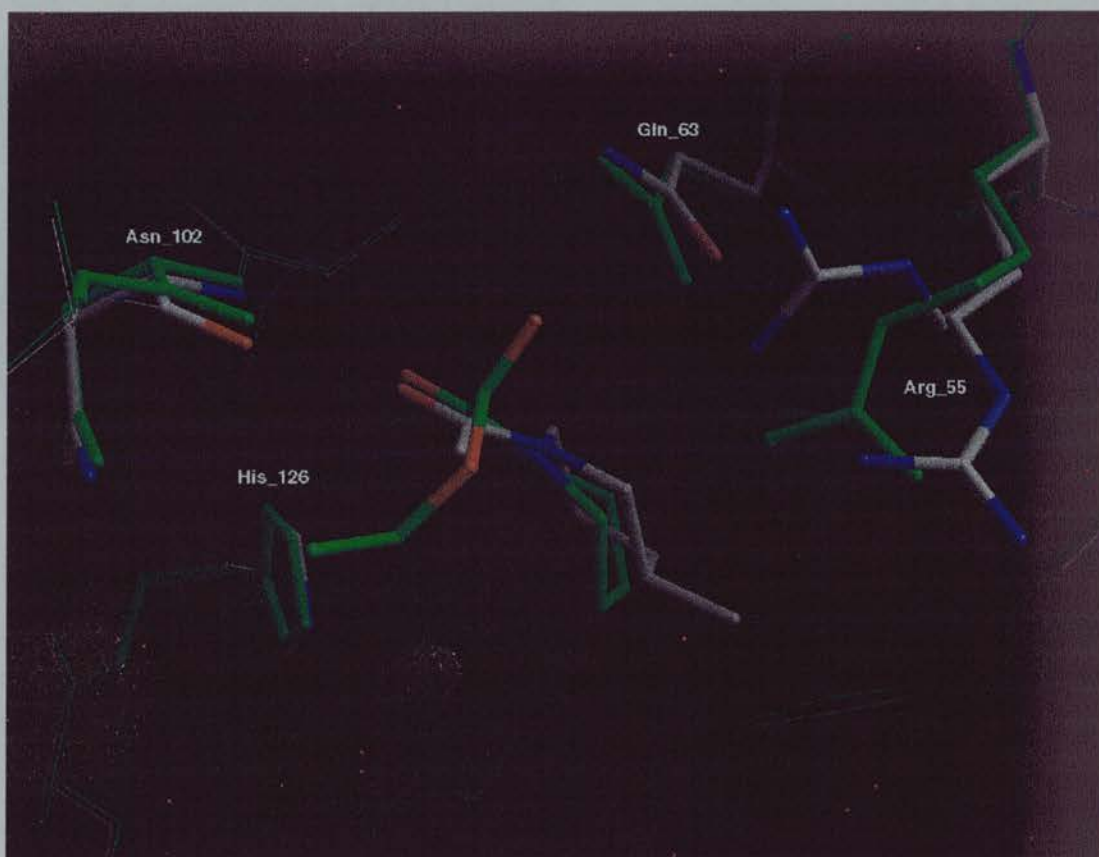


Fig. 7.53: Overlay of CypA-ACMPIP and CypA-ETPIP (ALT1) structures. ETPIP (ALT1) structure is in green. The side chain of the Arg 55 in the ACMPIP structure adopts two alternate positions. ACMPIP was the most structurally similar molecule found at that time and binds as predicted in the same position as the ETPIP.

Differences between the native protein structure and the structure with ACMPIP in the binding site are: the movement of the side chain of Met 61 observed in all other small ligand structures with CypP; the replacement of six water molecules (W_105, W_106, W_198 W_109 and W_208) by ACMPIP and the surprisingly different conformation of the Arg 55 side chain (Fig. 7.54). The rest of the side chains in the binding site are practically the same.

W_105 was replaced by the oxygen atom of ACMPIP and W_106 was replaced by a carbon atom of ACMPIP. This is comparable to the situation in the ETPIPG structure. W_198, W_109 and W_208 are displaced due to bad contacts with the ligand (less than 1.9 Å O/W to C/ACMPIP). W_208 also makes a bad contact with the NH1 of Arg 55/ALT2 (1.3 Å).

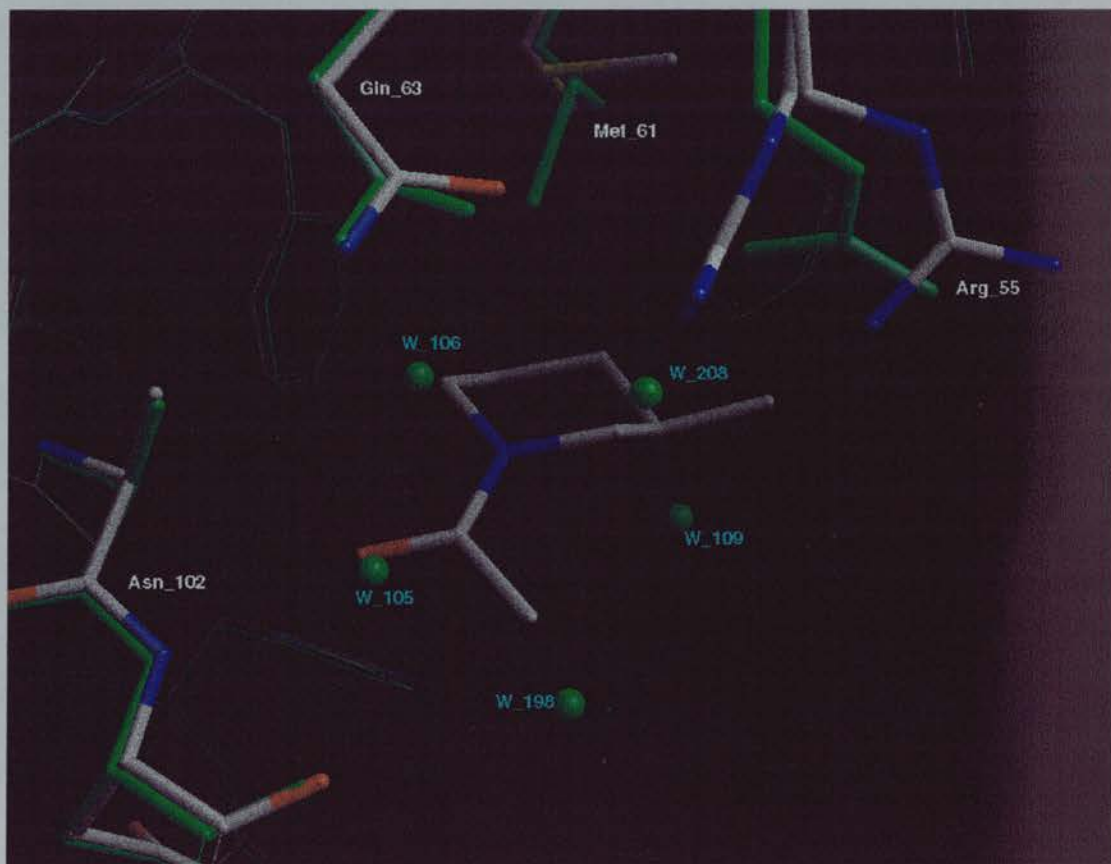


Fig. 7.54: Overlays of native CypA with the CypA-ACMPIP complex. CypA native structure is in green. Differences between the native protein structure and the structure with ACMPIP in the binding site are: the movement of the side chain of Met 61 observed in all other small ligand structures with CypP; the replacement of six water molecules (W_105, W_106, W_198 W_109 and W_208) by ACMPIP and the surprisingly different conformation of the Arg 55 side chain.

As a result of ACMPIP binding, side chains in the binding site of Cyp-A become more rigid than in the unliganded structure. The difference in the overall temperature factor of protein atoms between native and ACMPIP structure is about 12 % higher in ACMPIP structure. The side chain of His 126 was very mobile in the native structure. The mean temperature factor for CG, CD2, ND1, CE1 and NE2 in the native structure is 10.47 Å² and 7.58 Å² (30 % difference) in the ACMPIP structure. Similar effects were observed for Phe 113 where, because of the contacts between the ACMPIP and Phe (see Fig. 7.27) the side chain became more rigid. The overall temperature factor for the five ring atoms (CD1, CD2, CE1, CE2 and CZ) is 31.62 Å² compared with 38.19 Å² in the native structure.

7. DCH

DCH has the best interaction with CypA for non peptide ligands tested. DCH binds in a similar fashion to that with DMSO and TMSO. However the DCH molecule has little structural similarity with DMSO or TMSO and therefore comprises a new ligand family of CypA. DCH is currently the only member of this family showing binding activity.

The main difference seen between the native protein structure and the structure with DCH in the binding site is in the movement of the side chain of Met 61, replacement of two water molecules (W_106 and W_109) by DCH and movement of the Arg 55 side chain (Fig. 7.55). W_106 was replaced by a carbon atom from DCH. This is comparable to the situation in the DMSO structure. W_109 has been replaced by an oxygen atom. The rest of the side chains in the binding site are practically the same. W_208 in the native structure is equivalent to W_219 in the DCH structure, in which it has been displaced by 1.25 Å as a result of ligand binding (Fig. 7.55).

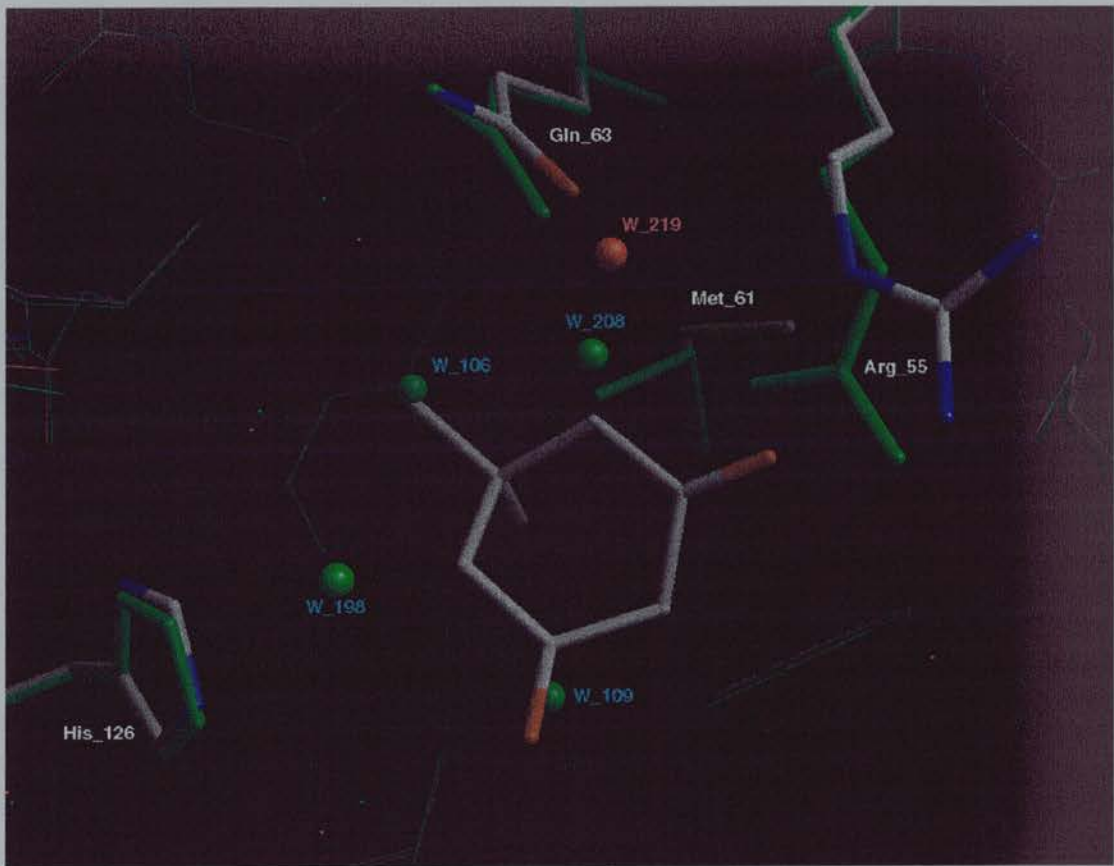


Fig. 7.55: Overlay of native CypA with the CypA-DCH complex. The CypA native structure is in green. The main difference seen between the native protein structure and the structure with DCH in the binding site is in the movement of the side chain of Met 61, replacement of two water molecules (W_106 and W_109) by DCH and movement of the Arg 55 side chain.

As a result of DCH binding, the side chains of Arg 55 (hydrogen bonding to DCH) become more rigid than in the unliganded structure. The difference in the overall temperature factor of protein atoms between native and DCH structure is about 20% higher than in the DCH structure. The side chain of Arg 55 was very mobile in the native structure, the mean temperature factor for NH1, NH2, CZ and NE being 41.37 \AA^2 dropping to 36.19 \AA^2 (a 32 % difference) in the DCH structure.

The DCH ligand binds in the same position as MeVal 11 of the CsA (see Fig. 7.56). The similarity in the binding is remarkable (see Fig. 7.57), given the very different sizes and structures of the two ligands (DCH has 10 non hydrogen atoms and CsA has 84 non hydrogen atoms). These structures show that this area of the binding site is a favourable pocket for dimethyl groups.

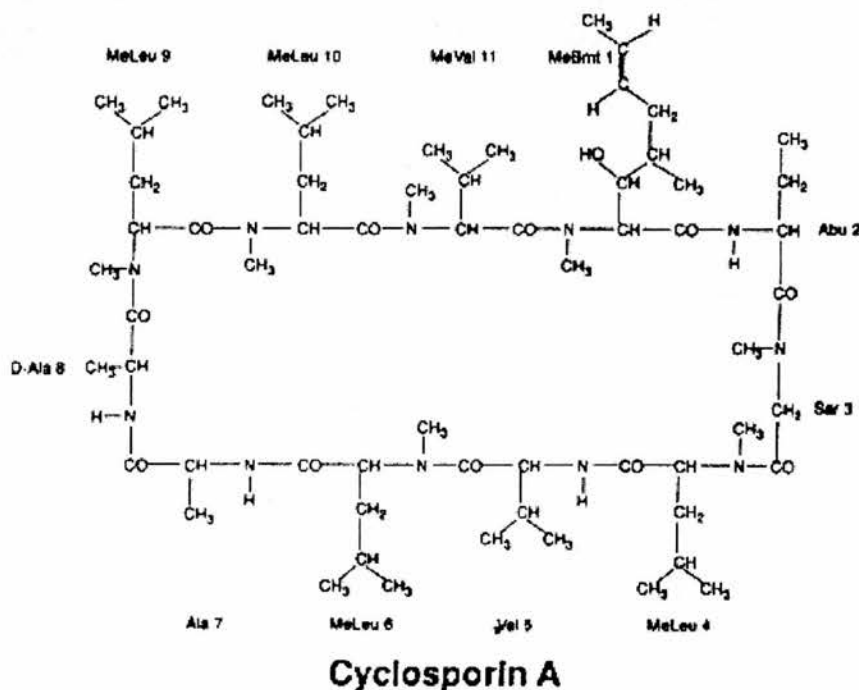


Fig. 7.56: Chemical formula of the immunosuppressant drug cyclosporin.

The similarities between CsA and DCH could be used to design new non peptide drugs, by extending DCH in the direction shown by the CsA molecule. The dimedone derivative molecule developed using the above approach would hopefully, possibly after several successive rounds of modification, significantly improve binding.

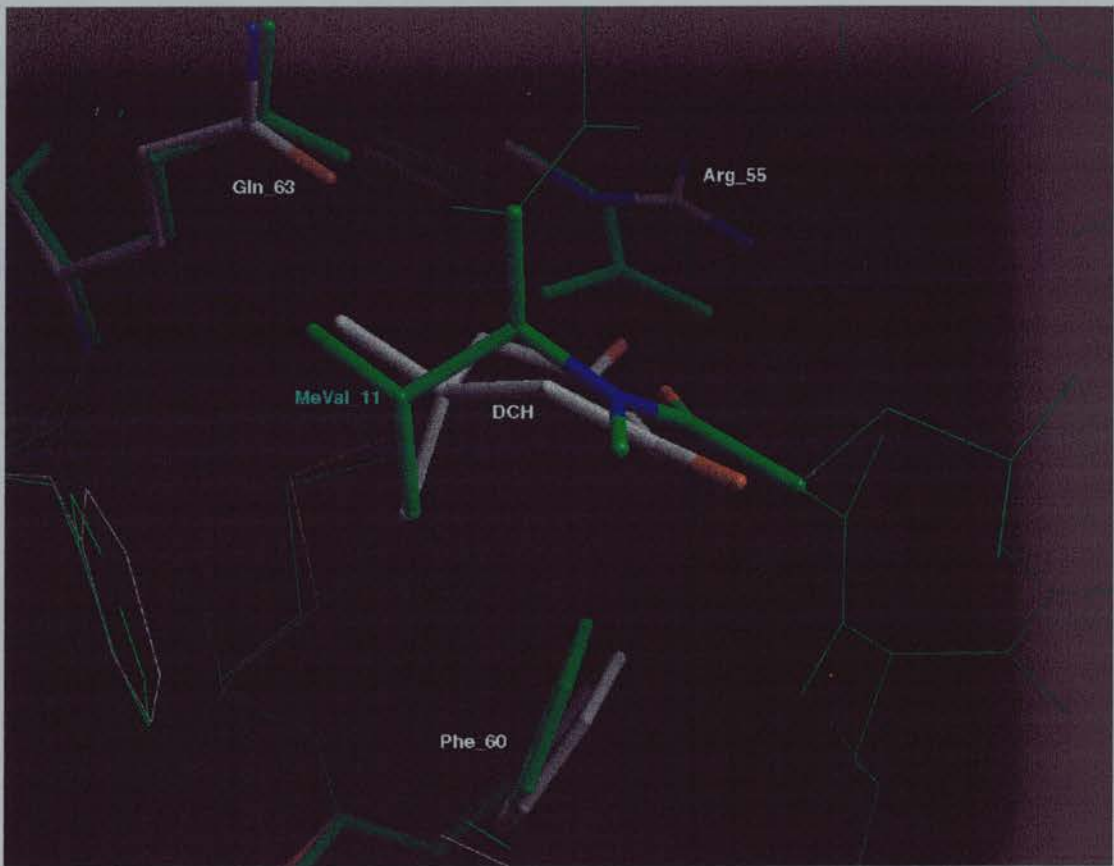


Fig. 7.57: Overlay of complex CypA-DCH with the CypA-CsA complex. The CypA-CsA structure is in green. The DCH ligand binds in the same position as MeVal 11 of the CsA. These structures show that this area of the binding site is a favourable pocket for dimethyl groups.

B) FKBP-12

The refined FKBP complex with cyclooctanone (oct_2) was compared with the available published x-ray structures of native FKBP-12 (1fkk, Keith et al 1995) and complexed with FK506 (1fkf, Duyne 1991). A least squares fit was carried out on to the 404 C, N, CA and O (main-chain atoms of residues 1 to 107) of the oct_2 molecule A with 1fkk and 1fkf structures. The 1fkk has an rmsd of 0.336 Å and the 1fkf a rmsd of 0.497 Å.

An overlay of 1fkk structure with the oct_2 structure in the binding site (Fig. 7.58) shows that three water molecules (W_110, W_112 and W_156) from the native structure have been replaced by the cyclooctanone. W_112 and W_156 make hydrophobic contacts (Fig. 7.59) and are likely to be replaced by a carbon atom as indeed happens when cyclooctanone binds (Fig. 7.58). W_110 is located in hydrophilic environment (see Fig. 7.59) and has been replaced by the oxygen atom of cyclooctanone (see Fig. 7.58).

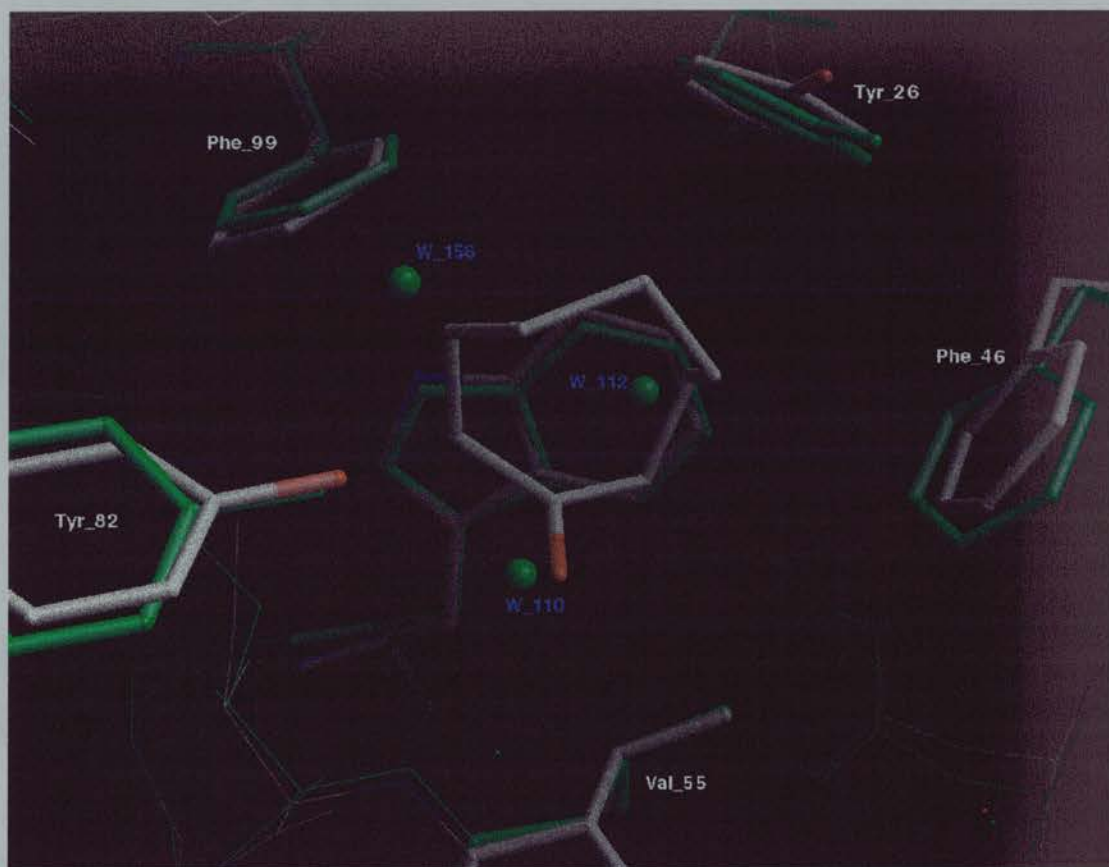


Fig. 7.58: Overlay of native FKBP12 structure with the FKBP12-Cyclooctanone complex. The FKBP12 native structure is in green. Three water molecules of the native structure have been replaced by cyclooctanone.

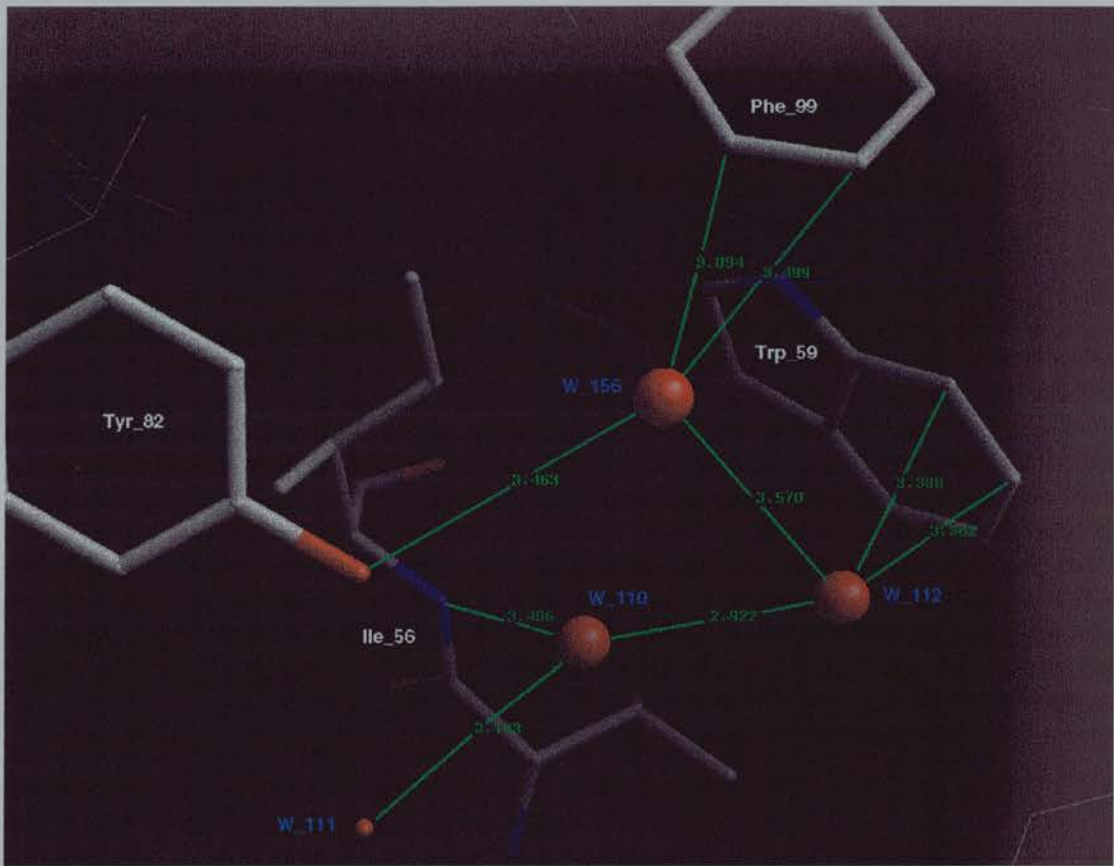


Fig. 7.59: Native (1fkk, Keith et al 1995) FKBP-12 structure with the three water molecules in the binding site. W_112 and W_156 make hydrophobic contacts and are likely to be replaced by carbon atoms. this happens when cyclooctanone binds (Fig. 7.58).

The cyclooctanone molecule is very flexible and is likely to adopt alternative conformations. When the CSD was searched using cyclooctanone as a template molecule there were no hits indicating that the cyclooctanone molecule can not be crystallized on its own because of the many alternate conformations which can be adopted in solution. The high flexibility of cyclooctanone molecule can be seen when the structure of 5 different cyclooctanone derivative crystal structures (randomly selected from CSD) are superimposed (Fig. 7.60). It is likely that a similar disorder occurs when cyclooctanone binds to the active site of FKBP-12. Unfortunately the data are not good enough to see and refine each alternate conformation.

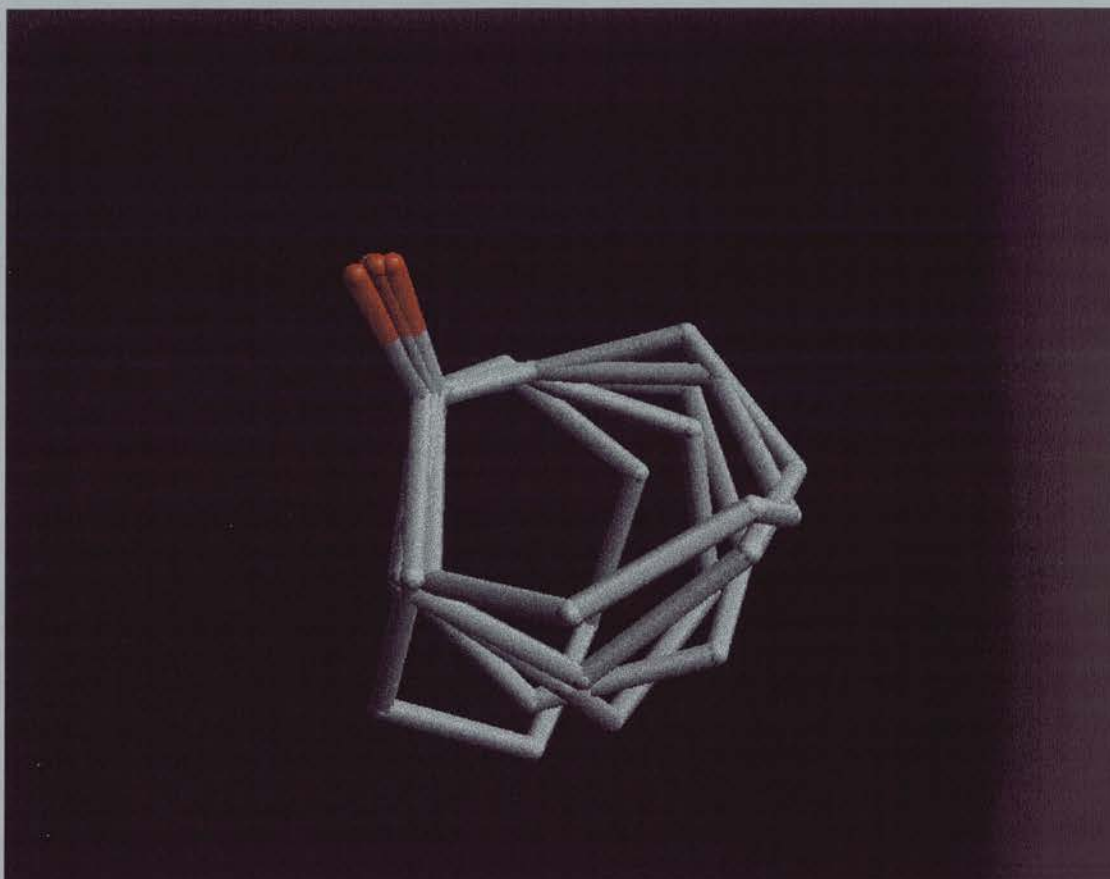


Fig. 7.60: An overlay of different structures of cyclooctanone found in CSD. The cyclooctanone molecules were part of larger structures selected randomly from the available examples in the CSD. The high flexibility of cyclooctanone molecule can be seen and it is likely that a similar disorder occurs when cyclooctanone binds to the active site of FKBP-12.

The high mobility or low occupancy of cyclooctanone can also be seen from the average value of the temperature factor of all atoms of cyclooctanone molecule which is much higher than the surrounding atoms of the protein. The average temperature factor for the nine protein atoms (listed in Table 7.21) that make contact with cyclooctanone is about 23 \AA^2 while the temperature factor for the cyclooctanone molecule is 40 \AA^2 . Also the six atoms (C1, C2, C3, C4, C5 and N7 see Fig. 7.61) of FK506 ligand from the 1fkf structure are located at the same position as the

cyclooctanone and make similar contacts with the protein. They have a mean temperature factor of about 6 \AA^2 . The mean temperature factor for the nine protein atoms (listed in Table 7.21) in 1fkf structure is 7.85 \AA^2 .

One application of protein-ligand complexes, demonstrated here by FKBP12-Cyclooctanone complex, could be the crystallization and structural studies of mobile or liquid molecules which are difficult to crystallize on their own.

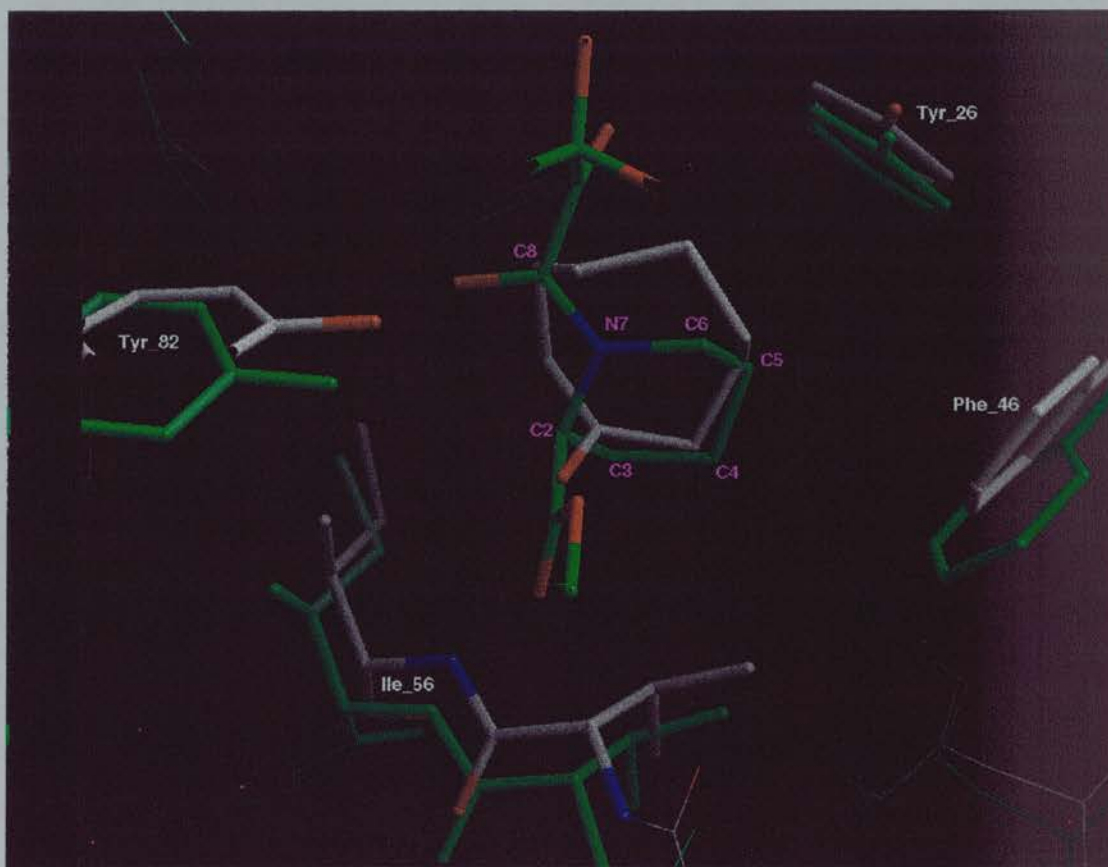


Fig. 7.61: Overlay of FKBP12-FK506 with the FKBP12-Cyclooctanone complex. The high mobility or low occupancy of cyclooctanone can also be seen from the average value of the temperature factor for the cyclooctanone molecule which is 40 \AA^2 . The six atoms (C1, C2, C3, C4, C5 and N7) of FK506 ligand from the 1fkf structure (in green) have a mean temperature factor of about 6 \AA^2 and they are located at the same position as the cyclooctanone and make similar contacts with the protein.

Table 7.21: Contacts of cyclooctanone ligand of molecule A in the asymmetric unit with surrounding atoms of the protein.

Ligand atom	Distance (Å)	Residue/Atom
CY4	3.01	Tyr_82/OH1
CY3	3.33	Tyr_82/OH1
CY3	3.55	Phe_99/CZ
CY7	3.3	Trp_59/CH2
CY7	3.48	Trp_59/CZ3
CY8	3.4	Trp_59/CE3
CY8	3.43	Trp_59/CZ3
CY8	3.42	Val_55/CG1
OA1	3.54	Ile_56/N

C) BrCyp

Discussion of the structural features of the BrCyp is restricted to the refined tetragonal crystal form. It is however worth noting that the inserted loop (51-KISGKPLH-58) adopts the same conformation in the trigonal structure and the tetragonal structure (described below) and is therefore likely to be independent of crystal packing effects.

The overall fold of BrCyp is similar that of the other cyclophilins structures (Braun, et al 1995) with an 8-stranded β -barrel capped by two α -helices. The comparison of BrCyp with hCypA is shown in Fig. 7.62. The rmsd between corresponding backbone atoms of 148 residues in hCypA and BrCyp is 0.56 Å. (divergent loops and N and C-terminii residues were not included).

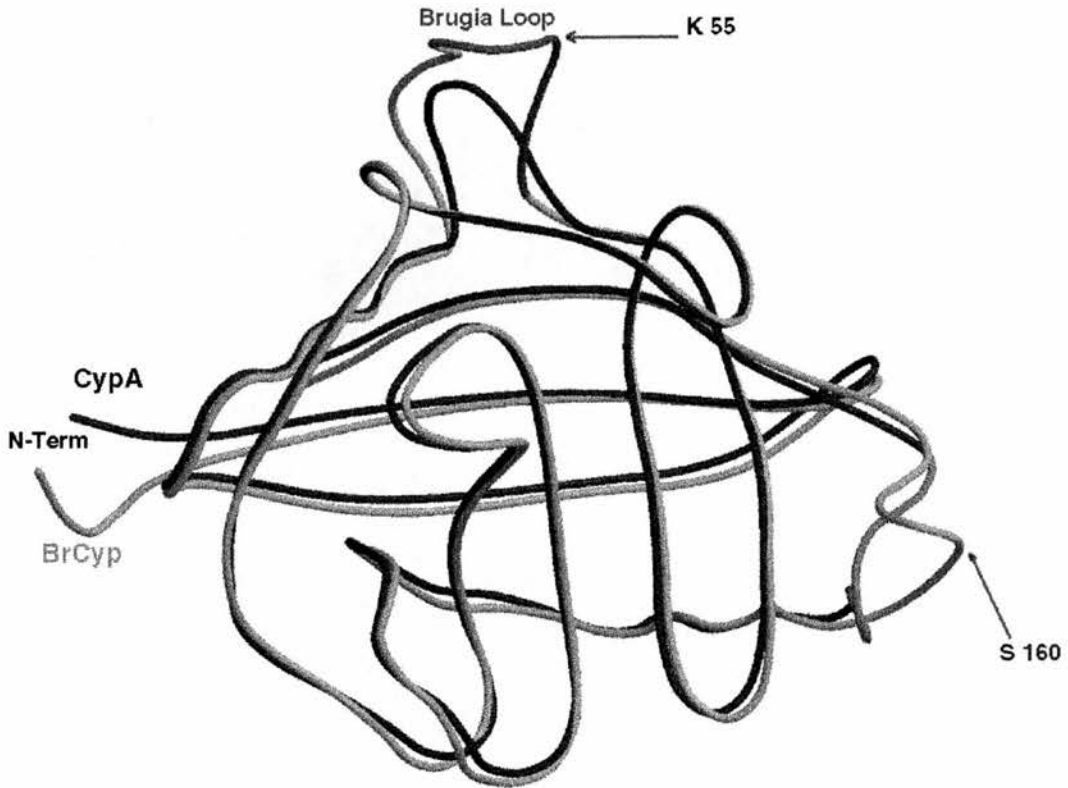


Fig. 7.62: Overlay of CypA with BrCyp. The CypA structure is in dark grey and the BrCyp in pale grey. The octapeptide loop (51KISGKPLH58) in BrCyp is labelled as Brugia loop.

The octapeptide loop (51KISGKPLH58) is one of the most distinctive structural features differentiating the BrCyp from all other available NMR or X-ray cyclophilin structures (Taylor et al 1997). The loop is held in place by a tight and very specific network of hydrogen bonds from the side-chain of Glu-87 (Fig. 7.63). Most cyclophilin homologues which have the octapeptide insert (including hCyp40, hnkCyp, and most plant cyclophilins) have an invariant glutamate in that position

while the group of cyclophilins without the octapeptide insert have a lysine at that position. This loop is a particularly common feature of the nematode cyclophilins, and is found in 7 of the 11 cyclophilin members from *C. elegans* (Page et al 1996). The Glu-87 locks the loop into a particular conformation which may be relevant for protein-protein recognition. This rather unusual role of a buried glutamate may even suggest a mechanism forcing a conformational change in the loop on protonation of the glutamate.

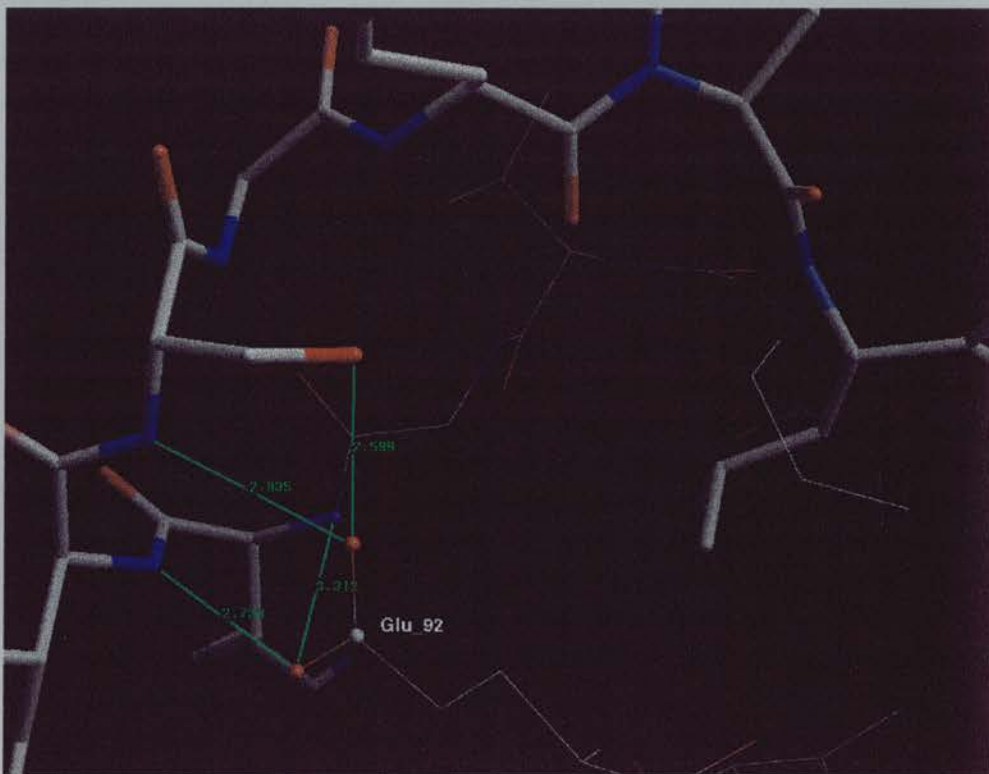


Fig. 7.63: The octapeptide loop of BrCyp (51KISGKPLH58 present with thick bonds). The four hydrogen bonds from the carboxy group on the side chain of Glu 92 locks the loop into a particular conformation.

Another loop (156-LKTNSKNRP-164) has significantly different conformation and sequence in hCypA. This loop also provides a subdivision of cyclophilins in which the sequence (and conformation) of this protruding loop is well conserved in the

divergent class of cyclophilins and is significantly different in hCypA as seen in Fig. 7.62 (labelled from S 160). The difference in conformation in this loop between CypA and CypB has been noted previously (Mikol et al 1994). The shape and distribution of charged amino acids on such protruding loops may well provide specific recognition signals for partner proteins in the cell.

Recombinant BrCyp has a $k_{cat}/K_m=7.9 \times 10^6 \text{ M}^{-1}\text{s}^{-1}$ using the substrate succinyl-Ala-Ala-Pro-Phe-p-nitroanilide, and is almost as efficient as hCypA which has a $k_{cat}/K_m=1 \times 10^7 \text{ M}^{-1}\text{s}^{-1}$ (Liu and Walsh 1990a). Both of the above values are close to those observed for the same protein purified during this work (chapter 4, section 3.B). Despite of the similar k_{cat}/K_m values, the concentration required to inhibit 50% of the BrCyp PPIase activity is rather high (860nM) compared with an IC₅₀ value of 19nM for human CypA (Liu et al 1990b). The X-ray structure of the BrCyp cyclophilin domain provides a probable explanation of the poor CsA binding.

The active site of the cyclophilins has been well characterised (Taylor et al 1997) and the 13 residues involved in binding the large inhibitor CsA are shown in Figure 7.64. All are conserved in BrCyp with the exception of Lys114 (usually Ala) and His132 (usually Trp). Other differences in the active site of BrCyp compared to that of hCypA are some small conformational changes in the side chains of Arg66 and Phe_71 (Fig. 7.64). It is interesting to note that the four most closely homologous divergent cyclophilins; bmCyp-1, ceCyp-8, hnkCyp and srCyp (Taylor et al 1998) all have the Trp to His and Ala to Lys/Arg mutations. In line with these observations, the enzymatically characterised hnkCyp was similarly found to have a low affinity for Csa, with an IC₅₀ value of 760nM (Rinferet et al 1994).

In this crystal structure Lys114 forms a hydrogen bond with the carbonyl oxygen atom of Gly72 (Fig. 7.64) and the side chain forms a gate-like barrier (see Fig. 7.65) over the 'Abu-pocket', which is one of the key recognition sites for cyclosporin binding (Braun et al 1995; Taylor et al 1997).

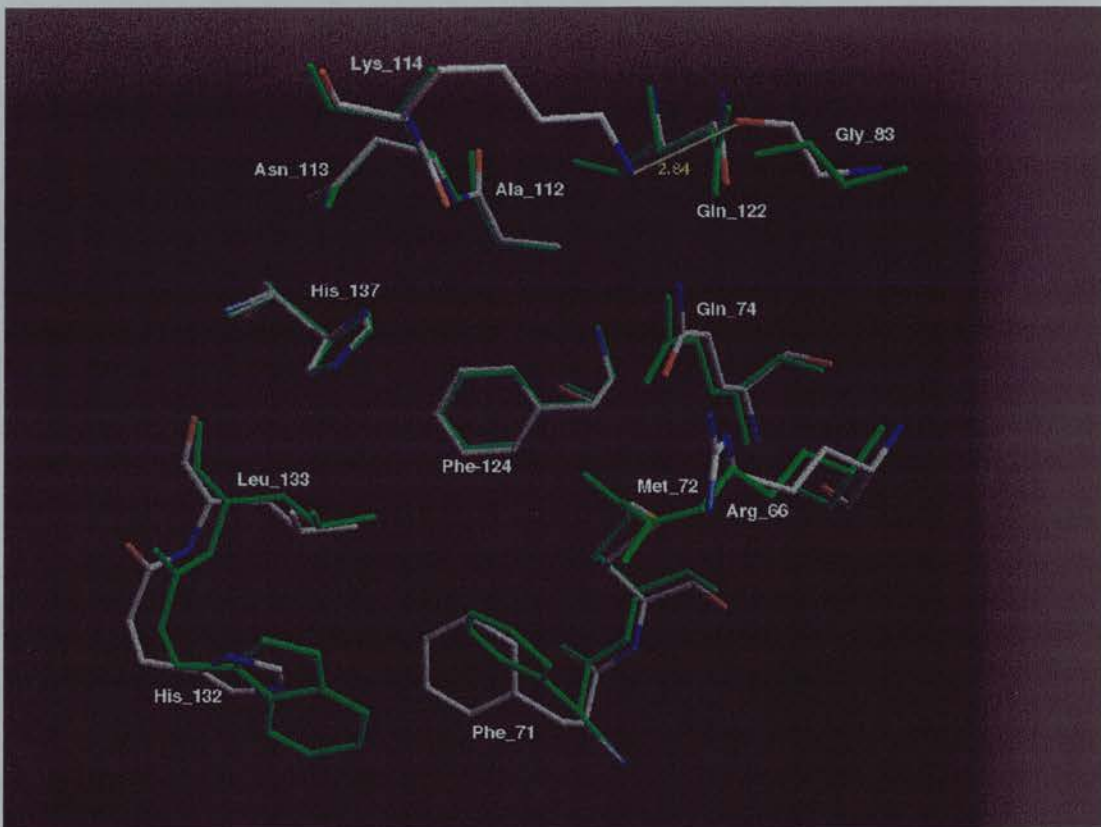


Fig. 7.64: Overlay of the active site of BrCyp with the CypA (green) showing the side chains of the 13 residues known to be involved in substrate and inhibitor binding of CypA. The main difference in the active site of BrCyp compared to that of hCypA are the Lys114 (instead of an Ala) and His132 (instead of Trp).

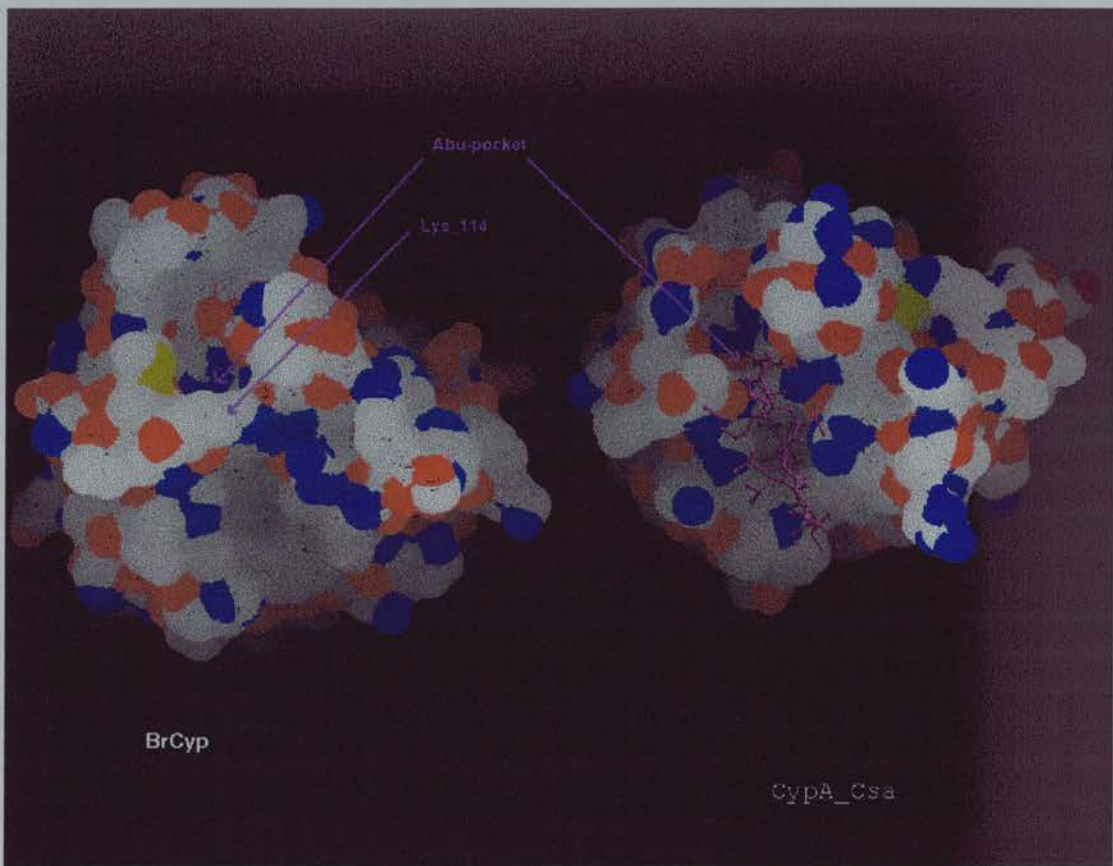


Fig. 7.65: CypA-CsA structure complex (right), shows how CsA binds to CypA. Side chain of Lys 114 of BrCyp (left) forms a hydrogen bond to the carbonyl O of Gly 83 and blocks the binding site for CsA. The side chain forms a gate-like barrier over the 'Abu-pocket', which is one of the key recognition sites for cyclosporin binding.

It is clear that Lys114 protruding into the recognition cleft of the PPIase active site of BrCyp will play a significant role in substrate recognition (Fig. 7.65). Even in solution it is likely that the steric bulk of the Lys114 side chain in most low-energy conformations will at least partially block the Abu-pocket. This will prevent tight binding of the bulky CsA ligand and explains the low affinity of the BrCyp/CsA complex.

Another interesting observation of the active site of BrCyp in the tetragonal crystal form is that is occupied by side chains from a crystallographically neighbouring

molecule (Fig. 7.66). This packing arrangement is such that the hydrophobic pocket is occupied by the side chain of Met46 which forms van der Waals contacts with Phe71, Met72, Phe124, Leu133 and His137 which comprise five of the 13 residues involved in CsA-binding in hCypA. The sulphur atom of Met46 bound in the active site corresponds closely to the position adopted by the valine side chain in Cyp-bound CsA (see Fig. 7.57) This crystal packing arrangement suggests that the Cyp active site may be rather promiscuous and acts as a binding site for different hydrophobic amino acid side chains (Fig. 7.66).

The arrangement of the side chain of Met46 from the crystallographically neighbouring molecule also shows similarities to the binding of DMSO molecule (Fig. 7.43) ligand of CypA-DMSO complex (section 3.6). This suggests that BrCyp binding site may be act as binding site for the DMSO family ligand found during this work.

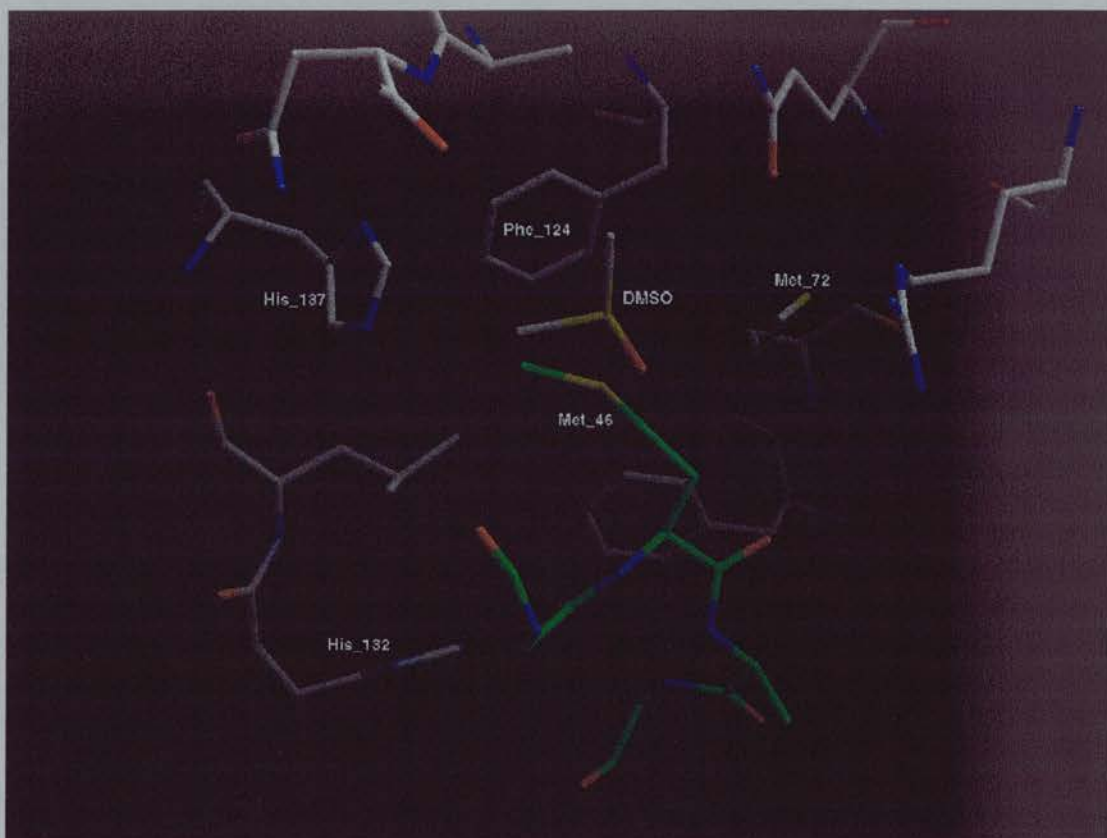


Fig. 7.65:The active site of BrCyp showing the position from a crystallographically related neighbouring molecule. Met_46 forms van der Waals contacts with Met_72, Phe_124, Leu_133 and His_137. Also the arrangement of the side chain of Met46 shows similarities to the binding of DMSO in the CypA-DMSO complex.

8 Conclusion

1. Cyp-A

The first non peptide ligands of CypA have been discovered and their X-ray structures determined. Six novel non peptide ligands belonging to three different families have been found and are all bound in the active site of Cyp. Each of these small ligands could be used as a starting point for developing novel non peptide ligands for CypA. The fact that they belong to three separate families has the advantage that different chemistry could be used to develop derivatives.

This is the first work where K_d values for small peptides and non peptide ligands of cyclophilins have been determined. The structures of a number of dipeptide and oligopeptide ligands bound to cyclophilins have been reported (see Taylor et al 1997a). However K_d values of those complexes have not been reported nor any other value related the strength of binding such as K_i or IC_{50} . The closest indication of how tightly Ala-Pro bound to CypA was given by Harrison and Stein (1990) who placed a conservative lower limit on K_i of 20 mM. A K_d (K_i and K_d are alternative symbols for the same constant) value of 18mM for Ala-Pro with CypA has been determined during this work. The K_d values of small non peptide ligands have also been determined and all lie in the millimolar range.

A new method for the calculation of IC_{50} and K_d has been developed. (Fischer et al 1989 see chapter 4 section 3). The method was tested for Cyclophilin A and CsA and the results were similar to those obtained by other well established methods. The main advantage of the new method is that it can estimate the IC_{50} without requiring greater than 50% inhibition. The method is more accurate in cases where the $[S] \ll K_m$.

Fluorescence was shown to be a very useful and fast method for the determination of K_d for protein-ligand complexes. The measurement of ligand binding by fluorescence spectroscopy requires that the optical properties of the protein-ligand complex differ from those of the free ligand and free protein (Bagshaw and Harris 1987).

There is a possibility that a complex of protein-ligand forms but is not revealed by fluorescence titration when the binding site is very rigid or the changes due to ligand binding have no effect on the surrounding environment of Trp. None of the small cyclophilin ligands found during this work were revealed by fluorescence titration. Ligation with small non peptide ligands does not change the overall structure of CypA. However small, but significant changes in the position and the B factors were observed for some residues in the binding site like Arg55, Met61, Gln63.

The CypA-CsA complex is a very good example where the CsA ligand is revealed by fluorescence titration (Kallen et al 1998). The above results could be expanded further by doing more experiments in order to find out which is the minimum distance (contact from ligand to Trp) required for change of a fluorescence signal in tryptophan titration. In the current work the minimum contact measured from crystal structure was the contact of 5.2 Å between NE1/Trp121 with O2/DCH.)

The CypA structures with the small ligands found during this work reveal new details of the CypA binding site.

1. The DMSO family of ligands revealed an amphiphilic area of the binding site. Water molecule 106 from the native structure is located in that area and it is replaced by a carbon atom when DMSO or TMSO is bound. This carbon atom is partially charged in the DMSO and probably in TMSO as well.
2. The replacement of one atom in a ligand molecule can have a dramatic effect in the way it is bound. The structures of TMSO and PNT with CypA show the

importance of the sulfoxy group and carbonyl group for the ligand binding. The replacement of a sulfur atom in the TMSO ligand by carbon leads to the PNT ligand which binds in a different position in the binding site of CypA.

3. The piperidine family of ligands bind similarly to peptide ligands containing proline residues and can be used as starting molecules for the design of a new family of tighter-binding ligands which share structural similarity with dipeptides or oligopeptides. A number of structures of CypA complexed with dipeptide and oligopeptide are available (Taylor et al 1997) and can be used as a template for further modification for new piperidine ligands.
4. The dimedone structure reveals a favoured binding site for the dimethyl group. This dimethyl binding site has been pointed out by two different docking programs. First the SANDOCK program (Burkhard 1995) found that dimedone is a putative ligand and later the LIDAEUS program found that 2,2,5-trimethyl-1,3 dioxane-4,6-dione is a putative ligand for that site. Both of the above compounds share a dimethyl group. Because of this dimethyl group dimedone can act as a novel valine mimic.

The similarities between N-Met-Val 11 of CsA and dimedone could be used to design new non peptide drugs, by extending dimedone in the direction shown in the CsA molecule. The dimedone derivative molecule developed using the above approach would hopefully, possibly after several successive rounds of modification, bind as tightly to CypA as CsA.

2. FKBP-12

The FKBP-12 structure with cyclooctanone has been solved to 2.05 Å with an R factor of 21.5 % and a free R factor 29.7 %. RMS deviation from ideality in bond length and bond angle are 0.005 Å and 1.67° respectively.

The overall structure of FKBP-12 does not change after cyclooctanone binding. The rmsd between backbone atoms (C, N, CA and O) of 107 residues in FKBP12/cyclooctanone and native FKBP12 is 0.336 Å.

The cyclooctanone molecule is very flexible ($B=40\text{Å}^2$) and it is likely to adopt multiple conformations. One application of protein-ligand complexes, demonstrated here by the FKBP12-cyclooctanone complex, could be the crystallization and structural studies of mobile or liquid molecules which are difficult to crystallize on their own.

3. BrCyp

BrCyp was crystallized in two different crystal forms (trigonal and tetragonal) and unit cell and space group have been determined for both. The trigonal form could not be refined to a reasonable R factor due to a possible twinned crystal.

The crystal structure of the tetragonal form has been solved to 1.95 Å resolution with R factor of 19.9 % and R free 23.4 %. RMS deviation from ideality in bond length and bond angle are 0.008 Å and 1.426° respectively.

The overall fold of BrCyp is similar that of the other X-ray and NMR structures with the the 8-stranded β -barrel capped by two α -helices. The rmsd between

corresponding backbone atoms of 148 residues in hCypA and BrCyp is 0.56 Å. (divergent loops and N and C-terminal residues were not included). The octapeptide loop (51KISGKPLH58) is one of the most distinctive structural features differentiating the BrCyp from all other available NMR or X-ray cyclophilin structures.

It is clear that Lys114 protruding into the recognition cleft of the PPIase active site of BrCyp will play a significant role in substrate recognition. Even in solution it is likely that the steric bulk of the Lys114 side chain in most low-energy conformations will at least partially block the Abu-pocket. This will prevent tight binding of the bulky CsA ligand and explains the low affinity of the BrCyp/CsA complex.

9. Appendix

Appendix 1

Amino acid sequence of proteins purified in current work.

Cyp-B human expressed in *E.coli*

```

      10      20      30      40
ADEKKKGPKV TVKVYFDLRI GDEDVGRVIF GLFGKT VPKT
      50      60      70      80
VDNFVALATG EKGFGYKNSK FHRVIKDFMI QGGDFTRGDG
      90     100     110     120
TGGKSIYGER FPDENFKLKH YGPGWVSMAN AGKDTNGSQF
     130     140     150     160
FITTVKTAWL DGKHVVFGKV LEGMEVVRKV ESTKTDSRDK
     170     180
PLKDVIIADC GKIEVEKPFA IAKE

```

Cyp-A human expressed in *E.coli*

```

      10      20      30      40      50
MVNPTVFFDI AVDGEPLGRV SFELFADKVP KTAENFRALS TGEKGFYKYG
      60      70      80      90     100
S CFHRIIPGF MCQGGDFTRH NGTGGKSIYG EKFEDEFIL KHTGPGILSM
     110     120     130     140
A NAGPNTNGS QFFICTAKTE WLDGKHVVFG KVKEGMNIVE
     150     160     165
AMERFGSRNG KTSKKITIAD CGQLE

```

BrCyp from *Brugia malayi* expressed in *E.coli*

```

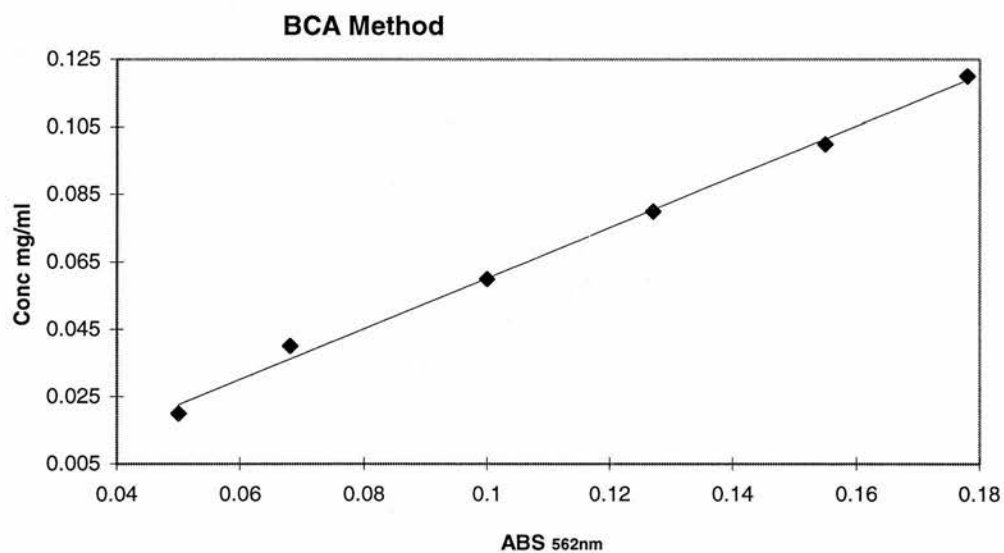
      10      20      30      40      50
MSKKDRRRVF LDVTIDGNLA GRIVMELYND IAPRTCNNFL MLCTGMAGTG
      60      70      80      90     100
KISGKPLHYK GSTFHRVIKN FMIQGGDFTK GDGTGGESY GGMFDDEEFV
     110     120     130     140     150
MKHDEPFVVS MANKGPNTNG SQFFITTPA PHLNNIHVVV GKVVSGQEVV
     160     170     177
TKIEYLKTNS KNRPLADVVI LNCGELV

```

Appendix 2

Table A1: Absorbance units for difference protein concentration using BCA method.

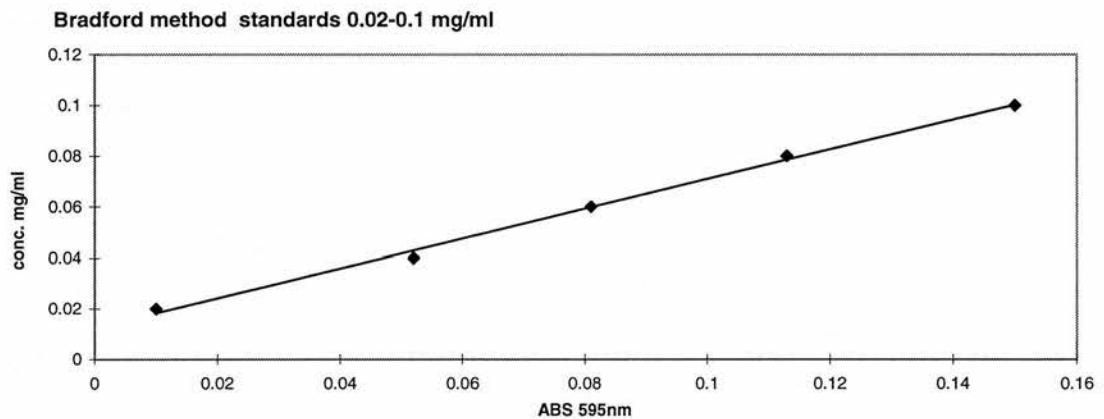
ABS 562nm	BSA Conc. mg/ml
0.05	0.02
0.068	0.04
0.1	0.06
0.127	0.08
0.155	0.1
0.178	0.12

**Plot 1:** Concentration of BSA solutions (table A1) plotted against absorbance units.

Using the least square method the series of points in plot 1 fit a linear equation $(\text{Conc.}) = 0.7515 * (\text{ABS}) - 0.014$. The points fits with a square correlation coefficient of $R^2 = 0.9963$.

Table A2: Absorbance units for difference protein concentration using Bradford method.

ABS	Conc. BSA (mg/ml)
0.01	0.02
0.052	0.04
0.081	0.06
0.113	0.08
0.15	0.1



Plot 2: Concentration of BSA solutions (table A2) plotted against absorbance units. Protein and Coomassie Brilliant Blue G-250 reagent, forms a chromophore absorbs at 595 nm. The absorbance is proportion to the protein concentration.

Using the list square method the series of points in plot 2 fit a linear equation $(\text{Conc.}) = 0.5846 (\text{ABS}) + 0.0125$. The points fits with a square correlation coefficient of $R^2 = 0.9967$.

10 References

- Allen, F. H., Bellard, S., Brice, M. D., Cartwright B. A., Doubleday, A., Higgis, H., Hummelink, T., Hummelink-Peters, B. G., Kennard, O., Motherwell, W. D. S., Rodgers, J. R. and Watson, D. G.** (1979) The Cambridge crystal data center: Computer-based search, retrieval, analysis, and display information. Acta Cryst. B 35, 2331-2339.
- Allen, F. H., Davies, J. E., Galloy, J. J., Jonson, O., Kennard, O., Macrae, C. F., Mitchell, E. M., Mitchell, F. F., Smith, J. M. and Watson, D. G.** (1991) The development of Versions 3 and 4 of the Cambridge structural database system. J. Chem. Inf. Comput. Sci. 31, 187-204.
- Amemiya, Y.** (1997) X-Ray Storage-Phosphor Imaging plate Detectors: High-Sensitivity X-Ray Area Detector in Methods in Enzymology ed **Abelson, N. J. and Simon, I., M.** Volume 276 Macromolecular Crystallography Part A **Carter, W. C. and Sweet, M. R. N.** ed pp Academic Press
- Anderson, S. K., Gallinger, S., Roder, J., Frey, J., Young, H. A. and Ortaldo, J. R.** (1993) A cyclosporin-related protein involved in the function of natural killer cells. Proc. Natl. Acad. Sci. U.S.A. 90, 542-546.
- Babine, R., Bleckman, T., Kissinger, C., Showalter, R., Pelletier, L., Lewis, C., Tucker, K., Moomaw, E., Parge, H. and Villafranca, E.** (1995) Design, synthesis and X-ray Crystallographic studies of novel FKBP-12 ligands. Biorganic & Med.Chem. Lett. 5 (15) 1719-1724.
- Bachinger, H. P.** (1987) The influence of peptidyl-prolyl *cis-trans* isomerases on the *in vitro* folding of type III collagen. J. Biol. Chem. 262, 17144-17148.
- Bagshaw, G. and Harris, D.** (1987) Measurement of ligand binding to proteins in Spectrophotometry and spectrofluorimetry a practical approach ed **Bashford C. and Harris D.** IRL Press

- Baker, E. K., Collen, N. J. and Zuker, C. S.** (1994) The cyclophilin homolog NinaA functions as a chaperone, forming a stable complex in vivo with its protein target rhodopsin. EMBO J. 13, 4886-4895.
- Becker, J. W., Rotonda, J., McKeever, B. M., Chan, H. K., Marcy, A. I., Wiederrecht, G., Hermes, J. D. and Springer, J. P.** (1993) FK-506-binding protein: three dimensional structure of the complex with the antagonist L-685,818. J. Biol. Chem. 268, 11335-11339.
- Bierer, B. E., Somers, P. K., Wandless, T.J., Burekoff, S. J. and Schreiber, S. L.**(1990) Probing immunosuppressant action with a non natural immunophilin ligand. Science 250 (4980), 556-559.
- Blundell, T. and Johnson, L.** (1976) Protein Crystallography. Academic Press New York.
- Böhm, J. H.** (1995) Site-directed structure generation by fragment-joining. Perspectives in Drug Discovery and Design 3, 21-33.
- Böhm, J. H.** (1996) Current computational tools for *de novo* ligand design. Current Opinion in biotechnology 7, 433-436.
- Brünger, A.** (1997) Patterson correlation searches and refinement in Methods in Enzymology ed **Abelson, N. J. and Simon, I. M.** Volume 276 Macromolecular Crystallography Part A **Carter, W. C. and Sweet, M. R. N.** ed pp Academic Press
- Braaten, D., Franke, E. K., and Luban, J.** (1996) Cyclophilin A is required for an early step in the life cycle of human immunodeficiency virus type 1 before the initiation of reverse transcription J. Virology 70 (6), 3551-3560.
- Bradford, M.** (1976) A Rapid and Sensitive Method for the Quantitation of Microgram Quantities of Protein Utilizing the principle of Protein_Dye Binding. Analytical Biochemistry 72, 248-254.
- Braun, W., Kallen, J., Mikol, V., Walkinshaw, M. D. and Wuthich, K.** (1995) Three-dimensional structure and actions of immunosuppressants and their immunophilins FASEB J. 9, 63-72.

- Bruenger, A. T.** (1992) Version 3.1 System for X-ray Crystallography and NMR. Yale University Press, New Haven and London.
- Bugg, E. C., Carson, M. W. and Montgomery, A. J.** (1993) Drus by Design Scin. American 269 (12), 60-66.
- Burkhard Kresze, G.** (1983) Methods for Protein Determination: in Methods of Enzymatic Analysis ed **Bergement, Ulrich, H.** Volume II Samples Reagents Assesment of Results. Academic Press, inc
- Burkhard, P.** (1995) Protein Ligand Interactions. PhD Thesis University of Basel Switzerland.
- Castellano, E. E., Oliva, G., Zinner, L. B. and Vicentini, G.** (1985) Syntesis and crystal-structure of hexa (mu-trifluoroacetato) tetrakis (tetramethylenesulfoxide) dilantanum (III) polymer and tetra (mu-trifluoroacetato)-bis (trifluoroacetato) tetrakis (tetramethylenesulfoxide) dineodymium (III) Inorganica Chimica Acta F block Elements Articles and Letters. 110 (2) 77-81.
- Compton, L. A., Davis, J. A., Nacdonald, J. R. and Bachinger, H. P.** (1992) Structural and functional characterisation of *Escherichia coli* peptidyl-prolyl *cis-trans*-isomerases. European Journal of Biochemistry 206, 927-934.
- Cudney, R., Patel, S., Weisgraber, K., Newhouse, Y. and McPherson, A.** (1994) Screening and optimisation strategies for macromolecular crystal growth. Acta Cryst. D50 (4) 414-423
- Cull, M. and McHenry, C.** (1990) Preparation of Extracts and Subcellular Fractionation: Preparation of Extracts from Prokaryotes in Methods in Enzymology ed **Abelson, J. and Simon, M.** Volume 182 Guide to Protein Purification **Deuthscher, M. ed pp** Academic Press.
- Dauter, Z.** (1997) Data collection Strategy in Methods in enzymology ed. **Abelson, J. and Simon, M.** Volume 276 Macromolecular Crystallography part A ed. **Carter, C and Sweet, R.** ACADEMIC PRESS.

- Deutscher, M.** (1990) Maintaining Protein Stability in Methods in Enzymology ed **Abelson, J. and Simon, M.** Volume 182 Guide to Protein Purification **Deutscher, M. ed pp** ACADEMIC PRESS, INC
- Ducruix, A. and Giegé, R.** (1990) Methods of Crystallization in Crystallization of Nucleic Acids and Proteins A Practical Approach **Ducruix, A. and Giegé, R. ed.,** Oxford University Press.
- Eberhardt, E. S., Loh, S. N., Hinck, A. P. and Raines, R. T.** (1992) Solvent effects on the energetics of prolyl peptide-bond isomerisation. J. Amer. Chem. Soc. 114 (13), 5437-5439.
- Emmel, E. A., Verweij, C. L., Durand, D. B, Higgins, K. M., Lacy, E. and Crabtree, G. R.** (1989) Cyclosporin A specifically inhibits function of nuclear proteins involved in T cell activation. Science 246, 1617-16290.
- Fersht, A.** (1984) Enzyme structure and mechanism W. H. Freeman and Company New York
- Fesik, S. W., Gampe, R. T., Jr., Eaton, H. L., Gemmecker, G., Olejniczak E. T., Neri, P., Holzman, T., F. Egan, D. A., Edalji R., Simmer, R., Helfrich, R., Hochlowski, J. and Jackson, M.** (1991) NMR studies of [U-13C]cyclosporin A bound to cyclophilin: bound conformation and portions of cyclosporin involved in binding. Biochemistry 30, 6574-6583.
- Fesik, S. W., Gampe, R. T., Jr., Holzman T. F., Egan, D. A., Edalji, R., Luly, J. R., Simmer R., Helfrich, R., Kishore, V. and Rich, D. H.** (1990) Isotope-edited NMR of cyclosporin A bound to cyclophilin: evidence for a trans 9,10 amide bond. Science 250, 1406-1409.
- Fischer, G. and Bang, H.** (1984) The refolding of urea-denatured ribonuclease A is catalyzed by peptidyl-prolyl *cis-trans* isomerase. Bioch. Biophys. Acta 828 39-42.
- Fischer, G., Bang, H. and Mech, C.** (1984) Nachweis einer enzymkatalyse für cis-trans-Isomerisierung der Peptidbindung in prolinhaltigen peptiden. Biomed. Biochim. Acta 43 (10) 1101-1111.

- Fischer, G., Berger, E. and Bang, H.** (1989b) Kinetic β -deuterium isotope effects suggest a covalent mechanism for the protein folding enzyme peptidylprolyl *cis/trans*-isomerase. FEB 250, 267-270.
- Fischer, G., Wittmann-Liebold, B., Lang, K., Kiefhaber, T. and Schmid, F.** (1989) Cyclophilin and peptidyl-prolyl *cis-trans* isomerase are probably identical proteins Lett. Nature 337 476-478.
- Fischer, G., Bang, H. and Mech, C.** (1984) Detection of enzyme catalysis for *cis-trans* isomerisation of peptide bonds using proline containing peptides as substrates., Biomed. Biochem. Acta 43, 1101-1112.
- Fischer, W., Bellus, D., Alder, A., Francotte, E. and Roloff, A.** (1985) New cyclic dimers of methacryloyl chloride. Chimia 39, 19.
- Franke, E., K., Yuan, H., E., H and Luban, J.** (1994) Specific incorporation of cyclophilin A into HIV-1 virions Nature 372 (6504), 359-362.
- Fransson, C., Freskgard P., O., Herbertsson, H., Johansson, A., Jonasson, P., Martensson, L., G., Svensson, M., Jonsson, B., H. and Carlsson, U.** (1992) *Cis-trans* isomerisation is rate-determining in the reactivation of denaturation human carbonic anhydrase-II as evidenced by proline isomerase. FEBS Lett. 296 (10), 90-94.
- Galat, A and Metcalfe, M., S.** (1995) Peptidylproline *cis/trans* Isomerases. Prog. Biophys. Molec. Biol. 63, 67-118.
- Galat, A., Lane, W. S., Standaert, R. F. and Schreiber, S. L.** (1992) A rapamycin-selective 25-kDa immunophilin, Biochemistry 31, 2427-2434.
- Garman, F. E. and Schneider, R. T.** (1997) Macromolecular Crystallography J. Appl. Cryst. 30 211- 237.
- Gewirth, D.** (1994) "The HKL Manual-A description of programs Denzo, Xdisplay and Scalepack, " 5th Ed. Yale University, New Haven, CT.
- Glusker, J., Lewis, M. and Rossi, M.** (1994) Crystal structure analysis for chemists and biologists. VCH Publishers.

- Greer, J., Erickson, J. W., Baldwin, J. J. and Varney, D. M.** (1994) Application of the three-dimensional structures of protein target molecules in structure-based drug design. J. Medicinal Chem. 37 (8), 1035-1054.
- Handschumacher, R., Harding, M., Rice, J. and Drugge, R.** (1984) Cyclophilin: A Specific Cytosolic Binding Protein for Cyclosporin A. Science 226, 544-547.
- Harding, M. W., Galat, A., Uehling, D. E. and Schreiber, S. L.** (1989) A reseptor for the immunosuppressant FK506 is a *cis-trans* peptidyl-prolyl isomerase. Nature 341, 758-760.
- Harding, M. W., Galat, A., Uehling, D. E., and Schreiber, S. L.** (1989) A reseptor for the immunosuppressant FK506 is a *cis-trans* peptidyl isomerase, Nature 341, 758-760.
- Harding, M. W., Handschumacher, R. E. and Schreiber, D. W.** (1986) Isolation and amino acid sequences of cyclophilin. J. Biol. Chem. 261, 8547-8555.
- Harrison, R. K. and Stein, R. L.** (1992) Mechanistic studies of enzymatic and nonenzymatic prolyl *cis-trans* isomerization. J. Am. Chem. Soc. 114 3464-3471.
- Harrison, R. K. and Stein, R. L.** (1990a) Mechanistic studies of peptidyl prolyl *cis-trans* isomerase-evidence for catalysis by distortion. Biochemistry 29 (7), 1684-1689.
- Harrison, R. K. and Stein, R. L.** (1990b) Substrate specificities of the peptidyl-prolyl *cis*↔*trans* isomerase activities of cyclophilin and FK-506 binding protein: evidence for the existence of a family of distinct enzymes. Biochemistry 29, 3813-3816.
- Herrler, M., Bang, H. and Marahiel, M. A.** (1994) Cloning and characterisation of ppiB, a *Bacillus subtilis* gene which encodes a cyclosporin A-sensitive peptidyl-prolyl *cis-trans* isomerase. Molec. Microbiol. 11, 1073-1083.
- Hohnson, J. L. and Toft, D. O.** (1994) A novel chaperone complex for steroid-receptors involving heat-shock proteins, immunophilins and P23. J. Biol. Chem. 269 (40), 24989-24993.
- Holzman, T., Egan, D., Edalji, R., Simmer, R., Helfrich R., Taylor, A. and Burren, N.** (1990) Preliminary characterization of a cloned neutral isoelectric form of the human peptidyl prolyl isomerase cyclophilin J. Biol. Chem. 266 (4), 2474-2479.

- Husi, H. and Zurini, M.** (1994) Comparative binding studies of cyclophilins to cyclosporin A and derivatives by fluorescence measurements. Anal. Bioch. 222 251-255.
- Jackosn, S. J. and Fersht, A. R.** (1991) Influence of peptidyl-prolyl *cis-trans* isomerisation on the folding kinetics and thermodynamic characterisation of the transition state folding. Biochemistry 30, 10436-10443.
- Jancarik J. and Kim, S.** (1991) Sparse- Matrix sampling-A screening method for crystallization of proteins J. Appl. Cryst. 24 409-411.
- Jin, Y. J., Albers, M. W., Lane, W. S., Bierer, B. E., Scriber, S. L., and Burakoff, S. J.** (1991) Molecular cloning of a membrane-associated human FK506 and rapamycin binding protein, FKBP-13, Proc. Natl. Acad. Sci., USA 88, 6677-6681.
- Jorgensen, W. L. and Gao, J.** (1988) Cis trans energy difference for the peptide-bond in the gas-phase and in aqueous-solution. J. Amer. Chem. Soc. 110 (13), 4211-4216.
- Kabsch, W. and Sander, C.** (1983) Dictionary of protein secondary structure: pattern recognition of hydrogen bonds and geometrical features Biopolymers 22 2577-2637.
- Kallen, J. and Walkinshaw, D. M.** (1992) The X-ray structure of a tetrapeptide bound to the active site of the Human cyclophilin A, FEBS Lett. 300, 286-290.
- Kallen J., Mikol V., Taylor P. and Walkinshaw D. M.** (1998) The X-ray structure and analysis of 11 cyclosporin derivatives complexed with cyclophilin A, J. Mol. Biol 283, 435-449.
- Kallen, J. and Walkinshaw, D. M.** (1992) The X-ray structure of a tetrapeptide bound to the active site of the Human cyclophilin A, FEBS Lett. 300, 286-290.
- Ke H.** (1992) Similarities and differences between human cyclophilin A and other β -barrel structures: structural refinement at 1.63 Å resolution, J. Mol. Biol. 228, 539-550.

- Ke, H., Mayrose D. and Cao W** (1993) Crystal structure of cyclophilin A complex with substrate Ala-Pro suggest a solvent-assisted mechanism of cis-trans isomerisation. Proc. Natl. Acad. Sci. USA 90 3324-3328.
- Ke H., Zydowsky, L. D., Liu, J. and Walsh, C. T.** (1991) Crystal structure of recombinant human T cell cyclophilin A at 2.5 Å resolution, Proc. Natl. Acad. Sci., USA 88 9483-9487.
- Ke, H., Mayrose, D. and Wei, Cao** (1993) Crystal structure of cyclophilin A complexed with substrate Ala-Pro suggests a solvent-assisted mechanism of *cis-trans* isomerization. Proc. Natl. Acad. Sci. USA. 90, 3324-3328.
- Keith, P. W., Yamashita, M. M., Sintchak, D. M., Rotstein, H. S., Murcko, A. M., Boger, J., Thomson A. J., Fitzgibbon, J. M., Black , R. J. and Navia A. M.** (1995) Comparative X ray structures of the major binding protein for the immunosuppressant FK506 (Tacrolimus) in unliganded form and in complex with FK506 and rapamycin. Acta Cryst. D51, 511-521.
- Kimball, P.M., Kerman, R.H. and Kahan, B.D.** (1991) Failure of Prolyl-peptidyl Isomerase to mediate cyclosporine suppression of intracellular activation signal generation. Transplan. 51 (20), 509-513.
- Kofron, J., Kuzmic, P., Kishore, V., Colon-Bonilla, E. and Rich, D.** (1991) Determination of kinetic constants for peptidyl-prolyl cis-trans isomerases by an improved spectrophotometric assay. Biochemistry 30, 6127-6134.
- Kraulis, P.J.** (1991) Molscript-a program to produce both detailed and schematic plots of protein structures. J. Appl. Cryst. 24, 946-950.
- Lang, K., Schmid, F. X. and Fischer, G.,** (1987) Catalysis of protein folding by prolyl isomerase. Nature 329, 268-270.
- Laskowsky, R. A., MacArthur, M. W., Moss, D. S. and Thornton, J. M.** (1993) PROCHECK: a program to check the stereochemical quality of protein structures. J. Appl. Cryst. 26, 283-291.
- Lehninger, A., Nelson, D. and Cox, M.** (1993) Principles of Biochemistry. Worth Publishers New York.

- Lepre, C. A., Pearlman, D. A., Cheng, J. W., DeCenzo, M. T., Livingston, D. J., and Moor, J. M.** (1994) Solution structure of FK506 bound to the R42K, H87V double mutant of FKBP-12. Biochemistry 33, 13571-13580.
- Levitt, M. and Park, B.** (1993) Water: now you see it, now you don't. Structure 1 (4) 223-226.
- Liu, J., Albers, M., Chen, C., Schreiber, S. and Walsh, C.** (1990) Cloning, expression, and purification of human cyclophilin in *Escherichia coli* and assessment of the catalytic role of cysteins by site-directed mutagenesis. Proc. Natl. Acad. Sci. 87, 2304-2308.
- Liu, J. and Walsh, C. T.** (1990a) Peptidyl Prolyl *cis-trans* isomerase from *Escherichia coli* a periplasmic homolog of cyclophilin that is not inhibited by cyclosporin A
- Lodish, H. F. and Kong, N.** (1991) Cyclosporin A inhibits an initial step in folding of transferrin within the endoplasmic reticulum. J Biol. Chem. 266, 14835-14838.
- Loh, C., Shaw, K. T. Y., Carew, J., Voila, J. P. B., Luo, C., Perrino, B. A. and Rao, A.** (1996) Calcineurin binds the transcription factor NFAT1 and reversibly regulates its activity. J. Biol. Chem. 271 (18), 10884-10891.
- Lorber, B. and Giegé, R.** (1990) Preparation and handling of biological macromolecules for crystallization in Crystallization of Nucleic Acids and Proteins A Practical Approach **Ducruix, A. and Giegé, R.** ed., pp 24 Oxford University Press.
- Luo, C., Burgeon, E., Carew, J. A., McCaffrey, P. G., Badalian, T. M., Lane, W. S., Hogan, P. G. and Rao, A.** (1996) Recombinant NFAT1 (NFATp) is regulated by calcineurin in T cells and mediates transcription of several cytokine genes. Molec. Cellular Biol. 16 (7), 3955-3966.
- Maki, N., Sekiguchi, F., Nishimaki, J., Miwa, K., Hayano, T., Takahashi, N., and Suzuki, M.** (1990) Complementary DNA encoding the human T cell FK506 binding protein, peptidyl-prolyl *cis-trans* isomerase distinct from cyclophilin, Proc. Natl. Acad. Sci., USA 87, 5440-5443.

- McPherson, A.** (1985) Crystallization of Macromolecules: General Principles in Methods in Enzymology ed **Colowick, S. P. and Kaplan, N. O.** Volume 114 Diffraction Methods for Biological Macromolecules **Wyckoff, H. W., Hirs, C. H. W and Timasheff, S. N.** ed pp Academic Press.
- McRee, D.** (1993) Practical Protein Crystallography pp 12-15 Academic Press.
- Michnick, S. W., Rosen, M. K., Wandless, T. J., Karplus, M., and Schreiber, S. L.** (1991) Solution structure of FKBP, a rotamase enzyme and receptor for FK506 and rapamycin Science 252, 836-839.
- Mikol, V. and Duc, D.** Crystallization of the complex between Cyclophilin A and Cyclosporin derivatives: the use of cross-seeding. Acta Cryst. D50, 543-549.
- Mikol, V., Kallen, J., Pflügl, G. and Walkinshaw, D. M.** (1993) X-ray structure of a monomeric cyclophilin A-cyclosporin A crystal complex at 2.1 Å resolution. J. Mol. Biol. 234, 000-012.
- Mikol, V., Kallen, J. and Walkinshaw, M. D.** (1994) X-ray structure of a cyclophilin B/cyclosporin complex: Comparison with cyclophilin A and delineation of its calcineurin-binding domain. Proc. Natl. Acad. Sci. USA 91, 5183-5186.
- Moore, J. M., Peattie, D. A., Fitzgibbon, M. J. and Thomson, J. A.** (1991) Solution structure of the major binding protein for the immunosuppressant FK506. Nature 351, 248-250.
- Morris, A. L., MacArthur, M. W., Hutchinson, E. G., Thornton, J. M.** (1992) Stereochemical quality of protein structure coordinates. Proteins 12 345-364.
- Navaza, J. and Saldudjian, P.** (1997) AMoRe: An automated molecular replacement program package in Methods in Enzymology ed **Abelson, N. J. and Simon, I. M.** Volume 276 Macromolecular Crystallography Part A **Carter, W. C. and Sweet, M. R. N.** ed pp ACADEMIC PRESS, INC.
- Otwinowski, Z.** "Oscillation data reduction program" in Proceedings of the CCP4 study weekend: "Data collection and processing", 29-30 January 1993, Compiled by: **L. Sawyer, N. Isaacs and S. Bailey**, SERC Daresbury laboratory, England, pp 56-62.

- Otwinowski, Z. and Minor, W.** (1997) Processing of X-ray diffraction data collected in oscillation mode in *Methods in Enzymology* ed **Abelson, N. J. and Simon, I. M.** Volume 276 Macromolecular Crystallography Part A **Carter, W. C. and Sweet, M. R. N.** ed pp Academic Press
- Page, A., Landry D., Wilson, G. and Carlow, C.** (1995) Molecular characterization of a cyclosporin A-Insensitive cyclophilin from the Parasitic Nematode *Brugia malayi*. *Biochem.* 34 (36), 11545-11550.
- Page, A., Kumar, S. and Carlow, C.K.S.** (1995b) Parasite Cyclophilins and Antiparasite activity of cyclosporine-A. *Parasitology Today* 11 (10), 385-388.
- Page, A., MacNiven, K. and Hengartner M.O.** (1996) Cloning and biochemical characterisation of the cyclophilin homologues from the free-living nematode *Caenorhabditis elegans*. *Biochem. J.* 317 (1), 179-185.
- Papageorgiou, C., Sanglier, J. J. and Traber, R.** (1996 a) Anti HIV-1 activity of a hydrophilic cyclosporin derivative with improved binding affinity to cyclophilin A. *Bioorg. Medic. Chem. Let.* 6 (1), 23-26.
- Pflügl, M. G., Kallen, J., Jansonius, N. J., and Walkinshaw, D. M.** (1994) The Molecular Replacement Solution And X-Ray Refinement To 2.8 Å Of A Decameric Complex Of Human Cyclophilin A With The Immunosuppressive Drug Cyclosporin. *J. Mol. Biol.* 244, 385-409.
- Price, R., Zydowsky, L., Jin, M., Baker, H., McKeon, F. and Walsh, C.** (1991) Human cyclophilin b: A second cyclophilin gene encodes a peptidyl-prolyl isomerase with a signal sequence. *Proc. Natl. Acad. Sci.* 88, 1903-1907.
- Radzicka, A., Acheson, S.A. and Wolfenden, R.** (1992) *Cis-trans* isomerisation at proline-desolvation and its consequences for protein folding. *Bioorg. Chem.* 20 (4), 382-386.
- Rinfret, A., Collins, C., Menard, R. and Anderson, S.** (1994) The N-Terminal Cyclophilin-Homologous domain of a 150-kilodaton tumor recognition molecule exhibits both peptidyl prolyl *cis-trans*-isomerase and chaperone activities *Biochemistry* 33, 1668-1673.

- Rodgers, W. D.** (1997) Practical Crystallography in Methods in Enzymology ed **Abelson, N. J. and Simon, I. M.** Volume 276 Macromolecular Crystallography Part A **Carter, W. C. and Sweet, M. R. N.** ed pp Academic Press
- Rossomando, E.** (1990) Purification Procedures: Chromatographic Methods in Methods in Enzymology ed **Abelson, J. and Simon, M.** Volume 182 Guide to Protein Purification **Deutscher, M.** ed pp ACADEMIC PRESS, INC
- Salemme, R. F. Spurlino, J. and Bone, R.** (1997) Serendipity meets precision: the integration of structure-based drug design and combinatorial chemistry for efficient drug discovery. Structure 5 319-324.
- Sambrook, J., Fritsch, F. E., Maniatis, T.** (1989) Molecular Cloning: A Laboratory Manual. Second Edition (Book 1) Cold spring Harbor Laboratory Press.
- Sambrook, J., Fritsch, F. E., Maniatis, T.** (1989) Molecular Cloning: A Laboratory Manual. Second Edition (Book 3) Cold spring Harbor Laboratory Press.
- Schulz, E.G. and Schirmer, H. R.** (1979) Principles of protein Structure. Springer-Verlag New York.
- Sheldrick, M. G. and Schneider, R. T.** (1997) SHELXL: High- Resolution Refinement in Methods in Enzymology ed **Abelson, N. J. and Simon, I. M.** Volume 277 Macromolecular Crystallography Part B **Carter, W. C. and Sweet, M. R. N.** ed pp Academic Press.
- Siekierka, J. J., Hung, S. H. Y., Poe, M., Lin, C. S., and Sigal, N. H.** (1989) A cytosolic binding protein for the immunosuppressant FK506 has peptidyl-prolyl isomerase activity but is distinct from cyclophilin, Nature 341, 755-757.
- Smith, T., Ferreira, L. R., Hebert, C., Norris, K. and Sauk, J. J.** (1995) Hsp47 and cyclophilin-b traverse the endoplasmic-reticulum with procollagen into pre-golgi intermediate vesicles a role for hsp47 and cyclophilin-b in the export of procollagen from the endoplasmic reticulum. J. Biol. Chem. 270, 18323-18328.
- Spik, G., Haendler, B., Delmas, O., Mariller, C., Chamoux, M., Maes, P., Tartar, A., Montreuil, J., Stedman, K., Kocher, H., Keller, R., Hiestand, P. and Movva,**

- N. (1991) A Novel secreted cyclophilin-like protein. (SCYLP) J. Biol. Chem. 226 (17), 10735-10738.
- Stanier, R., Ingraham, J., Wheelis, M. and Painter, P.** (1986) General Microbiology, (page 17). The Macmillan Press LTD.
- Steinmann, B., Bruckner, P. and Supertifuga, A.** (1991) Cyclosporin a slows collagen triple-helix formation in *vivo*-indirect evidence for a physiological-role of peptidyl-prolyl *cis-trans* -isomerase. J. Biol. Chem. 266, 1299-1303.
- Stellwagen, E.** (1990) Purification Procedures: Chromatographic Methods in Methods in Enzymology ed **Abelson, J. and Simon, M.** Volume 182 Guide to Protein Purification **Deuthscher, M. ed pp** ACADEMIC PRESS, INC
- Stoscheck, M.** (1990) Quantitation of Protein in Methods in Enzymology ed **Abelson, J. and Simon, M.** Volume 182 Guide to Protein Purification **Deuthscher, M. ed pp** Academic Press
- Stout, G. and Jensen, L.** (1989) X-ray structure determination a practical guide. Willey publication.
- Stura, E. A., Feinstein, A. and Wilsow, A.** (1987) Crystallization and preliminary crystallographic data for an antiprogestosterone monoclonal-antibody FAB' and steroid-FAB' complexes J. Mol. Biol. 193 (1), 229-231.
- Stura, E. A. and Wilson, I. A.** (1990) Seeding techniques in Crystallization of Nucleic Acids and Proteins A Practical Approach **Ducruix, A. and Giegé, R.** ed., Oxford University press.
- Takahashi, N., Hayano, T. and Suzuki, M.** (1989) Peptidyl-prolyl *cis-trans* isomerase is the cyclosporin A-binding protein cyclophilin Lett. Nature 337 473-476.
- Tal, M., Silderstein, A. and Nusser, E.** (1980) Why Does Coomassie Brilliant Blue R Interact Differently with different Proteins? J. Biol. Chem. 260 (18), 9976-9980.
- Tanaka, H., Kuroda, A., Marusawa, H., Hatanaka, H., Kino, T., Goto, T. and Hashimoto, M.** (1987) Structure of FK506: a novel immunosuppressant isolated from *streptomyces*, J. Am. Chem. Soc. 109, 5031-5033.

- Tatlock, J., Kalish V., Parge, K., Knighton, D., Showalter, R., Lewis, C., French, J. and Villafranca, E.** (1995) High-Affinity FKBP-12 ligands derived from (r)-(-)-Carvone . Synthesis and evaluation of FK506 pyranose ring replacements. *Biorganic & Med.Chem. Lett.* 5 (21) 2489-2494.
- Taylor, P., Husi, H., Kontopidis, G. and Walkinshaw, M.** (1997) Structures of cyclophilin-ligand complexes. *Prog. Biophys. Molec. Biol.* 67 155-181.
- Taylor, P., Page, P. A., Kontopidis, G., Husi, H. and Walkinshaw, M.** (1998) The X-ray structure of a divergent cyclophilin from the nematode parasite *Brugia malayi*. *FEBS letters* 425 361-366.
- Thali, M., Bukovsky, A., Kondo, E., Rosenwirth, B., Walsh, C. T., Sodroski, J. and Gottlinger, H. G.** (1994) Functional association of cyclophilin A with HIV-1 virions. *Nature* 372 (6504), 363-365.
- Theriault, Y., Logan, T. M., Meadows, R., Yu, L., Olejniczak, E. T., Holzman, T. F., Simmer, R. L. and Fesik, S. W.** (1993) Solution structure of the cyclosporin A/cyclophilin complex by NMR. *Nature* 361, 88-91.
- Trandinh, C. C., Pao, G. M. and Saier, M. H. Jr.** (1992) Structural and evolutionary relationships among the immunophilins: two ubiquitous families of peptidyl-prolyl *cis-trans* isomerases. *FASEB J.* 6, 3410-3420.
- Van Duyne, G. D., Standaert, R. F., Karplus, M., Schreiber, S. L. and Clardy, J.** (1991) Atomic structure of FKBP-FK506, an immunophilin-immunosuppressant complex, *Science* 252, 839-842.
- Van Duyne, G. D., Standaert, R. F., Karplus, P. A., Schreiber, S. L. and Clardy, J.** (1993) Atomic structure of FKBP-12 complexes with FK506 and rapamycin. *J. Mol. Biol.* 229, 105-124.
- van Duyne, G. D., Standaert, R. F., Karpus, P. A., Schreiber, S. L. and Clardy, J.** (1991) Structure of Immunophilin-immunosuppressant complex. *Science* 252, 839-842.
- Verlinde, LMJ. C. and Hol, GJ. W.** (1994) Structure-based drug design: progress, results and challenges. *Structure* 2 (7), 577-587.

- Walkinshaw, M.D., Kallen, J., Weber, H. P., Widmer, A., Widmer, H. and Zurini, M.** (1992) Immunophilin Structure: A template for immunosuppressive drug desing? Transp. Proceedings 24 (4), 8-13.
- Wayne, A., Hendrickson, A. and Ogata, M.** (1997) Phase determination from multiwavelength anomalous diffraction measurement in Methods in Enzymology ed **Abelson, N. J. and Simon, I. M.** Volume 276 Macromolecular Crystallography Part A **Carter, W. C. and Sweet, M. R. N.** ed pp Academic press.
- Weber, C., Wider, G., von Freyberg, B., Traber, R., Braun, W., Widmer, H. and Wüthrich, K.** (1991) The NMR structure of cyclosporin A Bound to cyclophilin in aqueous solution. Biochemistry 30, 6563-6574.
- Widmer, A.** (1997) WITNOTP: A computer program for molecular modelling. Sandoz AG, Basel.
- Wiechelmann, K., Braun, R. and Fitzpatrick, J.** (1988) Investigation of the bicichoninic acid protein assay: identification of the groups responsible for colour formation. Anal. Biochem. 175, 231-237.
- Wilson, K. P., Yamashita, M. M., Sintchak, M. D., Rotstein, S. H., Murcko, M. A., Boger, J. B., Thomson, J. A., Fitzgibbon, M. J., Black, J. R. and Navia, M. A.** (1995) Comparative X-ray structures of the major binding protein for the immunosuppressant FK506 (Tacrolimus) in Unligated form and in complex with FK506 and Rapamycin. Acta Cryst. D51, 511-521.
- Yeh, J. and Hol, W.** (1998) A flash-annealing technique to improve diffraction limits and lower mosaicity in crystals of glycerol kinase. Acta Cryst. D(54) 479-480.
- Zhao, Y. D. and Ke, H. M.** (1996 a) Mechanistic implication of crystal structures of the cyclophilin-dipeptide complexes. Biochemistry 35, 7362-7368.
- Zhao, Y. D. and Ke, H. M.** (1996 b) Crystal structure implies that Cyclophilin predominantly catalyzes the *trans* to *cis* isomerization. Biochemistry 35, 7356-7361.